Structural Studies of Liquid Crystals and Silyl Solutes

Paul James Mathieson

A thesis presented for the
Degree of Doctor of Philosophy
in the Faculty of Science
of the University of Edinburgh, 1995

DECLARATION

This thesis has not been submitted, in whole or in any part, for any degree at this or any other university. The work is original and my own, carried out under the direction of Prof. D.W.H.Rankin; where this is not so credit has been duly given.

21/11/95

Acknowledgements

I would like to thank all the people at Edinburgh University who helped me throughout my time there. In particular, thanks go to Dr David Reed and Dr John Miller for running the LCNMR spectra, Dr Steve Henderson for assistance with practical work and Dr Paul Brain for his help and encouragement on a variety of topics and Dr Sandy Blake for collecting the data for my crystal structures. Thanks also go to Dr Naresh Mooljee for his invaluable advice and support in all aspects of computing and to Ewan, Charles, Murray and Pete for moral support.

Special thanks go to my supervisor Prof. David Rankin for his assistance and continued optimism throughout and to Dr Bob Gould for his patience and assistance with all things crystalline.

Finally, I would like to express my gratitude to Dow Corning and to the Science and Engineering Research Council who funded this CASE award.

Abstract

The deviations in structure from that of the gas phase have been examined when the technique of liquid crystal nuclear magnetic resonance (LCNMR) spectroscopy is applied to a series of simple silyl compounds. Both conventional vibrational corrections and an additional correction to account for the correlation between vibration and reorientation of the molecules were applied. This has indicated that the main structural differences are as a result of specific interactions between polar groups from the liquid crystal and the silicon. This interaction takes the form of an S_N2 interaction intermediate as is found in the crystal structures of these silyl compounds. In addition, the crystal structure of two liquid crystals, 4'-*n*-heptyl-4-cyanobiphenyl (*7*-CB) and 4'-methoxy-4-cyanobiphenyl (*1*-OCB) have been determined. The molecular packing of *7*-CB and the first seven members of the *n*-OCB series were then examined and found to be related to the mesogenic properties of these compounds on melting.

Contents

Chapter 6 - A Study of Silyl Containing Compounds in the Liquid Crystal Environment

Chapter 1

Introduction

1. Introduction

In the past there has been much work carried out at Edinburgh concerning the structures of main group compounds. In particular the structures of simple Silicon and Germanium compounds (of which those containing -SiH_3 and -GeH_3 groups are the simplest) and Phosphorus compounds have been studied. [1,2,3,4]

The main structural technique used in studying these has been electron diffraction (with or without the aid of microwave spectroscopy). However, these techniques can not always accurately determine the positions of light atoms, particularly hydrogen, and so the technique of Liquid Crystal NMR (LCNMR) is often used to compliment these other structural techniques. A structure more precise than that determined by any single technique is then obtained by means of combined analysis.[5,6,7]

In using LCNMR data in combined analysis studies, it is assumed that the structure determined in the liquid crystal solvent (solution phase) is the same as that obtained in the gas phase. This is found to be the case when the solute molecule being studied is fairly rigid and does not interact with the liquid crystal solvent. [8-13]

Unfortunately few inorganic compounds are rigid systems, and there has not been so much success using LCNMR data in combined structural analysis with them.[14,15] It has been found that many liquid crystal solvents are reactive, reacting with inorganic solutes or co-ordinating weakly to the solute molecules, thereby changing their structures.[16]

The compounds of particular interest at Edinburgh have been the silyl compounds. Typically, it is found that there is a two degree increase in the HSiH angle of the silyl group.[1,2] An explanation of this could be that the basic solvent groups, most frequently cyanide, co-ordinate to the silyl groups, i.e. a Lewis acid-base interaction, as is observed in the crystal phase for these silyl compounds.[2,17-26] This is analogous to a snap shot of an S_N2 intermediate as is shown in Figure 1.1.

Figure 1.1 S_N2 intermediate. The incoming isonitrile displaces the bound nitrile group

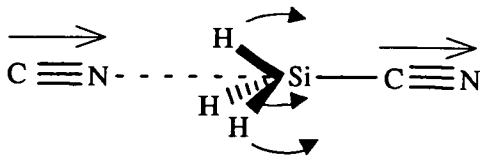

The purpose of this work was to investigate this further and to determine whether or not it would possible in the future to use results from LCNMR spectroscopy in combined analysis studies of inorganic compounds. The technique of LCNMR spectroscopy is explained in Chapter 2.

Chapter 3 describes the first approach taken to this problem, which was to examine the crystal structures of silyl compounds and the liquid crystals themselves. It was then hoped that crystals of adducts formed between the liquid crystal molecules and silyl compounds could be obtained. Crystals of an adduct formed between silyl chloride and diethyl ether had previously been obtained at Edinburgh[26] and it was thought that a similar approach would work in this case. However, no such crystals were obtained.

Chapter 4 describes the crystal structures of two different, but related, liquid crystal molecules. These are 4-*n*-heptyl-4-cyanobiphenyl (*7*-CB) and 4-*n*-methoxy-4-cyanobiphenyl (*1*-OCB). The trends in crystal packing of the first seven members of the *n*-OCB series are then analysed in Chapter 5, and the interactions and mode of crystal packing correlated to the mesogenic behaviour exhibited by these compounds on melting.

In order to further examine the deformations observed in silyl compounds dissolved in liquid crystals, Chapter 6 details experiments carried out using a variety of liquid crystals obtained from Merck Ltd. on silyl compounds of the general formula SiH_3X (X=Br, Cl, I, F, CN, CH_3). It was discovered that each compound distorted in the same manner and by a similar amount in each solvent. Interestingly, it was observed that the structure obtained by LCNMR depended almost totally on the type of functional group present in the liquid crystal molecules. The HSiH angle was

consistently smaller than the gas phase value for each compound when a non polar solvent was used. Angles around 0.5° and 2.0° larger than the gas phase values were found in fluorinated and cyano containing solvents respectively.

This was also reflected in the ^1H chemical shift of the silyl compounds which tended to be larger in the cyano containing liquid crystals. This is expected if an interaction similar to that depicted in Figure 1.1 was adopted. As the silicon changes from four to five co-ordinate, the SiH bonding will change from sp^3 to sp^2 hybridisation. This results in the bonds having increased s character and hence the hydrogen becomes more deshielded, resulting in an increased chemical shift.

In Chapter 7 the approach adopted by Lounila and Diehl[27,28], where an additional correction is introduced to the direct couplings in the LCNMR data to account for the correlation between the vibration and reorientation of the solute molecule within the liquid crystal environment, was applied. They successfully used this technique to account for, and correct, apparent deformations in the methyl geometry of methyl fluoride and iodide.[29] This required using extra information from a 'probe' molecule dissolved in the NMR tube along with the solute. The molecule they used was methane, as this is a good approximation to the methyl groups being studied. In this work silane was therefore used as a probe molecule. The documentation for the program MASTER[30] required to calculate this correction is included as Appendix A.

Unfortunately, only partial success was found with this technique. In almost every case this correction resulted in a slight improvement between the gas phase and LCNMR structures, but three distinctly different structures remained. It is concluded that the non-polar liquid crystal solvent that does not contain any functional groups likely to interact with the silyl solute molecules gives a structure in reasonably good agreement with the gas phase values in almost every case. The HSiH angle in the fluorinated and the cyano containing solvents is consistently 0.4° and 1.9° larger respectively than this.

Finally, the results obtained in the conclusions from this work are summarised in Chapter 8, along with some suggestion for further work.

References

[1] C.A.Brookman, '4th Year Honours Project', University of Edinburgh (1989)

[2] P.D.Blair, A.J.Blake, R.W.Cockman, S.Cradock, E.A.V.Ebsworth and D.W.H.Rankin, J. Mol. Struct., 193, (1989), 279

[3] P.D.Blair, J. Mol. Struct, 97, (1983), 147

[4] A.J.Blake, E.A.V.Ebsworth and M.Dyrbusch, Acta. Cryst., Sect. C, 43, (1987), 1683

[5]K.Kuchitsu and M.Nakata, "Stereochemical Applications of Gas-phase Electron Diffraction", Part A, Ch.7, eds. I.Hargittai and M.Hargittai, VCH, New York, (1988), 227

[6]R.K.Heenan and A.G.Robiette, J. Mol. Struct., 54, (1979), 135

[7]K.Tamagawa, T.Iijima and M.Kimura, J. Mol. Struct., 30, (1976), 243

[8]P.Diehl and W.Niederberger, J. Magn. Reson., 9, (1973), 495

[9]J.W.Emsley, J.C.Lindon and J.Tabony, J. Chem. Soc., Farad. Trans., 71, (1975), 579

[10]N.J.D.Lucas, Mol. Phys., 22, (1971), 233

[11]S.Cradock, P.B.Liescheski, D.W.H.Rankin and H.E.Robertson, J. Amer. Chem. Soc., 110(9), (1988), 2759

[12]P.B.Liescheski and D.W.H.Rankin, J. Mol. Struct., 196, (1989), 1

[13]S.Cradock, P.B.Liescheski and D.W.H.Rankin, J. Magn. Reson., 91, (1991), 316

[14]E.E.Burnell and P.Diehl, Canad. J. Chem., 50, (1972), 3566

[15]J.W.Emsley and J.C.Lindon, Mol. Phys., 29, (1975), 531

[16] T.Väänänen, J.Jokisaari, A.Kääriäinen and J.Lounila, J. Mol. Struct., 102, (1983), 175

[17] A.J.Blake, E.A.V.Ebsworth and A.J.Welch, Acta. Cryst., Sect. C, 40, (1984), 895

[18] D.G.Anderson, A.J.Blake, S.Cradock, E.A.V.Ebsworth, D.W.H.Rankin and A.J.Welch, Angew. Chem., Int. Edn. Engl., 25, (1986), 107

[19] D.G.Anderson, A.J.Blake, S.Cradock, E.A.V.Ebsworth, D.W.H.Rankin, H.E.Robertson and A.J.Welch, J. Chem. Soc., Dalton Trans., (1987), 3035

[20] A.J.Blake, E.A.V.Ebsworth and A.J.Welch, Acta. Cryst., Sect. C, 40, (1984), 895

[21] D.G.Anderson, A.J.Blake, S.Cradock, E.A.V.Ebsworth, D.W.H.Rankin and A.J.Welch, Angew. Chem., Int. Edn. Engl., 25, (1986), 107

[22] D.G.Anderson, A.J.Blake, S.Cradock, E.A.V.Ebsworth, D.W.H.Rankin, H.E.Robertson and A.J.Welch, J. Chem. Soc., Dalton Trans., (1987), 3035

[23] M.J.Barrow and E.A.V.Ebsworth, J.Chem. Soc., Dalton Trans., (1982), 211

[24] A.J.Blake, S.G.D.Henderson, E.A.V.Ebsworth and A.J.Welch, Acta Cryst., Sect. C, 41, (1985), 1141

[25] A.J.Blake, S.G.D.Henderson, E.A.V.Ebsworth and A.J.Welch, Acta Cryst., Sect. C, 44, (1988), 1337

[26] A.J.Blake, S.Cradock, E.A.V.Ebsworth and K.C.Franklin, Angew. Chem., 29, (1990), 76

[27]J.Lounila and P.Diehl, J. Magn. Reson., 56, (1984), 254

[28]J.Lounila and P.Diehl, Mol. Phys., 52, (1984), 827

[29]J.Lounila, P.Diehl, Y.Hiltunen and J.Jokisaari, J. Magn. Reson., 61, (1985), 272

[30]R.Wasser, M.Kellerhals and P.Diehl, Magn. Reson. Chem., 27, (1989), 335

Chapter 2

Liquid Crystal Nuclear Magnetic Resonance (LCNMR) Spectroscopy

2. Introduction - Liquid Crystals

The Austrian botanist Friedrich Reintzer is generally credited for 'discovering' liquid crystals in 1888, when he observed that cholesteryl benzoate had 'two melting points'. Since then, it has emerged that around 0.5% of all organic compounds form some type of phase between the liquid and crystalline phases. These are referred to as mesophases.

The mesophases possess a greater degree of order than that found in the liquid phase, but maintain the essential liquid property of rapid, random translational motion. Different mesophases have different degrees of order, with the least ordered being the 'nematic' mesophase. This is normally formed by compounds containing rod-like molecules, and can be thought of as forming because the molecules prefer to align with their rod axes lying parallel rather than perpendicular to one another (Figure 2.1). Normally a nematic liquid crystal will have many areas of local order, where all the molecules can be described as pointing along a vector called the 'director', no overall order existing because the different directors throughout the bulk of the sample point in different directions. However, if the liquid crystal is placed in an electrical or magnetic field, all the local directors can be made to point in the same direction and the liquid becomes anisotropic. Alignment of the liquid crystal will also cause alignment of any solute molecules, and it is this effect that is used in LCNMR experiments.

Obviously, when aligning a sample in such a way, it is important to have some measure of the degree of order/anisotropy of the sample. It turns out that the most convenient way to describe this is as the average of the Legendre polynomial $P_2=\frac{1}{2}\left(3\cos^2\theta-1\right)$, where θ is the angle each molecule makes with the director. This function is conveniently formulated so that an isotropic liquid would have an order of zero, and a perfectly aligned solid would have a value of one. Typical values for liquid crystals range from 0.3 to 0.9.

Figure 2.1 A time-averaged representation of the nematic mesophase

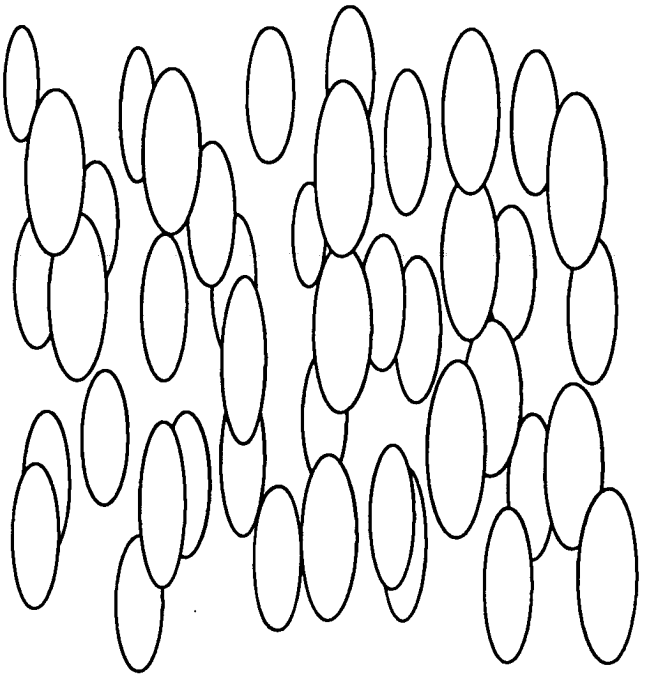

A special case of the nematic mesophase is the cholesteric or chiral nematic mesophase. This is formed by optically active molecules and differs from the nematic mesophase in that, in an aligned sample, the directors do not arrange themselves all pointing in the same direction but are slightly displaced with one another. This results in the direction in space of the director rotating as you move through the sample. A new term called the 'pitch' is introduced to define the distance through the sample required for the director to complete one full revolution. This type of mesophase is not of much use for high resolution NMR experiments (unless strong field strengths are used), but is important because of its optical properties which can be used in display applications and the fact that the pitch, and hence optical properties, are sensitive to temperature/pressure as well as the strength of any applied electric/magnetic fields.

A third class of mesophase is the smectic mesophase. These types of mesophase have a higher degree of order than the nematic mesophase because, as well as the small degree of orientational order, there is also a small amount of positional order. This positional order arises because the molecules tend to form into distinct layers. There

are several different varieties of smectic mesophase. Two common examples are the smectic A phase, in which the director is perpendicular to the planes, and the smectic C phase, in which the director makes an angle other than 90 ° to the planes (Figures 2.2 and 2.3).

These mesophases are all formed by compounds containing molecules which are all essentially rod-like in shape (calamatic liquid crystals). A further type of liquid crystal was discovered in India in 1977, and is formed by molecules which are disk-like in shape. These types of liquid crystals are classed 'discotic'. They also exhibit a wide range of mesophases including nematic, chiral nematic and smectic (or columnar). This serves only to give an insight into what is an interesting subject in its own right, but we shall not digress. An easily readable introduction to liquid crystals and some of their applications is given by Collings[1]. It is best now to have a brief introduction into how liquid crystals are used in LCNMR to obtain structures of solute molecules.

Figure 2.2 A time-averaged representation of the smectic A mesophase

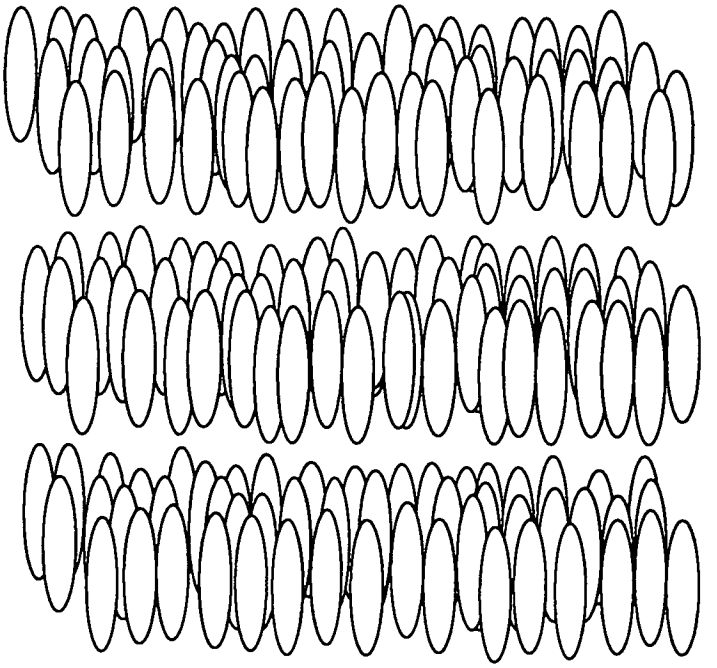

Figure 2.3 A time-averaged representation of the smectic C mesophase

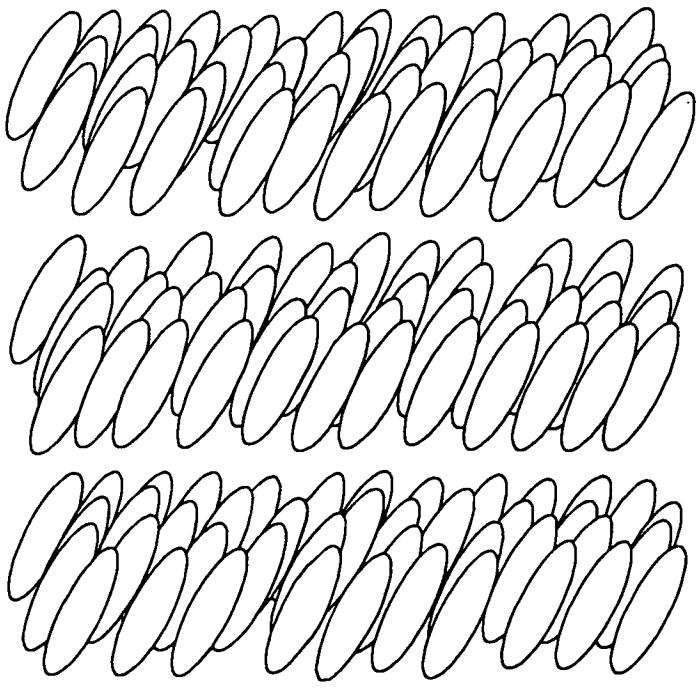

2.1 Theory

As is mentioned above, a liquid crystal NMR experiment is carried out by taking advantage of the anisotropic properties of a nematic liquid crystal when it is caused to align under the influence of an external field. It is found that any small solute molecules experiencing this anisotropic environment also experience a degree of ordering.

A typical NMR experiment carried out using an isotropic solvent yields spectra which are dependent on both the chemical shifts (ω_i) of each nuclei observed and an indirect coupling constants (J_{ij}) between all observed nuclei. A third set of parameters, the direct dipolar coupling constants (D_{ij}), is not observed. Unlike the indirect coupling constants, which are transmitted through bonds, these direct coupling constants are transmitted through space. Their magnitudes are therefore dependent upon both the distances between the nuclei concerned, and on the direction through space of the vectors between them. In the isotropic solvent, where the molecules tumble randomly

in solution, these are averaged out to zero. In the liquid crystal environment, where a degree of anisotropy is introduced to the solute molecules, these dipolar couplings no longer average to zero. It must be remembered that the molecules still tumble in all directions, the anisotropy arising because the molecules spend longer in some orientations than in others. The molecules are said to be partially oriented.

The magnitude of these direct dipolar couplings are given by the equation

$$D_{ij} = -\frac{\mu_0 \hbar \gamma_i \gamma_j}{4\Pi^2} \frac{S_{ij}}{r_{ij}^3} \qquad \textbf{Eq. 2. 1}$$

where D_{ij} is the direct coupling between nuclei i and j, μ_0 is the permittivity of vacuum, $\hbar$ is Diracs constant, γ_I is the magnetogyric ratio of nuclei i, r_{ij} is the internuclear distance, and $S_{ij}=\frac{1}{2}\left(3\cos^2\theta_{ij}-1\right)$. θ_{ij} is the angle between the internuclear vector and the direction of the spectrometer's magnetic field.

From Equation 2.1 it is clear that for every direct coupling constant obtained, there are two variables which are unknown (r_{ij} and S_{ij}). This can be simplified, however, by defining a tensor S which describes the average orientation of the whole molecule. The average orientation of the vectors joining nuclear pairs in the molecule is then expressed as a function of this tensor.

$$D_{ij} = -\frac{\mu_0 \hbar \gamma_i \gamma_j}{4\Pi^2 r_{ij}^3} \begin{pmatrix} S_{zz}\cos^2\theta_{ijz} + S_{yy}\cos^2\theta_{ijy} + S_{xx}\cos^2\theta_{ijx} \\ +2S_{xz}\cos\theta_{ijx}\cos\theta_{ijz} + 2S_{yz}\cos\theta_{ijy}\cos\theta_{ijz} \\ +2S_{xy}\cos\theta_{ijx}\cos\theta_{ijy} \end{pmatrix} \qquad \textbf{Eq. 2. 2}$$

where $\theta_{ij\alpha}$ is the angle between the internuclear vector and an axis α, and $S_{\alpha\beta}$ are the elements of the orientation tensor,

$$S = \begin{pmatrix} S_{xx} & S_{yx} & S_{zx} \\ S_{yx} & S_{yy} & S_{zy} \\ S_{xz} & S_{yz} & S_{zz} \end{pmatrix}$$ which are determined by $S_{\alpha\beta} = \frac{1}{2}\left\langle 3\cos\theta_\alpha \cos\theta_\beta - \delta_{\alpha\beta} \right\rangle$.

θ_α is the angle between the molecular α-axes and the molecular field, and $\delta_{\alpha\beta}$ is the Kronecker delta.

Because the orientation tensor S is symmetric and traceless (i.e. $S_{xx}+S_{yy}+S_{zz}=0$), there is only a maximum of five orientation parameters required to define the orientation between all nuclear pairs in a given molecule. This number is reduced further by taking the symmetry of the molecule being studied into account (Table 2.1).

Table 2.1 Number of orientation parameters required to describe orientation of molecules with given symmetries.

Point Group	No. of Orientation Parameters
C_1, C_i	5
C_2, C_{2h}, C_s	3
C_{2v}, D_2, D_{2h}	2
Symmetric tops	1
Spherical tops	0

2.2 Experimental

Samples for LCNMR are prepared in much the same way as in any NMR experiment, the main difference being the use of a liquid crystal solvent in place of an isotropic solvent. In choosing a suitable liquid crystal, the main factors to consider are the temperature the experiment is to be carried out at (i.e. the desired mesophase must be present at the required temperature), and the liquid crystal must not react with the solute molecules. This second requirement is not normally a problem but for example, the liquid crystal p-methoxybenzylidene-p-n-butylaniline (MBBA) was found to react with silyl compounds (see Chapter 6). The mesophase chosen is also quite important. LCNMR experiments can be carried out using almost any mesophase under the right conditions but, in practise, the nematic phase is found to give spectra of higher resolution. Only nematic liquid crystals are used in Edinburgh at present.

The final decision to be made concerns the spectrometer used to obtain the spectra. The direct dipolar constants are usually much larger than the indirect coupling constants and can sometimes be thousands of Hertz. As a result of this these

couplings are often of comparable magnitude to, or greater than, the differences in chemical shift of the nuclei being observed, which leads to second order spectra. This and the fact that, unlike in conventional NMR experiments, coupling may occur between magnetically equivalent nuclei, leading to spectra containing many more lines than might be expected, means that it is often best to use a high field spectrometer. Moreover, for a solvent aligning parallel to the applied magnetic field, use of a spectrometer with a superconducting magnet allows rotation of the sample, reducing effects of field inhomogenity At Edinburgh, the preferred spectrometer is the Bruker WH360 MHz, although it is the BRUKER AL250 which is often used if ^{19}F spectra may also be required.

Before submitting a sample for LCNMR there are several factors which must be considered. In order to solve the LCNMR spectra, the chemical shifts and indirect couplings for the solute must be known. These are normally obtained from the literature or by running the solute in an isotropic solvent. There are some errors introduced here, however, due to solvent effects on the chemical shifts and indirect couplings. These effects are normally small and, in the case of the chemical shifts, are normally unimportant. This is because, in refining the LCNMR spectrum, the chemical shifts will be refined and optimised for the liquid crystal solvent that was used. This is not always possible for the indirect couplings, however, because these are often highly correlated with the direct couplings, preventing any satisfactory refinement. To get round this it is often best to run the LCNMR sample at a temperature at which the liquid crystal is in the isotropic phase. This allows the chemical shifts and indirect couplings to be measured in the solvent used for the LCNMR experiment.

A further consideration is what is expected to be observed in the LCNMR spectrum. If low abundance satellites are required then samples will have to spend longer in the spectrometer. If this is the case it may also be advisable to increase the concentration of solute molecule in the sample, although this lowers the solid-nematic and nematic-liquid transition temperatures, and narrows the temperature range of (or even eliminates) the nematic phase.

2.3 LCNMR spectra - analysis

When an LCNMR spectrum is obtained, the liquid crystal gives a very broad featureless spectrum due to the large number of couplings involved. Fortunately, the solute molecules normally provide relatively sharp peaks which can be easily identified and accurately measured in frequency and intensity. These are made clearer by subtracting the spectrum of the solvent from that of the solute and/or levelling the background, leaving just the sharp peaks attributable to the solute. In obtaining the D couplings from the spectrum there are two main routes, determined by whether the spectrum is first or second order.

2.3.1 First order spectra

In a first order spectrum, the direct couplings can be calculated directly from the line frequencies. Two different types of splitting occur. If the two nuclei concerned would normally give rise to an observable indirect coupling in an isotropic solvent, the coupling observed is $T_{ij} = 2D_{ij} + J_{ij}$, and where nuclei i and j are equivalent, so that no indirect coupling would normally be observed, the coupling is $T_{ij} = 3D_{ij}$.

Care must be taken, however, because a further complication arises from the fact that both direct and indirect couplings can be positive or negative. Double resonance experiments are normally used to determine the sign of indirect couplings in isotropic NMR. Even when these are known, however, assumptions about the structure of the molecule concerned are normally made to determine the relative signs of the indirect and direct couplings. This is done by assuming a structure and using Eq. 2.1 to calculate the direct couplings for various values of S. It is also possible to determine the signs of the direct couplings experimentally, but in practice, where there is any ambiguity, all possible combinations of signs are tried and it is usually apparent which is the correct combination.

2.3.2 Second order spectra

As mentioned above, because the direct couplings between nuclei are often of comparable magnitude to the differences in chemical shift of the nuclei concerned, second order spectra are often obtained in LCNMR experiments. These can be solved in two ways.

First, one can solve them analytically by taking into account the spin systems of the nuclei concerned. This approach is explained in the book by Emsley and Lindon[2]. It is useful to know about, although not as practicable when computer simulations etc. are available. Its advantages are that the theory predicts many features of LCNMR spectra that are not always apparent when using other techniques. One recent example at Edinburgh is actually highlighted in the book. The ^1H spectra of *p*-chlorofluorbenzene can be simulated by the spin system $[AB]_2X$. This is predicted to give rise to two sub-spectra of the $[ab]_2$ type corresponding to the case where the spin of the ^{19}F is $\pm\frac{1}{2}$. In solving this, it was found that only the sum of the two different direct couplings to the ^{19}F could be determined. By referring to the book it was confirmed that this is the case because of the relatively small difference in chemical shift of the two types of ^1H in the molecule. However, it was predicted that weak lines ought to be present in the middle of the spectrum which would allow further refinement to take place. These had not been observed at this point but, on closer scrutiny of the experimental spectra these lines were indeed found. This is just one example of a situation in which a better understanding of the type of spectrum being analysed can aid in finding the final and correct solution.

The second method for solving second order spectra is to the use computers and solve the spectra using iterative methods. It is this method that is used at Edinburgh with the aid of the programs LCSIM and SLIQUOR. These programs are based on the modified NMR analysis program LEQUOR[3].

The output of LCSIM and SLIQUOR was modified to make use of the new technology available in the Chemistry Department at Edinburgh. This has allowed

direct graphical comparison of experimental and calculated spectra to be made interactively on a SUN running X-Windows, with the option for a hard copy available as well. The subroutines which make this possible[4] make extensive use of the UNIRAS graphics libraries.[5]

LCSIM is a simulation program which does not refine the spectrum, but is a visual tool used to simulate the spectrum which corresponds to a particular set of orientation parameters. The program requires the user to input a trial structure for the molecule concerned. Also required are the chemical shifts and indirect couplings. The program then uses this information to calculate the direct couplings for any choice of orientation parameters. This is simplified by using a graphics window to compare the experimental and calculated spectra visually. The user then works systematically through a range of possible orientations and chooses the one which gives the best match of the two spectra. Once this is done, the calculated values of the direct couplings are taken and used in the refinement program SLIQUOR.

It should be remembered that it will seldom be possible to find any orientation parameter which exactly matches the experimental and calculated spectra. One reason for this is that the trial structure given in the input file is unlikely to be exactly the same as the structure of the molecule dissolved in the liquid crystal. The aim of LCSIM, therefore, is to obtain approximate orientation parameters which give a match between the spectra good enough for some of the lines occurring in both spectra to be identified with a reasonable degree of confidence. A more precise set of orientation parameters will be determined later when the final calculated direct couplings are used to determine the structure of the molecule in the program ED92[6,7]. For samples which produce spectra containing many lines within a small range of frequencies, it is sometimes beneficial to apply vibrational corrections to the calculated direct couplings. This has been shown to help in line assignment when deciding which lines from the simulated spectra should be assigned in SLIQUOR.

SLIQUOR is used to refine the spectral parameters (D_{ij}, J_{ij} and ω_i) to fit the experimental spectrum. In this program the assumptions about the structure, and

therefore orientation parameters, are removed and refinement is carried out by a least squares adjustment of NMR parameters to match the experimental and calculated spectra. Initially it calculates the same spectrum found using LCSIM. In SLIQUOR, refinement is carried out using frequencies that particular lines in the calculated spectrum are observed at in the experimental spectrum. It is very important in doing this to take care not to make any wrong assignments. These are often impossible to detect but will prevent proper refinement of the spectrum being achieved. For this reason it is especially important to make sure that, once a refinement is complete, there are no lines in the experimental spectrum that cannot be accounted for, and that there are no predicted lines which are unaccountably absent. Another good indication that something has gone wrong is the rms. fit of the spectral lines. For a proton spectrum it is not uncommon to obtain an rms. fit of ≤ 0.5 Hz. If this is not achieved, it is advisable to check the refinement by starting again, perhaps assigning lines from a different part of the spectrum first, or by trying to swap lines which are close in frequency.

From SLIQUOR it is normally possible to determine direct couplings with uncertainties of less than 0.3 Hz. The limiting factor is often the uncertainty in the experimental frequencies. In refining satellite spectra, larger uncertainties can often be found due to the small number of lines which my be assigned. It is not uncommon for satellites to be lost under peaks from the more intense parent spectrum, and often those found have higher uncertainties in their frequencies because of the lack of intensity. A more detailed description of the working and use of these programs is given by E.Brown[8].

2.4 Advantages and disadvantages of LCNMR

LCNMR is a structural technique in its own right, but at Edinburgh it is used most often to obtain structures not on its own but by combined analysis. These involve refining structural data from several different structural techniques together, and

generally provide structures more precise than those obtained by any one of the techniques alone.[9,10,11]

When a combined analysis is carried out, it is normally electron diffraction (ED), LCNMR, and often rotational spectroscopy that are used. The main advantage of LCNMR is that it can provide a precise geometry for the light atoms in the molecule, whereas ED can have trouble locating light atoms, particularly hydrogen, in the presence of heavy atoms, and it is also very difficult to resolve interatomic distances that are of a similar length. Rotational spectroscopy, although very precise, is restricted to the number of isotopomers available for study.

LCNMR does have its own disadvantages, however, with one generally being the restriction to the use of dipolar couplings between nuclei of spin ½. Also, due to the difficulty in separating the anisotropic indirect coupling contribution from the total anisotropic coupling, great care must be taken if couplings are to be used that do not involve hydrogen.

One final drawback of LCNMR is the need to determine the orientation parameters. Because of the need to use some of the direct couplings to determine this, it is normally only possible to measure ratios of distances and angles by LCNMR. This means it is virtually always necessary to use some form of external information in order to determine the overall size of a molecule.

2.5 Vibrational Corrections

When determining the structure of a molecule, the structure obtained is averaged over all the intermolecular motions the molecule underwent while being observed by the technique used. This leads to the problem that different structural techniques yield different average structures for the same molecule, because the averaging processes are different. This is a major problem when comparing structures obtained by different structural techniques, or in the case of combined analysis, when data from

several techniques are to be refined together to obtain one structure. Three different types of structure are identified below,

ED	$r_a \propto \left\langle \frac{1}{r} \right\rangle^{-1}$
Microwave Spectroscopy	$r_0 \propto \left\langle \frac{1}{r^2} \right\rangle^{-2}$
LCNMR	$r_d \propto \left\langle \frac{1}{r^3} \right\rangle^{-3}$

where r_a refers to the apparent distance between two nuclei obtained from an ED experiment, r_0 is the distance between nuclei derived from rotation constants in microwave spectroscopy, and r_d is the distance calculated from the direct dipolar couplings in LCNMR, r being the instantaneous internuclear distance.

In order that data can be combined from these different techniques, or the respective structures compared with one another, it is necessary to make corrections so that all will lead to equivalently averaged structures.

The most fundamental definition of an internuclear distance is often considered to be that of the equilibrium distance r_e. This gives an idealised structure where there is no molecular vibration and corresponds to the internuclear separation at which the potential energy function is a minimum. This is the type of structure obtained by ab initio calculations. In most cases it is not possible to obtain an r_e structure experimentally, so different structural definition is required.

The preferred equilibrium structure used is the r_α structure. This averages the nuclear positions over a Boltzman distribution of vibrational states at a given temperature. This is closely related to the r_α^0 (or r_z) structure, which is defined as the distance between the average nuclear positions in the ground vibrational state.

To convert an LCNMR structure from an r_d to an r_α structure, the approach used by Sykora et al.[12] is used. This involves converting the direct dipolar couplings observed

from the LCNMR experiment (D^0) to the corrected D^α values using the program BMGV[13]. This uses the equations:

$$D^\alpha = D^0 - d^h \qquad \text{Eq. 2. 3}$$

where d^h is the harmonic correction term, given by

$$d^h = -\frac{\mu_0 \hbar \gamma_\gamma \gamma_j}{8\Pi^2} Tr\left(S\Phi^h\right) \qquad \text{Eq. 2. 4}$$

where Tr() denotes the trace of the enclosed tensor product and S is the orientation tensor.

The elements of the tensor Φ^h are given by

$$\Phi^h_{\alpha\beta} = \left[C_{\alpha\beta} - 5\sum_\gamma \zeta_\gamma \left(C_{\alpha\gamma}\zeta_\beta + C_{\beta\gamma}\zeta_\alpha\right) + \frac{5}{2}\zeta_\alpha\zeta_\beta \sum_{\gamma\delta} C_{\gamma\delta}\left(7\zeta_\gamma\zeta_\delta - \delta_{\gamma\delta}\right)\right] \Big/ r^5 \qquad \text{Eq. 2. 5}$$

where ζ_α is the cosine of the angle between the internuclear vector and the α-axis of the molecular co-ordinate system, $\delta_{\gamma\delta}$ is the Kronecker delta and $C_{\alpha\beta}$ are the elements of the covariance matrix.

The covariance matrix describes how the vectors joining nuclei in the molecule change as the molecule vibrates. This is obtained from an harmonic force field analysis of the molecule. This is done using a vibrational analysis program such as GAMP[14] or ASYM20/40[15], or from the molecular mechanics program MM3[16] adapted to give the covariance matrix by Brown[8].

In conventional LCNMR, these are all the corrections deemed necessary. To ensure that this is the case, it is important to compare the structures obtained with those determined by other structural techniques. Diehl and Niederberger[17] demonstrated that the structure of benzene obtained by LCNMR analysis agreed, to within experimental error, with the r_α structure determined by ED. Similar results have been obtained for a number of other molecules, including pyridine[18] and cyclopropane[19]. In fact, the r_α structure obtained by LCNMR will always agree, within experimental errors, of the r_α structure obtained by ED, as long as the molecule being studied is

fairly rigid, (see below) and the degree of interaction between the liquid crystal used and the solute is low (c.f. pyrrole[20]).

In obtaining these structures by LCNMR, no particular attention has been paid to the actual liquid crystal used in the experiment. This is because, for these rigid molecules, the choice of liquid crystal solvent is largely unimportant. Structural changes observed on using different liquid crystals are generally very small and fall within experimental errors. Unfortunately, especially in the case of less rigid molecules, this is not always the case. Marked differences in structure have been observed at Edinburgh when comparing the r_α structure of silyl compounds[21,22] with the structures found by microwave spectroscopy. On further analysis using different liquid crystal solvents, it was found that the structure obtained by LCNMR for these compounds depended largely on the liquid crystal solvent used (see chapter 6). This has been observed elsewhere in the case of the methyl halides[23,24]. To account for these differences, a further correction has been developed by Lounila and Diehl[27,28] which allows for a correlation between vibration and reorientation of partially aligned solute molecules in the LCNMR experiment.

2.6 Correlation between vibration and rotation of partially oriented molecules

As described above, it is a relatively simple matter to determine orientation parameters for fairly rigid solute molecules and then use these to perform vibrational corrections to the experimentally observed direct couplings so that an r_α structure may be calculated.

However, because the forces experienced by a solute molecule in a liquid crystal environment may alter as the solute molecules undergo configurational changes, it is likely that the relationship between molecular internal motion and reorientation will become important. This would be particularly true for those molecules which undergo large amplitude internal motions.

Effects due to this correlation between vibration and rotation of the solute can be observed, even for molecules which have small amplitude vibrational motions. For example, tetrahedral molecules, such as methane, have been found to give rise to dipolar couplings when dissolved in various liquid crystals[25]. In a conventional LCNMR experiment, CH_4 is of T_d symmetry and hence ought to have an orientation parameter which is zero. This means that no D couplings should be observed. However, if a correlation between vibration and rotation is allowed, on undergoing an asymmetric stretch, the T_d symmetry is broken and the methane molecule can adopt a non-zero orientation parameter. This results in the observance of non-zero D couplings in the LCNMR experiment.

A theory to account for this effect in methanes was developed by Snijders et al.[26]. This tackles two different effects observed in the methanes, the rigid molecule orientation effect which is found in partially deuteriated methanes, and a non-rigid effect which is described above. It appears that the non-rigid contribution in the methanes can be derived from the well-known harmonic force field. The average deviations from tetrahedral symmetry of the deuteriated compounds, and hence the contribution to the D couplings from this rigid molecule effect, can be derived from the cubic anharmonic force field.

Lounila and Diehl[27,28] adopted the same form of vibration-rotation interaction Hamiltonian as was used by Snijders et al.[26] and obtained essentially the same result, but with the big difference that Lounila and Diehl used the theory to describe more general molecules and not just the special case of the methanes. The smaller rigid effect was also ignored in this treatment of the theory. An outline of the mathematics involved is given below.

2.6.1 The orienting potential

If the orienting forces experienced by a molecule in an LCNMR experiment are assumed to be described by a single particle potential energy U_{ext}, then the Hamiltonian for molecular motion (ignoring the electronic structure) is

$$H = T + U_{int} + U_{ext} \qquad \text{Eq. 2. 6}$$

where T is the kinetic energy and U_{int} is the internal potential energy of the molecule. T can then be separated into T_{trans}, T_{rot} and T_{int}, representing the translation, rotation and internal motion of the molecule respectively by introducing the Eckart axis system. This means that only small amplitude internal motion will be considered. The vibrational normal co-ordinates, Q_k, defined in the molecular frame are then used as the internal co-ordinates. In general U_{ext} is slightly dependent on the normal co-ordinates, so some correlation between the internal motion and the reorientation of the molecule will now be allowed.

If Ω is used to represent the laboratory fixed frame and the Q_k dependence of $U_{int}(Q_k)$ and $U_{ext}(\Omega, Q_k)$ is approximated by the leading terms of the Taylor series around the equilibrium geometry, then the Hamiltonian can be rewritten as

$$H = T_{trans} + T_{rot} + \frac{1}{2}\sum_k p_k^2 + U_{ext}^e(\Omega) + \sum_k U_k(\Omega) Q_k + \frac{1}{2}\sum_k w_k^2 Q_k^2 \qquad \text{Eq. 2. 7}$$

where p_k's are the momenta canonically conjugate to the Q_k's, w_k is the k^{th} angular frequency and

$$U_k(\Omega) = \left.\frac{\partial U_{ext}(\Omega, Q_k)}{\partial Q_k}\right|_e \qquad \text{Eq. 2. 8}$$

The quadratic terms in the expansion of $U_{ext}(\Omega, Q_k)$ are left out because when compared with the molecular forces, the orienting force is only weakly dependent on the internal co-ordinates. The potential energy for Q_k is that of a harmonic oscillator having frequency w_k

$$\bar{Q}_k(\Omega) = -\frac{U_k(\Omega)}{w_k^2} \qquad \text{Eq. 2. 9}$$

If the new variable $\xi_k = Q_k - \bar{Q}_k$ is introduced, the Hamiltonian becomes

$$H = T_{trans} + T_{rot} + \frac{1}{2}\sum_k p_k^2 + U_{ext}^e(\Omega) - \frac{1}{2}\sum_k w_k^2 \overline{Q}_k^2(\Omega) + \frac{1}{2}\sum_k w_k^2 \xi_k^2 \qquad \textbf{Eq. 2. 10}$$

Since the vibrational motion is much faster than the molecular reorientational diffusion motion, the equilibrium positions of the normal co-ordinates, $Q_k(\Omega)$, move much more slowly than Q_k. This allows the p_k, the momenta conjugate to Q_k, to be replaced by the momenta conjugate to ξ_k. The Hamiltonian then separates conveniently into parts for the translational, rotational and ξ_k variables.

This dependence of the orienting potential on the internal co-ordinates, therefore, results in two effects

a) A slightly different orienting potential is experienced by the molecule.

$$U'_{ext}(\Omega) = U_{ext}^e(\Omega) - \frac{1}{2}\sum_k w_k^2 \overline{Q}_k^2(\Omega)$$

b) The geometry is orientation dependent because, in the orientation Ω, the average geometry is defined by the set of normal co-ordinates $\overline{Q}_k(\Omega)$.

The conclusion from this is that the small correlation that exists between the molecular vibrational and reorientational motion does not alter the vibrational frequencies or amplitudes, only the equilibrium positions.

2.6.2 Application to LCNMR

Now we can take a look at how this should effect the relationship between the experimental data we obtain and the final structural parameters.

The NMR spectral parameters can be expressed in terms of the average values of the second-rank tensor elements parallel to the liquid crystal director.

$$\langle T_{\parallel} \rangle = \langle T_0 \rangle + \frac{2}{3}\sum_{\alpha,\beta} \langle T_{\alpha\beta}, S_{\alpha\beta} \rangle \qquad \textbf{Eq. 2. 11}$$

T_0 is 1/3 of the trace of the tensor, having elements $T_{\alpha\beta}$ in the molecular frame, and

$$S_{\alpha\beta} = \frac{3}{2}\cos\theta_{\alpha}\cos\theta_{\beta} - \frac{1}{2}\delta_{\alpha\beta} \qquad \text{Eq. 2. 12}$$

with θ_{α} being the angle between the α axis and the director.

The tensors $T_{\alpha\beta}$ describe molecular properties such as nuclear shielding, electric field gradient, indirect spin-spin coupling or direct dipolar coupling, and the interesting quantities are their elements in the (undistorted) equilibrium structure $T^{e}_{\alpha\beta}$.

$T_{\alpha\beta}$ can be expanded as a Taylor series in terms of the normal co-ordinates around $T^{e}_{\alpha\beta}$ and the series is transformed to the ξ_k variables. This leads to

$$\overline{T}_{\alpha\beta}(\Omega) = T^{e}_{\alpha\beta} + T^{h}_{\alpha\beta} + \sum_{k} T_{\alpha\beta,k}\overline{Q}_{k}(\Omega) + \ldots \qquad \text{Eq. 2. 13}$$

where $T^{h}_{\alpha\beta}$ is the contribution arising from the harmonic vibrations

$$T^{h}_{\alpha\beta} = \frac{\hbar}{4}\sum_{k} T_{\alpha\beta,kk}\frac{1}{w_k}\coth\left(\frac{\hbar w_k}{2k_B T}\right) \qquad \text{Eq. 2. 14}$$

If the perturbations in $T_{\alpha\beta}$ arise only from the distortions of the molecular geometry, the only orientation dependent quantities are the $\overline{Q}_{k}(\Omega)$. The final averaging over the orientational motion therefore gives

$$\langle T_{\parallel}\rangle = \langle T_0\rangle + \frac{2}{3}\sum_{\alpha,\beta}\left(T^{e}_{\alpha\beta} + T^{h}_{\alpha\beta}\right)S^{D}_{\alpha\beta} + \frac{2}{3}\sum_{k}\sum_{\alpha,\beta} T_{\alpha\beta,k}\langle\overline{Q}_{k}s_{\alpha\beta}\rangle \qquad \text{Eq. 2. 15}$$

$$\langle T_0\rangle = \frac{1}{3}\sum_{\alpha}\left(T^{e}_{\alpha\alpha} + T^{h}_{\alpha\alpha}\right) + \frac{1}{3}\sum_{k}\sum_{\alpha} T_{\alpha\alpha,k}\langle\overline{Q}_{k}\rangle \qquad \text{Eq. 2. 16}$$

where $S^{D}_{\alpha\beta} = \langle s_{\alpha\beta}\rangle$ and is the ordering matrix (referenced to the director).

These two equations demonstrate that the harmonic vibrational corrections to the spectral parameters are independent of the correlation effects. The contributions arising from the correlation depend only on $\overline{Q}_{k}$, i.e. only on the deformations in the molecular geometry.

These results are valid for an arbitrary orienting potential energy $U_{ext}(\Omega, Q_k)$. Its functional dependence on the molecular orientation Ω can be expressed as a series expansion in terms of the direction cosines of the director in the molecular frame, $\cos\theta_\mu$

$$U_{ext}(\Omega, Q_k) = -\sum_{\mu,\nu} A_{\mu\nu}(Q_k) s_{\mu\nu}(\Omega) \qquad \text{Eq. 2. 17}$$

Therefore, if the orienting potential is approximated by $U_{ext}(\Omega, Q_k)$, the orientation dependent distortions in the molecular geometry are

$$\overline{Q}_k(\Omega) = \frac{1}{w_k^2} \sum_{\mu,\nu} A_{\mu\nu,k} s_{\mu\nu} s(\Omega) \qquad \text{Eq. 2. 18}$$

where $A_{\mu\nu,k} = \left.\frac{\partial A_{\mu\nu}}{\partial Q_k}\right|_e$

The problem now is to determine the rotational averages $\langle s_{\alpha\beta} s_{\mu\nu} \rangle$. Theoretical values can be obtained using classical Boltzman statistics with the deformed orienting potential $U_{ext}(\Omega)$. But, since the form of the potential $U_{ext}(\Omega, Q_k)$ is only an approximation, this does not make a good starting point. It is more reasonable to approximate the orientational distribution function as a function of the experimentally determined ordering matrix elements $S_{\alpha\beta}^D$ (which are nevertheless indispensable for the determination of the values of the interaction tensor elements $A_{\mu\nu}$).

First, the orientational probability distribution is expanded in terms of the direction cosines of the director in the molecular frame, $\cos\theta_\alpha$.

$$P(\Omega) = \frac{1}{4\Pi}\left[1 + 5\sum_{\alpha,\beta} S_{\alpha\beta}^D \cos\theta_\alpha \cos\theta_{\beta+\ldots}\right] \qquad \text{Eq. 2. 19}$$

The effect of molecular distortion on the potential is inherent. By truncating the series at second order terms, we obtain:

$$\left\langle S_{\alpha\beta} S_{\mu\nu} \right\rangle = -\frac{1}{10}\partial_{\alpha\beta}\partial_{\mu\nu} + \frac{3}{20}\left(\partial_{\alpha\mu}\partial_{\beta\nu} + \partial_{\alpha\nu}\partial_{\beta\mu}\right) - \frac{2}{7}\left(S^D_{\alpha\beta}\partial_{\mu\nu} + \partial_{\alpha\beta}S^D_{\mu\nu}\right)$$
$$+\frac{3}{14}\left(S^D_{\alpha\beta}\partial_{\beta\nu} + S^D_{\alpha\nu}\partial_{\beta\mu} + \partial_{\alpha\mu}S^D_{\beta\nu} + \partial_{\alpha\nu}S^D_{\beta\mu}\right) \quad \textbf{Eq. 2. 20}$$

On dropping the antisymmetric parts of the tensors, $T_{\alpha\beta,k}$, and both the antisymmetric and isotropic parts of the tensor $A_{\mu\nu,k}$, the contributions arising from the correlation effect are

$$\left\langle T^d_{\parallel} \right\rangle = \left\langle T^d_0 \right\rangle + \frac{2}{3}\sum_k \sum_{\alpha,\beta} T_{\alpha\beta,k}\left\langle \overline{Q}_k S_{\alpha\beta} \right\rangle$$
$$= \left\langle T^d_0 \right\rangle + \frac{2}{3}\sum_k \sum_{\alpha,\beta,\mu,\nu} \frac{1}{w_k^2} T_{\alpha\beta,k} A_{\mu\nu,k}\left\langle S_{\alpha\beta} S_{\mu\nu} \right\rangle$$
$$+\sum_k \frac{1}{w_k^2}\left[\frac{1}{5}\sum_{\alpha,\beta} T_{\alpha\beta,k}A_{\alpha\beta,k} + \frac{1}{7}\sum_{\alpha,\beta,\mu} S^D_{\alpha\beta}\left(T_{\mu\mu,k}A_{\alpha\beta,k} + 4T_{\alpha\mu,k}A_{\beta\mu,k}\right)\right] \quad \textbf{Eq. 2. 21}$$
$$\left\langle T^d_0 \right\rangle = \frac{1}{3}\sum_k \frac{1}{w_k^2}\sum_{\alpha,\beta,\mu} T_{\mu\mu,k}A_{\alpha\beta,k}S^D_{\alpha\beta}$$

This results in the same equation for D_{ij} as before, but with an extra term which is the deformation correction arising from the correlation between vibration and reorientation of the solute molecule, i.e.

$$D_{ij} = D^e_{ij} + D^h_{ij} + D^d_{ij} + \ldots \quad \textbf{Eq. 2. 22}$$

The deformation correction is given by the equation

$$D^D_{ij} = -S_{zz}K_{ij}\sum_k \frac{1}{w_k^2}\left[\frac{3}{10}\sum_{\alpha,\beta}\phi_{\alpha\beta,k}A_{\alpha\beta,k} + \frac{2}{7}\sum_{\alpha,\beta,\mu} S^D_{\alpha\beta}\left(3\phi^{ij}_{\alpha,\mu,k}A_{\beta\mu,k} - \phi^{ij}_{\mu\mu',k}A_{\alpha\beta,k}\right)\right] \quad \textbf{Eq. 2. 23}$$

2.6.3 Practical Aspects

The orienting forces are in general not known. This means the molecular interaction tensor $A_{\alpha\beta}$ cannot be expressed in terms of the fundamental properties of the molecule and its environment. Therefore, the derivatives of the $A_{\alpha\beta}$, with respect to the normal co-ordinates, $A_{\alpha\beta,k}$, are not directly available. These can be determined experimentally, together with the structural parameters, by using the spectral data.

In order that this can be done, some model must be used to relate the terms $A_{\alpha\beta,k}$ using only a few primary parameters. Such a model is the group additivity of the molecular interaction tensor.

This assumes that the torque acting on the molecule is the sum of the torques acting on the segments (bonds or groups) of the molecule. The molecular interaction tensor is therefore the sum of the segmental interaction tensors $A_{\alpha\beta}{}^{n}$.

If the principal axes system is known then, at most, two independent parameters are required to specify the traceless segmental interaction tensor. These may be chosen as the anisotropy of the tensor

$$\Delta A_n = A_L^n - \frac{1}{2}\left(A_T^n + A_V^n\right)$$

and the asymmetry of the tensor

$$\eta_n = \frac{A_T^n - A_V^n}{A_L^n}$$

where A_L^n is the longitudinal principal value (e.g. in the bond direction) and A_T^n and A_V^n are the transverse principal values of the n^{th} segmental interaction tensor, thus

$$A_L^n = \frac{2}{3}\Delta A_n$$

$$A_T^n = -\frac{1}{3}\Delta A_n\left(1-\eta_n\right)$$

$$A_V^n = -\frac{1}{3}\Delta A_n\left(1+\eta_n\right)$$

The torque acting on the relatively rigid segment of the molecule can be expected to bend the segment as a whole and not to effect the internal state (such as the bond length). This allows the principal values of the segmental interaction tensor to be treated as being constant (independent of any molecular deformation). This means that in this case the dependence of the molecular interaction tensor $A_{\alpha\beta}$ on the deformations arises entirely from the rotations of the principal axes of the segmental tensors with respect to the fixed frame.

The tensor $A_{\alpha\beta}$ can therefore be expressed as a function of the molecular geometry and the set of parameters ΔA_n and η_n, and the derivatives $A_{\alpha\beta,k}$ can be calculated in terms of these primary parameters.

It is now found that

$$A_{\alpha\beta,\underline{k}} = \sum_i \sum_\mu b_{i\mu}^k \left. \frac{\partial A_{\alpha\beta}}{\partial A_{i\mu}} \right|_e$$

where $b_{i\mu}^k = c_{i\mu}^k / \sqrt{m_i}$ and $c_{i\mu}^k$ is the $i\mu$ component of the k^{th} normalised eigenvector of the dynamical matrix $W_{i\mu j\nu} = F_{i\mu j\nu} / \sqrt{m_i m_j}$. $F_{i\mu j\nu}$ is an element of the force constant matrix in Cartesian co-ordinates.

Because the parameters ΔA_n and η_n determine the molecular interaction tensor $A_{\alpha\beta}$, they also specify the ordering tensor $S_{\alpha\beta}^D$. This means that the order parameters cannot be fitted independently of the terms ΔA_n and η_n. Both the equilibrium and harmonic vibrational corrections to the spectral parameters depend on ΔA_n and η_n only through the order parameters. Since they are usually the dominating contributions, the order parameters are fitted as such, and the interdependent relationships are correspondingly introduced into the set of ΔA_n and η_n.

According to the classical Boltzman statistics

$$S_{\alpha\beta}^D = \frac{1}{Z_C} \int s_{\alpha\beta} e^{-\frac{U_{ext}}{k_B T}} d\Omega, \text{ where } Z_C = \int e^{-\frac{U_{ext}}{k_B T}} d\Omega. \qquad \textbf{Eq. 2. 24}$$

Here U_{ext} is the orienting potential energy containing both the equilibrium and deformational contributions. This means the fitted order parameters include both of these contributions inherently.

Using the principal axis system of the $A_{\alpha\beta}^e$, and dropping the orientation-independent term,

$U'_{ext} = A\left(\cos^2 \Theta_y + R\cos^2 \Theta_z\right)$, where $A = \frac{3}{2}\left(A^e_{xx} - A^e_{yy}\right)$ and $R = \frac{A^e_{zz} - A^e_{xx}}{A^e_{xx} - A^e_{yy}}$

The relationships between the order parameter and the functions A and R are obtained by numerical integration using this form of the potential energy.

References

[1] P.J.Collings, "Liquid Crystals: Natures' Delicate Phase of Matter", Adam Hilger, Bristol, (1990)

[2] J.W.Emsley and J.C.Lindon, "NMR Spectroscopy Using Liquid Crystal Solvents", Pergamon press, 1975

[3] P.Diehl, H.P.Kellerhals and W.Niederberger, J. Magn. Reson., 4, (1971), 352

[4] these routines were written jointly with E.M.Brown. The source code can be found in the OUTPUT section of Appendix AIII, E.M.Brown, PhD Thesis, University of Edinburgh, (1994)

[5]UNIRAS Ltd., "FGL/GRAPHICS User Guide - Version 6", Manchester Computing Centre, 1st edition IUCC reprint, (1989)

[6] A.S.F.Boyd, G.S.Laurenson and D.W.H.Rankin, J. Mol. Struct., 71, (1981), 217

[7] D.M.Bridges, J.M.Freeman, G.C.Holywell and D.W.H.Rankin, J. Organomet. Chem., 32, (1971), 87

[8] E.M.Brown, Ph.D. Thesis, University of Edinburgh, (1994)

[9] K.Kuchitsu and M.Nakata, "Stereochemical Applications of Gas-phase Electron Diffraction", Part A, Ch. 7, eds. I.Hargittai and M.Hargittai, VCH, New York, (1988), 227

[10] R.K.Heenan and A.G.Robiette, J. Mol. Struct., 54, (1979), 135

[11] K.Tamagawa, T.Lijima and M.Kimura, J. Chem. Struct., 30, (1976), 243

[12] S.Sykora, J.Vogt, H.Bösiger and P.Diehl, J. Magn. Reson., 36, (1979), 53

[13] S.Cradock, private communication

[14] S.Cradock, G.S.Laurenson and D.W.H.Rankin, J. Chem. Soc., Dalton Trans., (1981), 187

[15] L.Hedberg and I.M.Mills, J. Mol. Spectr., 160, (1993), 117

[16] P.Aped and N.L.Allinger, J. Am. Chem. Soc., 114, (1992), 1. The MM3 program is available through the Quantum Chemistry Program Exchange.

[17] P.Diehl and W.Niederberger, J. Magn. Reson., 9, (1973), 495

[18] J.W.Emsley, J.C.Lindon and J.Tabony, J. Chem. Soc., Faraday Trans., 71, (1975), 579

[19] N.J.D.Lucas, Mol. Phys., 22, (1971), 233

[20] T.Vaananen, J.Jokisaari, A.Kaariainen and J.Lounila, J. Mol. Struct., 102, (1983), 175

[21] C.A.Brookman, 4th Year Project, University of Edinburgh, (1988)

[22] P.D.Blair, A.J.Blake, R.W.Cockman, S.Cradock, E.A.V.Ebswoth and D.W.H.Rankin, J. Mol. Struct., 193, (1989), 279

[23] J.Jokisaari and Y.Hiltunen, Mol. Phys., 50, (1983), 1013

[24] L.Lounila, P.Diehl, Y.Hiltunen and J.Jokisaari, J. Magn. Reson., 61, (1985), 272

[25] E.E.Burnell and C.A.Lange, J. Magn. Reson., 39, (1980), 461, and references therein.

[26] J.G.Snijders, C.A.Lange and E.E.Burnell, J. Chem. Phys., 77(11), (1982), 5386

[27] J.Lounila and P.Diehl, J. Magn. Reson., 56, (1984), 254

[28] J.Lounila and P.Diehl, Mol. Phys., 52, (1984), 827

Chapter 3

The Structures of Silyl Compounds in the Crystalline Phase

3. Introduction to the structures of silyl compounds

LCNMR spectroscopy has been shown to be particularly useful at obtaining structures of fairly rigid, inert molecules, especially when data from electron diffraction and / or rotational spectroscopy is also used in a combined analysis.[1,2,3]

However, significantly different structures were obtained by LCNMR for norboradiene when two different solvents were used.[4,5] At Edinburgh there has been particular interest in studying silyl compounds. It was discovered, however, that there was a two degree increase in the HSiH angle in the liquid crystal phase from that of the gas phase.[6,7]

A possible explanation for this could be that cyanide groups present in the liquid crystals used in these experiments, co-ordinate in the solution to the silyl groups. This is thought to appear similar to a snap shot of an S_N2 intermediate as is shown in Figure 3.1

Figure 3.1 Possible mechanism for distorted silyl geometry in the liquid crystal

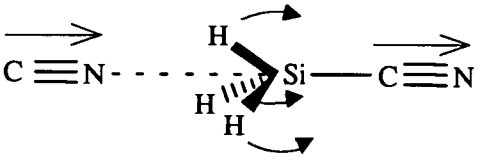

To investigate this further, the crystal structure of the silyl compounds, the liquid crystal solvents and any adducts of the two were studied.

3.1 The structures of some silyl compounds

It has already been demonstrated in studies of the molecular structures of silyl compounds that intermolecular Lewis acid-base interactions can lead to major structural changes. These interactions have normally involved silyl groups acting as electron pair acceptors, while the donor atoms have included nitrogen,[7,8 9,10]

oxygen,[11,12] sulphur[13] and halogens.[14,15] From these, perhaps the most striking example is the crystalline structure of (dimethyl) silylamine[8] (SiH_3NMe_2) which consists of five co-ordinate, trigonal bipyramidal silicon atoms and tetrahedrally co-ordinated nitrogen atoms in a cyclic pentameric structure.

Figure 3.2 Cyclic pentameric structure of (dimethyl) silylamine[8]

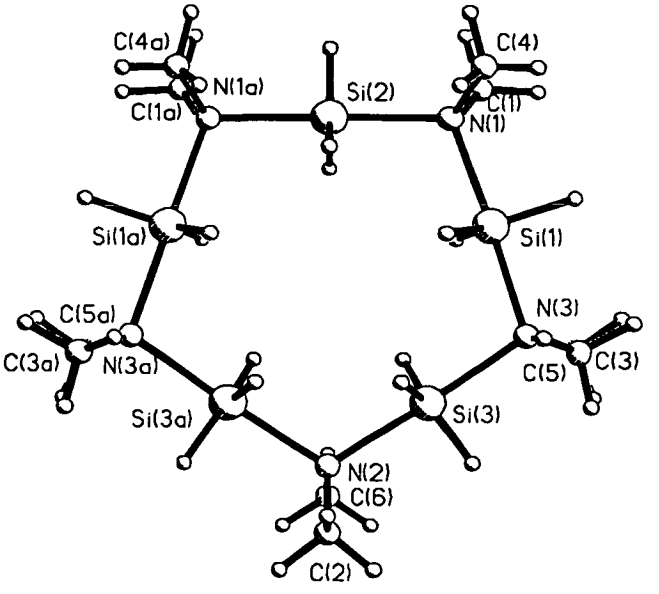

Of more interest in this work is the crystalline structure of silyl cyanide.[7] The molecules lie on crytsallagrophic mirror planes and are arranged in chains with short non-bonded Si...N contacts of 2.79 Å, compared with 3.6 Å for the sum of the van der Waals radii of silicon and nitrogen. Shorter Si...N contacts are however found elsewhere, with a contact of 2.05 Å being found in the dimers of (chlorosilyl) dimethylamine.[9]

Figure 3.3 Chain like packing of silyl cyanide[7]

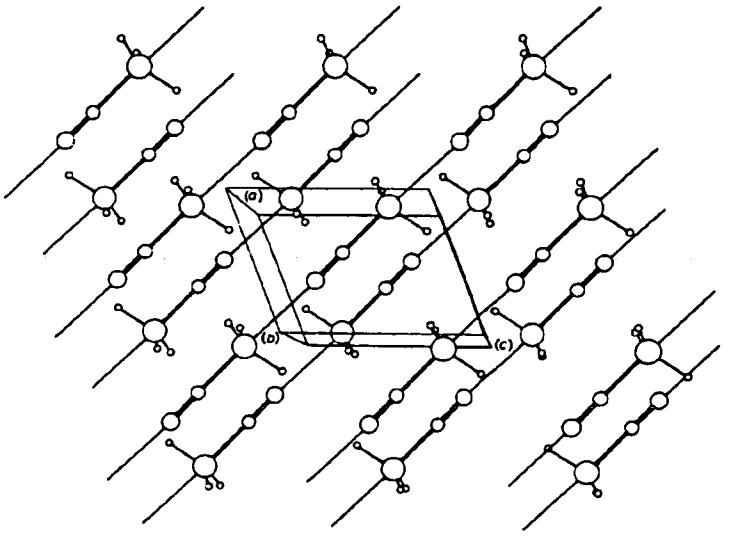

The SiC and CN bonds are lengthened by 0.05 Å and 0.01 Å respectively from their gas phase values and the HSiH angle is increased by around 5°. This is consistent with the crystal structure showing a snapshot of an S_N2 substitution intermediate, with an incoming isonitrile group displacing the bound nitrile group. This is in fact consistent with what is observed in the crystal structures of other silyl compounds.

The crystal structures of silyl fluoride[14] and silyl iodide[15] both consist of infinite zigzag chains with the intermolecular Si...F and Si...I distances being less than the sum of the van der Waals radii in both cases, Figure 3.4 and Figure 3.5.

Figure 3.4 Crystal packing of silyl fluoride[14]

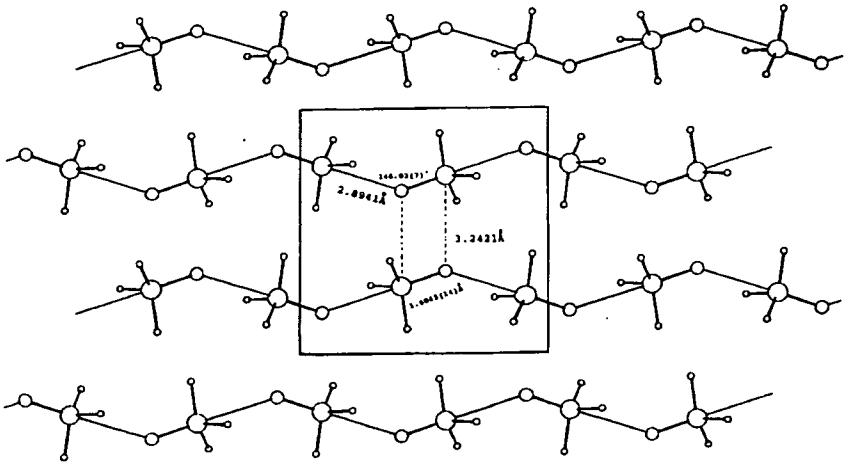

Figure 3.5 Crystal packing of silyl iodide[14]

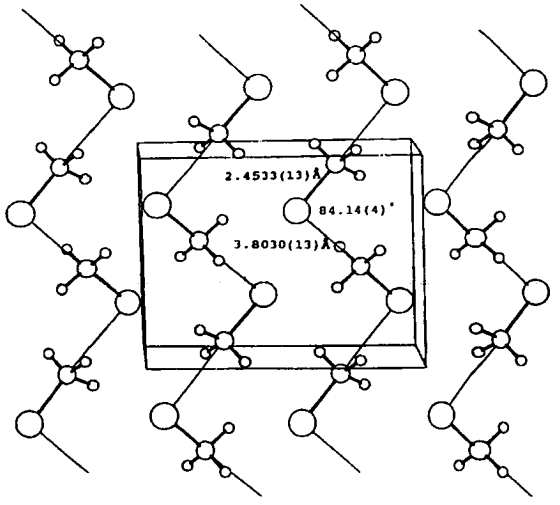

It has not been possible, so far, to grow single crystals of silyl chloride or silyl bromide due to the occurrence of phase transitions below the freezing point of both these compounds, although X-ray powder diffraction studies have shown them to be isostructural with germyl chloride[16] which packs in a similar fashion to silyl fluoride and silyl iodide.

It is therefore evident that the structures of these silyl compounds are markedly dependent on the phase in which the structure is obtained. In the LCNMR experiments where the HSiH angle was observed to widen by around two degrees from the gas phase value, the concentration of silyl compound in the NMR sample tube was too low for this type of interaction to be significant. However, the liquid crystal solvent used in these experiments consists of molecules which contain cyano groups. This allows an interaction to occur not between the solute molecules themselves but between the solute and the liquid crystal solvent. This raises the question of whether these adducts could be further investigated by perhaps growing crystals of them.

3.2 Adducts of silyl compounds

Adducts of the halogenosilanes with bases have been known for a long time[17,18], but due to their reactivity there has not been a great deal of structural work carried out

upon them. With respect to this work, the most interesting adducts formed are those of dimethyl ether with silyl[19] and germyl[20] halides. The adducts formed were 1:1 adducts of dimethyl ether with silyl chloride, silyl bromide and germyl chloride. These were all found to be stable only below their melting points. A single crystal of the silyl chloride adduct was found to consist of simple, non interacting adduct molecules, Figure 3.6. The silyl bromide adduct was found to be isostructural with this by X-ray powder diffraction.

Figure 3.6 Adduct of silyl chloride and dimethyl ether[19]

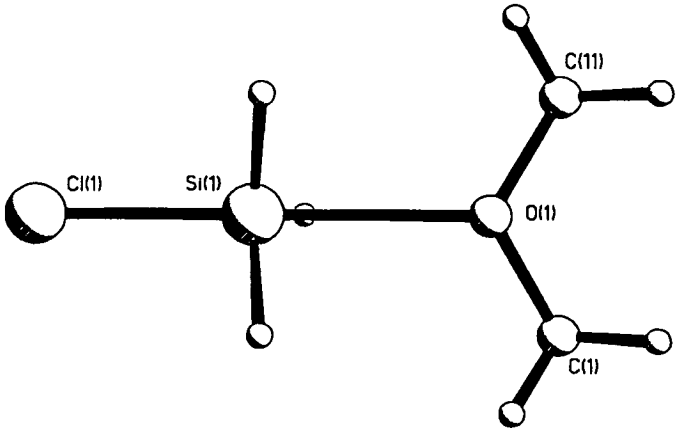

The Si...O bond in the silyl chloride adduct is 2.272 (1) Å making it shorter than many other Si...O bonds characterised to date. It is comparable to the longer Si...N bond found in the (chlorosilyl) dimethylamine dimer[9]. This has an Si...N bond 2.054 (13) Å, Figure 3.7. Like the silyl chloride adduct, however, this is only stable in the solid phase.

The shortness of these bonds can be explained in terms of the basicity of the donor atoms involved. Oxygen bound to silicon is much less basic[17] than an oxygen in normal alkyl ethers, while nitrogen is intrinsically more basic than oxygen. Because of the silyl group acting as a weak electron acceptor, it allows the formation of distinctly stronger, and shorter, secondary bonds with dimethyl ether than between molecules of disiloxane, and even stronger, shorter bonds to the nitrogen of (chlorosilyl) dimethylamine.

Figure 3.7 Pentameric structure of the (chlorosilyl) dimethylether adduct[9]

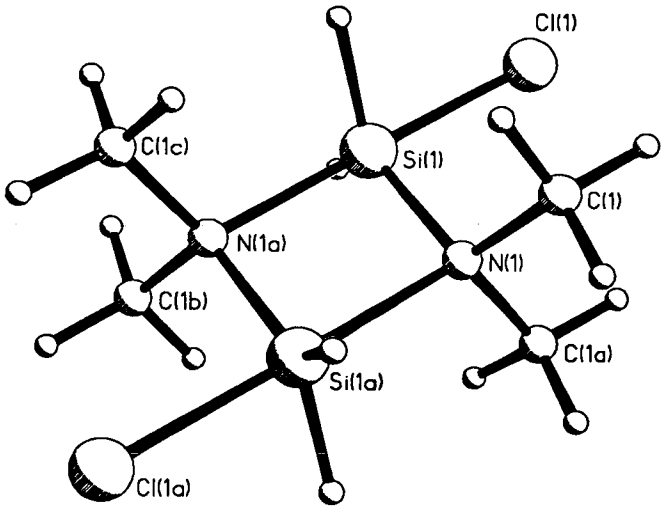

3.3 Growing crystals of liquid crystals and liquid crystal - silyl adducts

The liquid crystal solvents used in earlier LCNMR studies of silyl compounds were called E 5 and E 7. These liquid crystals do not contain single compounds but are eutectic mixtures of alkyl and alkoxy cyanobiphenyls. This is because, by using an eutectic mixture, one can increase the temperature range of the nematic phase. For X-ray studies, however, it was necessary to use a single compound liquid crystal. Four different liquid crystal which are present in the these eutectic mixtures previously used for LCNMR analyses were therefore obtained from BDH Limited. These were,

5-CB	4-cyano-4-n-pentylbiphenyl
7-CB	4-cyano-4-n-septylbiphenyl
1-OCB	4-cyano-4-n-methoxybiphenyl
8-OCB	4-cyano-4-n-octoxybiphenyl

As can be observed from Figure 5.2 (Chapter 5), *5*- and *7*-CB are both nematic liquid crystals while *1*-OCB is a monotropic nematic liquid crystal and *8*-OCB is both a smectic and nematic liquid crystal.

The introduction to Chapter 5 details some of the work which has been carried out on nematogenic and smectogenic compounds. Almost all of this has concentrated on the mesophases and it is only comparatively recently that much crystallographic work has been done. It is now thought that the nature of the packing of the molecules in the solid state and other molecular characteristics can give valuable insights into the nature of the nematic or smectogenic liquid crystal mesophase. This is discussed in more detail in Chapter 5 where the packing of the first seven molecules in the *n*-OCB series has systematically been analysed, allowing predictions on how the next member of the series, *8*-OCB, will pack in the solid phase and why this compound exhibits both the smectic and nematic mesophases.

Of the four liquid crystals chosen here, only the crystal structure of *1*-OCB was previously known[21], although this had been obtained at ambient temperature and no hydrogen positions had been refined. In order to determine conditions in which crystals of any adducts were likely to grow and to discover how these liquid crystals packed on their own, it was attempted to grow single crystals of these liquid crystals. Having a partially ordered mesophase just above the solid phase it was not surprising to discover that these compounds all formed microcrystalline solids. A large variety of solvents and conditions were tried but only suitable crystals of *1*-OCB and *7*-CB were obtained. The crystal structure determination and packing of these are discussed in Chapters 4 and 5. Data for *1*-OCB and *7*-CB were collected at 150 K and the structure obtained for *1*-OCB was found to be in good agreement with the previous crystal structure determination. Data for *7*-CB was also collected at ambient temperature to determine whether any phase change occurred on cooling of the crystal, but this data was found to be in good agreement with that at low temperature.

Large plate-like crystals of *8*-OCB were obtained but found not to diffract. This was attributed to a layer structure in which each layer was randomly oriented. The sample was therefore placed in a magnetic field to induce alignment of the liquid crystal molecules before crystallisation but this did not appear to make any difference.

No successful attempts were made at obtaining single crystals of any adducts formed between these liquid crystals and halogenosilanes. In line with previous work which examined adducts formed between halogenosilanes and the organic bases pyridine, trimethylamine and tetramethylenediamine,[17] samples were prepared by adding the silyl compound to an excess of liquid crystal. When no crystals were obtained a wide variety of different mixtures and concentrations were tried but to no avail.

The main problem encountered was maintaining the purity of the silyl compounds. They decomposed on contact with moisture to form disiloxane and hydrogen halide gas. This was observed as a yellowish discolouration of the sample. Also, when potential crystals were obtained, there was difficulty in handling them. Attempts were made to coat them in oil or to place them in glass capillaries but these proved to be unsuccessful.

An attempt was also made to grow crystals both of the liquid crystals and any adducts directly in a capillary tube on the diffractometer. This removed the difficulties in handling the crystals and allowed use to be made of the accurate temperature control of the diffractometer. This again proved unsuccessful but is perhaps the most suitable route for future attempts at this kind of work.

It may also be advantageous to use more polar silyl compounds. Many of the attempts made in this work involved silyl bromide but with hindsight, it may have been wiser to use silyl chloride, fluoride or even cyanide. This is because the Si...N interaction will be stronger in these compounds compared to that of silyl bromide. This may have some bearing on the inability of earlier studies in obtaining single crystals of silyl bromide or silyl chloride and the adduct of silyl bromide with dimethyl ether.

References

[1]S.Cradock, P.B.Liescheski, D.W.H.Rankin and H.E.Robertson, J.Amer.Chem.Soc., 110(9), (1988), 2759

[2]P.B.Liescheski and D.W.H.Rankin, J.Mol.Struct., 196, (1989), 1

[3]S.Cradock, P.B.Liescheski and D.W.H.Rankin, J.Magn.Reson., 91, (1991), 316

[4]E.E.Burnell and P.Diehl, Canad.J.Chem., 50, (1972), 3566

[5]J.W.Emsley and J.C.Lindon, Mol.Phys., 29, (1975), 531

[6] C.A.Brookman, '4th Year Honours Project', University of Edinburgh (1989)

[7] P.D.Blair, A.J.Blake, R.W.Cockman, S.Cradock, E.A.V.Ebsworth and D.W.H.Rankin, J. Mol. Struct., 193, (1989), 279

[8] A.J.Blake, E.A.V.Ebsworth and A.J.Welch, Acta. Cryst., Sect. C, 40, (1984), 895

[9] D.G.Anderson, A.J.Blake, S.Cradock, E.A.V.Ebsworth, D.W.H.Rankin and A.J.Welch, Angew. Chem., Int. Edn. Engl., 25, (1986), 107

[10] D.G.Anderson, A.J.Blake, S.Cradock, E.A.V.Ebsworth, D.W.H.Rankin, H.E.Robertson and A.J.Welch, J. Chem. Soc., Dalton Trans., (1987), 3035

[11] M.J.Barrow, E.A.V.Ebsworth and M.M.Harding, Acta. Cryst., Sect. B, 35, (1979), 2093

[12] A.J.Blake, M.Dyrbusch, E.A.V.Ebsworth and S.G.D.Henderson, Acta. Cryst., Sect. C, 44, (1988), 1

[13] M.J.Barrow and E.A.V.Ebsworth, J.Chem. Soc., Dalton Trans., (1982), 211

[14] A.J.Blake, S.G.D.Henderson, E.A.V.Ebsworth and A.J.Welch, Acta Cryst., Sect. C, 41, (1985), 1141

[15] A.J.Blake, S.G.D.Henderson, E.A.V.Ebsworth and A.J.Welch, Acta Cryst., Sect. C, 44, (1988), 1337

[16] A.J.Blake, E.A.V.Ebsworth and M.Dyrbusch, Acta. Cryst., Sect. C, 43, (1987), 1683

[17] H.J.Campbell-Ferguson and E.A.V.Ebsworth, J. Chem, Soc., Sect. A, (1966), 1508

[18] H.J.Campbell-Ferguson and E.A.V.Ebsworth, J. Chem. Soc., Sect. A, (1967), 705

[19] A.J.Blake, S.Cradock, E.A.V.Ebsworth and K.C.Franklin, Angew. Chem., 29, (1990), 76

[20] A.J.Blake, S.Cradock, K.C.Franklin and S.G.Fraser, J. Chem. Soc., Dalton Trans., (1990), 1663

[21] L.Walz, H.Paulus and W.Haase, Z. Krist., 180, (1987), 97

Chapter 4

The crystal structures of 4'-*n*-heptyl-4-cyanobiphenyl (*7*-CB) and 4'-methoxy-4-cyanobiphenyl (*1*-OCB).

4 Introduction

In recent years, several X-ray investigations of liquid crystalline materials have been carried out.[1,2,3,4,5,6,7,8,9,10] The aim of these investigations has been to gain some understanding as to how the molecules interact within the liquid crystal mesophase. It is thought that the crystalline phase of any mesogen, with a low enthalpy of crystallisation, should be very similar to that of the mesogenic phase. Further evidence to support this comes from measurements of density and volume changes in liquid crystalline substances as the temperature (and phase) is varied[11]. These measurements indicate that the changes in volume at phase transitions are too small for significant changes in local molecular organisation to occur.

In this work, the liquid crystals of interest are those used as solvents for LCNMR experiments at Edinburgh University. These are mixtures of single compound liquid crystals from the 4'-*n*-alkyl/alkoxy-4-cyanobiphenyls. The two liquid crystals examined here are 4'-*n*-heptyl-4-cyanobiphenyl (*7*-CB), and 4'-methoxy-4-cyanobiphenyl (*1*-OCB). Both compounds were supplied by BDH Ltd.

4.1 The crystal structure of 4'-*n*-heptyl-4-cyanobiphenyl (*7*-CB).

4.1.1 Experimental

Suitable colourless ingot shaped single crystals were obtained by slow evaporation from a solution of methylene chloride. Lattice constants and intensity measurements were performed on a STADI-4 diffractometer using monochromatic MoKα radiation. The crystal data collected at 150 K is presented in Table 4.1. The structure was solved using the SHELX-86 program[12]. Least-squares refinement with anisotropic thermal parameters on all non-hydrogen atoms lead to R = 0.044. The co-ordinates of all hydrogen atoms were found from the Patterson map and all hydrogen atoms were refined isotropically.

It has been observed in related compounds that more than one crystalline phase may occur for these types of compounds.[6,8,10] Since the main concern here is that it is the crystalline phase immediately preceding the liquid crystal mesophase that is studied, measurements were also made at 293 K in order to establish that no phase transition had occurred on cooling the crystal. The crystal data for this refinement is given in Table 4.2. This structure was solved using the non-hydrogen skeleton obtained from the refinement at 150 K. As before, the co-ordinates of all hydrogen atoms were found from the Patterson map and all hydrogens were refined isotropically.

Table 4.1 Crystal data and structure refinement for *7*-CB at 150 K.

Identification code	*7*-CB
Empirical formula	$C_{20}H_{23}N$
Formula weight	277.39
Temperature	150(2) K
Wavelength	0.71073 Å
Crystal system	Triclinic
Space group	$P\bar{1}$
Unit cell dimensions	a = 9.596(9) A α = 90.69(6) ° b = 11.35(2) A ß = 98.90(5) ° c = 15.72(2) A γ = 106.97(7) °
Volume	1615(4) $Å^3$
Z	4
Density (calculated)	1.141 Mg/m^3
Absorption coefficient	0.065 mm^{-1}
F(000)	600
Crystal size	0.175 x 0.31 x 0.51 mm
Theta range for data collection	2.63 to 22.54 °
Index ranges	-10<=h<=10, -12<=k<=12, 0<=l<=16
Reflections collected	4791
Independent reflections	4231 [R(int) = 0.0522]
Refinement method	Full-matrix least-squares on F^2
Data / restraints / parameters	4219 / 0 / 563
Goodness-of-fit on F^2	1.243
Final R indices [I>2sigma(I)]	R1 = 0.0442, wR2 = 0.1161
R indices (all data)	R1 = 0.0863, wR2 = 0.1508
Largest diff. peak and hole	0.159 and -0.206 $e.Å^{-3}$

Table 4.2 Crystal data and structure refinement for 7-CB at 293 K

Identification code	7-CB
Empirical formula	$C_{20}H_{23}N$
Formula weight	277.39
Temperature	293(2) K
Wavelength	0.71073 Å
Crystal system	Triclinic
Space group	$P\bar{1}$
Unit cell dimensions	a = 9.7553(8) Å α = 91.664(10)° b = 11.5301(10) Å ß = 99.006(5)° c = 15.877(2) Å γ = 107.245(5)°
Volume	1679.1(3) $Å^3$
Z	4
Density (calculated)	1.097 Mg/m^3
Absorption coefficient	0.063 mm^{-1}
F(000)	600
Crystal size	0.51 x 0.31 x 0.175 mm
Theta range for data collection	2.61 to 22.49°
Index ranges	-10<=h<=10, -12<=k<=12, 0<=l<=17
Reflections collected	4391
Independent reflections	4391 [R(int) = 0.0000]
Refinement method	Full-matrix least-squares on F^2
Data / restraints / parameters	4381 / 0 / 563
Goodness-of-fit on F^2	1.078
Final R indices [I>2sigma(I)]	R1 = 0.0426, wR2 = 0.1069
R indices (all data)	R1 = 0.1100, wR2 = 0.1528
Largest diff. peak and hole	0.101 and -0.153 $eÅ^{-3}$

4.1.2 Results and Discussion

The labeling scheme for all non-hydrogen atoms is given in Figure 4.1 which is a projection perpendicular to the best fit plane of the two independent molecules.

Figure 4.1 Labeling scheme used for non-hydrogen atoms for both molecules of 7-CB.

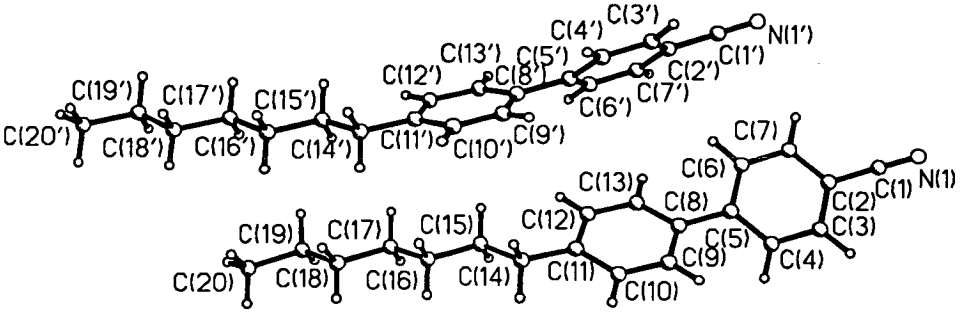

It can be seen from this that both molecules adopt an extended conformation.

There are no significant deviations between the crystal structures at the two temperatures. Although the following discussion is applicable to either structure, it is the data recorded at 150 K that is discussed below.

The final positional and thermal parameters are listed in Table 4.3 and Table 4.7 using the same labelling scheme as in Figure 4.1. The anisotropic displacement parameters for the non-hydrogen atoms are given in Table 4.6 and the bond lengths and bond angles are given in Table 4.4 and Table 4.5. These are found to be comparable with those of other mesogenic compounds[1-10]. It was noticed, however, that there is no shortening of the C(2)-C(7) bond as has been observed in other mesogens[2, 13, 14], although it is perhaps significant that this shortening is absent for other molecules in the alkyl series. The torsion angles between the two phenyl rings are 28.7 ° and 35.7 ° which are in agreement with the observations of Walz et al[1] for a cyanobiphenyl with an alkyl tail of this length.

Figure 4.2 shows a packing diagram which highlights the two most important features concerning the way in which *7*-CB packs. The most obvious of these being the $[0\bar{2}3]$ plane which was found from the crystallographic data to have an intensity four times that of any other plane. These planes or sheets are separated from one another by around 3.5 Å. The other feature being the alternating aromatic and hydrocarbon regions, which can be interpreted as being analogous to the layers observed in a smectic liquid crystal. In this case, the molecules have arranged themselves so that they lie at an angle of around 50° with respect to the layer.

In attempting to explain how the molecules pack, it is simplest to show how they interact within one of the $[0\bar{2}3]$ planes. This is shown in Figure 4.3. The molecules can be thought of as forming infinite chains via the parallel cyano-tail interaction (P1) discussed in Chapter 5. Each chain contains both independent molecules and is held together by weak N...H contacts. The shortest contact being 2.92 Å. This is closer than might be expected on comparison with Table 5.8, where it is seen that the closest contact for this interaction in *6*-OCB was 3.12 Å. *7*-OCB, which packs in a similar manner to *7*-CB, showed no interaction at all. This small difference in the contacts of *7*-CB and *7*-OCB must be as a result of the oxygen atom present in the tail of *7*-OCB.

These chains arrange themselves in such a way that stacks of molecules are formed, each stack comprising just one type of molecule. Two different antiparallel interactions occur within each stack and a third occurs between them (Figure 4.3).

Figure 4.2 Crystal packing of *7*-CB showing the distinct layers which form along [0$\bar{2}$3]

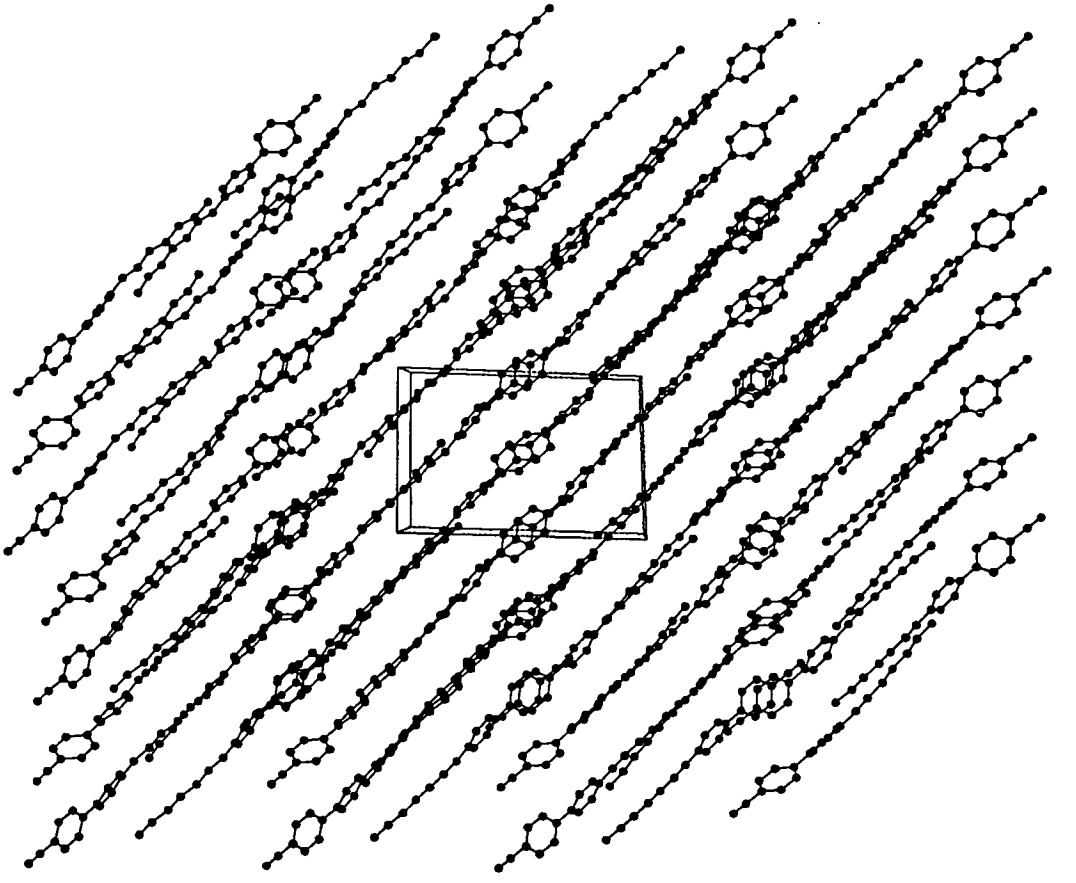

Figure 4.3 Crystal packing of *7*-CB showing a view perpendicular to one of the sheets along [0$\bar{2}$3].

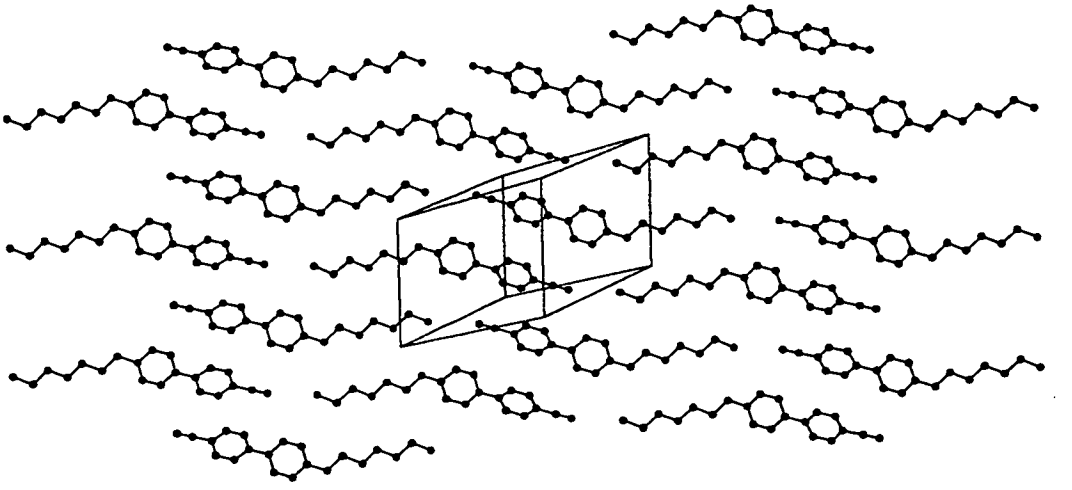

The first of these is the antiparallel cyano-phenyl interaction A2 (Figure 5.3). A2 can be described in terms of inter ring contacts. The phenyl rings are planar to one another with ring centres separated by 4.9 Å. This is different from the equivalent interaction in 7-OCB (Chapter 5), where the centre of the rings were only 3.9 Å apart. This difference is because unlike in 7-OCB where the cyano group lay over the phenyl ring, in 7-CB the cyano group lies to one side of the phenyl ring. This allows contacts to be made between the nitrogen from the cyano group and hydrogens from the ring 2 of the other molecule. The closest contact being N...H(13) at 2.93 Å for molecule 1 and N'...H(13') at 2.86 Å for molecule 2. In the *n*-OCB series, no significant contacts were observed with the hydrogens of ring 2 in this interaction.

The next interaction formed in these sheets of molecules is the antiparallel head-to-tail interaction A3 (Figure 5.4). This can also be described in terms of inter ring contacts with the closest contact being 4.9 Å between the centres of the two ring 1s which lie planar to one another. The inter ring contact between ring 1 and ring 2 is 6.4 Å and 6.3 Å for molecules one and two respectively with the angles between rings being 30.4° and 36.2°. As in A2, the cyano group lies to the side of ring 2 rather than over it, with the closest N...H contacts N...H(10) at 3.05 Å and N'...H(10') at 3.10 Å. This is different from what was observed in the *n*-OCB series as there are no nitrogen contacts with the tails of the molecules.

The final interaction occurring in these sheets is the antiparallel large tail-tail interaction A6 (Figure 5.7). This is very similar to that found in the *n*-OCB series, with the shortest contacts now H(10)...H(20') at 2.64 Å and H(10')...H(20) at 2.66 Å. These are very similar to the contact distances observed in 7-OCB.

The other interactions found in 7-CB all occur between these sheets of molecules. There is another interaction of the A3 type which forms, this time, between different molecules. This involves hardly any contact distances, but is interesting in that the closest N...H contact is now 3.14 Å to an H(14). This is also reflected in the shorter

inter ring contact between ring 1 and ring 2 of 4.7 Å, with the rings now lying at an angle of 53.0° to one another.

The strongest interaction occurring between the sheets of molecules is the large parallel interaction P4 (Figure 5.12). This involves different molecules lying parallel to one another but slightly displaced so that there is contact between the nitrogen of one molecule and H(7') of the other. This is 2.90 Å in *7*-CB. Again this interaction can be described in terms of inter ring contacts. This time the shortest distance between centres of rings is 4.8 Å between ring 1 and ring 2 with the angle between the planes of the two rings being 59.4°. The closest H...H contact is 2.50 Å and is formed between an H(19) and an H(15'). This interaction is again very similar to that found in *7*-OCB, and the *n*-OCB series in general.

Next is the antiparrallel tail-tail interaction A7 (Figure 5.8). This differs from that observed in the *n*-OCB series in that it involves a shortest contact of 2.61 Å between an H(16) and an H(20). The equivalent contacts in the *n*-OCB series are of comparable distance, but involve hydrogens nearer the end of the alkoxy tails.

The final interaction is the antiparallel biphenyl-tail interaction A5 (Figure 5.6). This has a closest contact of 2.43 Å between an H(6') and an H(20'). Although there are no oxygen contacts as in the *n*-OCB series, this interaction is very similar to what is found for the *n*-OCBs. The biphenyl unit lies along the tail of the other molecule in such a way that the cyano end of ring 1 extends past the end of the tail.

In terms of relating how the crystalline phase of *7*-CB will melt to form the nematic phase, a similar argument to that used in chapter 5 for *5*-, *6*-, and particularly *7*-OCB, is applicable. Figure 4.4 is a projection of the *ac*-plane, showing molecules from several sheets arranging in infinite stacks.

Figure 4.4 Crystal packing of 7-CB showing a projection of the *ac*-plane. It can be seen that stacks of molecules arrange in dimers of the A2 and A3 type.

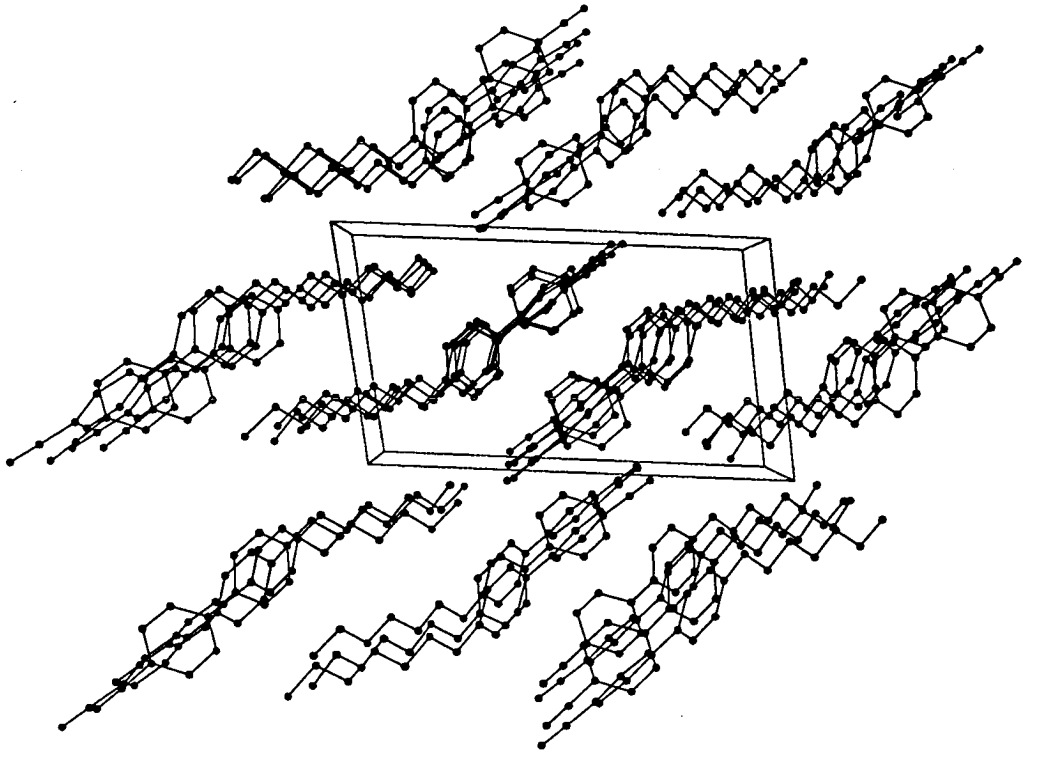

There are two types of antiparrallel dimers here which involve cyanobiphenyl overlap. These are the cyano-phenyl (A2) interaction and the head-to-tail (A3) interaction. In agreement with the conclusions of chapter 5, the stronger dimer is assumed to be that formed by the A3 interaction. This is in good agreement with diffraction experiments outlined in the introduction to chapter 5. These dimers are actually slightly longer than those of the *n*-OCB series, as a result of less biphenyl overlap. This is explained by the absence of the oxygen atom which increases the size of the aromatic core in the *n*-OCBs. As a result of the decrease in the biphenyl overlap, these dimers support the idea of a partial bilayer model of the cyano-biphenyls as discussed by Haase et al.[14]

However, whichever of these dimers (A2 or A3) is chosen as being the dominant one, it can be seen that the dimers are arranged in an imbricated fashion with respect to one another. On melting, it is easy to understand how the tail contacts can be broken down as the molecules gain energy. If the weaker cyano-phenyl contacts also

break down, the slightly stronger head-to-tail contacts persist into the nematic mesophase. Of course, it will not be quite as simple as this and, as is highlighted in the introduction to chapter 5, diffraction experiments have indicated that a small degree of layer formation occurs in the nematic phase of *7*-CB. This is not surprising considering the 'smectic-like' layer structure of the crystal and the fact that *8*-CB, which has just one more carbon atom in the alkyl tail, melts to form the smectic phase.

Table 4.3 Atomic co-ordinates (x 10^4) and equivalent isotropic displacement parameters (A^2 x 10^3) for 7-CB. U(eq) is defined as one third of the trace of the orthogonalised Uij tensor

	x	y	z	U(eq)
N(1)	361(3)	-2096(2)	3329(2)	51(1)
C(1)	1022(3)	-1385(2)	3882(2)	36(1)
C(2)	1848(3)	-511(2)	4578(2)	32(1)
C(3)	2932(3)	-781(2)	5169(2)	39(1)
C(4)	3740(3)	67(2)	5828(2)	38(1)
C(5)	3489(3)	1214(2)	5923(1)	29(1)
C(6)	2384(3)	1458(2)	5328(2)	32(1)
C(7)	1579(3)	626(2)	4661(2)	33(1)
C(8)	4404(3)	2158(2)	6600(1)	30(1)
C(9)	5884(3)	2243(2)	6903(2)	33(1)
C(10)	6768(3)	3175(2)	7489(2)	35(1)
C(11)	6242(3)	4087(2)	7801(2)	32(1)
C(12)	4759(3)	3985(2)	7520(2)	36(1)
C(13)	3866(3)	3050(2)	6934(2)	35(1)
C(14)	7271(3)	5136(3)	8401(2)	36(1)
C(15)	6554(3)	5863(3)	8927(2)	36(1)
C(16)	7680(3)	6862(3)	9536(2)	35(1)
C(17)	6988(3)	7531(3)	10114(2)	35(1)
C(18)	8090(3)	8506(3)	10748(2)	36(1)
C(19)	7386(3)	9181(3)	11317(2)	39(1)
C(20)	8490(4)	10099(3)	11977(2)	52(1)
N(1')	137(3)	2915(2)	3449(2)	58(1)
C(1')	876(3)	3622(3)	3987(2)	40(1)
C(2')	1820(3)	4504(2)	4656(2)	34(1)
C(3')	3143(3)	5306(2)	4501(2)	36(1)
C(4')	4032(3)	6155(2)	5143(2)	33(1)
C(5')	3632(2)	6219(2)	5957(1)	29(1)
C(6')	2301(3)	5405(2)	6101(2)	32(1)
C(7')	1402(3)	4551(2)	5464(2)	34(1)
C(8')	4595(3)	7153(2)	6627(1)	31(1)
C(9')	6129(3)	7489(2)	6706(2)	36(1)
C(10')	7032(3)	8394(2)	7301(2)	37(1)
C(11')	6451(3)	9015(2)	7860(1)	31(1)
C(12')	4918(3)	8661(2)	7796(2)	34(1)
C(13')	4011(3)	7752(2)	7196(2)	33(1)
C(14')	7481(3)	10032(3)	8482(2)	37(1)
C(15')	6766(3)	10730(2)	9031(2)	35(1)
C(16')	7899(3)	11756(3)	9612(2)	36(1)
C(17')	7223(3)	12530(3)	10123(2)	37(1)
C(18')	8355(3)	13558(3)	10699(2)	36(1)
C(19')	7703(3)	14399(3)	11167(2)	37(1)
C(20')	8865(3)	15428(3)	11727(2)	42(1)

Table 4.4 Bond lengths [Å] for the two molecules of *7*-CB.

N(1)-C(1)	1.151(3)	N(1')-C(1')	1.152(3)
C(1)-C(2)	1.434(4)	C(1')-C(2')	1.442(4)
C(2)-C(3)	1.391(4)	C(2')-C(3')	1.388(4)
C(2)-C(7)	1.396(4)	C(2')-C(7')	1.395(4)
C(3)-C(4)	1.376(4)	C(3')-C(4')	1.380(4)
C(4)-C(5)	1.401(4)	C(4')-C(5')	1.400(4)
C(5)-C(6)	1.396(4)	C(5')-C(6')	1.393(4)
C(5)-C(8)	1.479(4)	C(5')-C(8')	1.479(4)
C(6)-C(7)	1.373(4)	C(6')-C(7')	1.381(4)
C(8)-C(13)	1.393(4)	C(8')-C(13')	1.392(3)
C(8)-C(9)	1.401(4)	C(8')-C(9')	1.394(4)
C(9)-C(10)	1.378(4)	C(9')-C(10')	1.374(4)
C(10)-C(11)	1.391(4)	C(10')-C(11')	1.394(3)
C(11)-C(12)	1.394(4)	C(11')-C(12')	1.394(4)
C(11)-C(14)	1.510(4)	C(11')-C(14')	1.509(4)
C(12)-C(13)	1.382(4)	C(12')-C(13')	1.381(4)
C(14)-C(15)	1.526(4)	C(14')-C(15')	1.525(4)
C(15)-C(16)	1.519(4)	C(15')-C(16')	1.517(4)
C(16)-C(17)	1.519(4)	C(16')-C(17')	1.520(4)
C(17)-C(18)	1.517(4)	C(17')-C(18')	1.514(4)
C(18)-C(19)	1.522(4)	C(18')-C(19')	1.523(4)
C(19)-C(20)	1.508(4)	C(19')-C(20')	1.514(4)

Table 4.5 Bond angles [°] for the two molecules of *7*-CB.

N(1)-C(1)-C(2)	179.3(3)	N(1')-C(1')-C(2')	179.2(3)
C(3)-C(2)-C(7)	119.5(2)	C(3')-C(2')-C(7')	119.8(2)
C(3)-C(2)-C(1)	120.4(3)	C(3')-C(2')-C(1')	120.4(2)
C(7)-C(2)-C(1)	120.1(2)	C(7')-C(2')-C(1')	119.8(3)
C(4)-C(3)-C(2)	120.3(3)	C(4')-C(3')-C(2')	119.9(3)
C(3)-C(4)-C(5)	121.2(3)	C(3')-C(4')-C(5')	121.2(3)
C(6)-C(5)-C(4)	117.4(2)	C(6')-C(5')-C(4')	118.0(2)
C(6)-C(5)-C(8)	121.0(2)	C(6')-C(5')-C(8')	122.0(2)
C(4)-C(5)-C(8)	121.5(2)	C(4')-C(5')-C(8')	119.9(2)
C(7)-C(6)-C(5)	122.1(3)	C(7')-C(6')-C(5')	121.4(2)
C(6)-C(7)-C(2)	119.5(3)	C(6')-C(7')-C(2')	119.7(3)
C(13)-C(8)-C(9)	116.6(2)	C(13')-C(8')-C(9')	117.0(2)
C(13)-C(8)-C(5)	121.8(2)	C(13')-C(8')-C(5')	121.6(2)
C(9)-C(8)-C(5)	121.5(2)	C(9')-C(8')-C(5')	121.3(2)
C(10)-C(9)-C(8)	121.6(3)	C(10')-C(9')-C(8')	121.9(2)
C(9)-C(10)-C(11)	121.8(3)	C(9')-C(10')-C(11')	121.3(3)
C(10)-C(11)-C(12)	116.8(2)	C(10')-C(11')-C(12')	117.0(2)
C(10)-C(11)-C(14)	120.1(2)	C(10')-C(11')-C(14')	119.6(2)
C(12)-C(11)-C(14)	123.1(2)	C(12')-C(11')-C(14')	123.5(2)
C(13)-C(12)-C(11)	121.7(3)	C(13')-C(12')-C(11')	121.7(2)
C(12)-C(13)-C(8)	121.6(2)	C(12')-C(13')-C(8')	121.2(2)
C(11)-C(14)-C(15)	116.8(2)	C(11')-C(14')-C(15')	116.7(2)
C(16)-C(15)-C(14)	112.7(2)	C(16')-C(15')-C(14')	112.3(2)
C(17)-C(16)-C(15)	113.5(2)	C(15')-C(16')-C(17')	113.7(2)
C(18)-C(17)-C(16)	114.5(2)	C(18')-C(17')-C(16')	113.7(2)
C(17)-C(18)-C(19)	114.1(2)	C(17')-C(18')-C(19')	114.5(2)
C(20)-C(19)-C(18)	113.6(3)	C(20')-C(19')-C(18')	113.1(2)

Table 4.6 Anisotropic displacement parameters ($A^2 \times 10^3$) for 7-CB. The anisotropic displacement factor exponent takes the form: $-2\pi^2[h^2 a^{*2} U11 + ... + 2 h k a^* b^* U12]$.

	U11	U22	U33	U23	U13	U12
N(1)	50(2)	49(2)	50(2)	-12(1)	0(1)	14(1)
C(1)	35(2)	36(2)	38(2)	-3(1)	4(1)	14(1)
C(2)	31(1)	32(1)	33(1)	2(1)	8(1)	7(1)
C(3)	47(2)	30(2)	42(2)	0(1)	2(1)	16(1)
C(4)	45(2)	35(2)	36(2)	1(1)	-2(1)	17(1)
C(5)	32(1)	28(1)	29(1)	3(1)	7(1)	10(1)
C(6)	31(1)	30(2)	35(2)	1(1)	5(1)	12(1)
C(7)	31(1)	34(2)	34(1)	3(1)	4(1)	12(1)
C(8)	34(1)	29(1)	29(1)	4(1)	6(1)	12(1)
C(9)	38(2)	34(2)	32(1)	0(1)	3(1)	17(1)
C(10)	33(2)	40(2)	34(1)	0(1)	-2(1)	17(1)
C(11)	34(2)	34(2)	29(1)	3(1)	4(1)	13(1)
C(12)	35(2)	38(2)	37(2)	-4(1)	4(1)	15(1)
C(13)	26(2)	44(2)	35(1)	-2(1)	1(1)	13(1)
C(14)	32(2)	41(2)	35(2)	-6(1)	0(1)	13(1)
C(15)	34(2)	40(2)	33(2)	0(1)	2(1)	13(1)
C(16)	33(2)	38(2)	33(2)	-2(1)	3(1)	12(1)
C(17)	33(2)	39(2)	35(2)	1(1)	5(1)	13(1)
C(18)	35(2)	37(2)	37(2)	-3(1)	2(1)	14(1)
C(19)	40(2)	44(2)	34(2)	-3(1)	5(1)	16(2)
C(20)	55(2)	62(2)	42(2)	-17(2)	-2(2)	29(2)
N(1')	45(2)	57(2)	68(2)	-27(2)	-7(1)	17(1)
C(1')	37(2)	36(2)	51(2)	-4(2)	3(1)	19(1)
C(2')	36(2)	32(2)	37(2)	-4(1)	-2(1)	19(1)
C(3')	40(2)	36(2)	32(2)	-1(1)	6(1)	13(1)
C(4')	37(2)	30(2)	33(2)	2(1)	9(1)	9(1)
C(5')	32(1)	29(1)	30(1)	4(1)	4(1)	15(1)
C(6')	32(1)	35(2)	33(2)	6(1)	8(1)	14(1)
C(7')	28(1)	29(2)	45(2)	5(1)	5(1)	10(1)
C(8')	32(2)	34(2)	29(1)	7(1)	6(1)	13(1)
C(9')	37(2)	40(2)	33(1)	-6(1)	7(1)	16(1)
C(10')	28(2)	45(2)	38(2)	-3(1)	9(1)	9(1)
C(11')	34(2)	36(2)	25(1)	3(1)	3(1)	13(1)
C(12')	37(2)	42(2)	28(1)	0(1)	7(1)	18(1)
C(13')	28(2)	40(2)	31(1)	3(1)	4(1)	12(1)
C(14')	36(2)	41(2)	36(2)	-2(1)	6(1)	12(1)
C(15')	35(2)	36(2)	32(1)	1(1)	8(1)	9(1)
C(16')	31(2)	39(2)	35(2)	-3(1)	5(1)	9(1)
C(17')	34(2)	39(2)	37(2)	0(1)	7(1)	11(1)
C(18')	33(2)	40(2)	36(2)	-3(1)	6(1)	11(1)
C(19')	38(2)	41(2)	34(2)	3(1)	8(1)	13(1)
C(20')	45(2)	45(2)	37(2)	-4(1)	11(1)	14(2)

Table 4.7 Hydrogen co-ordinates (x 10^4) and isotropic displacement parameters (A^2 x 10^3) for *7*-CB.

	x	y	z	U(eq)
H(3)	3155(26)	-1577(25)	5088(15)	44(7)
H(4)	4496(29)	-106(24)	6246(17)	48(8)
H(6)	2183(27)	2262(26)	5365(15)	48(8)
H(7)	806(27)	808(22)	4242(16)	41(7)
H(9)	6308(25)	1640(22)	6679(15)	37(7)
H(10)	7799(29)	3182(22)	7691(15)	43(7)
H(12)	4347(28)	4590(24)	7737(16)	45(7)
H(13)	2841(28)	3016(21)	6733(15)	36(7)
H(14A)	7935(30)	5742(25)	8045(17)	52(8)
H(14B)	7923(27)	4740(22)	8809(15)	39(7)
H(15A)	5882(27)	5275(23)	9268(16)	43(7)
H(15B)	5979(27)	6285(22)	8531(16)	38(7)
H(16A)	8238(27)	7407(23)	9196(16)	35(7)
H(16B)	8347(28)	6478(22)	9892(16)	39(7)
H(17A)	6372(26)	6954(23)	10440(15)	35(7)
H(17B)	6348(26)	7936(22)	9727(15)	36(7)
H(18A)	8763(28)	9194(24)	10438(16)	46(7)
H(18B)	8679(27)	8088(23)	11123(16)	39(7)
H(19A)	6677(28)	8609(24)	11581(16)	43(8)
H(19B)	6824(27)	9663(23)	10921(16)	40(7)
H(20A)	8039(29)	10481(24)	12382(17)	49(8)
H(20B)	9154(34)	10742(29)	11712(19)	63(10)
H(20C)	9101(33)	9671(28)	12360(19)	67(9)
H(3')	3495(26)	5323(22)	3928(16)	40(7)
H(4')	4948(27)	6700(23)	5045(15)	35(7)
H(6')	2013(25)	5433(21)	6653(15)	32(6)
H(7')	490(28)	3984(23)	5563(15)	40(7)
H(9')	6589(26)	7112(22)	6316(15)	40(7)
H(10')	8146(29)	8626(23)	7348(15)	44(7)
H(12')	4475(30)	9071(25)	8176(17)	53(8)
H(13')	2959(29)	7509(21)	7166(14)	34(6)
H(14D)	8132(29)	9615(24)	8857(16)	47(7)
H(14E)	8109(30)	10681(26)	8136(17)	53(8)
H(15D)	6082(28)	11116(23)	8655(16)	42(7)
H(15E)	6158(25)	10143(21)	9382(14)	31(6)
H(16D)	8547(31)	12294(26)	9260(18)	58(8)
H(16E)	8543(25)	11370(20)	10023(14)	27(6)
H(17D)	6596(28)	12902(24)	9709(17)	45(7)
H(17E)	6570(30)	12019(25)	10475(17)	51(8)
H(18D)	9035(30)	14094(25)	10335(17)	52(8)
H(18E)	8947(30)	13203(26)	11141(18)	53(8)
H(19D)	7089(26)	14777(22)	10727(15)	37(7)
H(19E)	7118(27)	13933(22)	11528(16)	34(7)
H(20D)	9525(28)	15955(23)	11351(16)	43(7)
H(20E)	9463(30)	15024(25)	12196(18)	56(8)
H(20F)	8497(33)	15994(29)	12051(20)	70(9)

4.2 The crystal structure of 4'-methoxy-4-cyanobiphenyl (*1*-OCB).

4.2.1 Experimental

Suitable colourless column-shaped single crystals of *1*-OCB were obtained by slow evaporation from a solution of methanol and methylene chloride. Lattice constants and intensity measurements were performed on a STADI-4 diffractometer using MoK_{α} radiation. The crystal data is presented below in Table 4.8.

The structure had previously been solved at ambient temperature by Walz et al.[1] The non-hydrogen atoms were taken from the structure given by them and least squares refinement with the anisotropic thermal parameters for all non-hydrogen atoms, led to R = 0.0542 for 2744 independent reflections. The co-ordinates of all hydrogen atoms were found directly from the Patterson map and all hydrogen atoms were refined isotropically. There was some disorder found in the position of a hydrogen from the methyl group of molecule 2 (H(14D)). This was overcome by refining the methyl hydrogens together as a group over several cycles until the shift/esd's settled down. Structure determination was then completed by allowing all atoms to refine isotropically.

Table 4.8 Crystal data and structure refinement for *1*-OCB.

Identification code	*1*-OCB
Empirical formula	$C_{14}H_{11}NO$
Formula weight	209.24
Temperature	293(2) K
Wavelength	0.71073 Å
Crystal system	Monoclinic
Space group	$P2_1/n$
Unit cell dimensions	a = 15.581(3) Å $\alpha = 90°$ b = 15.054(10) Å ß = 93.15(2)° c = 9.298(4) Å $\gamma = 90°$
Volume	2178(2) $Å^3$
Z	8
Density (calculated)	1.276 Mg/m^3
Absorption coefficient	0.081 mm^{-1}
F(000)	880
Crystal size	0.62 x 0.31 x 0.3 mm
Theta range for data collection	2.58 to 22.52°
Index ranges	0<=h<=16, -16<=k<=0, -10<=l<=8
Reflections collected	2810
Independent reflections	2744 [R(int.) = 0.0236]
Refinement method	Full-matrix least-squares on F^2
Data / restraints / parameters	2736 / 0 / 358
Goodness-of-fit on F^2	1.131
Final R indices [I>2sigma(I)]	R1 = 0.0542, wR2 = 0.1461
R indices (all data)	R1 = 0.0715, wR2 = 0.1618
Extinction coefficient	0.0009(4)
Largest diff. peak and hole	0.503 and -0.196 $e.Å^{-3}$

4.2.2 Results and Discussion

The molecular structure is presented in Figure 4.5 as a projection perpendicular to the best fit plane of the molecules and the labelling of the non-hydrogen atoms are given for both independent molecules.

Figure 4.5 Two independent molecules of *1*-OCB indicating the numbering scheme used.

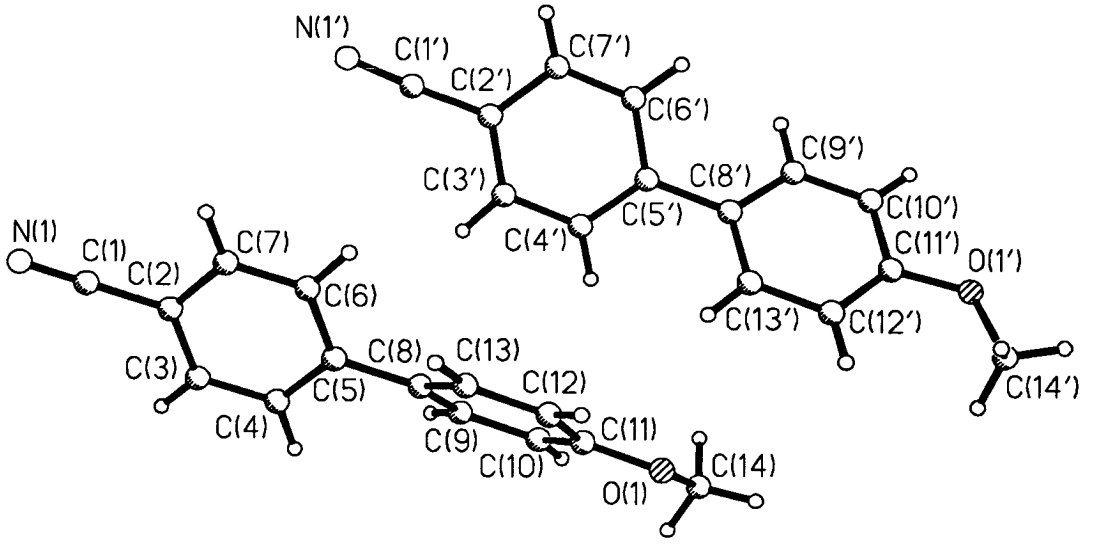

The final positional and thermal parameters are listed in Table 4.9 and Table 4.12, with the anisotropic displacement parameters in Table 4.11. The bond lengths and bond angles are given in Table 4.10 and are found to be comparable to those found in other mesogenic compounds.[1-10]

The structure obtained here compares favourably with that previously determined (the only differences being due to the lower temperature of this study and the fact that the hydrogen atom positions are found in this case directly from the Patterson map). As was observed in the previous structure, the thermal parameters for molecule one have, in the majority, lower temperature factors than molecule two.

The torsion angle between the two phenyl rings in *1*-OCB was found to be 44.7(5)° and 43.5(5)°, which agrees very well with the values of 44.1° and 43.6° found previously.

A discussion of the crystal packing and monotropic behaviour of *1*-OCB is given in chapter 5 (section 5.3.1), where the monotropic behaviour is linked to the low degree of imbrication in the crystal.

Table 4.9 Atomic co-ordinates (x 10^4) and equivalent isotropic displacement parameters (A^2 x 10^3) for *1*-OCB. U(eq) is defined as one third of the trace of the orthogonalised Uij tensor.

	x	y	z	U(eq)
O(1)	3772(1)	2954(1)	-1073(2)	33(1)
N(1)	3890(2)	-4374(2)	-1045(3)	49(1)
C(1)	3867(2)	-3608(2)	-1077(3)	33(1)
C(2)	3825(2)	-2659(2)	-1106(3)	29(1)
C(3)	4098(2)	-2184(2)	-2291(3)	28(1)
C(4)	4056(2)	-1273(2)	-2299(3)	26(1)
C(5)	3751(2)	-796(2)	-1134(3)	24(1)
C(6)	3483(2)	-1283(2)	46(3)	26(1)
C(7)	3509(2)	-2197(2)	59(3)	29(1)
C(8)	3727(2)	182(2)	-1136(3)	23(1)
C(9)	3432(2)	657(2)	-2354(3)	26(1)
C(10)	3425(2)	1581(2)	-2376(3)	27(1)
C(11)	3726(2)	2048(2)	-1168(3)	24(1)
C(12)	4007(2)	1588(2)	64(3)	29(1)
C(13)	4005(2)	673(2)	85(3)	26(1)
C(14)	3380(2)	3453(2)	-2243(4)	37(1)
O(1')	1268(1)	5471(2)	1185(2)	40(1)
N(1')	981(2)	-1855(2)	1228(4)	66(1)
C(1')	1023(2)	-1072(2)	1170(4)	41(1)
C(2')	1060(2)	-136(2)	1140(3)	33(1)
C(3')	1567(2)	294(2)	166(4)	33(1)
C(4')	1628(2)	1206(2)	154(3)	31(1)
C(5')	1173(2)	1727(2)	1096(3)	28(1)
C(6')	654(2)	1285(2)	2054(3)	31(1)
C(7')	600(2)	377(2)	2093(4)	35(1)
C(8')	1233(2)	2709(2)	1094(3)	26(1)
C(9')	490(2)	3224(2)	1200(3)	32(1)
C(10')	531(2)	4136(2)	1221(3)	32(1)
C(11')	1315(2)	4565(2)	1148(3)	28(1)
C(12')	2058(2)	4074(2)	1030(3)	30(1)
C(13')	2016(2)	3155(2)	1011(3)	29(1)
C(14')	2037(2)	5953(3)	1358(4)	46(1)

Table 4.10 Bond lengths [Å] and angles [°] for *1*-OCB.

O(1)-C(11)	1.368(4)	O(1')-C(11')	1.366(4)
O(1)-C(14)	1.431(4)	O(1')-C(14')	1.402(4)
N(1)-C(1)	1.154(4)	N(1')-C(1')	1.182(4)
C(1)-C(2)	1.431(5)	C(1')-C(2')	1.410(5)
C(2)-C(7)	1.398(4)	C(2')-C(3')	1.393(4)
C(2)-C(3)	1.400(4)	C(2')-C(7')	1.401(4)
C(3)-C(4)	1.373(4)	C(3')-C(4')	1.376(5)
C(4)-C(5)	1.404(4)	C(4')-C(5')	1.398(4)
C(5)-C(6)	1.403(4)	C(5')-C(6')	1.403(4)
C(5)-C(8)	1.472(4)	C(5')-C(8')	1.482(4)
C(6)-C(7)	1.376(4)	C(6')-C(7')	1.370(5)
C(8)-C(9)	1.396(4)	C(8')-C(13')	1.398(4)
C(8)-C(13)	1.403(4)	C(8')-C(9')	1.400(4)
C(9)-C(10)	1.392(4)	C(9')-C(10')	1.374(5)
C(10)-C(11)	1.385(4)	C(10')-C(11')	1.388(4)
C(11)-C(12)	1.389(4)	C(11')-C(12')	1.384(4)
C(12)-C(13)	1.378(4)	C(12')-C(13')	1.385(4)
C(11)-O(1)-C(14)	117.0(2)	C(11')-O(1')-C(14')	118.2(3)
N(1)-C(1)-C(2)	179.0(3)	N(1')-C(1')-C(2')	178.2(4)
C(7)-C(2)-C(3)	119.4(3)	C(3')-C(2')-C(7')	118.9(3)
C(7)-C(2)-C(1)	120.0(3)	C(3')-C(2')-C(1')	120.1(3)
C(3)-C(2)-C(1)	120.6(3)	C(7')-C(2')-C(1')	121.0(3)
C(4)-C(3)-C(2)	119.9(3)	C(4')-C(3')-C(2')	120.7(3)
C(3)-C(4)-C(5)	121.7(3)	C(3')-C(4')-C(5')	121.1(3)
C(6)-C(5)-C(4)	117.6(3)	C(4')-C(5')-C(6')	117.5(3)
C(6)-C(5)-C(8)	121.0(3)	C(4')-C(5')-C(8')	121.7(3)
C(4)-C(5)-C(8)	121.3(3)	C(6')-C(5')-C(8')	120.8(3)
C(7)-C(6)-C(5)	121.3(3)	C(7')-C(6')-C(5')	121.9(3)
C(6)-C(7)-C(2)	120.1(3)	C(6')-C(7')-C(2')	119.9(3)
C(9)-C(8)-C(13)	117.4(3)	C(13')-C(8')-C(9')	117.7(3)
C(9)-C(8)-C(5)	121.3(3)	C(13')-C(8')-C(5')	122.2(3)
C(13)-C(8)-C(5)	121.3(3)	C(9')-C(8')-C(5')	120.0(3)
C(10)-C(9)-C(8)	121.7(3)	C(10')-C(9')-C(8')	121.1(3)
C(11)-C(10)-C(9)	119.6(3)	C(9')-C(10')-C(11')	120.3(3)
O(1)-C(11)-C(10)	125.0(3)	O(1')-C(11')-C(12')	125.6(3)
O(1)-C(11)-C(12)	115.5(3)	O(1')-C(11')-C(10')	114.5(3)
C(10)-C(11)-C(12)	119.6(3)	C(12')-C(11')-C(10')	119.8(3)
C(13)-C(12)-C(11)	120.6(3)	C(11')-C(12')-C(13')	119.7(3)
C(12)-C(13)-C(8)	121.1(3)	C(12')-C(13')-C(8')	121.3(3)

Table 4.11 Anisotropic displacement parameters ($A^2 \times 10^3$) for *1*-OCB. The anisotropic displacement factor exponent takes the form:
$-2\pi^2 [h^2 a^{*2} U11 + ... + 2 h k a^* b^* U12]$

	U11	U22	U33	U23	U13	U12
O(1)	34(1)	25(1)	39(1)	3(1)	2(1)	-2(1)
N(1)	64(2)	31(2)	53(2)	-2(1)	15(2)	2(1)
C(1)	37(2)	36(2)	26(2)	-4(1)	6(1)	0(1)
C(2)	27(2)	29(2)	30(2)	-1(1)	-1(1)	0(1)
C(3)	27(2)	33(2)	23(2)	-4(1)	3(1)	1(1)
C(4)	24(2)	32(2)	23(2)	4(1)	4(1)	-3(1)
C(5)	18(2)	29(2)	24(2)	0(1)	0(1)	-1(1)
C(6)	28(2)	29(2)	23(2)	-4(1)	5(1)	2(1)
C(7)	34(2)	32(2)	23(2)	3(1)	7(1)	0(1)
C(8)	16(1)	31(2)	23(2)	0(1)	6(1)	-1(1)
C(9)	24(2)	29(2)	24(2)	-1(1)	6(1)	-1(1)
C(10)	24(2)	35(2)	23(2)	7(2)	6(1)	3(1)
C(11)	18(2)	26(2)	30(2)	2(1)	6(1)	1(1)
C(12)	24(2)	31(2)	29(2)	-4(2)	-1(1)	-4(1)
C(13)	25(2)	30(2)	24(2)	4(1)	0(1)	0(1)
C(14)	35(2)	31(2)	45(2)	5(2)	4(2)	5(2)
O(1')	44(1)	35(1)	41(2)	0(1)	3(1)	4(1)
N(1')	66(2)	58(3)	74(3)	1(2)	9(2)	-6(2)
C(1')	40(2)	30(2)	50(2)	-13(2)	-10(2)	7(2)
C(2')	24(2)	38(2)	36(2)	-2(2)	-1(1)	-1(1)
C(3')	23(2)	38(2)	37(2)	-9(2)	1(1)	4(1)
C(4')	23(2)	40(2)	29(2)	-2(2)	8(1)	2(1)
C(5')	21(2)	37(2)	27(2)	0(1)	0(1)	4(1)
C(6')	27(2)	38(2)	29(2)	-3(2)	7(1)	2(1)
C(7')	31(2)	41(2)	34(2)	-1(2)	8(2)	-5(2)
C(8')	24(2)	34(2)	20(2)	-1(1)	5(1)	3(1)
C(9')	26(2)	41(2)	30(2)	3(1)	10(1)	4(1)
C(10')	29(2)	38(2)	28(2)	4(1)	10(1)	11(2)
C(11')	39(2)	28(2)	19(2)	0(1)	4(1)	7(1)
C(12')	31(2)	37(2)	23(2)	4(1)	3(1)	0(2)
C(13')	27(2)	35(2)	26(2)	-2(1)	5(1)	7(1)
C(14')	46(2)	56(2)	37(2)	0(2)	3(2)	-8(2)

Table 4.12. Hydrogen co-ordinates (x 10^4) and isotropic displacement parameters (A^2 x 10^3) for *1*-OCB.

	x	y	z	U(eq)
H(3)	4300(19)	-2511(20)	-3061(34)	33(2)
H(4)	4263(19)	-946(20)	-3066(34)	33(2)
H(6)	3241(19)	-982(20)	806(34)	33(2)
H(7)	3317(19)	-2515(20)	895(34)	33(2)
H(9)	3237(19)	342(20)	-3181(35)	33(2)
H(10)	3253(19)	1892(20)	-3240(36)	33(2)
H(12)	4198(19)	1910(21)	827(35)	33(2)
H(13)	4190(19)	354(21)	901(35)	33(2)
H(14A)	3435(19)	4095(23)	-1944(32)	35(3)
H(14B)	2757(21)	3304(19)	-2407(32)	35(3)
H(14C)	3669(20)	3322(20)	-3155(36)	35(3)
H(3')	1912(19)	-34(20)	-457(33)	33(2)
H(4')	1987(20)	1492(20)	-516(34)	33(2)
H(6')	335(20)	1651(20)	2724(33)	33(2)
H(7')	282(20)	98(20)	2749(35)	33(2)
H(9')	-66(21)	2963(20)	1251(32)	33(2)
H(10')	14(20)	4468(20)	1252(32)	33(2)
H(12')	2588(21)	4343(20)	983(32)	33(2)
H(13')	2534(20)	2822(20)	951(31)	33(2)
H(14D)	1671(20)	6553(21)	1317(32)	35(3)
H(14E)	2380(20)	5771(19)	2277(36)	35(3)
H(14F)	2415(20)	5890(20)	502(36)	35(3)

References

[1] L.Walz, H.Paulus and W.Haase, Z. Kristallogr., 180 (1987), 97

[2] P.Mandal and S.Paul, Mol. Cryst. Liq. Cryst., 131, (1985), 223

[3] M.A.Kravers, V.I.Kulishov, A.J.Polischuk and A.S.Tolochko, Sov. Phys. Crystallogr., 37(3), (1992), 375

[4] K.Hori, Y.Koma, A.Uchida and Y.Ohashi, Mol. Cryst. Liq. Cryst., 225, (1993), 15

[5] L.Walz, W.Haase and I.H.Ibrahim, Mol. Cryst. Liq. Cryst., 200, (1991), 43

[6] W.Haase, J.Loub, H.Paulus, M.A.Mokhles and I.H.Ibrahim, Mol. Cryst. Liq. Cryst., 197, (1991), 57

[7] G.V.Vani, Mol. Cryst. Liq. Cryst., 99, (1983), 21

[8] W.Haase, J.Loub and H.Paulus, Z.Kristallogr., 202, (1992), 7

[9] W.Haase, H.Paulus, Z.X.Fan, I.H.Ibrahim and M.Mokhles, Mol. Cryst. Liq. Cryst. (letters), 6(4), (1989), 113

[10] W.Haase, H.Paulus and R.Pendzialek, Mol. Cryst. Liq. Cryst., 100, (1983), 211.

[11] A.J.Leadbetter, J.L.Durrant and M.Rugman, Mol. Cryst. Liq.Cryst. (letters), 34, (1977), 231

[12] G.M.Sheldrick, SHELX-86, program of crystal-structure solution, University of Göttingen, Germany, (1986)

[13] A.J.Leadbetter and M.A.Mazid, Mol. Cryst. Liq. Cryst., 51, (1979), 85

[14] W.Haase, H.Paulus and H.T.Muller, Mol. Cryst. Liq. Cryst. 97, (1983), 131

Chapter 5

Intermolecular interactions in Liquid Crystals

5 Introduction

Although the bulk properties of nematic liquid crystal phases are well understood, the various distribution functions describing the molecular organisation within these phases are less well known. One experimental technique that has been employed to shed light on this problem is X-ray diffraction of the liquid crystal phase.

A typical experiment of this kind[1] would involve placing a sample in a container between opposite poles of two permanent magnets (B~1T) on a rotating stage, the stage being part of an oven so that the sample temperature can be controlled. Proper alignment of the sample can then be attained, and X-ray diffraction patterns obtained using a focusing horizontal diffractometer.

By measuring the positions of the equatorial arcs it is possible to determine the intermolecular spacing perpendicular to the long axes of the molecules. This tends not to vary a great deal from one liquid crystal to another. However, the meridional scattering (parallel to the long axes of the molecules) is found to be much more dependent on the liquid crystal being studied.

Leadbetter et al.[2] examined five different liquid crystals in this way. The liquid crystals studied were three Schiffs bases, p-methoxybenzylidene-p-n-butylaniline (MBBA), p-ethoxybenzylidene-p-n-butylaniline (EBBA) and p-methoxybenzylidene-p-cyanoaniline (MBCA) and two cyanobiphenyls, 4'-n-pentyl-4-cyanobiphenyl (5-CB) and 4'-n-septyl-4-cyanobiphenyl (7-CB).

The equatorial scattering indicated that all five liquid crystals had intermolecular spacings of ~5.0 Å perpendicular to their long axes. This implies that there must be some restriction to the rotation of the molecules round their long axes since the diameter of a freely rotating molecule is around 6.5 Å. It was also found that in all cases the distribution of the projections of the molecular centres onto a plane perpendicular to the local director is random beyond about five molecular diameters. The 'orientational' correlation of the long molecular axes was found to extend over

very much greater distances even in unoriented samples. This confirms that in the nematic phase, although the molecules align themselves parallel to the director, the degree of positional order remains low.

The meridional scattering of the five liquid crystals indicates that three distinct patterns exist. If the Bragg spacings are compared with the maximum molecular lengths of the different liquid crystals, it is found that in MBBA and EBBA they match the molecular length to within a few percent, but that in MBCA they are significantly smaller. In the biphenyls the Bragg spacing is much bigger than the molecular length. This suggests the existence of more than one kind of nematic phase, each having a different local molecular organisation.

The local molecular organisation for EBBA and MBBA can be explained by the observation that, even when there is extensive correlation of the z co-ordinates of the molecules (parallel to the molecular axes), they tend not to form into independent files. Instead, the molecules show a weak tendency to form into layers, although each layer only extends over a few molecular diameters.

For MBCA, the observation that the Bragg spacing is less than the molecular length is attributed to some well-defined local molecular packing. Although the crystal structure of MBCA has not been determined, it can be inferred from the crystal packing of related compounds[3,4].

Of particular interest to this work are the diffraction patterns of the two biphenyls. The two diffraction patterns are very similar to each other but differ markedly from those of MBBA, EBBA and MBCA. In fact, the diffraction patterns from the biphenyls are very similar to those found from smectic materials[5] but with more diffuse reflections. It is found that both biphenyls have a negligible file-like correlation along the z-axis but exhibit some short range ordering with a pronounced layer character. In each layer, the distribution of the projections of the molecular centres onto a plane perpendicular to the local director is random beyond about 5 molecular diameters for 7-CB and 4 molecular diameters for 5-CB. The distribution

parallel to the director is found to be 4.5 for both *5*- and *7*-CB The lateral ordering of the molecules is little affected on heating from the nematic to the isotropic phase. It is clear, therefore, that 5-CB and 7-CB have quasi-smectic A ordering on a local scale which increases with alkyl chain length up to *8*-CB which has a smectic A phase.

Perhaps the most striking observation is that the repeat unit along the texture axis is about 1.4 molecular lengths. It is assumed that this repeat distance results from strong molecular association due, presumably, to the high dipole moments in cyanobiphenyls. To fit with these observations the 'head-to-tail' configuration was proposed, Figure 5.1. This has the added advantage that it also implies a tendency to layer formation which is indeed observed. Another reason to support this type of bimolecular association is that ferroelectric properties have never been found in liquid crystals through alignment of the long axis direction. The 'head-to-tail' arrangement of the molecules gives the smallest repeat unit that would account for this.

Further evidence for this 'head-to-tail' configuration is provided by Leadbetter et al.[6] in a study of various liquid crystals of the cyanobiphenyl type. They found that if the length of the biphenyl unit (rigid core of the molecule) is defined as '*a*' and the remainder of the tail as '*b*', then a plot of '*a*+2*b*' versus the Bragg spacing gives a straight line.

X-ray and neutron diffraction experiments were also used to test the hypothesis of the formation of a bimolecular group which involves overlapping tails (A) or with overlapping cores (B). Model B is a good fit to experiment for <ß> in the range 0-35 ° (ß is the angle molecules make with respect to the director). On the other hand, model A would be acceptable if <ß>~35 °. However for a typical S_A phase, the distribution of molecular axes orientation f(ß) has <P2> ≥ 0.7, which would require <ß> to be less than 25 °, where $<P_2>$ is the second Legendre polynomial and is used as a shortcut to represent the order of the liquid crystal, i.e. $<P_2>$ is the average value of the expression $\frac{1}{2}\left(\overline{\cos\beta}^2 - 1\right)$. This establishes model B with the overlapping

cores as a good representation of the average structure in the smectic A and nematic phases.

Figure 5.1 The 'head-to-tail' configuration of bimolecular association accounts for the observed repeat unit of 1.4 times the length of an isolated molecule

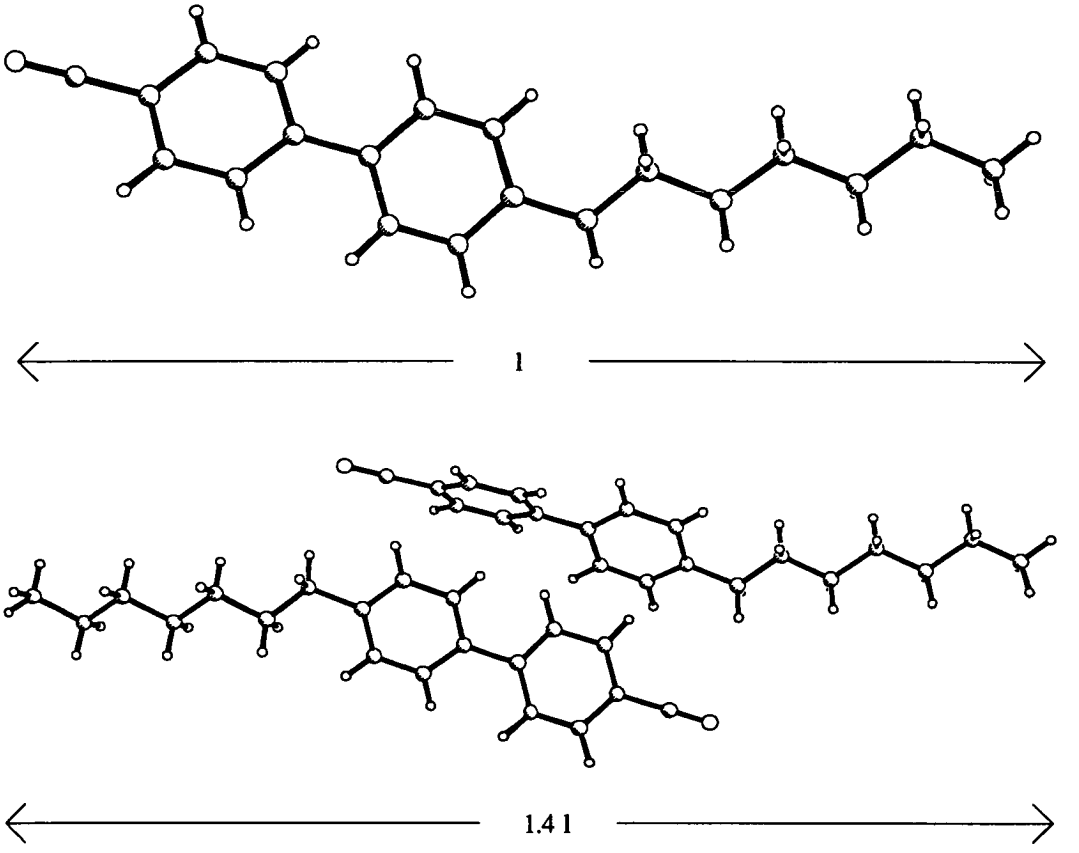

Another approach to the problem is to measure the density and volume changes in liquid crystalline substances, as the sample temperature (and phase) is varied.[7] These measurements show that, at phase transitions, the changes in volume are too small for significant changes in local molecular organisation to occur. This is consistent with the above observations that structural changes at these transitions are essentially changes in long range order with the average local structure remaining little changed. These volume measurements are used to predict a 'free volume' in the smectic A phase of 5-10% in *8*-CB. This is very similar to the 'free volume' found from similar experiments in CBOOA (N-p-cyanobenzylidene p-octyloxyaniline).[8] These

measurements rule out some of the possible structures proposed for the smectic A phase which involve "interpenetration" of tails and/or cores. These types of local structure would have low average packing and high average molecular volume caused by essentially identical areas of core and tail. The actual packing must, in fact, be more efficient and is probably based on a bilayer type structure composed from molecules adopting the 'head-to-tail' configuration.

Cladis et al.[9] also give support to this 'head-to-tail' configuration as a means of interpreting re-entrant nematic - bilayer smectic A transitions. A re-entrant phase is a phase which reappears either on cooling a liquid crystal or by increasing the pressure on the liquid crystal sample, e.g. nematic→smectic→nematic, the second nematic phase being termed the re-entrant phase. Normally for a smectic liquid crystal, the enhanced tendency for the polar parts of the molecules to interact preferentially with other polar groups via fairly long range electrostatic forces, and for the non-polar parts to interact with similar groups via fairly short range forces, is the "key" to smectic layering[10]. This leads to 'monolayer' smectic A phases for the majority of liquid crystals since they tend to have the polar segments of the molecules in the middle with the hydrocarbon layers extending outwards. For cyanobiphenyls which have the polar core of the molecule at one end, it is obvious that some kind of dimerization is likely. This is assumed to be responsible for the bilayer smectic A phase.

When a liquid crystal with a six-unit hydrocarbon chain (nematic) is added to a liquid crystal with an eight-unit chain (smectic), the smectic layer becomes more susceptible to rupture with stress indicating that the strength of the bilayer has been weakened. It is therefore understood that the short range attractive interactions of the non-polar tails stabilise the smectic layers - the strength of this interaction being proportional to the number of carbon atoms in the tail.

To account for transitions between less dense smectic and more dense nematic character, it is assumed that the polar-polar and the nonpolar-nonpolar interactions are maintained for the bilayer smectic A phase to remain stable under pressure, but

that the layer spacing expands due to the increasing repulsive interaction of the aromatic rings with increasing pressure.

However, another possibility for bimolecular association is the dimer suggested by Haase et al.[11] where it is suggested that the cyano group of one molecule overlaps with the cyano substituted phenyl ring of its neighbour and vice versa (see later, Figure 5.4). The length of the dimer measured by diffraction experiments of the nematic phase ought to be related to the tail conformation adopted by the molecules and also to the ordering in the liquid crystalline phase. If a value of 0.65 is chosen for the average order parameter $\langle P_2 \rangle$ then the longer dimers suggested here would fit within the experimentally measured layer spacing.

The argument used to support this is that the 'head-to-tail' interaction would ideally require a dihedral angle between the rings of the biphenyl group of close to 0°. However, NMR measurements obtained by Sinton and Pines[12] indicate that this angle in the nematic phases of *4*- and *5*-CB is around 32°.

Leadbetter et al.[6] estimate spatial disorder normal to the layers of around 20 %. This is calculated assuming that in each layer, a normal Maier-Saupe distribution centred at $\beta = 0$ and with $\langle P_2 \rangle \approx 0.7$ is found. This high degree of disorder is required to give the correct density measurements and makes it possible for the 'head-to-tail' dimer to occupy the average structure of the layers. The crystal-like representation of the 'head-to-tail' bimolecular association cannot fill space to give the correct density without allowing for disorder of this magnitude.

It is also possible to examine phase transitions of liquid crystals using Molecular Dynamics (MD) or Monte Carlo (MC) simulations. One such simulation[13] was performed on the liquid crystal molecules *5*-, *6*-, *7*- and *8*-OCB. It was found that the molecular ordering and motion in the nematic phase could be reproduced for all four compounds. One interesting observation was that the structural anisotropy was clearly larger in the nematic phase than the isotropic phase. This is because, at the phase transition from isotropic to nematic, the probability distribution of anisotropy

becomes much narrower as the majority of molecules adopt a conformation with a more extended tail. This again highlights the role played by the alkyl/alkoxy tails in determining the type and range of mesophase formation.

In summary, it is clear that the 'head-to-tail' configuration is present in cyanobiphenyl liquid crystals. In fact, this bimolecular association has been shown to exist in the nematic, smectic and even the isotropic phases of these materials.[2] It can also be understood that as the hydrocarbon chain length increases, it is the short range attractive interactions of the non-polar tails which stabilise smectic layer formation. This would suggest that for a liquid crystal such as *8*-OCB, which has both a smectic and a nematic mesophase, we could account for its liquid crystalline behaviour as follows:

In the isotropic phase the molecules are fairly energetic, but many of the molecules will exist as 'dimers' adopting the 'head-to-tail' configuration due to the relatively strong electrostatic forces between the polar groups in the cyano biphenyl units. There will even be some interactions of these 'dimers' forming small regions of local order. On cooling the sample to the nematic phase, the average intermolecular spacing perpendicular to the long axis of the molecules gradually decreases by around 0.1 - 0.2 Å to around 5 Å, resulting in ordered regions becoming larger and more common as the molecules are now less energetic and the dipole interactions become more influential. Also, the short range van der Waals interactions between the non-polar tails will now take some effect, causing the ordered regions to have more of a layer structure. Each ordered region would only persist for 4 to 5 layers at most, but this would result in more regions aligning with a common z-axis. On further cooling the sample to the smectic phase, these tail-tail van der Waals contacts become stronger still. The layer structure grows and what we recognise as the smectic mesophase is formed.

Diffraction experiments[2] show that no sudden change in interatomic distances occur at phase transitions. This would suggest a mechanism similar to that predicted by molecular dynamics as discussed previously. This entails the molecules adopting

more anisotropic conformations at phase transitions rather than suddenly adopting any preferred interaction.

Using this model as a guide, it would imply that in the *n*-OCB series, when $n < 8$ the van der Waals interactions between the tails is not of a sufficient strength to allow formation of a smectic phase before the crystalline phase is formed.

5.1 The 4'-alkoxy-4-cyanobiphenyls (*n*-OCB's)

It has been shown[7] that no significant changes to the molecular organisation of liquid crystals occur at phase transitions. Therefore, in order to examine the processes which result in nematic behaviour further, the crystal structures and intermolecular contacts of a series of cyanobiphenyl liquid crystals have been examined. The 4'-alkoxy-4-cyanobiphenyls (*n*-OCB's) were chosen because crystal structures of the first seven in the series have been published.[14,15,16] This makes it possible to compare intermolecular contacts in the crystal phase as the number of carbon atoms in the alkoxy chain increases. The alkoxy homologues also have the advantage over their alkyl counterparts of having a larger dipole moment. This ought to result in stronger intermolecular interactions.

Before looking at the interactions found in the crystal phase it is useful to make a note of the properties of the alkoxy cyanobiphenyl series[17] (Figure 5.2).

The liquid crystal properties of the series vary significantly as the alkoxy chain length increases. The first four molecules in the series do not actually exhibit a liquid crystal phase on melting. It is only on cooling that a nematic mesophase is found. These molecules are therefore termed monotropic liquid crystals. The next three compounds in the series, *n* (No. of carbon atoms in the tail)=*5,6* or *7*, are nematic liquid crystals. The next two, $n = 8$ or *9*, have both smectic A and nematic phases whilst the remaining molecules, $n = 10, 11$ or *12* have only a smectic A phase.

Figure 5.2 Transitions observed in the n -OCB series

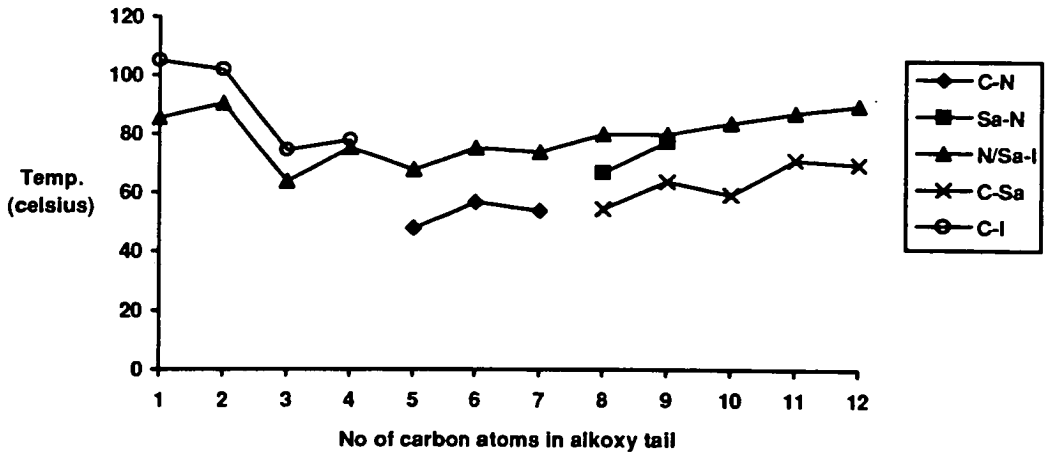

On observing the transition temperatures, T_{N-I} in Figure 5.2, an odd-even effect is observed.[18] This is attributed to the fact that each odd-numbered carbon atom added to the chain elongates the molecule without increasing its width, while each even-numbered carbon atom tends to increase the width more than the molecular length. Since T_{N-I} is related to the overall molecular anisotropy it can be seen that the molecules having alkyl/alkoxy chains of odd parity will have higher T_{N-I} values than those with an even parity.

In an effort to unravel the differences in how the *n*-OCBs pack in their crystalline phases, it was decided to separate and classify all the different types of interactions found. This was done by extracting the co-ordinates for each liquid crystal from the Cambridge Structural Data Base[19,20] and compiling intermolecular contact tables using the program CALC.[21] Hydrogen atom co-ordinates were only available for *1*- and *5*-OCB. The most probable hydrogen positions were obtained using the program XP[22] for all other molecules. All interactions which had intermolecular contact distances of ≤ (2.5 Å + the sum of the van der Waals radii) were then generated using XP and are summarised in Figure 5.4 - Figure 5.15 It was also necessary to correct the bond length between the last two carbons in the second molecule of *4*-OCB which was too short due to disorder in the crystal structure.

Each interaction has been classified as being either antiparallel (A1-A7), indicating that the cyano groups of the two molecules involved point in opposite directions, or parallel (P1-P5), indicating that the cyano groups point in the same direction. Each interaction is accompanied, where appropriate, with a table giving selected intermolecular contact distances and a brief explanation of that interaction, including any significance it may have on liquid crystal behaviour. Finally, Table 5.14 summarises which type of interactions appear in each liquid crystal. The numbering scheme used in the following tables is shown in Figure 5.3 for the largest compound studied, 7-OCB.

Figure 5.3 A molecule of 7-OCB showing the numbering system used

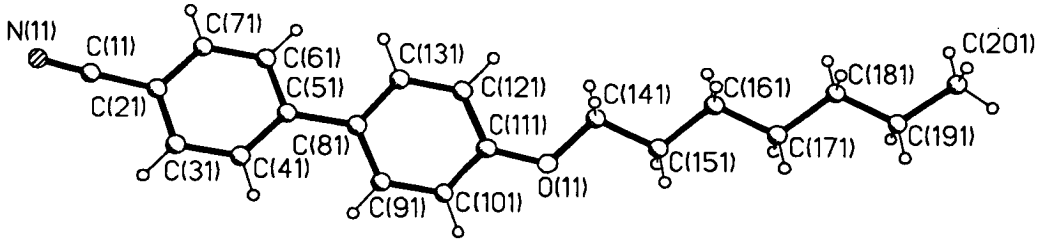

Interaction A1: Cyano-cyano interaction

Figure 5.4 Cyano-cyano interaction (A1)

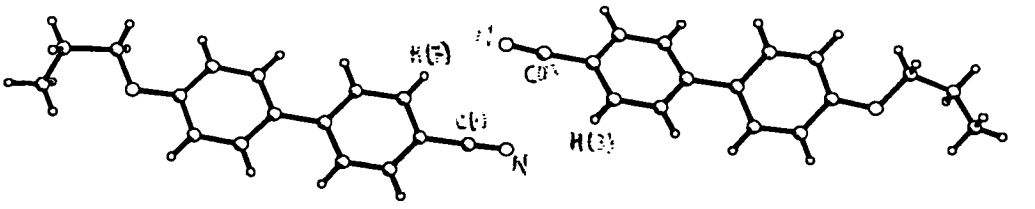

Table 5.1 Selected intermolecular contacts (Å) for the A1 interaction.

		H(3)/H(7)	C(3)/C(7)	C(1)	N	C(2)
1-OCB	N	2.71	3.59			
	N	2.89	3.61			
2-OCB	N	2.86	3.58			
3-OCB	N	2.54	3.43	3.47	3.50	3.93
5-OCB	N	2.56	3.44	3.34	3.32	3.86
6-OCB	N	2.84	3.69		3.56	3.56
	N	2.85	3.46	3.40		3.74
7-OCB	N	2.49	3.38	3.57	3.64	3.95
	N	2.74	3.48	3.40	3.52	3.82

All liquid crystals in this series except for *4*-OCB, exhibit the A1 interaction. The intermolecular contact distances do not vary significantly from one compound to another although a slight odd-even effect is observed when looking at the N...H contacts.

Interaction A2: Cyano-ring 1 interaction

Figure 5.5 Cyano-ring 1 interaction (A2)

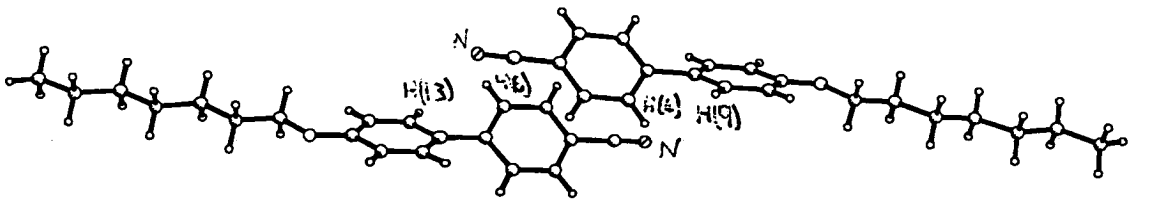

Table 5.2 Selected interatomic contacts (Å) for the A2 interaction.

		H(9)/H(13)	H(4)/(6)	C(5)	C(4)/(6)
1-OCB	N	3.11		3.90	3.96
2-OCB	N	2.82	3.58		3.62
7-OCB	N	2.916			3.68
	N		2.84	3.51	

Interaction A2 closely resembles the dimer proposed by Haase et al.[11] It only occurs in *1*- and *2*-OCB, which have monotropic behaviour, and in *7*-OCB, which is a nematic liquid crystal but crystallises with a 'smectic-like' packing structure. All compounds have adopted twisted biphenyl moieties with dihedral angles ranging from 33° to 46°.

This interaction can also be described in terms of the inter ring contacts between the cyanophenyl rings of the two molecules. The simplest way to describe this is in terms of the angle in degrees between the best fit planes of the two rings (ø), the distance between the centres of gravity of the two rings (r), the horizontal displacement / offset (r_{xy}) and the perpendicular distance between the two planes (r_z). These are given in Table 5.2.1 for the A2 interaction.

Table 5.2.1 Inter ring contacts for the A2 interaction

	ø	r	r_{xy}	r_z
1-OCB	0.0	4.61	2.63	-3.79
2-OCB	27.1	4.59	2.97	3.50
7-OCB	2.8	3.88	1.70	3.49

It is seen that in *1*- and *7*-OCB the rings are approximately parallel to one another but displaced by 2.6 Å and 1.7 Å respectively. In *2*-OCB the rings interact at an angle of 27.1° while remaining displaced by 3.0 Å. The closest inter ring contact being in *7*-OCB.

In *1*-OCB the interaction occurs between two equivalent molecules, but in *2*- and *7*-OCB the interaction is only found between crystallographically different molecules.

Interaction A3: Head-to-tail interaction

Figure 5.6 Head-to-tail interaction (A3)

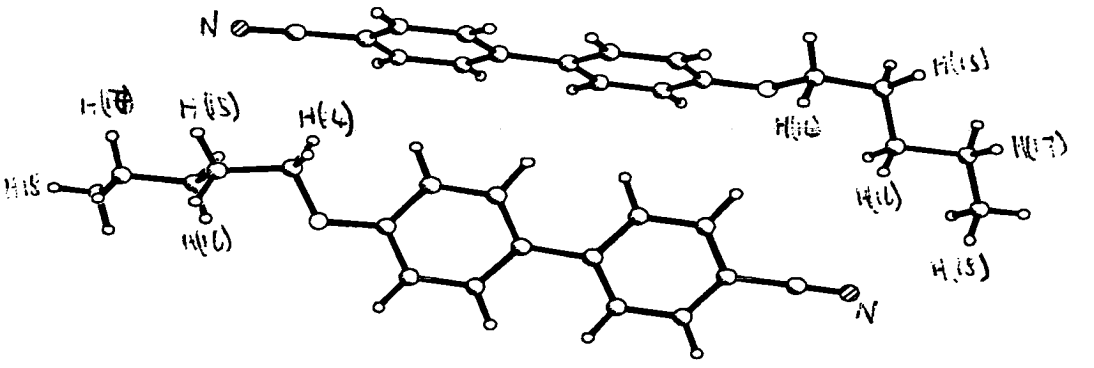

Table 5.3 Selected intermolecular contacts (Å) for the A3 interaction

		H(14)	H(15)	H(16)	H(17)	H(18)
3-OCB	N	3.29	3.51	3.44		
5-OCB	N	3.24	3.13	3.37	3.78	
	N			3.58		2.83
6-OCB	N	3.43		2.88		
	N	3.60	2.95			

This interaction closely resembles the dimer proposed by Leadbetter and others [1,2,5,6,7,9,23] and is generally believed to be present in the mesogenic and even isotropic phases of cyanobiphenyl liquid crystals. Although not shown in the above table, all the liquid crystals, except *2*- and *4*-OCB, were found to exhibit this interaction. The intermolecular contact distances do not vary significantly from one liquid crystal to the next, but there is some variation in the intermolecular ring 1-ring 2 angles. Compounds highlighted in the above table are those which happen to have contacts between the nitrogen from the cyanide group and hydrogens from the alkoxy tail. In *1*- and *7*-OCB, no such contacts are observed as the tail points away from the cyanide group. An alternative description of this interaction is in terms of the inter ring contacts. The main interaction is between ring 1 from one molecule and ring 2 from

another, but there are also some longer contacts between similar rings from both molecules. These contacts are given in Table 5.3.1.

Table 5.3.1 Inter ring contacts for the A3 interaction

	Ring 1 / Ring 2				Ring 1/2 / Ring 1/2			
	ø	r	r_{xy}	r_z	ø	r	r_{xy}	r_z
***1*-OCB**	44.2	4.41	0.80	4.34	0.0	5.56	4.69	2.98
***3*-OCB**	47.4	4.81	4.38	1.97				
***5*-OCB**	62.1	4.86	1.18	4.72	61.8	5.68	3.19	4.70
***6*-OCB**	9.6	5.00	3.14	3.89	32.2	5.88	5.73	1.30
	56.0	4.74	1.03	4.62				
***7*-OCB**	37.1	5.04	2.65	4.29				

Only *1*-, *5*- and *6*-OCB show contacts between similar rings of the molecules. In all three cases the rings are relatively far apart with the shortest distance between ring centres occurring in *1*-OCB at 5.56 Å. As expected there are many more inter ring contacts involving the first and second rings of the molecules. These occur with angles ranging from 9.6° in *6*-OCB to 62.1° in 5-OCB. The closest inter ring interaction is in *1*-OCB where the distance between ring centres is 4.4 Å. Perhaps of most significance is the ring displacement (r_{xy}) which is the shortest observed in these interactions at 0.8 Å. For *1*-OCB this can be explained as there are no interactions observed between the cyano nitrogen and hydrogens from the tail of the other molecule. It is assumed that in *3*-, *5*-, and *6*-OCB, hydrogen contacts between the tail and the cyano group are responsible for larger horizontal displacements of the rings. In *7*-OCB the rings are displaced but no N...H contacts are observed with the tail of the other molecule. However, the large tail - tail interaction (P2) is present, and the cyano group can instead 'see' the hydrogens from the tail of a different molecule to that involved in the A3 interaction.

Interaction A4: Ring 2-ring 2 interaction

Figure 5.7 Ring 2-ring 2 interaction (A4)

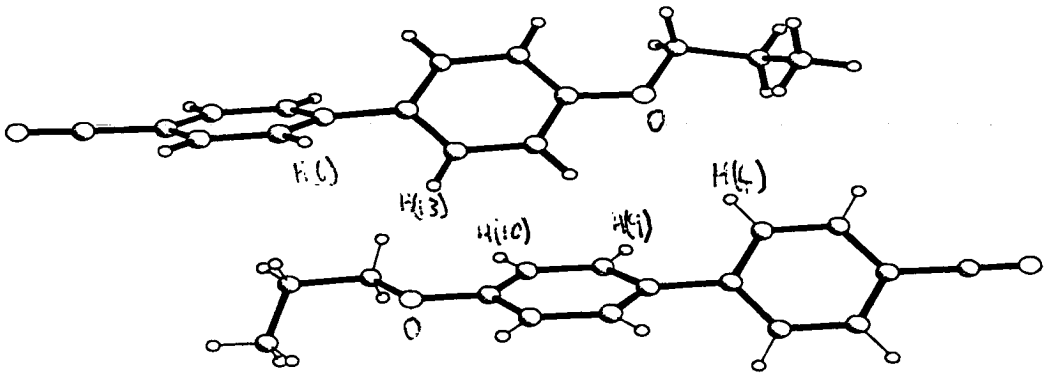

Table 5.4 Selected intermolecular contacts (Å), for the A4 interaction.

		H(4)/H(6)	H(9)/H(13)	H(10)/H(12)		H(18)	H(19)
1-OCB	O	3.29					
	O	2.80	3.42				
2-OCB	O	3.43	2.78	3.76			
	O	3.11	3.19				
3-OCB	O	3.01					
	O	2.90					
6-OCB	O	2.82	3.81		N	3.57	
					N	3.33	3.12

Interaction A4 is observed in all the liquid crystals studied except *4*- and *5*-OCB, although no significant intermolecular contacts are observed for *7*-OCB either. The main variation in intermolecular contacts is a slight odd-even effect observed as the oxygen appears to be a little closer to the tail of the other molecule when *n* is even. This can also be observed by considering the inter ring contacts involved in this interaction, Table 5.4.1.

Table 5.4.1 Inter ring contacts for the A4 interaction

	ø	r	r_{xy}	r_z
1-OCB	75.3	4.85	1.13	4.72
	0.00	5.99	5.47	2.43
2-OCB	74.0	4.81	0.42	4.79
	74.0	5.02	1.65	4.74
3-OCB	40.8	4.63	1.91	4.22
6-OCB	49.8	4.96	4.30	2.46
7-OCB	4.8	6.14	5.77	2.10

It was observed that the angle between rings varied from 0° in *1*-OCB to 74° in *2*-OCB, with the closest inter ring distance being 4.6 Å in *3*-OCB.

It is also observed that in *6*-OCB the tail is long enough that it comes into contact with the cyano group from the other molecule. This may give some added stability to compounds with sufficient carbons in the alkoxy tail to make this possible.

Interaction A5: Biphenyl-tail interaction

Figure 5.8 Biphenyl-tail interaction (A5)

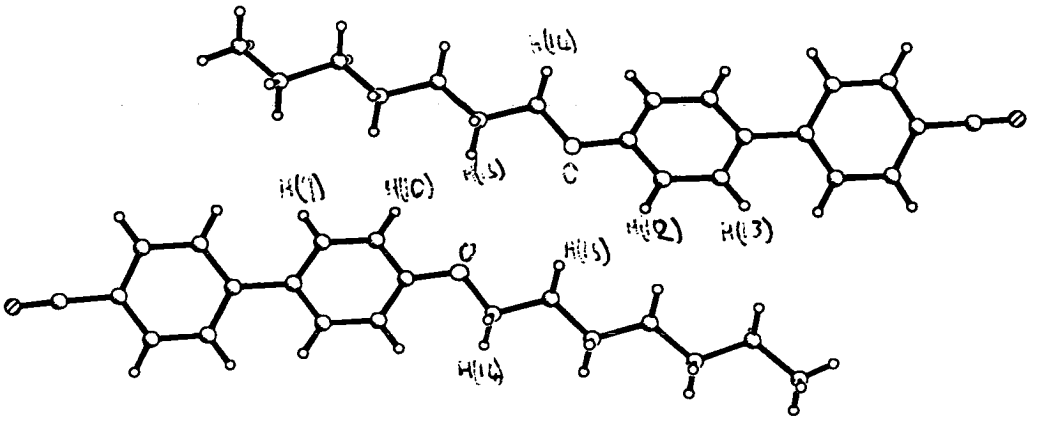

Table 5.5 Selected intermolecular contacts (Å), for the A5 interaction.

		H(9)/(13)	H(10)/H(12)	O	H(14)	H(15)
1-OCB	O	3.72	2.96			
2-OCB	O		2.67			
	O	2.87	3.46			
5-OCB	O			3.73	3.13	3.75
	O		2.72			
6-OCB	O		4.13	3.77	3.45	
	O			3.87	3.55	3.16
7-OCB	O					3.16

This interaction is more prominent in the liquid crystals exhibiting the nematic mesophase. This is not so unexpected as it is only when the tail is of a comparable length to that of the biphenyl core that this interaction can occur. The molecules always arrange themselves so that the cyano end of ring 1 extends beyond the end of the tail. As a result of this, the two molecules can be seen to be sliding past each other as the chain length increases as can be observed by following the intermolecular

contacts from the oxygen in the above table. This is of particular interest here because it results in less biphenyl overlap for those compounds with longer tails.

Interaction A6: Large tail-tail interaction

Figure 5.9 Large tail-tail interaction (A6)

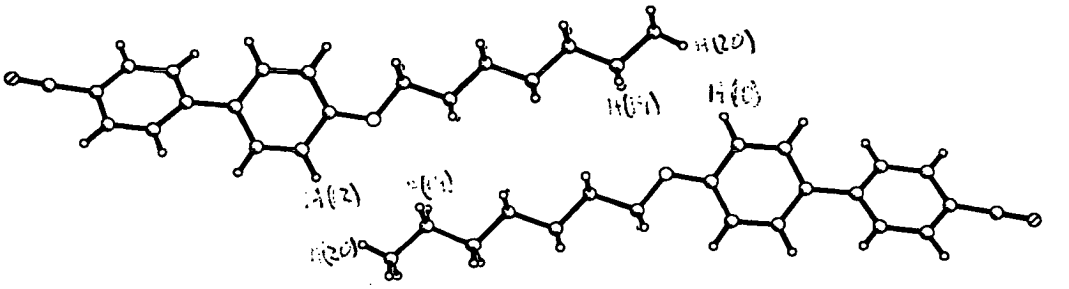

Table 5.6 Selected intermolecular contacts (Å), for the A6 interaction.

		H(10)/H(12)
6-OCB	H(19)	3.24
7-OCB	H(20)	2.70

This interaction only occurs in *6*- and *7*-OCB, and involves the entire length of the tails. This is actually very similar to one of the models which Leadbetter et al.[6] used in examining the results of X-ray and neutron diffraction experiments. It was concluded that this form of dimer would be acceptable for a smectic liquid crystal only if $<\beta> \approx 35^{\circ}$. Both *7*-CB and *7*-OCB pack in a 'smectic like' manner, each being joined by interactions of this type, but these are observed to have values of ß around 50° and 64° respectively.

Interaction A7: Tail-tail interaction

Figure 5.10 Tail-tail interaction (A7)

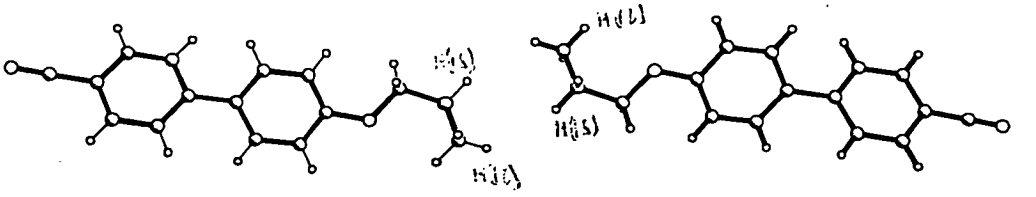

Table 5.7 Selected intermolecular contacts (Å), for the A7 interaction

		H(15)	H(16)	H(17)	H(18)	H(19)
3-OCB	H(16)	2.52				
	H(16)		2.54			
5-OCB	H(18)			2.50		
	H(18)				3.10	
6-OCB	H(19)					2.86
	H(18)				2.57	

Interaction A7 involves the tips of the tails of each molecule just 'seeing' the tips of the tails of the other molecule. As is observed from the table, no significant differences are observed between compounds. The main contribution to molecular packing from this interaction is the increased separation of the biphenyl cores as the tails of the molecules become longer.

Interaction P1: Cyano-tail interaction (Chain-like)

Figure 5.11 Cyano-tail interaction (P1)

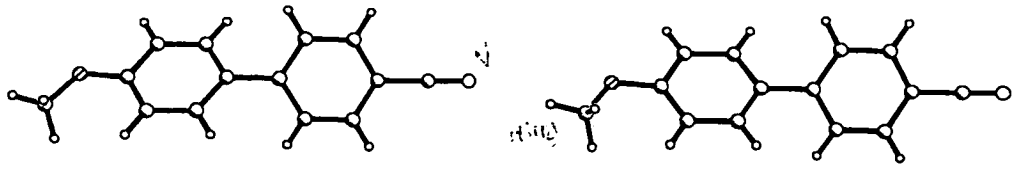

Table 5.8 Selected intermolecular contacts (Å), for the P1 interaction.

		H(7)/(3)	N
1-OCB	H(14)	2.75	
	H(14)		2.55
	H(14)		2.58
	H(14)	2.78	2.91
2-OCB	H(15)	2.99	
	H(15)		2.95
	H(15)		3.34
	H(15)	3.11	3.41
3-OCB	H(16)	3.48	
	H(16)		3.32
	H(16)		3.58
5-OCB	H(16)	2.79	
	H(17)		3.37
6-OCB	H(19)		3.12
	H(19)		3.36
	H(19)		3.39
	H(19)	2.60	3.44

Interaction P1 is observed in all the compounds except *4*- and *7*-OCB. As can be seen from the right hand column of Table 5.8, 'N', the intermolecular contact distance

between the last hydrogen in the tail of each liquid crystal and the nitrogen in the other molecule increases as the tail gets longer.

Interaction P2: Biphenyl-tail interaction (odd chain length)

Figure 5.12 Biphenyl-tail interaction (P2)

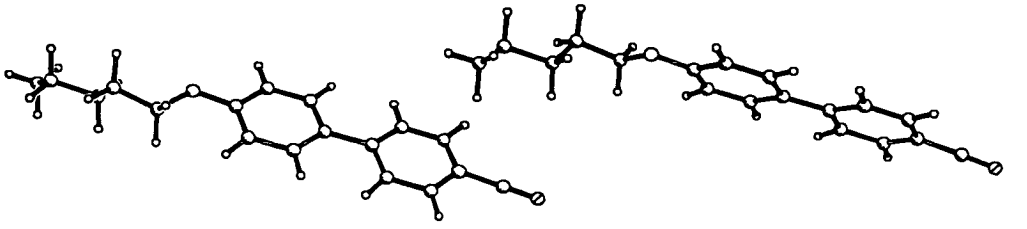

Interaction P3: Biphenyl-tail interaction (even chain length)

Figure 5.13 Biphenyl-tail interaction (P3)

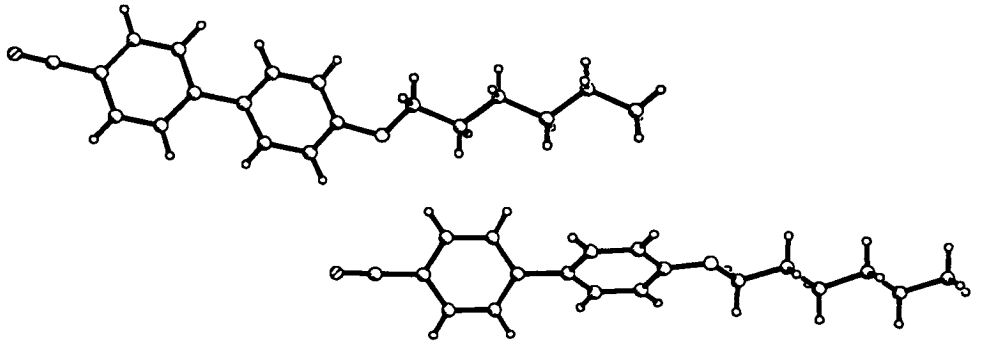

The interaction P2 is observed in *1*-, *5*- and *7*-OCB which all have an odd number of carbon atoms in their tail. In this interaction, the end of the tail interacts with ring 1 of the other molecule. Interaction P3, however, is only found in *6*-OCB which has an even number of carbons in the tail. In this interaction the whole biphenyl core of one molecule lies along the tail of the other molecule.

Interaction P4: Large parallel interaction

Figure 5.14 Large parallel interaction (P4)

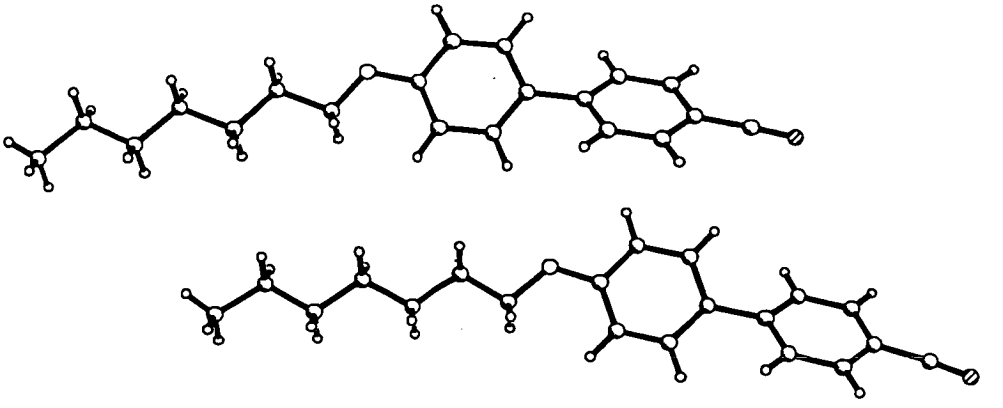

Interaction P5: Large parallel interaction (soldier like)

Figure 5.15 Large parallel interaction (P5)

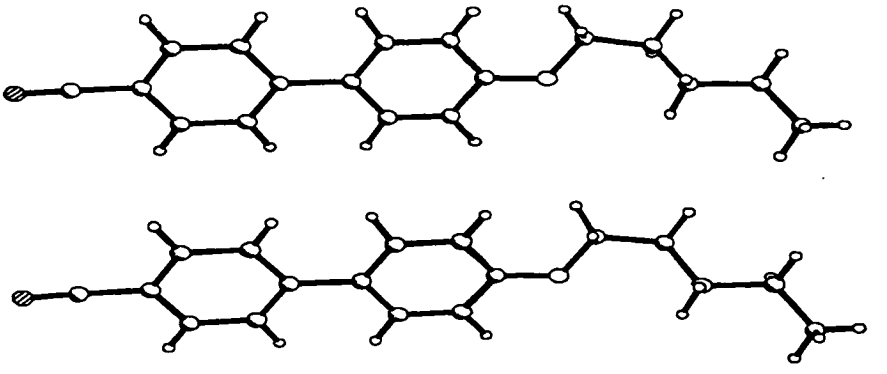

Both interactions P4 and P5 involve a lot of H...H contacts at less than 3 Å. A natural consequence of this type of interaction is that it will become stronger as the tail length increases due to the increasing number of intermolecular contacts being formed. Interaction P4 occurs in all the liquid crystals studied, except for *3*- and *5*-OCB, which instead adopt the interaction P5.

Both of these interactions are best described in terms of inter ring interactions. The main one in P4 being between ring 1 of one molecule and ring 2 of the other, but longer contacts between similar rings are also observed. Interaction P5 consists of contacts between rings which all lie planar to one another. The contacts are relatively distant with the closest distance between ring centres being 5.7 Å in *5*-OCB, Table 5.8.

Table 5.8 Inter ring contacts for the P4 and P5 interactions

a) P4

	Ring 1 / Ring 2				Ring 1/2 / Ring 1/2			
	ø	r	r_{xy}	r_z	ø	r	r_{xy}	r_z
***1*-OCB**	43.9	5.70	3.15	4.75	17.1	5.96	5.70	1.74
	60.5	4.68	4.31	1.81	75.3	5.86	3.85	4.41
***2*-OCB**	45.9	4.84	1.31	4.65	29.7	4.89	3.20	3.70
	60.1	4.81	4.57	1.50	74.0	5.86	5.48	2.07
***4*-OCB**	52.3	4.64	4.09	2.20	43.6	5.30	3.16	4.26
	59.8	4.83	1.12	4.69	67.8	5.06	1.70	4.77
***6*-OCB**	10.7	5.56	5.18	2.24				
***7*-OCB**	34.8	5.00	4.56	2.04	37.1	4.81	4.27	2.22
	39.6	4.63	3.82	2.60				

b) P5

	Ring 1 / Ring 1				Ring 2 / Ring 2			
	ø	r	r_{xy}	r_z	ø	r	r_{xy}	r_z
***3*-OCB**	0.0	5.95	5.31	2.70	0.0	5.95	5.58	2.08
***5*-OCB**	0.0	5.70	4.87	2.95	0.0	5.70	4.89	2.92

The interactions observed for each compound of the *n*-OCB series are summarised in Table 5.9. A 'Y' is used to indicate the occurrence of a specific interaction and an 'N' indicates that the interaction is absent.

Table 5.9 Summary of interactions found in each compound of the *n*-OCB series.

	A1	A2	A3	A4	A5	A6	A7	P1	P2	P3	P4	P5
1-OCB	Y	Y	Y	Y	Y	N	N	Y	Y	N	Y	N
2-OCB	Y	Y	N	Y	Y	N	N	Y	N	N	Y	N
3-OCB	Y	N	Y	Y	N	N	Y	Y	N	N	N	Y
4-OCB	N	N	N	N	N	N	N	Y	N	Y	Y	N
5-OCB	Y	N	Y	N	Y	N	Y	Y	Y	N	N	Y
6-OCB	Y	N	Y	Y	Y	Y	Y	Y	N	Y	Y	N
7-OCB	Y	Y	Y	Y	Y	Y	N	N	Y	N	Y	N

The next step is to look at the crystal structure of each liquid crystal and to interpret the properties of that liquid crystal in terms of the interactions observed.

5.2 Crystal Structures of the 4'-alkoxy-4-cyanobiphenyls

5.2.1 4'-methoxy-4-cyanobiphenyl (*1*-OCB)

As discussed previously, *1*-OCB is a monotropic liquid crystal. This is of relevance when discussing its crystal packing because, unlike other nematogens (e.g. *5*-, *6*- and *7*-OCB), the nematic phase is not observed on melting the crystal but only on cooling the sample from the isotropic phase. This implies that for *1*-OCB, the packing forces are such that the 'head-to-tail' dimers believed to be present in the nematic and smectic phases of cyanobiphenyl compounds, are broken up on melting of the crystal.

The crystal structure for *1*-OCB was obtained by Walz et al.[14], with the hydrogen atoms being placed in idealised positions, and also as part of this work (see Chapter 4) at low temperature and with the hydrogen atoms included in the refinement. Both crystal structures are essentially the same, and it is the co-ordinates from the low temperature study that have been used in examining intermolecular contacts.

1-OCB crystallises with the space group $P2_1/n$ and has eight molecules in the unit cell. This means that there are two independent molecules in the asymmetric unit. The dihedral angles in the biphenyl groups of the two molecules are 44.1 ° and 43.6 ° which is close to the gas phase value in biphenyl, calculated to be 42 °.[24] The crystal packing can be seen in Figure 5.16 where the molecules are extended parallel to one another with the longest axis along [010].

Figure 5.16 Packing diagram for 1-OCB showing molecules extended along [010].

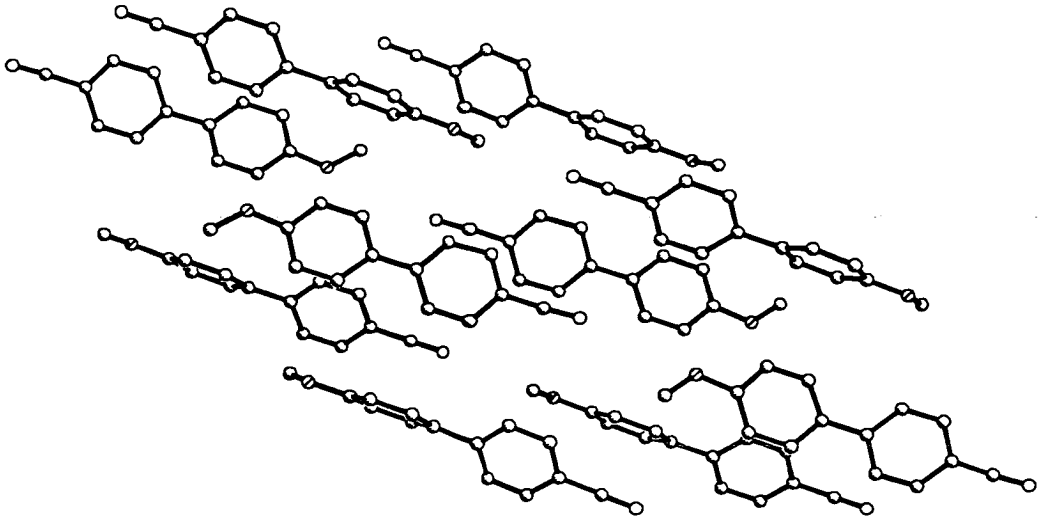

Walz et al.[14] concluded that the most significant interactions are the weak cyano phenyl contacts formed between one set of crystallographically equivalent molecules, the other half of the molecules not undergoing any noteworthy interactions. The weak cyano-phenyl contact referred to is the interaction classified as (A2, Figure 5.5) and is discussed below.

From Table 5.9 it is seen that *1*-OCB exhibits all the interactions listed except A6, A7, P3 and P5. It is now possible, starting with the anti-parallel interactions first, to take each interaction observed and make a few comments regarding its likely effect on nematogenic behaviour, the cyano-cyano interaction (A1, Figure 5.4), is typical of that found in other compounds in the *n*-OCB series. In *1*-OCB the cyano groups from the two molecules overlap in such a way that the closest contact is actually 2.71 Å between the nitrogen of the cyanide in one molecule and the hydrogen adjacent to the cyanide in the other. This allows for efficient packing in the crystal but is unlikely to be present in the liquid crystal phase because of the close proximity of the polar cyano groups, and because any dimer persisting in the solution phase would be likely to consist of a larger degree of overlap of the molecules involved.

Next is the cyano-phenyl interaction (A2, Figure 5.5). This is only observed in *1*-, *2*- and *7*-OCB. It involves the cyano group of one molecule lying over the phenyl ring of the other. This closely resembles the dimer proposed by Haase et al.[11] (see earlier), and is referred to above as being the most noteworthy interaction. As in the interaction A1, this is more likely a means of packing efficiently in the crystal and is unlikely to be found in the liquid crystal phase. The dihedral angle in the biphenyl group is 43.6 ° in molecules undergoing this interaction.

The head-to-tail interaction (A3, Figure 5.6) is present in all the compounds studied except for *2*- and *4*-OCB. This interaction involves the biphenyl units slipping over one another with the cyanide group able to interact with the tail of the other molecule. This closely resembles the dimer proposed by Leadbetter and others[1,2,5,6,7,9,10,23] and is generally believed to be present in the nematic and smectic phases of cyanobiphenyl liquid crystals. There are no significant differences in the intermolecular contact distances throughout the series, but the biphenyl dihedral angles vary from compound to compound. In *1*-OCB, the angle is 44.2 °.

Interaction A4 (Figure 5.7), the ring 2-ring 2 interaction, is observed in all the liquid crystals studied except for *4*-OCB. This involves the molecules slipping over one another so that the second phenyl ring of one molecule lies over the second phenyl ring of the other. In *6*-OCB this allows the cyanophenyl of each molecule to interact with the tail of the other molecule. However, for the smaller compounds, such as *1*-OCB, this is not possible. The extent of this interaction can conveniently be followed by observing the hydrogen contacts made to the oxygen in the alkoxy tail. In *1*-OCB the shortest H...O contact is 2.81 Å.

The biphenyl-tail interaction (A5, Figure 5.8) involves the biphenyl unit of one molecule interacting with the tail of another. This is more prominent in compounds with longer tails where the interaction involves many weak biphenyl-tail contacts. It is unlikely that this interaction is of great importance for *1*-OCB.

The first parallel interaction observed is the cyano-tail interaction (P1, Figure 5.11). This involves the tendency of the molecules to form infinite chains, formed by N...H contacts between the cyanide of one molecule and a hydrogen in the terminal methyl group of another. This distance increases, and hence the contact becomes less important, as the number of carbons in the alkoxy chain increases. In *1*-OCB the shortest N...H contact is 2.55 Å.

The biphenyl-tail interaction (P2, Figure 5.12) is only observed in those compounds of the *n*-OCB series with *n* odd. It consists of the end of the alkoxy chain interacting with the first phenyl ring of another molecule. This interaction does not vary a great deal with increased chain length and is unlikely to be strong enough to influence the formation of the liquid crystal phase.

The final interaction of note is the large parallel interaction (P4, Figure 5.14). This involves many relatively short H...H contacts of less than 3 Å. The number of these contacts, and hence the influence of the interaction increases with increased chain length. This interaction probably plays a large part in influencing the parallel alignment of the molecules in the crystal and nematic phases.

In order to describe the mesogenic behaviour of *1*-OCB in terms of these interactions it is necessary to consider what will happen as the crystal melts. Although interaction A1 is present in all the crystal structures studied, it is unlikely to persist in the nematic or isotropic phases. Indeed, it is probable that interactions A1 and A2 can be treated together. For *1*-OCB to form the nematic phase on melting, the molecules would be required to slide over one another (or break up and recombine) to form dimers similar to those represented by interaction A3. These dimers would then remain aligned with one another under the influence of the parallel interaction P4.

The reason *1*-OCB melts to form an isotropic phase, and not a nematic phase, is related to the shortness of the alkoxy chain. This results in a smaller contribution from interaction P4 and a stronger contribution from interaction P1. The other interaction observed in *1*-OCB, which is dependent on the chain length, is interaction

A4. If the tail was longer, the biphenyl overlap would be reduced and perhaps the tail would help pull the molecules apart. This is discussed more later but hints at the real significance of the tail. As it becomes longer, molecules in different layers of the crystal become displaced with respect to one another, thereby resulting in a more imbricated mode of crystal packing. This results in more weak interactions between the biphenyl unit and the tail of the molecule which can break down on melting, allowing the crystal to partially melt with some of the stronger, polar cyanobiphenyl antiparallel interactions persisting into the liquid crystalline or even isotropic phases.

5.2.2 4'-ethoxy-4-cyanobiphenyl (*2*-OCB)

As with *1*-OCB, *2*-OCB is a monotropic liquid crystal and it must be remembered that, although the nematic phase is obtained on cooling the sample from the liquid phase, the nematic phase is not obtained on melting the crystal.

The crystal structure of *2*-OCB was obtained by Walz et al.[14] In looking at the intermolecular contacts the hydrogen atoms have been placed in idealised positions using the molecular graphics package XP.[22]

2-OCB crystallises with the space group C2/c and has sixteen molecules in the unit cell. This means there are two independent molecules in the asymmetric unit. The dihedral angles in the biphenyl groups of the two molecules being 44.9 ° and 33.4 °. This suggests that the biphenyl unit in one set of crystallographically equivalent molecules is more affected by packing forces than the other. The crystal packing can be seen in Figure 5.17 where the molecules are extended along [$20\bar{1}$].

Walz et al.[14] concluded that the most significant interactions are the weak cyano-phenyl contacts (A2). In *2*-OCB these occur between unequivalent molecules in the asymmetric unit, whereas in *1*-OCB, this interaction was only observed between crystallographically equivalent molecules.

Figure 5.17 Crystal packing of 2-OCB with the molecules extended along [20$\bar{1}$]. Molecules with labels are all in the same plane.

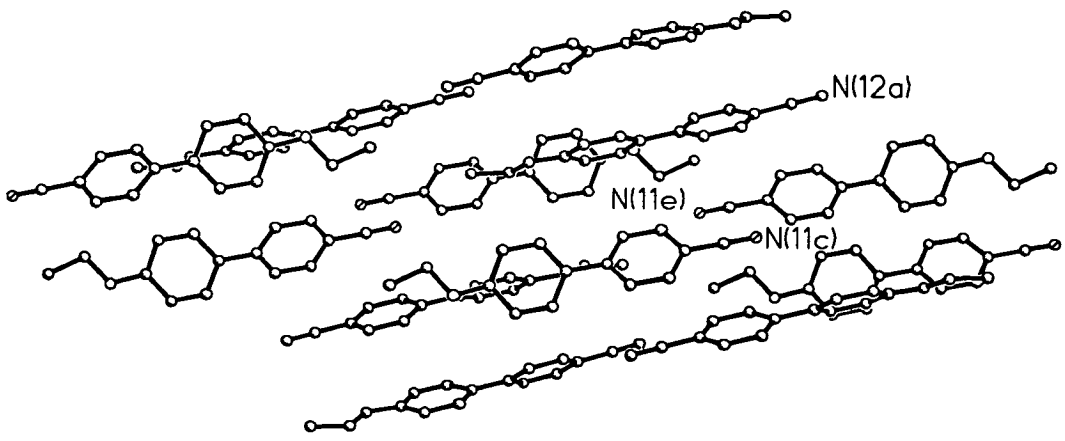

From Table 5.9 it can be seen that *2*-OCB does not exhibit any interactions not observed for *1*-OCB, but that interactions A3 and P2 are missing. The omission of the head-to-tail interaction (A3) can be explained because in *1*-OCB, one set of crystallographically equivalent molecules underwent the cyano-phenyl interaction (A2) and the other set underwent the head-to-tail interaction (A3). In *2*-OCB, both sets of molecules combine to form the interaction A2, thereby preventing formation of the A3 type interaction.

The absence of the biphenyl-tail interaction (P2) is also a consequence of the above argument. Because both molecules interact together in the cyano-phenyl (A2) interaction, the crystal consists of layers containing these dimers. The packing is too dense to allow a molecule from another layer to penetrate sufficiently for the P2 interaction to occur.

A comparison with the interactions observed in *1*-OCB now follows, with the anti-parallel interactions first. The cyano-cyano contact (A1) is similar to that found in *1*-OCB, but with the shortest N...H contact slightly longer at 2.84 Å. As mentioned above, the cyano-phenyl interaction occurs between crystallographically inequivalent molecules in *2*-OCB, making this interaction more prominent than in *1*-OCB. The ring 2-ring 2 interaction (A4) is similar to that found in *1*-OCB, the shortest H...O

contact in *2*-OCB being 2.78 Å. This indicates that the molecules are displaced a little relative to one another so that the oxygen now lies closer to ring 2 than it was in *1*-OCB, thereby slightly reducing the amount of ring 2-ring 2 overlap. The biphenyl-tail interaction (A5) is a little stronger than that observed in *1*-OCB due to the extra carbon atom in the alkoxy chain. The closest contact is between the oxygen of one molecule and the ring 2 hydrogen atom adjacent to the oxygen in the other (2.67 Å).

Comparing the parallel interactions the cyano-tail contact (P1) is not as strong as in *1*-OCB, with the shortest N...H contact being 2.95 Å in *2*-OCB. The other interaction of note is the large parallel interaction P4 which is slightly stronger in *2*-OCB due to the extra H...H contact from the alkoxy tail.

Since the only difference between the molecules of *1*-OCB and *2*-OCB is the addition of a carbon in the alkoxy tail, this must somehow be responsible for the differences in crystal packing between the two compounds. The crystal structure indicates that the alkoxy tail in *2*-OCB adopts an extended structure resulting in an enhanced structural anisotropy than if the tail did not adopt the extended confirmation. This is the basis for the odd-even effect (see previously 5.2). The higher T_{N-C} for *2*-OCB (Figure 5.2) must be related to this. In the nematic phase, the molecules are more likely to align parallel to one another than in *1*-OCB. Because of this, the molecules will find it easier to form the dimers found in the crystalline phase, and the compound crystallises at a higher temperature than *1*-OCB.

Conversely, because of the shortness of the tail, an argument similar to that used for *1*-OCB can explain why *2*-OCB is monotropic in behaviour: because of the low degree of imbrication, the strong polar contacts hold the molecules firmly together and prevent melting to form the nematic phase.

5.2.3 4'-propoxy-4-cyanobiphenyl (*3*-OCB)

Like *1*- and *2*-OCB, *3*-OCB is a monotropic liquid crystal. The crystal structure was obtained by Walz et al.[14] then later by Kravers et al.[26] These two structures are essentially the same and it is the co-ordinates from Walz et al., with the hydrogens added in idealised position using the program XP[22], that are used here.

3-OCB crystallises with the space group $P2_1/c$ and has four molecules in the unit cell. This means that all molecules are crystallographically equivalent in the asymmetric unit. The dihedral angle of the biphenyl group is 47.4 °. The crystal packing can be seen in Figure 5.18 where the molecules are extended parallel to [403].

Figure 5.18 Molecular packing in 3-OCB showing the molecules extended along [403]. Molecules that have been labeled are all in the same plane and interact via the cyano-cyano (A1) interaction.

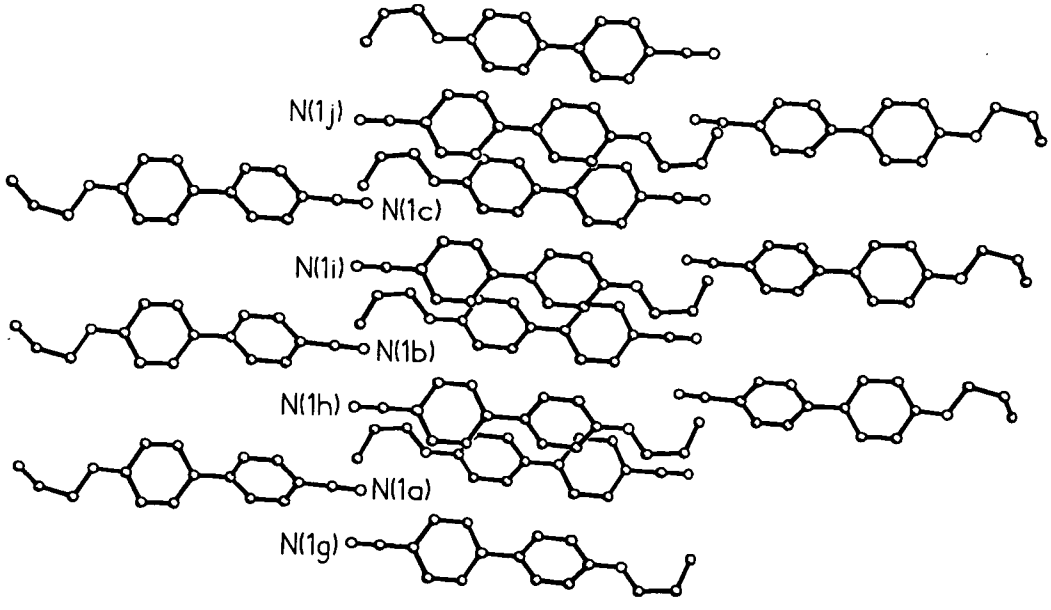

Walz et al.[14] concluded that the most significant interactions are the weak cyano-cyano contacts which arrange themselves in an infinite stack along the crystallographic *b* axis. This is the interaction classified as A1 (Figure 5.4).

From Table 5.9 it is observed that *3*-OCB exhibits slightly different interactions from those observed in *1*- and *2*-OCB. The interactions A2, A5 and P4 are missing and, in keeping with *2*-OCB, so is the interaction P2. However, *3*-OCB exhibits two different interactions which are not observed in either *1*- or *2*-OCB. These are the tail-tail interaction A7, (Figure 5.10) and the large parallel interaction P5, (Figure 5.15).

The parallel interaction P5, (Figure 5.15) appears to be most influential regarding the crystal packing of *3*-OCB. This interaction involves the two molecules standing exactly alongside one another. Interestingly, it is only observed in *3*- and *5*-OCB. Its presence in *3*-OCB can conveniently be used to explain the absence of the cyano-phenyl interaction A2.

Interaction A2 often occurs between two layers or sheets of molecules in the crystal. As these molecules are related by the interaction P5, molecules interacting in an antiparallel arrangement are no longer displaced with respect to one another and the cyano-cyano interaction (A1) occurs instead. Similarly, the antiparallel interaction, A5, is not formed either.

The appearance of the antiparallel tail-tail interaction A7, (Figure 5.10) is also attributed to the parallel interaction P5. Interaction A7 is merely the tail-tail contact between two molecules involved in the P5 interaction. If it were not for the interaction P5, the two molecules involved in interaction A7 would overlap to a greater extent, causing the molecules to adopt the antiparallel biphenyl-tail interaction (A5) instead.

The other interactions present can be compared to those found in *1*- and *2*-OCB as follows. Taking the antiparallel interactions first, the cyano-cyano contact (A1) is similar to that found in *1*- and *2*-OCB, but with a shortest N...H contact of 2.54 Å. This is shorter than is observed in *1*- and *2*-OCB and, on looking at Table 5.1, it is noticeable that there is an odd-even effect present in these weak N...H contacts. Those compounds with an odd number of carbon atoms in the alkoxy tail show

shorter contacts than those with an even number of carbons. This also appears to be related to the presence of the P5 interaction. The absence of this interaction in *1*-OCB explains why the shortest N...H contact is only marginally shorter than that found in *2*- and *6*-OCB, and longer than those found in *3*-, *5*- and *7*-OCB.

The head-to-tail interaction (A3) differs from that found in *1*-OCB mainly in that the dihedral angle in the biphenyl group of *3*-OCB is 47.6°, whereas in *1*-OCB it was 44.2°.

The ring 2-ring 2 interaction (A4) follows the pattern from *1*- and *2*-OCB, in that the shortest H...O contact is 2.90 Å, with the hydrogen in this case being one of the hydrogens on ring 2 closest to the cyanophenyl ring. This is longer than was observed in *2*-OCB but shorter than the distance observed in *1*-OCB, as would be expected if the odd-even effect observed for this interaction is real.

Finally, the parallel cyano-tail contact (P1) also follows the trend observed in *1*- and *2*-OCB. In *3*-OCB, the shortest N...H contact is greater still at 3.32 Å.

In relating these observations to the monotropic behaviour exhibited by *3*-OCB, it is worth examining how its properties compare to *1*- and *2*-OCB, by looking again at Figure 5.2. There is a marked drop in T_{C-I} from *1*- and *2*-OCB to *3*-OCB. This indicates that the crystal is not as strongly held together in *3*-OCB as it is for the smaller molecules. Again, the difference can only have been caused by the addition of one carbon atom to the alkoxy tail and so it must be explained in terms of how the crystal packing has altered to accommodate this.

As mentioned above, the biggest effect the additional carbon has had on the crystal packing is the introduction of the parallel interaction P5. This was shown above to account for the prevention of the formation of the antiparallel cyano-phenyl dimer (A2), and results in the formation of more antiparallel cyano-cyano dimers (A1). A possible explanation for this is that, for efficient packing in the crystal phase, the molecules arrange themselves in dimers with maximum structural anisotropy. Since a

tail with an odd number of carbon atoms has a reduced structural anisotropy to a tail with an even number, the molecules compensate for this by forming the cyano-cyano (A1) dimer instead.

To explain the lower melting point of *3*-OCB, it is considered that the A1 dimers will be less strongly held together than the cyano-phenyl A2 dimers. This is most likely the largest effect, but the reduced ring 2-ring 2 overlap in the antiparallel interaction A4, and the further weakening of the parallel interaction P1, will also contribute. It is also significant that, as the alkoxy tail becomes longer, an ever increasing proportion of intermolecular contacts consist of the weak van der Waals tail contacts, which would be expected to break down more easily than the polar cyano-cyano or cyano-biphenyl contacts. The monotropic behaviour of *3*-OCB is accounted for by arguments similar to those presented for *1*- and *2*-OCB.

5.2.4 4'-butoxy-4-cyanobiphenyl (*4*-OCB)

As in the first three members of the *n*-OCB series, *4*-OCB is a monotropic liquid crystal. The crystal structure was determined by Walz et al.[14] and the hydrogen atoms were added in idealised positions using the program XP.[22]

4-OCB crystallises with the space group $Pca2_1$ and has eight molecules in the unit cell. This means there are two independent molecules in the asymmetric unit. The dihedral angles in the biphenyl groups being -29.9° and 39.0°. The crystal packing can be seen in Figure 5.19. It is observed that the molecules pack in layers, each layer interacting with the next via cyano-tail interactions. Each layer has all the molecules pointing in the same direction so that there exists an anisotropy in the crystal with the cyano dipoles averaged over several layers pointing along [100].

This is permitted by the acentric space group. It is, however, markedly different from what is found in the crystal packing of all other members of the *n*-OCB series of compounds, because it results in the crystalline phase being polar. As a consequence

of this, no antiparallel interactions are found in the crystal. This different mode of packing in the crystal can only be explained in terms of the stability of the parallel P4 interaction. On comparing the crystal densities of the *n*-OCB series (Figure 5.20 ***Plot of crystal density (dc) versus carbon chain length (n) for the first seven molecules in the n-OCB series***

) it is seen that *4*-OCB packs less efficiently than might be expected.

Figure 5.19 Crystal packing of 4-OCB. Although cyano dipoles point on average along [100], it can be seen that molecules arrange themselves in layers, with each layer being approximately 100 ° to one another.

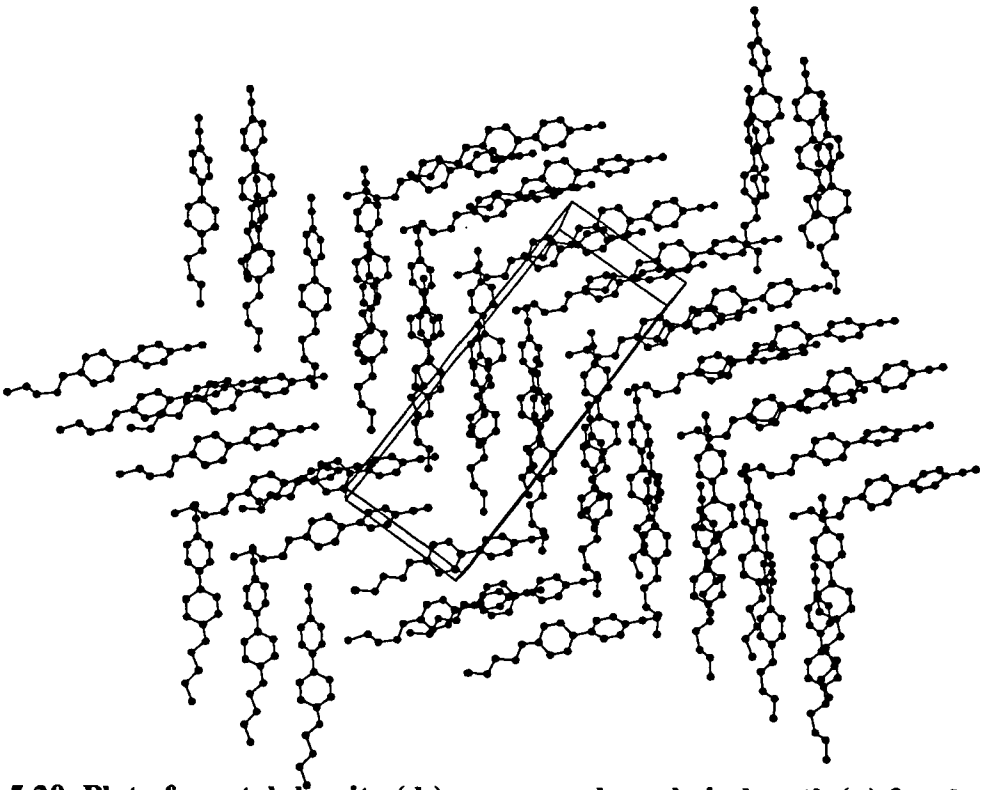

Figure 5.20 Plot of crystal density (d_c) versus carbon chain length (n) for the first seven molecules in the n-OCB series

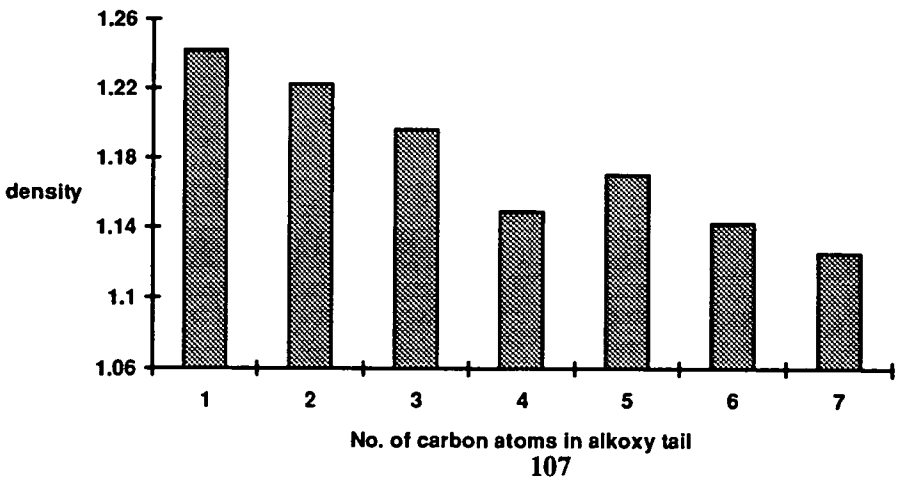

From Table 5.9 it can be seen that the only interactions observed for *4*-OCB are the parallel interactions P1, P3 and P4. It is simplest to describe the packing in terms of layers comprising both crystallographically independent molecules. Each layer is perpendicular to the *c*-axis, with the molecules in each layer making an angle of approximately 50 ° to the *c*-axis. Within each layer, all the molecules interact via the large parallel interaction P4, and the other interactions occur between these layers. Although specified as being P1 and P3, these are different to the interactions observed in other compounds in the series because, instead of the molecules aligning parallel to one another, the angle between molecules in *4*-OCB is approximately 100 °.

On comparing these interactions to those found in the first three compounds of the *n*-OCB series, the large parallel interaction P4 only differs from that of the other compounds in the extra contacts formed by the slightly longer alkoxy tail. It is perhaps significant that, in *4*-OCB, the tail is long enough for a tail-tail contribution in this interaction to take place: the shortest contact is H(14)...H(17) at 2.95 Å.

The 'parallel' cyano-tail interaction, P1, differs from those of the first three compounds in that the molecules no longer align truly parallel to one another. The shortest N...H contact is 3.09 Å. This is shorter than the contact of 3.32 Å found in *3*-OCB, but, as the angles between the molecules are different in the two cases, there can be no valid direct comparison.

The parallel biphenyl-tail interaction P3 is found for the first time in the series in *4*-OCB. The most significant contact is between the nitrogen of the cyano group of one molecule and a hydrogen on ring 2, adjacent to the oxygen, of 2.62 Å. However, because the two molecules lie at an angle of approximately 100 ° to one another, it is not possible for any 'real' interaction to take place between the biphenyl unit and the tail of the two molecules.

When considering how these interactions are likely to influence the liquid crystal properties of *4*-OCB, it is useful to refer back to Figure 5.2. It is seen that $T_{C\text{-}N}$ has risen a little from that of *3*-OCB and that $T_{I\text{-}N}$ is very close to $T_{C\text{-}I}$. Since it seems

clear that the formation of the nematic phase requires the presence of antiparallel dimers similar to interaction A3, it is not surprising that crystals of *4*-OCB melt to form the isotropic phase. In fact, since this cannot happen until the large parallel interaction (P4) is broken down, the higher melting point can be attributed largely to the strength of this interaction.

These interactions, and the lack of them, also help to explain the different packing arrangement adopted by *4*-OCB. This has the shortest tail which permits the parallel P3 interaction, and it is clear that the length of the tail prevents the formation of the A5 interaction (as does the shorter tail length in *3*-OCB), as this would result in an unfavourable interaction between the oxygen of both molecules. The tail length in *4*-, and *5*-OCB also appears to be unfavourable for the antiparallel A4 interaction. Its absence in these compounds is attributed to the lack of beneficial contacts to the cyanophenyl ring from hydrogens on the final carbon of the tail, which since *n* is even, points away from the phenyl ring in both cases. This interaction being stabilised for *6*- and *7*-OCB because the tail is now long enough for some weak N...H contacts to form with the cyano group.

5.2.5 4'-pentoxy-4-cyanobiphenyl (*5*-OCB)

5-OCB is the first compound in the *n*-OCB series which forms the nematic phase on melting the crystal as well as on cooling from the isotropic phase. This means that the crystalline phase is now a precursor to the nematic phase.

The crystal structure of *5*-OCB was determined by Mandal and Paul[15], and then later by Kravers et al.[26] Again the two structure determinations are essentially the same and it was that obtained by Mandal and Paul that was used in this study.

5-OCB crystallises with the space group $P2_1/n$ and has four molecules in the unit cell. This means that all molecules are crystallographically equivalent in the asymmetric unit. The dihedral angle of the biphenyl group is 0.82 ° in *5*-OCB. This indicates that

the molecules have adopted a favourable packing arrangement to overcome the preference of the biphenyl unit to have a dihedral angle of around 42°.[25] The energy required to enable this planar biphenyl arrangement is estimated at around 2 kJ mol^{-1}.[26] The crystal packing can be seen in Figure 5.21 where the molecules are extended with their biphenyl units parallel to the *ab*-plane.

Figure 5.21 Molecular packing of 5-OCB demonstrating how the molecules associate in dimers by both the cyano-cyano (A1) and the head-to-tail (A3) interactions.

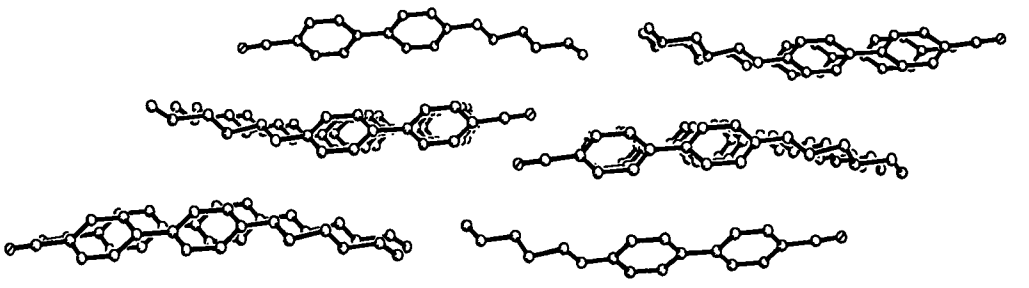

Mandal and Paul[15] observed that the most significant interaction in the crystal is the antiparallel cyano-cyano interaction between pairs of molecules related by an inversion centre. This is the interaction A1 as defined earlier. It is also proposed that because the interatomic distance in the nematic phase is close to the value of the crystal *b*-axis, the molecular stacking along the *c*-axis breaks down on melting the crystal. The dimers observed in the nematic phase (A3) could then be formed by a shift of the associated molecules with respect to each other along the crystal *a*-axis.

On examining Table 5.9, it is observed that *5*-OCB adopts the same interactions as were found for *3*-OCB but that two extra interactions now take place. These are the antiparallel biphenyl-tail interaction A5 (Figure 5.8) and the parallel biphenyl-tail interaction P2 (Figure 5.12).

The main difference between the packing of *3*- and *5*-OCB is that the alkoxy tail is two carbons longer in *5*-OCB. This results in an important change in the way the molecules fit together. In *3*-OCB the infinite stacks of cyano-cyano interactions were

explained in terms of the parallel interaction P5, and how that contributed to preventing overlap of cyano groups with phenyl rings as happens in *1*- and *2*-OCB. However, this was assisted in *3*-OCB by the contribution from the antiparallel interaction A3. In *3*-OCB, the alkoxy chain does not extend significantly further than the nitrogen from the cyano group of the other molecule, thereby helping to maintain an orderly packing (i.e. without imbrication). However, in *5*-OCB, the alkoxy chain does extend further than the nitrogen when the molecules adopt this packing arrangement. This forces the molecules to pack in a more imbricated fashion resulting in the reappearance of the interactions A5 and P2.

Before comparing the other interactions, it is worth discussing these two extra ones. The antiparallel biphenyl-tail interaction (A5) is significant in that *5*-OCB is the first compound in the *n*-OCB series which has an alkoxy tail long enough that the oxygen of one molecule does not lie over ring 2 of the other molecule, but now has contacts with the tail of the other molecule. The absence of this interaction in *3*- and *4*-OCB is attributed to unfavourable contacts between the oxygen atoms of the two molecules with no additional attractive interactions being made to compensate for this. The importance of this when considering liquid crystalline behaviour, is that there has been a reduction of the 'core-core' overlap which can be interpreted as the molecules moving towards forming distinct regions of aliphatic and hydrophilic character in the crystal (i.e. layers).

The parallel biphenyl-tail interaction (P2) is formed largely as a consequence of the interaction A5. Because the molecules interact in an imbricated fashion, molecules between layers are displaced with respect to one another along their long axis. This results in the formation of the interaction P2, which is a weak interaction, unlikely to be influential in liquid crystal behaviour.

Comparing the other interactions, the antiparallel cyano-cyano contact A1 is again similar to that found for *1*-, *2*- and *3*-OCB, in that it has a shortest N...H contact of 2.56 Å. This is consistent with the observations made in discussing *3*-OCB, when it was observed that these N...H contacts followed a slight odd-even effect. The head-

to-tail interaction (A3) differs from that found previously in that the biphenyl dihedral angle is now approximately 0°, and the nitrogen from the cyano group is able to make a relatively short contact of 2.83 Å with a hydrogen from the methyl group in the tail of the other molecule. The tail-tail interaction (A7) is again unlikely to be significant in liquid crystalline behaviour and occurs more as a consequence of the parallel interaction P5.

Of the parallel contacts, the large parallel interaction P5 is similar to that observed in *3*-OCB. It is interesting to observe that interaction P4 was not found in *5*-OCB. This is again attributed to the fact that it is only the even numbered carbons in the alkoxy tail that appear to contribute actively to the strength of the interaction. Meanwhile, the interaction P5 only occurs when there is an odd number of carbons in the tail.

In considering how the nematic phase is formed on melting from the crystal, these observations agree with the conclusions of Mandal and Paul above. The head-to-tail and biphenyl-tail interactions may break down and the molecules form dimers by sliding over one another on melting. Alternatively, and more likely, is that it is the cyano-cyano contacts which break down and the head-to-tail contacts which persist, a process which would result in less molecular rearrangement. This would require the head-to-tail interaction to be stronger than the cyano-cyano interaction. However, the cyano-cyano contact, although more significant in terms of the closeness of the interaction, involves relatively few contacts, whereas the head-to-tail interaction involves a lot of slightly more distant contacts. This may be particularly important in *5*-OCB because, in the crystal, the cyano group interacts with the whole alkoxy tail of the other molecule. It is therefore likely that nematic behaviour on melting is due largely to this interaction and the fact that the overall crystal packing is of an imbricated nature.

5.2.6 4'-hexyloxy-4-cyanobiphenyl (*6*-OCB)

Like *5*-OCB, *6*-OCB forms the nematic phase on melting from the crystalline phase as well as on cooling from the isotropic phase. The crystal structure of *6*-OCB was determined by Hori et al.[16] and the hydrogen atoms were added in idealised positions using the program XP.[22]

6-OCB crystallises with the space group $P2_1/a$ and has eight molecules in the unit cell. This means there are two crystallographically independent molecules in the asymmetric unit (the dihedral angles of the biphenyl groups being 36° and 26°). The crystal packing can be seen in Figure 5.22, where the molecules are arranged in a parallel fashion and stack along the *b*-axis.

Figure 5.22 Crystal packing of 6-OCB demonstrating the molecules stacking along the b-axis. Again, examples of both the cyano-cyano (A1) and head-to-tail (A3) interactions can be seen.

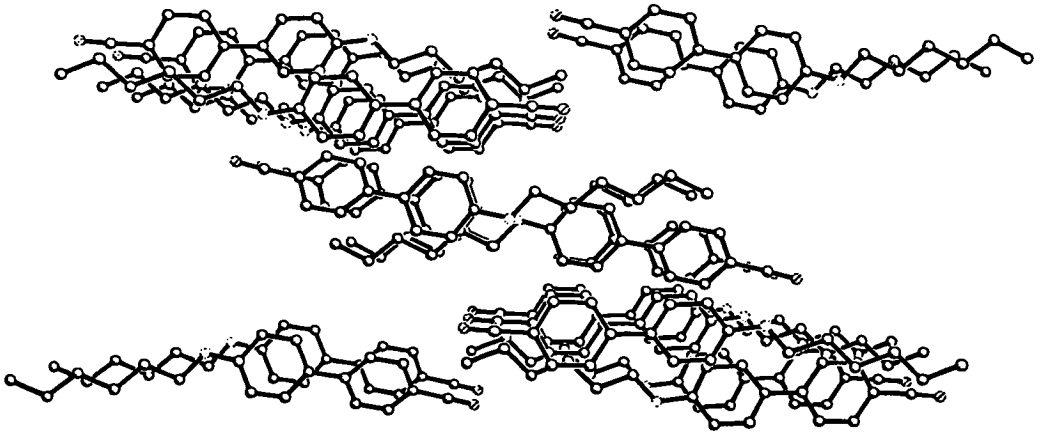

K Hori et al.[16] observed that unequivalent molecules (A, B) interact to form the antiparallel cyano-cyano contacts (A1), and also that there is a short O...O distance (3.87 Å) between members of the second set of molecules (B), the pair of molecules being related by an inversion centre. This contact is actually part of the antiparallel biphenyl-tail interaction A5.

On examining Table 5.9, it is clear that molecules of *6*-OCB experience all the observed interactions except for the antiparallel cyano-phenyl contacts (A2), the biphenyl-tail interaction (P2) and the large parallel interaction (P5).

Comparing these interactions with those observed for other molecules, the cyano-cyano contacts (A1) are formed between crystallographically unequivalent molecules (A, B) and follow the odd-even trend observed previously with the closest N...H contact for *6*-OCB is 2.84 Å. The head-to-tail interaction (A3) also occurs between molecules A and B and differs from that found previously as there is less biphenyl overlap than was found in *5*-OCB. This is reflected in the shortest contact to the nitrogen being from H(16) at 2.88 Å.

The ring 2-ring 2 interaction (A4) is similar to that observed in *2*-OCB, in that the oxygen again reaches over ring 2 of the other molecule, the closest contact this time being 2.82 Å with a hydrogen on ring 2 adjacent to ring 1 of the other molecule. The main difference in this interaction from that observed in *2*-OCB is that the nitrogen is now able to interact with the tail of the other molecule.

Next is the biphenyl-tail interaction (A5). As mentioned above, these contacts only involve molecule B. This is very similar to what is observed in *5*-OCB, with the O...O contact now slightly larger.

The large tail-tail interaction A6 (Figure 5.9) is observed for the first time in *6*-OCB. This involves a hydrogen from the terminal methyl group of one molecule being in contact with a hydrogen adjacent to the oxygen on ring 2 of the other. This interaction only involves molecule A. The main significance of this interaction is that it involves many weak H...H contacts between the tails of the molecules, and results in a dimer with maximum dipole separation. It is this type of interaction which could result in the layering of the crystal into regions of hydrophilic and aliphatic character.

The final antiparallel interaction is the tail-tail interaction (A7). This is similar to that observed in *3*- and *5*-OCB, in that the shortest contact is between hydrogens on the second last carbon of the alkoxy tail. In *6*-OCB this distance is 2.57 Å.

The first parallel interaction is the cyano-tail interaction (P1). This occurs between the molecules A and B and again follows the observed trend with the closest N...H contact being 3.12 Å.

The parallel biphenyl-tail interaction (P3) is only really observed in *6*-OCB. It is recorded in Table 5.9 as being present for *4*-OCB, but in *4*-OCB the molecules interact at such an angle that this cannot really count. In *6*-OCB, the biphenyl unit of one molecule lies right along the tail of another, with the cyano group just reaching ring 2. This interaction occurs between pairs of B molecules and between A and B molecules, but not between pairs of A molecules. Curiously, because the biphenyl unit lies along the tail of another molecule, the cyano groups no longer align parallel to the rings, as is seen in other compounds in the series (excluding *4*-OCB). The angle, as a result of this interaction, is around 25 ° (Figure 5.23).

The final interaction observed in *6*-OCB is the large parallel interaction (P4). Again, this does not change significantly from one compound to another, but in *6*-OCB there is an extra H...H contact between a hydrogen on C(19) and a hydrogen on C(16).

When considering how *6*-OCB will melt to form the nematic phase, a very similar argument to that used for *5*-OCB is applicable. Broadly speaking, the crystal packing of *6*-OCB is very similar to that of *5*-OCB when viewed perpendicular to the *ac* plane (Figure 5.21 and Figure 5.22). This is not altogether unexpected since both compounds undergo transitions with approximately the same ΔH (28.9 kJ mol^{-1} for *5*-OCB and 29.7 kJ mol^{-1} for *6*-OCB) on melting to form their nematic phases, and the structural order in the nematic phases of *5*- and *6*-OCB is very similar.

Figure 5.23 Crystal packing of *6*-OCB demonstrating that although *6*-OCB packs in a similar manner to the other compounds in the series, it is also similar to *4*-OCB in that the sheets of molecules are no longer parallel.

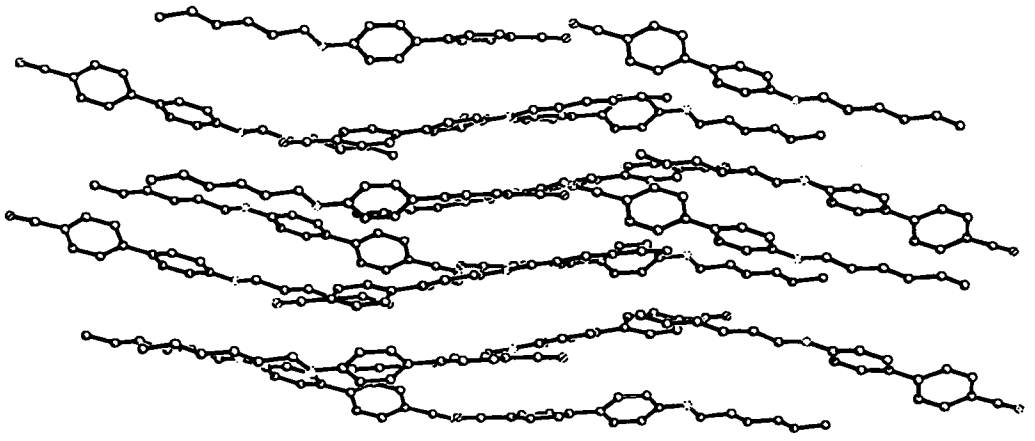

It is therefore assumed that *6*-OCB melts by breaking down the contacts perpendicular to the cyano-cyano dimers in Figure 5.22. As in *5*-OCB, it is a little unclear whether the dominant dimers will come from the cyano-cyano (A1) interactions or the head-to-tail (A3) interactions. As before, although the interaction A1 involves a few relatively strong contacts, the interaction A3 comprises many more, slightly weaker ones. The A3 interaction must, however, be favoured because this involves much less rearrangement of the molecules on melting.

5.2.7 4'-septoxy-4-cyanobiphenyl (*7*-OCB)

Like *5*- and *6*-OCB, *7*-OCB forms the nematic phase on melting from the crystalline phase as well as on cooling from the isotropic phase. The crystal structure of *7*-OCB was determined by Hori et al.[16] and the hydrogen atoms were added in idealised positions using the program XP.[22]

7-OCB crystallises with the space group $P\bar{1}$ and has four molecules in the unit cell. This means that there are two crystallographically independent molecules in the asymmetric unit (the biphenyl moieties being 37 ° and 40 °). The crystal packing can

be seen in Figure 5.24 where the molecules arrange themselves in a 'smectic-like' layer structure. Each layer being parallel to the *ac*-plane.

Figure 5.24 Crystal packing of 7-OCB showing the 'smectic-like' layer formation. N.B. Only every other layer is shown for clarity.

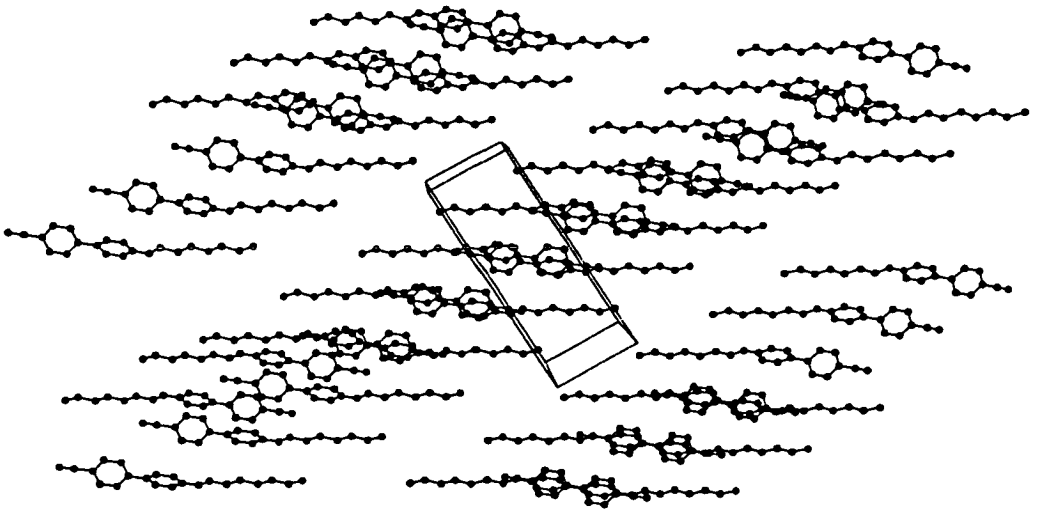

Figure 5.25 demonstrates the packing within each layer by showing two parallel sheets of molecules. Within each sheet, the molecules interact mainly via the cyano-cyano interaction, with the cyano-phenyl and the head-to-tail interactions occurring between sheets.

Figure 5.25 Crystal packing of 7-OCB. This view is perpendicular to two sheets of molecules which contribute to form the layers. The labeled molecules are all in the same sheet.

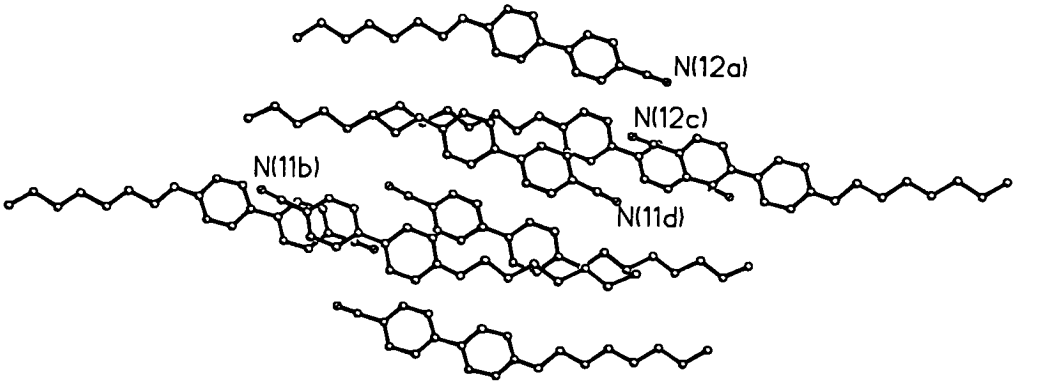

K Hori et al.[16] found that inequivalent molecules (A, B) interact to form the antiparallel cyano-cyano contacts (A1). It is these dimers which then arrange themselves into the 'smectic-like' layer structure observed in Figure 5.24.

On referring to Table 5.9, it is seen that *7*-OCB molecules experience all the interactions listed except for the antiparallel tail-tail interaction (A7), the cyano-tail interaction (P1) and the biphenyl-tail interaction (P3). The omission of these can, however, readily be explained.

The cyano-tail interaction (P1) is not observed because, as a result of the molecules packing in layers via the A1 interaction, the cyano group now tends to be either too far away for an N...H contact to be observed, or the cyanophenyl and the tail overlap to result in the parallel P2 interaction. Although this is a surprising omission from the intermolecular contacts, it does fit in with the trend that, as the alkoxy tail becomes longer, the N...H contact increases. Similarly, the antiparallel interaction A7 is too distant to be observed in the table of closest intermolecular contacts used to determine these interactions.

Finally, the interaction P3 would involve biphenyl-tail overlap which is not possible in the 'smectic-like' layer structure the molecules adopt.

On comparing the interactions which are present with those found previously, the antiparallel cyano-cyano interaction (A1) has a shortest N...H contact at 2.49 Å. This is slightly shorter than that observed in other compounds in the series, but again follows the odd-even trend which is observed.

Apart from *1*- and *2*-OCB, *7*-OCB is the only compound in which the cyano-phenyl interaction (A2) is observed. This takes place between the sheets of molecules shown in Figure 5.25. It is presumably this contact which stabilises the formation of the 'smectic-like' layer structure in the crystal. This may occur in *7*-OCB for exactly the same reason as it occurs in *1*- and *2*-OCB. In the small molecules the tail was about the same length as a phenyl ring. This results in packing where two molecules lying

antiparallel to one another can be displaced by about one phenyl ring along their long axis. Because of this displacement, the molecules can adopt the cyano-phenyl interaction (A2) instead of the cyano-cyano interaction (A1) as seen in other molecules.

The antiparallel head-to-tail interaction (A3) is prominent on looking at the molecular packing (Figure 5.25) but differs from that observed in *5*- and *6*-OCB in that there are now no contacts between the cyano group and the alkoxy tail. The angle between the two interacting rings, ring 1 and ring 2 is 143.1 °.

The antiparallel ring 2-ring 2 interaction (A4) differs from those found in previous compounds in that there are no contacts involving the oxygen atom. This is because the interaction takes place between two molecules related by an inversion centre, so that the two ring 2s are parallel to one another. The shortest contact observed is 2.40 Å between a hydrogen adjacent to the cyano group on ring 1, and a hydrogen of C(16) of the tail.

The biphenyl-tail interaction (A5) continues the trend previously observed in that the closest oxygen contact is 3.16 Å from a hydrogen on C(15). This is a significant achievement in terms of molecular packing because there is now no contact at all between the cores of the two molecules. Just as importantly, the molecules are separated so the cyano groups of the molecules participate in antiparallel cyano-cyano contacts (A1) with molecules in the 'next layer'. The major significance of this is that the addition of one more carbon to the alkoxy chain (*8*-OCB) ought to result in a further separation of the cores in the interaction A5 (perhaps resulting in A6 instead) and make it likely that the cyano-cyano interaction observed in *7*-OCB would be replaced in *8*-OCB by a cyano-phenyl interaction. This would give a much more distinct layer structure to the crystal and, assuming that it is the head-to-tail interaction (A3) which is predominant in liquid crystal formation, would allow the smectic phase to be formed on melting. It is this that is believed to be responsible for the smectic phase observed in 8-OCB. However, at higher temperatures the tails of the molecules are not quite long enough to support these dimers (i.e. insufficient

interlayer penetration by the tails) and the smectic layer structure is broken down to form the nematic phase as the molecules rearrange to achieve greater tail-tail and biphenyl-tail contacts, resulting in the more imbricated arrangement associated with the nematic phase.

The large tail-tail interaction (A6) is similar to that found in *6*-OCB, with the H...H contact between the methyl and the hydrogen on ring 2 now being much shorter at 2.70 Å. The extra strength of this interaction must be influential in formation of the layer structure of the crystal.

Of the parallel interactions, the biphenyl-tail interaction (P2) is similar to that found in *5*-OCB and is again attributed to the imbricated mode of packing.

The large parallel interaction P4 is again influential in keeping the molecules aligned and will be stronger than observed in previous molecules due to the extra carbon in the alkoxy tail.

As mentioned above, this type of crystal packing is more like what would be expected for a smectic liquid crystal than a nematic one. It is not surprising, therefore, on looking at Figure 5.2, to observe that *7*-OCB is the largest compound in the *n*-OCB series which does not exhibit smectic behaviour. The reason for *7*-OCB remaining a nematic liquid crystal is that, although the crystal phase exhibits a much more pronounced layer structure, the molecules/dimers lie at an angle of 64 ° to the plane of the layer. This means there is still a large degree of imbrication within each layer. The layers consist of sheets of dimers related by the cyano-cyano (A1) dimer but similar dimers in adjacent sheets are displaced so that cyano-phenyl (A2) and head-to-tail (A3) interactions occur between sheets. On melting, it is these which are dominant and result in the nematic behaviour of *7*-OCB.

5.3 Conclusion

It is clear that this analysis has given a further insight into how molecules from the *n*-OCB series interact to form the nematic and smectic mesophases.

For the first four compounds in the series, only monotropic behaviour is observed. This can be attributed to the lack of imbrication in the crystal structure and to the fact that all molecules are bound tightly in the crystal by the strong polar interactions.

The next three compounds exhibit nematic behaviour on melting from the crystal. This is explained in terms of imbrication of the molecular packing which results in molecules being bound together by both the strong polar interactions, as previously, and the weaker van der Waals contacts. These weaker contacts can break down more easily on melting and the nematic phase is formed by 'dimers' associated by the head-to-tail (A3) interaction.

The next two compounds in the series melt to form the smectic phase, but are unstable so that on continued warming the compound undergoes a further phase change to the nematic phase. Although no crystal structures of these compounds have been obtained to date, it is logical that they will pack in a similar fashion to 7-OCB. An extra carbon in the alkoxy tail may result in a slightly larger biphenyl overlap in the sheets of molecules seen in 7-OCB so that interactions A1 and A2 occur. By introducing the A2 type of interaction, the dimers formed in the sheets of molecules will be more tightly bound and therefore may persist on melting to enable the smectic phase to form. On further heating, these will be broken down and the liquid crystal reverts to the nematic phase.

The remaining compounds in the series form only the smectic phase. Following the arguments above, it is reasonable to assume that the molecules lying within the sheets will adopt a still larger biphenyl overlap (the addition of two carbons to the tail may displace the biphenyl cores by another phenyl ring). This can result in dimers forming which involve both the A2 and A3 interactions as is seen between sheets. Because

these dimers will now be as strong in the sheets of molecules as they are between them, the smectic phase is formed and persists until a sufficient temperature is reached for these interactions to be broken down and the isotropic phase is formed.

References

[1] W.Haase, Z.X.Fan and H.J.Müller, J.Chem. Phys., 89(5), (1988), 3317

[2] A.J.Leadbetter, R.M.Richardson and C.N.Colling, J.Phys. (Paris) Colloq., 1, (1975), 37

[3] G.V.Vani and K.Vijayan, Acta. Cryst., B33, (1977), 2236

[4] R.F.Bryan, P.Forcier and R.W.Miller, J. Chem. Soc. - Perkin II, (1978), 368

[5] S.Diele, P.Brand and H.Sackmann, Mol. Cryst. Liq. Cryst., 16, (1972), 105

[6] A.J.Leadbetter, J.C.Frost, J.P.Gaughan, G.W.Gray and A.Mosley, J.Phys. (Paris) Colloq., 40, (1979),375

[7] A.J.Leadbetter, J.L.A.Durrant and M.Rugman, Mol. Cryst. Liq. Cryst. (letters), 34, (1977), 231

[8] S.Torza and P.E.Cladis, Phys. Rev. Letts., 32, (1974), 997

[9] P.E.Cladis, R.K.Bogardus, W.B.Daniels and G.N.Taylor, Phys. Rev. Lett., 39(11), (1977), 720

[10] D.Guillon and A Skoulios, Mol. Cryst. Liq. Cryst., 38, (1977), 31

[11] W.Haase, H.Paulus and R.Pendzialek, Mol. Cryst. Liq. Cryst., 100, (1983), 211

[12] S.Sinton and A.Pines, Chem. Phys. Lett., 76, (1980), 263

[13] I.Ono and S.Kondo, Bull. Chem. Soc. Jpn., 66, (1993), 633

[14] L.Walz, H.Paulus and W.Haase, Z. Krist., 180, (1987), 97

[15] P.Mandal and S.Paul, Mol. Cryst. Liq. Cryst., 131, (1985), 223

[16] K.Hori, Y.Koma, A.Uchida and Y.Ohashi, Mol. Cryst. Liq. Cryst., 225, (1993), 97

[17] Catologue data, BDH Chemicals Ltd.

[18] S.Macelia, J. Chem. Phys., 60, (1974), 3599

[19].G.M.Sheldrick, SHELX-86, program of crystal-structure solution, University of Göttingen, Germany, (1986)

[20] G.M.Sheldrick, SHELX-93, program of crystal-structure solution, University of Göttingen, Germany, (1986)

[21] R.O.Gould and P.Taylor, CALC. program for molecular geometry calculations, University of Edinburgh, Scotland, (1985)

[22] XP, interactive molecular graphics v4.3 for MSDOS, Siemans Analytical Xray Inst. Inc., (1992)

[23] A.De Vries, Mol. Cryst. Liq. Cryst., 10, (1970), 31

[24] P.Meurisse, F.Laupretreand, C.Noel, Mol. Cryst. Liq. Cryst. (Lett.), 110 (1984), 41

[25] C.P.Brock and R.P.Minton, J. Amer. Chem. Soc., 111(13), (1989), 4586

[26] M.A.Kravers, V.I.Kulishov, A.J.Polishchuk and A.S.Tolochko, Sov. Phys. Crystallogr., 37(3), (1992), 375

Chapter 6

A Study of Silyl Containing Compounds in the Liquid Crystal Environment

6 Introduction

In order to examine the solvent dependence on the structure of silyl containing compounds in LCNMR studies, the structures of a series of compounds of the general formula SiH_3X have been studied, where X = Br, Cl, I, F, CN and CH_3.

The solvents chosen for this study were selected to be as chemically different from one another as possible. This was so that any solute structural variations observed between liquid crystal solvents would be highlighted. The liquid crystals chosen are detailed in Table 6.1

Table 6.1 Liquid crystals used in this work

E5 / E7	eutectic mixtures of alkyl and alkoxy cyano biphenyl compounds (*1*-OCB, *8*-OCB,*4*-CB and *7*-CB)
ZLI 1167	a mixture of cyano cyclohexyls (4'-n-propyl/pentyl/heptyl-*trans,trans*-bicyclohexyl-4'-carbonitriles)[12]
ZLI 4792	a mixture containing super fluorinated compounds
ZLI 3086	a mixture containing only non-polar molecules
ZLI 1083	a mixture of esters
Mixt. 1	84.3 % wt E7 + 15.7 % wt ZLI 1167

All of the above were purchased from BDH Ltd. BDH declined to give any further information on the composition of ZLI 4792, ZLI 3086 and ZLI 1083. Other liquid crystals including EBBA (p-ethoxybenzylidene-p-n-butylaniline) and MBBA (p-methoxybenzylidene-p-n-butylaniline) and mixtures involving these and ZLI 1167 were also tried, but found to react with the solutes used.

In the analysis of methyl iodide by Jokisaari and Hiltunen[1], it was observed that the sample colour changed after a day or so when EBBA was used as liquid crystal solvent. It is likely, therefore, that some slow reaction takes place between the liquid

crystal and the methyl iodide solute. It is not surprising then, that the more reactive silyl compounds react more quickly with the liquid crystal solvent. Samples involving EBBA and MBBA were observed to discolour immediately on warming to room temperature. The sample changing from a colourless mixture to a lumpy yellowish brown mixture.

As was highlighted in chapter 2, one technique which has recently been used with some success to 'probe' the liquid crystal environment in an NMR experiment, is the observance of the distortions a methane molecule undergoes in the same tube as the molecule being studied. The apparent 'deformation' of the methane from tetrahedral symmetry being a measure of how much the solute molecule will itself be distorted by the orienting forces of the liquid crystal.

In this study, it was decided to adopt a similar approach, but to use silane in place of the methane as a 'deformation probe'. The reason for doing so being that silane is much more chemically similar to the silyl compounds being studied than is methane, and it was hoped that the deformations observed in the silane would be more closely correlated with distortions in the silyl compounds being observed.

The silane used in these experiments was prepared in the following manner:

$$SiCl_4 + 4\ LiAlH_4 \rightarrow SiH_4$$

Tetrachlorosilane (1 g) (dried over molecular sieve) in dibutylether (25 ml) (dried over sodium) were placed in a pressure equalising dropping funnel. This was added dropwise to a suspension of lithium aluminium hydride (1 g) in dibutylether (100 ml) in a 3-necked flask. Gaseous products were passed through a -78 ° C (acetone / CO_2) condenser via a swivel link attachment to a vacuum line, and collected using four liquid nitrogen traps in series. The reaction being carried out under nitrogen with continual spiral monitoring to ensure there is no pressure build up. Initially, the nitrogen pressure was 25 cm / Hg, but as the reaction progressed the pressure was

bled to an equilibrium pressure of around 10 cm/Hg. Products were purified by repeated fractionation through a -160 ° C (40 - 60 pet. ether) slush bath. Purity being monitored by FT-IR spectroscopy.

6.1 Silyl Bromide.

6.1.1 Experimental

Silyl bromide was prepared in the following manner.

$$C_{10}H_{12} + 4\ Br_2 \rightarrow C_{10}H_8Br_4 + 4\ HBr$$

$$Si(C_6H_5)H_3 + HBr \rightarrow SiH_3Br + C_6H_6$$

Tetrahydranapthalene (150 ml) was placed in a 3-necked flask fitted with a pressure equalising dropping funnel and a -78 ° C (acetone/CO_2) condenser. The condenser has a swivel link attached to it, through which gaseous products can be passed to a vacuum line and collected using four liquid nitrogen traps in series. Care was taken throughout in ensuring that all apparatus and reagents were dry, as the presence of water greatly reduces the yield of gaseous hydrogen bromide.

Reaction is carried out by adding the bromine dropwise from the pressure equalising dropping funnel. The hydrogen bromide produced is purified by repeated fractionation through a -120 ° C (diethyl ether) slush bath.

The hydrogen bromide (120 mmol) was then added to phenylsilane (55-60 mmol) at 77 K in a bulb ampoule (250 ml). The ampoule placed in a -78 ° C (acetone / CO_2) bath and left in a fume cupboard overnight. The reaction is observed to have taken place when the benzene which is formed appears as a solid in the bulb.

The gaseous silyl bromide was then transferred to a vacuum line and purified. The more volatile component being dealt with first. This was achieved by fractionating the reaction mixture at -120 ° C (diethyl ether). Both fractions are checked by FT-IR spectroscopy but only the hydrogen bromide passed the -120 ° C bath. The benzene was then removed by fractionating at -78 ° C and finally any traces of hydrogen bromide are removed by again fractionating at -120 ° C.

Sample tubes were prepared using a variety of liquid crystals, and ^{1}H spectra were recorded using a BRUKER AL250 spectrometer at Edinburgh University. All experiments were carried out at 298 K except for the sample in the solvent ZLI 1167 which had to be run at 310 K to prevent the solvent-solute mixture from solidifying. This sample was also analysed without spinning the NMR tube as ZLI 1167 orients perpendicular to the applied magnetic field.

6.1.2 Analysis

All spectra were first order and the silyl bromide contribution consists of a strong triplet arising from the direct dipolar coupling between the hydrogen nuclei, and a much weaker triplet of doublets arising from coupling to the much lower abundance ^{29}Si.

The two direct couplings (D_{ij}) can be taken directly from the spectra because the ^{1}H peaks are separated by a coupling of 3 D_{HH} and the ^{29}Si satellites are separated by 2 D_{SiH} + J_{SiH}. Some example spectra are given in Appendix B.

The silane spectrum consists of a singlet due to the ^{1}H coupling and again a weak doublet due to the coupling to the lower abundance ^{29}Si. As above, the ^{29}Si satellites are separated by $2D_{SiH} + J_{SiH}$.

Attempts to measure the value of the indirect couplings J_{SiH} of both silyl bromide and silane by recording an isotropic spectra of each sample were unsuccessful because in many cases the peaks arising from the liquid crystal masked the much weaker silyl peaks, and in some cases it appeared that the silyl compounds may have decomposed. A value of J_{SiH} = -235.7 (6) Hz for silyl bromide and J_{SiH} = -203.0 (6) Hz for silane was obtained in liquid crystal ZLI 1167. These are in agreement with values of -235 and -202.99 Hz used by Brookman[2]

It was found, however, from calculating the structures of silyl fluoride and silyl cyanide, that there is a solvent dependence on the indirect couplings. There was insufficient time to obtain the isotropic spectra of all the compounds studied in each different solvent, but the indirect couplings were instead predicted on the basis of the chemical shifts of the silyl compounds in different solvents (see page 145). Therefore, the value J_{SiH} of silyl bromide dissolved in the solvents ZLI 4792 and ZLI 3086 were taken as -240.5 Hz and -240.9 Hz respectively.

At this point there is still some ambiguity concerning the sign of the two couplings D_{HH} and D_{SiH}. This is resolved on structural grounds as it turns out that the ratio of $\frac{D_{SiH}}{D_{HH}}$ must be of the order of -0.65 for a reasonable structure to be obtained. This allows the sign of the D_{SiH}, and hence the sign of the D_{HH} coupling to be fixed. The direct couplings obtained are presented in Table 6.2.

Table 6.2 Experimental dipolar couplings for Silyl Bromide and Silane (Hz)

Solvent	D_{HH}	D_{SiH}	D_{SiH} (SiH_4)
ZLI 1167	-487.62 (19)	332.83 (78)	1.11 (38)
ZLI 3086	110.25 (18)	-65.35 (77)	1.64 (37)
ZLI 4792	351.45 (18)	-221.15 (77)	-0.20 (37)
ZLI 1083	853.28 (20)	-585.41 (80)	-1.76 (40)*
Mixt. 1	696.13 (20)	-490.32 (80)	-0.80 (40)
E 7	712.50 (20)	-501.84 (80)	-0.82 (40)

* This value of D_{SiH} for silane was obtained in a separate experiment.

The next step was to apply vibrational corrections to the dipolar couplings of silyl bromide. This was done using the ab initio force field calculated by Schneider and Thiel[3]. The covariance matrix required by the program BMGV[4], to calculate the harmonic corrections to the dipolar couplings, was derived from the force field using the program ASYM20[5]. The vibrationally corrected data thereby obtained are presented in Table 6.3.

Table 6.3 Vibrationally corrected dipolar couplings (Hz)

Solvent	D_{HH}	D_{SiH}
ZLI 1167	-498.36 (109)	347.82 (169)
ZLI 3086	112.68 (30)	-68.29 (103)
ZLI 4792	359.19 (79)	-231.11 (161)
ZLI 1083	872.08 (189)	-611.78 (276)
Mixt. 1	711.46 (155)	-512.41 (235)
E 7	728.19 (158)	-524.44 (240)

N.B. Vibrational corrections are 1.02203*D_{HH} and 1.04504*D_{SiH}.

The errors quoted for the vibrationally corrected dipolar couplings are 1 e.s.d. and have been calculated in such a way that both the uncertainty in the experimental line frequencies and the uncertainty in the vibrational corrections have been taken into account. This is done as follows :

1 e.s.d. = SQRT((uncertainty in uncorrected D_{ij})^2 + (10 % vibrational correction)^2)

Next the structure of silyl bromide in these different solvents is calculated. Because of the need to determine the orientation parameter in each case, it is only possible to determine one structural parameter per molecule. The most sensible structural parameter to determine is the HSiH angle, because it is unlikely that the SiH bond length will vary significantly between liquid crystal solvents, or between gas phase and solution phase.

The bond angles were calculated using the equations:

$$\left(\frac{r_{HH}}{r_{SiH}}\right)^5 - 2\left(\frac{r_{HH}}{r_{SiH}}\right)^3 - \frac{D_{SiH}}{D_{HH}}\frac{\gamma_H}{\gamma_{Si}} = 0, \qquad \text{Eq. 6.1}$$

$$\text{and } HSiH = 2\sin^{-1}\left(\frac{1}{2}\frac{r_{HH}}{r_{SiH}}\right) \qquad \text{Eq. 6.2}$$

These are derived from Equation 2.1 and the geometry of the silyl group.[2,30] This leads to the final values given in Table 6.4

Table 6.4 Final HSiH angles from vibrationally corrected data

Solvent	D_{SiH} / D_{HH}	HSiH (deg)	D_{SiH} (SiH_4) / Hz
ZLI 1167	-0.698 (5)	112.45 (12)	1.11 (38)
ZLI 3086	-0.606 (11)	110.20 (28)	1.64 (37)
ZLI 4792	-0.643 (6)	111.12 (38)	-0.20 (37)
ZLI 1083	-0.702 (5)	112.56 (12)	-1.76 (40)
Mixt 1	-0.720 (5)	112.98 (12)	-0.80 (40)
E 7	-0.720 (5)	112.98 (12)	-0.82 (40)

It is evident that the six calculated structures do not agree within experimental error. A clearer comparison of the silyl geometry is given in Figure 6.1 where the HSiH angle is plotted against the D_{SiH} coupling observed in silane. This also demonstrates that the HSiH angle and the observed coupling of silane are not strongly correlated to one another for these samples.

Figure 6.1 Plot of HSiH angle versus silane coupling (D_{SiH}) for SiH_3Br

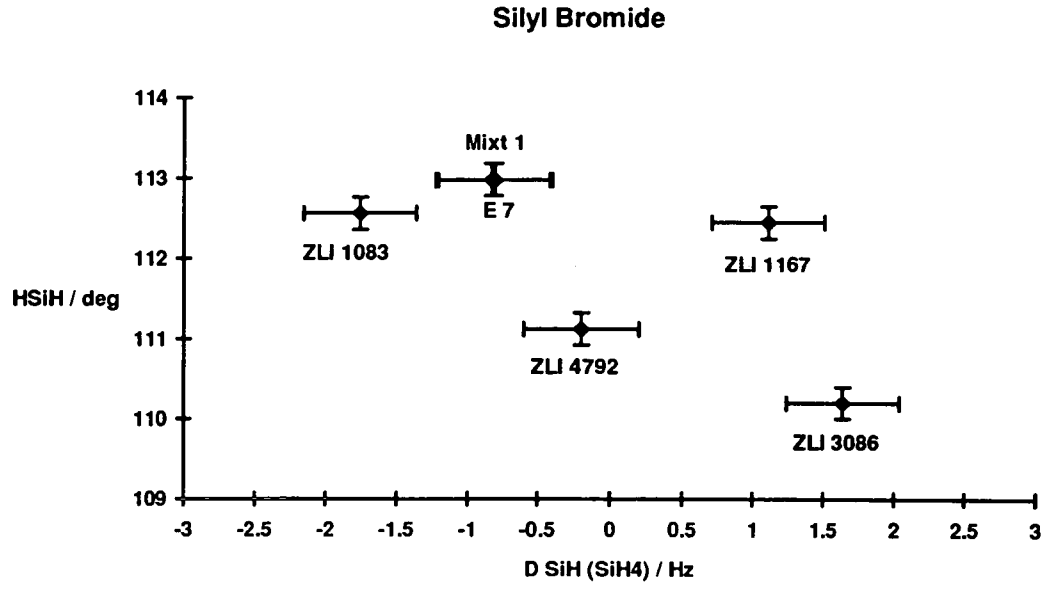

If the silane is to be used as a probe in the same manner as methane was used previously[1], then it is expected that the solvent giving rise to the silane coupling closest to zero should lead to the HSiH angle closest in agreement with that found in the gas phase. This is the sample recorded in the liquid crystal solvent ZLI 4792 with a silane D_{SiH} coupling of -0.20 (37) Hz, and an HSiH angle of 111.12 (38)°. This can be compared to the values of 111.0° and 110.4° for the r_s and r_0 structures obtained by Kewley et al.[6] and the r_o value 110.7° obtained by Duncan et al.[7]. It is clear, therefore, that the value obtained in liquid crystal ZLI 3086 of 110.20 (28)° is in closer agreement with the r_0 structure. This does however have a relatively large D_{SiH} silane coupling of 1.64 (37) Hz. The correlation between the coupling of silane and the resulting HSiH angle is further discussed in Chapter 7.

6.2 Silyl Chloride

6.2.1 Experimental

Silyl chloride was prepared in the following manner:

$SiH_3Br + HgCl_2 \rightarrow SiH_3Cl$

Silyl bromide (5-10 mmol) was passed repeatedly through a mercury chloride ($HgCl_2$) column and the resulting product monitored by FT-IR spectrometry. Once all the silyl bromide had reacted, any impurity, hydrogen chloride or disiloxane, must be removed. This was achieved by fractionating at -140 ° C (40-60 pet ether) to remove the hydrogen chloride. Disiloxane is inseparable from silyl chloride and can only be removed by converting silyl chloride to trisilylamine.

$3\ SiH_3Cl + 4\ NH_3 \rightarrow (SiH_3)_3N + 3\ NH_4Cl$

Reaction was carried out using a double-bulb ampoule. The one used had a large bulb (1000 ml) and a smaller bulb (250 ml) with the bulbs being separated from one another by a greaseless tap.

Ammonia (13 mmol) was placed in the smaller bulb and silyl chloride (10 mmol) in the larger bulb. Both bulbs were allowed to warm to room temperature before the connecting tap was opened very slightly and a white cloud of ammonium chloride formed in the larger bulb. The two reagents were allowed to react as slowly as possible and then left overnight. The impurities, silane and disiloxane, were removed by fractionating at -96 ° C (toluene).

To get back to the silyl chloride, the trisilylamine was reacted with hydrogen chloride:

$(SiH_3)_3N + 4\ HCl \rightarrow 3\ SiH_3Cl + NH_4Cl$

Reaction was again carried out using the double-bulb apparatus, the hydrogen chloride being placed in the smaller bulb and the trisilylamine in the larger bulb. Excess hydrogen chloride was removed by fractionating at -140 ° C (40-60 pet. ether) and purity confirmed by FT-IR spectrometry.

NMR samples were prepared with the same liquid crystals as used in the case of silyl bromide. However, the liquid crystal, Mixt 1, was omitted since for silyl bromide no significant differences were found between the results obtained in E 7 and Mixt. 1. ^1H spectra were recorded using a BRUKER AL250 spectrometer at Edinburgh University. As before, all experiments were carried out at 298 K except for the sample involving ZLI 1167 which was analysed at 310 K and without spinning of the tube.

6.2.2 Analysis

Because of the strong structural and chemical similarities between silyl bromide and silyl chloride, the spectra obtained for both compounds are almost identical in appearance. The D_{HH} and D_{SiH} couplings for silyl chloride were therefore taken directly from the spectra, as was the D_{SiH} coupling of silane (see Appendix B).

The values used for the indirect coupling J_{SiH} of silyl chloride are given below. As in the case of silyl bromide, it was not possible to obtain isotropic spectra in all solvents so the indirect couplings have been estimated by taking into consideration the chemical shift of silyl chloride in the various solvents used (see page 145). The values used are -238.1 Hz for liquid crystal ZLI 4792 , -238.4 Hz for ZLI 3086 and -240 Hz for E7, Mixt 1 and ZLI 1083. The indirect coupling for silane was assumed not to vary between solvents and a value of -203.0 Hz was used.

The signs of the direct couplings were assigned using the same arguments as used for silyl bromide. The direct couplings obtained are presented in Table 6.5.

The dipolar couplings of silyl chloride are then vibrationally corrected using the program BMGV. This is done using the covariance matrix obtained from ASYM20 with the harmonic force field of silyl chloride calculated by Schneider and Thiel.[3] The vibrationally corrected data obtained are presented in Table 6.6.

Table 6.5 Experimental dipolar couplings for Silyl Chloride and Silane (Hz)

Solvent	D_{HH}	D_{SiH}	D_{SiH} (SiH_4)
ZLI 1167	-401.78 (13)	273.22 (70)	1.13 (30)
ZLI 3086	92.05 (18)	-53.70 (77)	1.95 (37)
ZLI 4792	304.01 (18)	-190.31 (77)	-0.18 (37)
ZLI 1083	747.24 (30)	-513.32 (95)	-1.76 (40)*
E 7	617.88 (18)	-425.46 (77)	-0.65 (37)

* This value of D_{SiH} silane was obtained in a separate experiment.

Table 6.6 Vibrationally corrected dipolar couplings (Hz)

Solvent	D_{HH}	D_{SiH}
ZLI 1167	-409.28 (76)	284.39 (131)
ZLI 3086	93.77 (25)	-55.90 (80)
ZLI 4792	309.70 (60)	-198.10 (110)
ZLI 1083	761.23 (143)	-534.31 (231)
E 7	629.45 (117)	-442.86 (191)

N.B. Vibrational corrections are $1.0187*D_{HH}$ and $1.0409*D_{SiH}$

The errors again take into account both the uncertainty in the line frequencies of the experimental spectra and the vibrational corrections (see page 130).

As before, due of the lack of information obtained from the dipolar couplings, the only structural parameter that has been calculated is the HSiH angle. This was again done using equations 6.1 and 6.2 (page 131) as in the case of silyl bromide and the results obtained are given in Table 6.7.

Table 6.7 HSiH angles calculated from vibrationally corrected data

Solvent	D_{SiH} / D_{HH}	HSiH (deg.)	D_{SiH} (SiH_4) / Hz
ZLI 1167	-0.695 (4)	112.38 (10)	1.13 (30)
ZLI 3086	-0.583 (10)	109.62 (25)	1.95 (37)
ZLI 4792	-0.640 (5)	111.05 (12)	-0.18 (37)
ZLI 1083	-0.702 (4)	112.55 (10)	-1.76 (40)
E 7	-0.704 (4)	112.60 (10)	-0.65 (37)

These structures do not agree within experimental error. This is made clear by plotting the HSiH angle against the silane coupling (Figure 6.2). There is again no strong correlation between the HSiH angle and the D_{SiH} coupling of silane.

Figure 6.2 Plot of D_{SiH} / D_{HH} versus silane coupling for SiH_3Cl

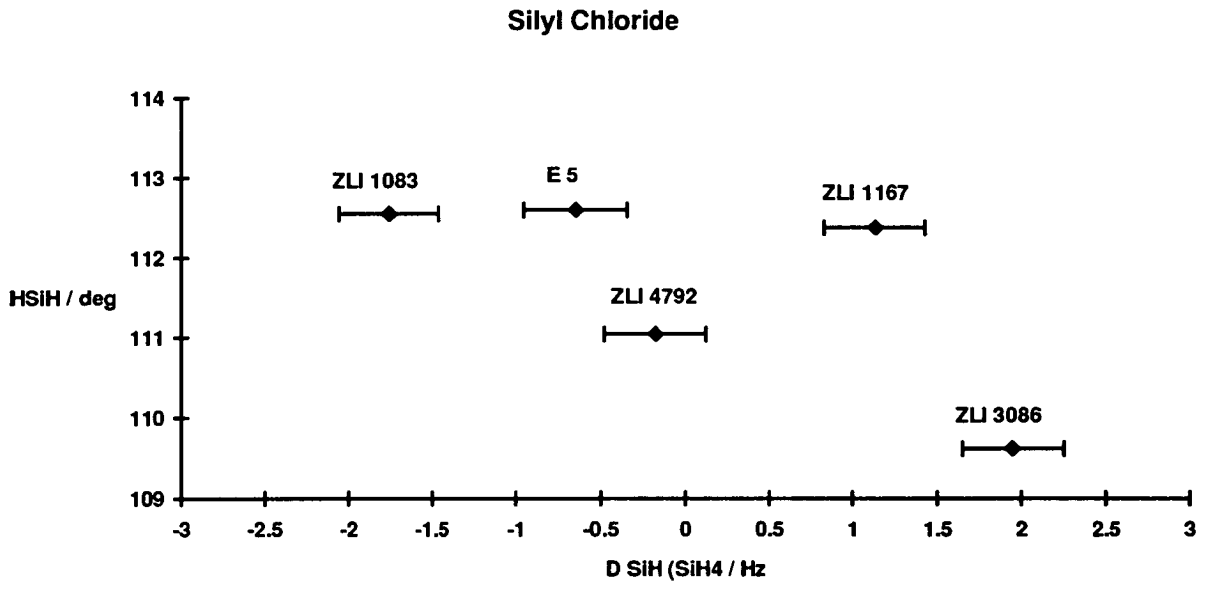

As in the case of silyl bromide, it was expected that the HSiH angle from the sample with the smallest silane coupling ought to be in best agreement with the HSiH angle obtained in the gas phase. This again corresponds to the sample run in liquid crystal ZLI 4792. This gives an HSiH angle of 111.05 (12) °, with a silane D_{SiH} coupling of -0.18 (37) Hz. This can be compared to values of 111.0 ° and 110.2 ° for the r_s and r_0

structures respectively obtained by Harmony et al.[8] and the r_0 value of 110.6° obtained by Duncan et al.[7] It appears that the value obtained in liquid crystal ZLI 3086 of 109.62 (2)° is in closer agreement to the r_0 value. Again this value is associated with a silane D_{SiH} coupling which is relatively large, 1.95 (37) Hz. The correlation between the coupling of silane and the resulting HSiH angle is further discussed in Chapter 7.

6.3 Silyl Iodide

6.3.1 Experimental

Silyl iodide was prepared in the following manner:

$$(SiH_3)_3N + 4\ HI \rightarrow 3\ SiH_3I + NH_4I$$

Using a double bulb apparatus, similar to that used for the trisilylamine synthesis, trisilylamine (10 mmol) was condensed into the larger bulb and hydrogen iodide (40 mmol) condensed into the smaller. Both bulbs were allowed to warm to room temperature before the hydrogen iodide was slowly added to the amine. Once addition was complete, all the volatiles were condensed at 77 K in the larger bulb. The apparatus was allowed to warm to room temperature and the reaction left overnight. The excess hydrogen iodide was removed by fractionating at -96° C (toluene) until the silyl iodide which remains has a vapour pressure of 12.7 cm / Hg at 0° C. It was not possible to monitor the purity of silyl iodide by FT-IR spectrometry due to the difficulty in detecting the presence of hydrogen iodide.

NMR samples were prepared using the same liquid crystal solvents used in the case of silyl chloride. ^1H spectra were recorded using a BRUKER AL250 spectrometer at Edinburgh University. A significant problem arose however, in that the silyl iodide appeared to react on warming the sample tubes to room temperature with all but two

of the liquid crystals used. This has resulted in results only being obtained silyl iodide in liquid crystals ZLI 4792 and ZLI 3086.

6.3.2 Analysis

The ^1H spectra of silyl iodide was very similar to those obtained for silyl bromide and silyl chloride. The dipolar couplings were therefore taken directly from the spectra and their signs determined as described previously in the case of silyl bromide (see Appendix B).

The values used for the indirect coupling J_{SiH} of silyl iodide were again determined by taking into account the chemical shift of each experiment (see page 145). The values used were -240.1 Hz for the sample run in ZLI 4792 and -240.5 Hz for the sample in ZLI 3086. The direct couplings obtained are presented in Table 6.8.

Table 6.8 Experimental dipolar couplings for Silyl Iodide and Silane (Hz)

Solvent	D_{HH}	D_{SiH}	D_{SiH} (SiH_4)
ZLI 3086	128.68 (18)	-77.04 (77)	1.99 (37)
ZLI 4792	414.36 (9)	-260.13 (64)	-0.23 (25)

The dipolar couplings are then vibrationally corrected using the program BMGV. This is done using the covariance matrix obtained from ASYM20 with the harmonic force field of Schneider and Thiel.[3] The vibrationally corrected data obtained are presented in Table 6.9.

Table 6.9 Vibrationally corrected dipolar couplings of Silyl Iodide (Hz)

Solvent	D_{HH}	D_{SiH}
ZLI 3086	131.93 (37)	-80.85 (86)
ZLI 4792	424.82 (105)	-272.98 (144)

N.B. Vibrational corrections are $1.0252*D_{HH}$ and $1.0494*D_{SiH}$.

The errors are calculated as described on page 130 to take into account both the uncertainty in the experimental frequencies and the vibrational corrections. The HSiH angles calculated are listed in Table 6.10.

Table 6.10 Final HSiH angles from vibrationally corrected data

Solvent	D_{SiH} / D_{HH}	HSiH (deg)	D_{SiH} (SiH_4) / Hz
ZLI 3086	-0.613 (8)	110.37 (20)	1.99 (37)
ZLI 4792	-0.643 (5)	111.12 (12)	-0.23 (25)

These two structures do not agree within experimental error. This is further emphasised by a plot of the HSiH angle versus the silane D_{SiH} coupling (Figure 6.3).

Figure 6.3 Plot of HSiH angle versus Silane coupling (D_{SiH}) for Silyl Iodide

It was again anticipated that the structure of the sample obtained in the liquid crystal solvent which gave rise to the silane D_{SiH} coupling closest to zero, would be closest to the structure observed in the gas phase. This corresponds to an HSiH angle of 111.12 (12)° obtained in ZLI 4792 which had an D_{SiH} (SiH_4) of -0.23 (37) Hz. This can be compared to the values of 111.1° and 110.5° for the r_s and r_0 structures obtained by Harmony et al.[8] and the value of 110.7° for the r_0 structure obtained by Duncan et al.[7] This indicated that the angle of 110.37 (20)° obtained in liquid crystal

ZLI 3086 was in best agreement with the r_o gas phase structure despite a silane coupling of 1.99 (25) Hz. The correlation between the observed structure and the silane coupling is further discussed in Chapter 7.

6.4 Silyl Fluoride

6.4.1 Experimental

Silyl Fluoride was prepared in the following manner:

$SiH_3Br + AsF_3 \rightarrow SiH_3F$

Silyl bromide (5 x 1 mmol) was passed through a column of AsF_3 (10 %) and silver sand (90 %) which had been dried in an oven for several days and pumped under vacuum for four days with occasional flaming to ensure that the column was as dry as possible. The silyl fluoride was then purified by fractionating through a -160 ° C (40-60 pet. ether) slush bath to remove any disiloxane and difluorsilane, and checked for purity by FT-IR spectrometry.

Samples using the solvents ZLI 3086, ZLI 4792, ZLI 1083 and E 7 were prepared and ^1H and ^{19}F spectra recorded using a BRUKER AL250 spectrometer at Edinburgh University.

6.4.2 Analysis

Due to the spin ½ ^{19}F nucleus, the ^1H spectrum for silyl fluoride was different from that observed for the other silyl halides. Each of the previously three ^1H lines was now split by the fluorine so that a triplet of doublets was observed. This resulted in the ^{29}Si satellites forming a weak triplet of doublets of doublets. Fortunately, spectra

were still first order and the direct couplings could be taken directly from them (see Appendix B).

The splittings are now 3 D_{HH}, 2 D_{HF} + J_{HF} and 2 D_{SiH} + J_{SiH}. The $^{1}H^{19}F$ couplings were double checked by analysing the ^{19}F spectra which consisted of a quartet due to the coupling with the spin ½ ^{1}H and a weak quartet of doublets due to the coupling with the spin ½ ^{29}Si nuclei.

Originally, it was assumed that the indirect couplings would be invariant in the liquid crystal solvents being used, and the couplings of -235.38 (10) and 47.23 (3) Hz for J_{SiH} and J_{HF} respectively, obtained by Brookman[2] in the isotropic phase of liquid crystal E 5, and -281 (3) Hz for the coupling J_{SiF} obtained by Ebsworth and Turner[9] were used.

The signs of the direct couplings were assigned using the same arguments as used for silyl bromide, and are given in Table 6.11.

Table 6.11 Experimental dipolar couplings for Silyl Fluoride and Silane

Solvent	D_{HH}	D_{SiH}	D_{HF}	D_{SiF}	D_{SiH} (SiH_4)
ZLI 3086	-37.59 (8)	28.97 (25)	32.74 (20)	-43.2 (31)	2.0 (23)
ZLI 4792	82.64 (25)	-50.16 (87)	-78.44 (62)	107.5 (34)	-0.24 (47)
ZLI 1083	504.49 (17)	-348.98 (50)	-471.55 (50)	646.1 (34)	-1.69 (36)
E 7	422.49 (17)	-292.50 (75)	-395.20 (50)	542.4 (34)	-0.81 (36)

It was observed that the direct couplings observed in solvent ZLI 3086 have the opposite signs to those in other solvents for silyl fluoride. This was unexpected as it is not observed for any other silyl compounds studied in this work using the solvent ZLI 3086. The opposite signs for the direct couplings is a consequence of silyl fluoride aligning perpendicular to the liquid crystal director in ZLI 3086. It was attempted to solve the spectra with the same sign of orientation parameter as is observed in all the other solvents but not all the ^{29}Si satellites could be found.

The dipolar couplings of silyl fluoride are then vibrationally corrected. This was done using the program BMGV with the covariance matrix produced by ASYM20 using the harmonic force field calculated by Schneider and Thiel.[3] The vibrationally corrected data are presented in Table 6.12.

Table 6.12 Vibrationally corrected dipolar couplings (Hz)

Solvent	D_{HH}	D_{SiH}	D_{HF}	D_{SiF}
ZLI 3086	-38.08 (9)	29.95 (10)	33.03 (34)	-43.2 (31)
ZLI 4792	83.71 (27)	-51.86 (89)	-79.10 (62)	107.2 (34)
ZLI 1083	511.01 (67)	-360.80 (140)	-475.74 (68)	644.0 (34)
E 7	427.95 (57)	-302.4 (124)	-398.70 (61)	540.6 (34)

N.B. Vibrational corrections are 1.01293*D_{HH}, 1.03386*D_{SiH}, 1.08889*D_{HF} and 0.99772*D_{SiF}.

The errors are again 1 e.s.d. and are calculated as described in 6.2 (page 131). For silyl fluoride it is clear that more structural information can now be obtained. As in the other silyl halides, the structure can be fully determined using just three parameters (two bond lengths and an angle). Because of the extra data from the ^{19}F couplings, we have four direct couplings. This should allow the orientation parameter and the structure to be fully determined. Unfortunately, because LCNMR can only give ratios of distances and not the absolute size of a molecule, it was not possible to refine all these parameters together. Instead, the Si-H bond length was fixed at 1.48 Å. This leaves three refining parameters which can be fitted using the four available direct couplings.

A further complication, however, arises due to one of these four couplings being between the two 'heavy' nuclei ^{29}Si and ^{19}F. This has the disadvantage that the indirect coupling, J_{SiF}, may have a significant anisotropic contribution. For this reason, it was decided that the direct coupling D_{SiF} be weighted out of the least square refinement by giving it an uncertainty of ± 100 Hz. The results of the refinement using the program ED92 are given in Table 6.13.

Table 6.13 Results of least squares refinement for Silyl Fluoride

Solvent	r Si-H (Å)	r Si-F (Å)	r Si-H / r Si-F	HSiH (°)	Szz
ZLI 3086	1.48	1.886 (2)	0.7847	114.54 (2)	-0.00979 (1)
ZLI 4792	1.48	1.507 (7)	0.9821	110.54 (6)	0.02007 (3)
ZLI 1083	1.48	1.632 (1)	0.9069	112.65 (1)	0.12718 (3)
E 7	1.48	1.631 (1)	0.9074	112.66 (1)	0.10653 (2)

Although the structures obtained in ZLI 1083 and E 7 are in good agreement with one another, it is clear that this is not the case for the structures obtained in ZLI 3086 and ZLI 4792. On comparing these to a bond ratio of 0.9257 (2) and HSiH angle of 110.6°, obtained by Duncan et al.[7] for the ground state microwave structure of silyl fluoride, it would appear that the Si-F bond length found in ZLI 1083 and E 7 is 0.03 Å longer than in the gas phase, whilst the corresponding bond length in ZLI 4792 is 0.09 Å shorter. The most anomalous result being in ZLI 3086 which gives a bond length 0.29 Å longer than expected.

These changes in bond length were clearly unreasonable. It was observed, however, that the two liquid crystals in which these anomalous structures are found, gave rise to direct couplings which were almost an order of magnitude smaller than those observed in the other two solvents. This implied that the direct couplings and hence the structure, were perhaps much more dependent on the value of the indirect couplings used than had previously been assumed. To test this, the structure of silyl fluoride was calculated in ZLI 4792, using the indirect couplings determined by Ebsworth and Turner[9] for an isotropic solvent, and found to be in much better agreement with both the microwave structure and the structures calculated in this work using the solvents E 7 and ZLI 1083. Another attempt was therefore made to obtain the isotropic spectra of silyl fluoride in these solvents.

There were again problems with overlapping solvent peaks, but the indirect couplings were obtained for silyl fluoride in liquid crystal solvent ZLI 3086. These were, J_{SiH} = -231.5 (3) Hz and J_{HF} = 46.2 (3) Hz. The ^{29}Si-^{1}H coupling of silane was

determined in the same experiment and found to be J_{SiH} = -202.9 (6) Hz. It was also decided to try some of the sample tubes which contained silyl cyanide, and the isotropic couplings of silyl cyanide were obtained in ZLI 3086 and ZLI 4792. It was realised from this that any variation in the indirect couplings between solvents would have to be taken into account. In deciding how to go about this, a graph was compiled showing the relationship of the chemical shifts of each compound with the solvent used. (Figure 6.4).

It was observed from this plot that each compound tends to follow the same trend in chemical shift variation from solvent to solvent, although an unexpectedly high chemical shift is found for silyl fluoride in liquid crystal E7, and a correspondingly small chemical shift is observed for methyl silane in this same solvent.

Figure 6.4 Plot of chemical shift (^{1}H) versus solvent for the silyl compounds studied

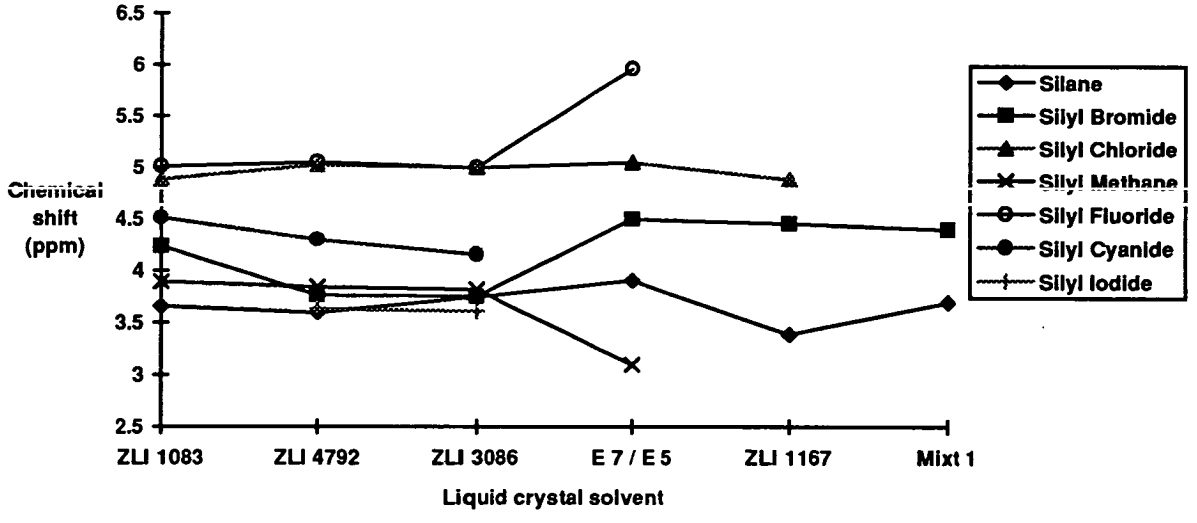

Assuming that the variation in indirect couplings will follow a similar trend to that of the chemical shift in these solvents and the fact that it appears from the structure of silyl fluoride that ZLI 4792 gives rise to similar indirect couplings as found by

Ebsworth and Turner for isotropic solvents, the indirect couplings for all the silyl halides have been estimated in Table 6.14.

Table 6.14 Indirect dipolar coupling for silyl compounds in various liquid crystal solvents

Compound	ZLI 1083	ZLI 4792	ZLI 3086	ZLI 1167	E 7	Mixt. 1
Silyl Bromide	-235.7	-240.5[a]	-240.9	-235.7[b]	-235.7	-235.7
Silyl Chloride	-240.0	-238.1[a]	-238.4	-240.0	-238.0	
Silyl Iodide		-240.1[a]	-240.5[b]			
Silyl Fluoride	-230.0	-229.0	-231.5[b]		-235.4[c]	
Silyl Cyanide	-236.0	-235.9[b]	-236.3[b]		-238.5[c]	

[a]Ebsworth and Turner[9] [b]Measured in this work [c]Blair et al.[16]

On using these indirect couplings for silyl fluoride, the results detailed in Tables 6.11 and 6.12 are recalculated to give Tables 6.15 and 6.16. The structure of silyl fluoride was again obtained from a least squares refinement using the program ED92. These final results are given in Table 6.17.

Table 6.15 Experimental dipolar couplings for Silyl Fluoride and Silane (Hz)

Solvent	D_{HH}	D_{SiH}	D_{HF}	D_{SiF}	D_{SiH} (SiH_4)
ZLI 3086	-37.59 (8)	28.97 (25)	32.74 (20)	-43.2 (31)	2.0 (23)
ZLI 4792	82.64 (25)	-50.16 (87)	-78.44 (62)	107.5 (34)	-0.24 (47)
ZLI 1083	504.49 (17)	-351.68 (50)	-471.55 (50)	646.1 (34)	-1.69 (36)
E 7	422.49 (17)	-292.50 (75)	-395.20 (50)	542.4 (34)	-0.81 (36)

Table 6.16 Vibrationally corrected dipolar couplings (Hz)

Solvent	D_{HH}	D_{SiH}	D_{HF}	D_{SiF}
ZLI 3086	-38.08 (9)	27.94 (32)	33.55 (34)	-41.7 (31)
ZLI 4792	83.71 (27)	-55.15 (65)	-78.11 (14)	107.2 (34)
ZLI 1083	511.01 (67)	-363.59 (140)	-475.74 (68)	644.0 (34)
E 7	427.95 (57)	-302.4 (124)	-399.31 (61)	538.4 (34)

N.B. Vibrational corrections are 1.01293*D_{HH}, 1.03386*D_{SiH}, 1.08889*D_{HF} and 0.99772*D_{SiF}.

Table 6.17 Results of least squares refinement for Silyl Fluoride

Solvent	r Si-H (Å)	r Si-F (Å)	r Si-H / r Si-F	HSiH (°)	Szz
ZLI 3086	1.48	1.797 (30)	0.8055 (135)	113.31 (20)	-0.00959 (11)
ZLI 4792	1.48	1.580 (12)	0.9363 (71)	111.51 (19)	0.02007 (13)
ZLI 1083	1.48	1.641 (7)	0.9019 (38)	112.78 (10)	0.12718 (13)
E 7	1.48	1.631 (6)	0.9074 (33)	112.67 (10)	0.10653 (12)

Relatively good agreement between the structures obtained in three of the solvents, ZLI 4792, ZLI 1083 and E 7 was obtained. The structure in ZLI 3086, however, although improved from previously, still had an Si-F bond much longer than was expected. On comparing these structures to the bond ratio of 0.9257 (2) and HSiH angle of 110.6° obtained by Duncan et al.[7] it is evident that the structure obtained in ZLI 4792 is in closest agreement. The structures obtained in E 7 and ZLI 1083 are consistent in that with larger HSiH angles they show longer Si-F bonds. This is consistent with the hypothesis that the silicon is becoming five co-ordinate in the solution. The resulting plot of HSiH angle versus D_{SiH} (SiH_4) is given in Figure 6.5.

Figure 6.5 Plot of HSiH angle versus Silane coupling (D_{SiH}) for Silyl Fluoride

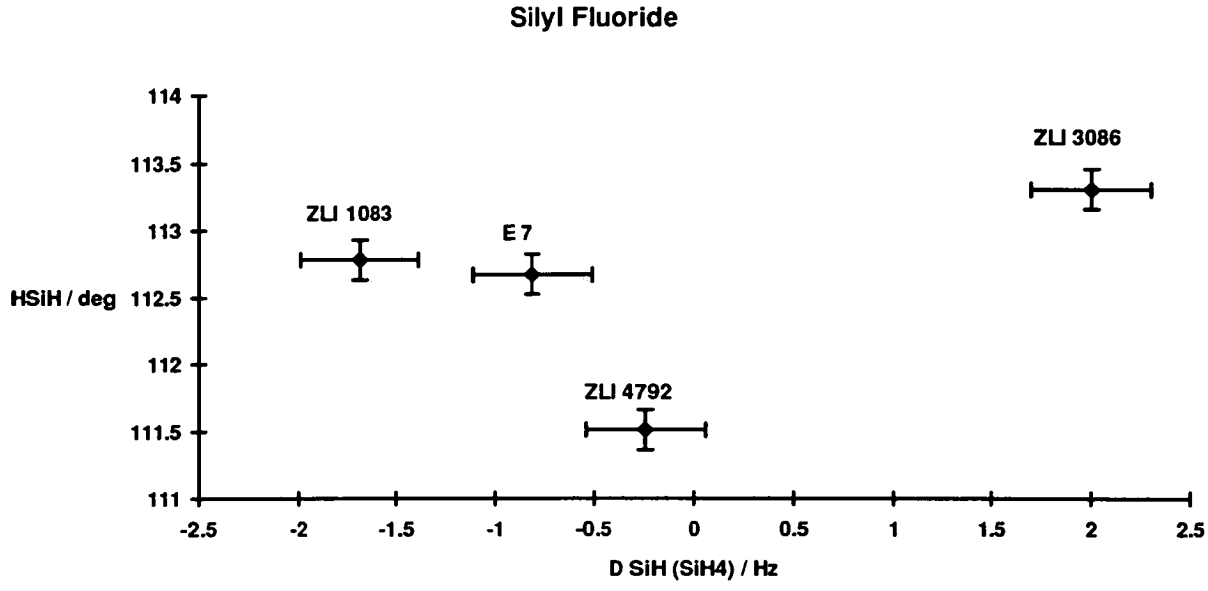

As mentioned previously, the result obtained in liquid crystal solvent ZLI 3086 is not as would be expected on a straight forward comparison of the results obtained using ZLI 3086 as solvent.

It had previously been anticipated that the silyl halides may interact with the liquid crystal solvent in an S_N2 type reaction intermediate. This would result in an increase in the HSiH angle and a small lengthening of the silyl halide bond (as is observed for the structure in E 7 and ZLI 1083). However, in the case of ZLI 3086, which is a non-polar solvent, this type of interaction can not take place.

A possible solution which would explain this widening HSiH angle and lengthening of the silicon halide bond only in the case of silyl fluoride, is if hydrogen bonding were taking place between the fluorine from the silyl fluoride and the liquid crystal molecule. An important feature of this is the orientation parameter. In all other cases where the liquid crystal has aligned parallel to the direction of the applied magnetic field, an orientation parameter has been determined where the silyl halide also aligns with the long axis in the magnetic field direction. For silyl fluoride dissolved in

ZLI 3086 this is not the case. If hydrogen bonding is taking place, then it would appear that the fluorine is not bonding to a terminal site in the liquid crystal (e.g. in E 7 the cyano group is a terminal group), but instead is bonded to a site somewhere in the body of the liquid crystal molecule. This, if it were taking place, would explain both the anomalous structure and orientation that was found here.

6.4.3 Anisotropy in J_{SiF}

The anisotropy of the indirect coupling J_{SiF} complicates the calculation of the direct coupling D_{SiF} because instead of the ^{29}Si satellites having a splitting of $2\,D_{SiF} + J_{SiF}$, the splitting now becomes $2\,D_{SiF} + J_{SiF} + J_{SiF}^{aniso}$, or more simply, $2\,(D_{SiF} + \frac{1}{2}\,J_{SiF}^{aniso}) + J_{SiF}$. This implies that by refining the structure of silyl fluoride as above with the D_{SiF} direct coupling weighted out, then the difference between the calculated direct coupling (dependent upon the refined structure and the orientation parameter) and the experimental direct coupling, will be $\frac{1}{2}\,J_{SiF}^{aniso}$. These are then compared as a percentage of the calculated direct coupling to see if there is any significant differences between solvents. The results for this are detailed in Table 6.18.

Table 6.18 Calculated values of J_{SiF}^{aniso} for Silyl Fluoride

Solvent	$\frac{1}{2}\,J^{aniso}$ (Hz)	$\lvert J^{aniso} / 2\,D^{calc} \rvert$ (%)	J^{aniso} / Szz (Hz)
ZLI 3086	-4.6 (3.1)	12.3 (80)	959 (646)
ZLI 4792	-9.0 (3.4)	7.7 (26)	-897 (334)
ZLI 1083	-2.8 (3.8)	0.4 (7)	-44 (60)
E 7	-17.9 (3.8)	3.2 (6)	-336 (72)

It is evident that J_{SiF}^{aniso} is not constant for the four samples. In examining the anisotropy of the indirect couplings of methyl fluoride, Ditchfield and Snyder[10] observed very large variations of the calculated anisotropies depending on the exact structure used. It is likely that this is why such a large variation was observed for the

four solvents. Previous studies of this kind have investigated J^{aniso} by assuming that the structure is invariant in the different solvents used[11, 12], but this was clearly not the case here. These studies also demonstrated that anisotropic effects are very small (often negligible) relative to the direct dipolar coupling when light nuclei are involved. This is supported by theoretical calculations.[13, 14]

A large contribution to the errors also arises due to the uncertainty of the indirect couplings in these different liquid crystal solutions. Only by obtaining more accurate values for these indirect couplings will more precise structural and anisotropy parameters be determined.

6.5 Silyl Cyanide

6.5.1 Experimental

Silyl Cyanide was prepared in the following manner:

$$AgNO_3 + KCN \rightarrow AgCN + KNO_3$$

$$SiH_3Br + AgCN \rightarrow SiH_3CN + AgBr$$

The silver cyanide salt (30 mmol) was prepared by the reaction of aqueous silver nitrate and potassium cyanide solutions. The precipitate was filtered off and washed with deionised water, alcohol then acetone, transferred to an ampoule and pumped dry overnight on a vacuum line.

Portions of silyl bromide (~5 mmol) were condensed onto the large excess of silver cyanide, and allowed to warm to room temperature for five minutes. The product was then fractionated at -78 ° C to remove traces of disiloxane and hydrogen cyanide and its purity checked by FT-IR spectrometry.

The ^1H spectrum of silyl cyanide had previously been determined by Blair[15] in liquid crystal solvent E 5, and so samples were prepared using only the solvents ZLI 1083, ZLI 3086 and ZLI 4792. ^1H spectra were recorded using a BRUKER WH360 spectrometer at Edinburgh University.

6.5.2 Analysis

The ^1H spectrum of silyl cyanide differs from the silyl halides because as well as a strong triplet from the three hydrogens, and the triplet of doublets from the ^{29}Si coupling, there are also a triplet of doublets from the ^{13}C and from the ^{15}N low

abundance isotopes. Fortunately, spectra are again first order and the direct couplings can be measured directly (see Appendix B).

The line splittings are 3 D_{HH}, 2 D_{SiH} + J_{SiH}, 2 D_{CH} + J_{CH} and 2 D_{NH} + J_{NH}. The indirect couplings were measured by Blair[15] in $CDCl_3$ as -238.6 (2), 4.6 (2) and -1.07 (2) Hz respectively for J_{SiH}, J_{CH} and J_{NH}. These were also obtained in this work for the isotropic phases of ZLI 3086 and ZLI 4792. The couplings observed were -236.4 (4) and 4.6 (4) Hz in ZLI 3086 and -235.9 (6), and 3.1 (2) Hz in ZLI 4792 for the J_{SiH} and J_{CH} couplings respectively. Both solvents yield smaller values for J_{SiH} and J_{CH} than were observed in $CDCl_3$, but the percentage changes are small as would be expected. It was found that the more cycles the NMR spectrometer accumulated, the broader was the central ^1H peak of the isotropic silyl cyanide spectrum. This was attributed to small temperature fluctuations in the probe of the spectrometer and prevented values of the smaller J_{NH} coupling being obtained even when the accumulation time was reduced. By comparing J_{SiH} with the chemical shifts of the silyl compounds in the different liquid crystal solvents used in this work, J_{SiH} for other compounds dissolved in these liquid crystals has been estimated (Table 6.14).

The signs of the direct couplings were assigned using the same arguments as used previously. The direct couplings obtained are presented in Table 6.19.

Table 6.19 Experimental dipolar couplings for Silyl Cyanide

Solvent	D_{HH}	D_{SiH}	D_{CH}	D_{NH}
ZLI 3086	198.97 (18)	-131.04 (29)	-45.25 (29)	9.68 (29)
ZLI 4792	483.18 (18)	-327.91 (29)	-108.80 (29)	23.03 (29)
ZLI 1083	985.48 (31)	-720.4 (9)	-224.55 (39)	46.78 (47)

Vibrational corrections were then applied to these direct couplings using the harmonic force field reported by Blair et al.[16] with the aid of the programmes ASYM20 and BMGV. The vibrationally corrected data are presented in Table 6.20. The errors

again take into account the uncertainty in the line frequencies of the experimental spectra and the vibrational correction (see page 131).

Table 6.20 Vibrationally corrected dipolar couplings (Hz)

Solvent	D_{HH}	D_{SiH}	D_{CH}	D_{NH}
ZLI 3086	203.76 (51)	-137.23 (168)	-45.95 (30)	9.67 (30)
ZLI 4792	494.80 (118)	-343.55 (161)	-110.48 (33)	23.01 (30)
ZLI 1083	1009.18 (239)	-754.76 (346)	-228.01 (52)	46.73 (48)

N.B. Vibrational corrections are 1.02407 *D_{HH}, 1.04770*D_{SiH}, 1.01541*D_{CH} and 0.99872*D_{NH}.

Because of the extra couplings obtained from the ^{13}C and ^{15}N satellites, in silyl cyanide it is possible to refine two of the three bond lengths as well as the HSiH angle and the orientation parameter. The results for this refinement are given in Table 6.21.

Table 6.21 Results of least squares refinement for Silyl Cyanide

Solvent	rCSi (Å)	rCN (Å)	rCSi / rSiH	rCN / rSiH	HSiH (°)	Szz
ZLI 3086	1.830 (29)	1.107 (66)	1.236 (20)	0.748 (45)	111.85 (17)	0.0502 (15)
ZLI 4792	1.870 (11)	1.124 (29)	1.2635 (74)	0.759 (20)	112.36 (12)	0.12254 (33)
ZLI 1083	1.900 (10)	1.163 (23)	1.2838 (68)	0.786 (16)	113.64 (11)	0.25548 (70)

These are then compared to the structure of silyl cyanide found previously in the gas, solution and crystalline phases[16] (Table 6.22).

Table 6.22 The structure of Silyl Cyanide

Phase	rCSi / rSiH	rCN / rSiH	HSiH (°)
Gas[a]	1.2436 (12)	0.7774 (9)	111.60 (4)
Solution[b]	1.2830 (51)	0.7836 (15)	113.68 (11)
Crystalline[c]	1.441 (19)	0.867 (12)	116.8 (4)

[a] r_{av} gas phase structure based on rotation constants and electron diffraction data.

[b] LCNMR structure calculated in Liquid Crystal solvent E 5 with data at three different temperatures.

[c] Low temperature crystal structure of Silyl Cyanide.

As was observed for other compounds in this work, results obtained in liquid crystal ZLI 1083 and in solvents E 5 / E 7 are closely related. Silyl cyanide is no exception to this. The HSiH angle of 113.64 (11) ° and the rCSi / rSiH ratio of 1.2838 (68) obtained in ZLI 1083 both agree within experimental error with the structure obtained when liquid crystal E 5 was used as solvent.

The errors in this work for the rCN bond length arise largely because it was not possible to measure the isotropic J_{NH} coupling from the isotropic ^1H spectra obtained of silyl cyanide in the above solvents.

As expected, it is found that the smaller the orientation parameter in any solvent, the more sensitive the structural parameters are to the indirect couplings. In silyl cyanide, a change in J_{NH} of 1 Hz resulted in a change in rCN of 0.23, 0.07 and 0.03 Å for the solvents ZLI 3086, ZLI 4792 and ZLI 1083 respectively. The same trend was found for rSiC with a 1 HZ change in J_{CH} resulting in a 0.09, 0.03 and 0.01 Å change in the bond length in these same three solvents.

Blair et al. observed that the LCNMR structure of silyl cyanide was mid-way between the structure found in the gas and the crystalline phases. In this work, however, the structure obtained in ZLI 3086 is in good agreement with that of the gas phase

structure and the structure obtained in ZLI 4792 lies mid-way between this and the structure observed in ZLI 1083 and E 5.

The structure in E 5 was reported as being a consequence of an S_N2 intermediate, with an incoming isonitrile group displacing the bound nitrile group as is observed in the crystalline phase of silyl cyanide. As E 5 is known to contain terminal cyano groups, this appears to be a reasonable assumption.

The exact functional groups present in the three liquid crystal used in this work were not known. It is clear that ZLI 3086, described to be a mixture of non-polar molecules, is unlikely to contain any polar groups, and that ZLI 4792, a mixture containing only super fluorinated compounds, will contain only fluorine. It is possible, however, that ZLI 1083, described as a mixture of esters, will contain terminal cyano groups. This would offer an explanation as to why the results obtained in ZLI 1083 and E 5/ E 7 are so similar.

This was therefore examined by FT-IR spectroscopy of the liquid crystal solvents. It was found that both E 7 and ZLI 1083 show absorption at 2226 cm^{-1} indicating the presence of cyanide groups, while no such absorption was found for ZLI 3086 or ZLI 4792. This lends strong support to the evidence that the silyl compounds do interact with the cyano group from the liquid crystal solvent as it is the structures obtained in these solvents which display the larger HSiH angle.

The differences in silyl geometry is further emphasised by plotting the HSiH angle versus D_{SiH} (SiH_4) for the four different solvents (Figure 6.6).

Figure 6.6 Plot of HSiH versus Silane coupling (D_{SiH}) for Silyl Cyanide

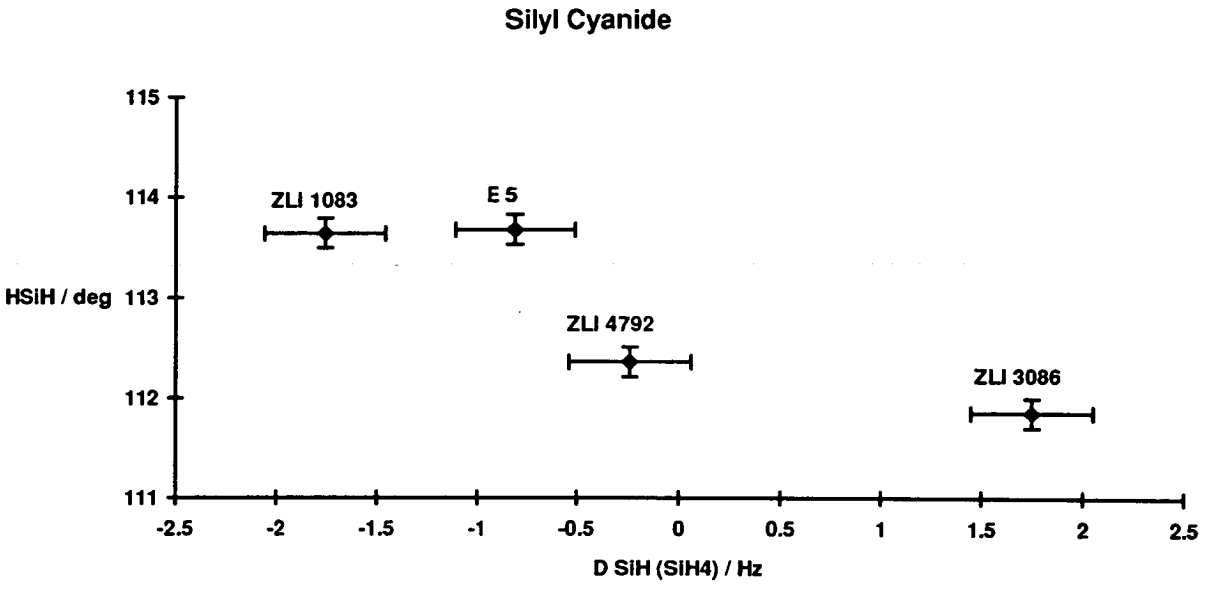

Figure 6.6 confirms the trend observed for previous compounds in these liquid crystals. It also demonstrates that the geometry of the silyl group is very similar for the structures determined in ZLI 1083 and E5, and that the structures determined in ZLI 4792 and ZLI 3086 are quite different from these. The correlation between the coupling of silane and the resulting HSiH angle is further discussed in Chapter 7.

6.6 Methyl Silane

6.6.1 Experimental

Methyl silane was prepared by the reduction of methyl trichlorosilane with lithium aluminium hydride.

$CH_3SiCl_3 + 3\ LiAlH_4 \rightarrow CH_3SiH_3$

The $LiAlH_4$ (3 g) was placed in a 250 ml, 3-necked flask and 100 ml of dry di-n-butyl ether was added. An -78 ° C (acetone/CO_2) condenser and a pressure equalised dropping funnel with a nitrogen inlet were attached to the flask. The apparatus was connected to a vacuum line via swivel links. The CH_3SiCl_3 (3.6 g) was diluted with di-n-butyl ether (50 ml) and added dropwise over a period of 30 minutes. The reaction was then left for a further 30 minutes, and volatile products were removed by trapping at liquid nitrogen temperature on the vacuum line. Purification consisted of repeated fractionation through a -78° C (acetone/CO_2) bath. Final purity was confirmed by FT-IR spectroscopy.

NMR samples were prepared using the liquid crystals ZLI 3086, ZLI 4792 and ZLI 1083 and ^1H spectra were recorded at 298 K on the University of Edinburgh Bruker WH360 spectrometer. The ^1H spectrum of methyl silane in liquid crystal E5 had been attained previously[17] at 298 K on the same spectrometer but had not been solved.

6.6.2 Analysis

Unlike the previous compounds in this work, methyl silane contains six hydrogens which give rise to a second order spectrum (see Appendix B). It was therefore not possible to determine the direct couplings directly and the program LCSIM[18] was

used instead to simulate the spectra. This is done using an experimental structure along with the chemical shifts and indirect couplings for the molecule being studied, and varying the orientation parameter until the calculated direct couplings produce a spectrum similar to the experimental spectrum being analysed.

Fortunately, methyl silane has C_{3v} symmetry and only one orientation parameter must therefore be found. Spectra were simulated for a wide range of solutions where Szz = -2 Sxx and when a suitable match to the experimental spectrum was obtained, the direct couplings predicted by LCSIM were transferred to the refinement program SLIQUOR[18]. This program requires the chemical shift of the nuclei involved and the indirect couplings as in LCSIM, but instead of an experimental structure, the direct couplings predicted by LCSIM are used. This enables lines in the experimental and calculated spectra to be matched up and the direct couplings, chemical shift and, in some cases, indirect couplings to be refined by a least squares method to obtain a more exact match between the two spectra.

In the program LCSIM, there are actually two possible solutions depending on whether Szz is positive or negative. The case of Szz being negative was ruled out by attempting to refine the direct couplings in the program SLIQUOR. It was found that a better match between experimental and calculated spectra was obtained with Szz positive. How well the experimental and calculated spectra match is given by the program SLIQUOR every time it carries out a refinement. This is given in terms of an rms. fit between the experimental and calculated frequencies of every line involved in the refinement.

The isotropic couplings (J_{ij}) used in this work were obtained from isotropic spectra using C_6D_6[17] as solvent. The trial structure used in LCSIM was the microwave structure of Duncan et al.[19] The estimated direct dipolar couplings (D_{ij}) were then entered into SLIQUOR for refinement. The labelling scheme used is shown in Figure 6.7 with the results of these refinements given in Tables 6.23 - 6.26. All errors are 1 e.s.d. and are those calculated from the refinement in SLIQUOR.

Figure 6.7 Labeling scheme for methyl silane

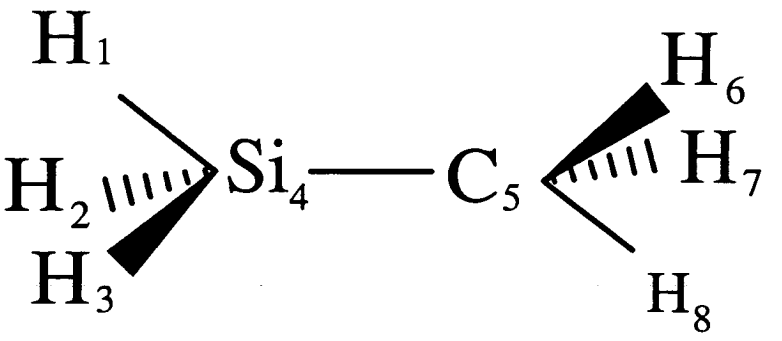

Previous studies of deuterated methyl silane[17, 20] found that the sign of J_{16} could not be determined due to a lack of experimental accuracy. In the present work, the ^1H spectrum of methyl silane in E5 was simulated with J_{16} both positive and negative. It was found that the r.m.s. fit between the observed and calculated frequencies was worse when J_{16} was negative even when all other parameters were refined. However, when J_{16} was included in the refinement, the solution with J_{16} positive was always found with little correlation existing between J_{16} and D_{16}. The values listed for J_{16} in Tables 6.23 - 6.26 are therefore the values obtained on refining the ^1H spectra. The other J_{ij} values, however, did not vary significantly on refinement, and as these were much more correlated to the related D_{ij} the errors obtained were large in every case.

This is consistent with the observations of Gerritson and Maclean[21] that for interactions between nuclei with largely differing magnetogyric ratios, only the Dij can be deduced from the spectra of oriented molecules. The values used in all solvents were, J_{15} = -4.5, Hz J_{56} = 121.8 Hz, J_{14} = 194.31 Hz and J_{46} = 7.954 Hz.

Table 6.23 Final refinement for Methyl Silane in liquid crystal E 5 (Hz)

Parameter	^1H-^1H Peaks	^1H-^{29}Si Peaks	^1H-^{13}C Peaks
Lines	66	54	29
r.m.s.	0.189	0.225	3.066
J_{16}	4.615(57)	4.615	4.615
W_1	1107.590(78)	1107.60(12)	1105.59(93)
W_6	-106.960(77)	-106.99(8)	-106.0(12)
D_{16}	-95.487(31)	-95.489(33)	-95.80(42)
D_{67}	404.176(44)	404.190(41)	404.22(52)
D_{12}	163.429(37)	163.423(56)	163.90(36)
D_{14}		-84.28(12)	
D_{46}		44.973(84)	
D_{15}			-34.38(86)
D_{56}			262.2(13)

Table 6.24 Final refinement for Methyl Silane in liquid crystal ZLI 4792 (Hz)

Parameter	^1H-^1H Peaks	^1H-29Si Peaks	^1H-^{13}C Peaks
Lines	51	69	12
r.m.s.	0.058	0.392	0.957
J_{16}	4.650(11)	4.650	4.650
W_1	1390.229(13)	1390.17(18)	1390.98(75)
W_6	157.993(13)	157.86(19)	158.01(62)
D_{16}	-110. 787(6)	-110.765(71)	-110.521(44)
D_{67}	470.954(9)	470.90(11)	470.90(33)
D_{12}	188.603(7)	188.593(83)	188.45(30)
D_{14}		-97.88(18)	
D_{46}		52.32(19)	
D_{35}			-39.55(60)
D_{15}			291.37(62)

Table 6.25 Final refinement for Methyl Silane in liquid crystal ZLI 3086 (Hz)

Parameter	^1H-^1H Peaks	^1H-^{29}SI Peaks	^1H-^{13}C Peaks
Lines	55	67	11
r.m.s.	0.049	0.297	0.356
J_{16}	4.633(11)	4.633	4.633
W_1	1378.354(13)	1378.25(17)	1382.13(79)
W_6	156.096(14)	156.16(86)	156.02(96)
D_{16}	-120.596(6)	-120.557(76)	-120.87(43)
D_{67}	508.466(11)	508.43(12)	510.86(247)
D_{12}	206.785(7)	206.780(87)	206.97(29)
D_{14}		-104.79(17)	
D_{46}		56.83(22)	
D_{15}			-42.36(72)
D_{56}			334.78(89)

Table 6.26 Final refinement for Methyl Silane in liquid crystal ZLI 1083 (Hz)

Parameter	^1H-^1H Peaks	^1H-^{29}SI Peaks	^1H-^{13}C Peaks
Lines	56	35	22
r.m.s.	0.073	0.295	0.603
J_{16}	4.621(11)	4.621	4.621
W_1	1406.196(13)	1406.10(26)	1406.16(74)
W_6	189.488(14)	189.47(30)	189.64(41)
D_{16}	-114.375(6)	-114.39(13)	-114.56(20)
D_{67}	485.464(9)	485.47(17)	485.66(20)
D_{12}	195.253(7)	195.25(14)	194.65(37)
D_{14}	-	-101.38(26)	-
D_{46}	-	54.03(29)	-
D_{15}	-	-	-39.62(64)
D_{56}	-	-	302.18(39)

The next step was to apply vibrational corrections to the dipolar coupling constants. This was done using the ab initio scaled harmonic force-field calculated by Kormonicki[22]. The program ASYM20 was used to calculate the covariance matrix and the program BMGV to calculate the harmonic corrections to the direct couplings. The vibrationally corrected data are presented in Table 6.27. Errors are calculated as described in 6.2 (page 130) and include contributions from the line uncertainties and vibrational corrections.

Table 6.27 Vibrationally corrected dipolar couplings for Methyl Silane (Hz)

D_{ij}	Correction	E5	ZLI 4792	ZLI 3086	ZLI 1083
D_{14}	1.0451	-88.09(40)	-102.29(48)	-109.52(50)	-105.92(53)
D_{12}	1.0214	166.93(35)	192.64(40)	211.21(44)	199.43(4)
D_{15}	1.0070	-34.62(86)	-39.83(60)	-42.66(72)	39.90(64)
D_{56}	1.0695	280.4(22)	311.62(212)	358.05(249)	323.1(1)
D_{67}	1.0336	417.76(136)	486.78(158)	525.55(171)	501.1(63)
D_{46}	1.0021	45.06(8)	52.43(19)	56.95(22)	54.14(29)
D_{16}	1.0013	-95.36(10)	-110.64(11)	-120.44(12)	-114.23(11)

The structure in each solvent was then obtained by a least squares refinement using ED92. Because of the need to choose a bond length with which the structure could be scaled, it was decided to fix rSiC at 1.8686 Å as determined in the gas phase by microwave spectroscopy[7]. Also, because methyl silane consists of a silyl and a methyl group joined together, it is possible to use the direct coupling between hydrogens from both groups (D_{16}) to obtain a value of the barrier to internal rotation. The results of this refinement are listed in Table 6.28.

The variation in silyl and methyl geometry is highlighted by plotting a graph of HSiH and HCH versus silane coupling for the four solvents (Figure 6.8).

Table 6.28 Final Structure and Internal Barrier to Rotation of Methyl Silane

Parameter	E5	ZLI 4792	ZLI 3086	ZLI 1083	Δ[a]
rCSi / Å	1.8686	1.8686	1.8686	1.8686	
rCH / Å	1.0895 (14)	1.1003 (2)	1.0885 (18)	1.0981 (85)	0.0118 (20)
HCH / °	108.26 (6)	107.617 (7)	108.48 (6)	107.71 (20)	0.86 (7)
rSiH / Å	1.4798 (13)	1.4924 (3)	1.4800 (21)	1.488 (11)	0.0124 (24)
HSiH / °	108.19 (4)	108.276 (5)	107.95 (4)	108.27 (15)	0.33 (5)
rCH / rSiC	0.5836 (7)	0.5888 (1)	0.5825 (10)	0.5877 (45)	
rSiH / rSiC	0.7919 (7)	0.7987 (2)	0.7920 (12)	0.7963 (59)	
Barr. / kJ mol^{-1}	4.97 (13)	4.95 (3)	4.51 (23)	4.88 (108)	0.46 (26)
Szz	3.830 (10)	4.540 (2)	4.824 (20)	4.66 (10)	

[a]Observed deviation in parameter over the four solvents.

Figure 6.8 Plot of HSiH and HCH versus Silane coupling for Methyl Silane

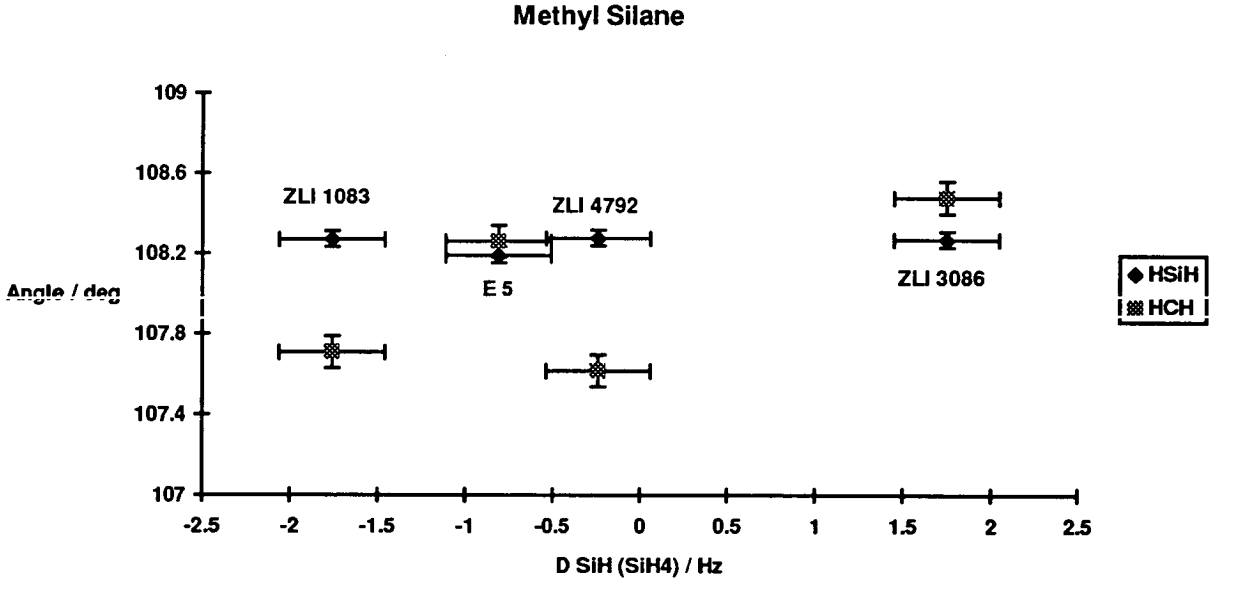

Table 6.28 demonstrates that with the C-Si bond length fixed, rCH and rSiH vary considerably between solvents. These variations in bond length are, however, correlated. The lengths of both bonds increase from ZLI 3086 - E5 - ZLI 1083 - ZLI 4792. At the same time as these bonds are increasing in length, the HSiH angle is

opening up and the HCH angle is closing. Figure 6.8 demonstrates how much larger the variation observed in the HCH angle is compared to HSiH. There does not, however, appear to be a strong correlation between the HSiH or HCH angles and the D_{SiH} coupling observed for silane. This is further discussed in Chapter 7.

These observations for the bond lengths and angles are remarkably similar to what would be seen if the liquid crystals ZLI 3086 - ZLI 1083 were successively better at nucleophilic attack, causing the silicon to tend toward a five co-ordinate system. This would be accompanied by a decrease in the ratio rSiH / rSiC as the HSiH angle becomes larger. This is not observed however for the data in Table 6.28.

In order to compare the structures obtained with the structure of methyl silane in the gas phase it is important to compare only the ratios of bond lengths and angles as these are not subject to the arbitrary scaling factor introduced to structures by assuming that rSiC was 1.8686 Å in the LCNMR structures. The best structure for methyl silane in the literature appears to be the microwave structure obtained by Duncan et al.[7] This r_0 structure is given in Table 6.29 along with the predicted r_e values for the C-H and Si-H bonds obtained by M^{c}Kean[23] from studies of isolated Si-H and C-H stretches in a wide variety of related compounds.

Table 6.29 The r_0 structure of methyl silane

PARAMETER	r_0	r_e
rSiC / Å	1.8686(2)	
rCH / Å	1.0957(5)	1.08526
rSiH / Å	1.4832(4)	1.47788
rCH / rSiC	0.5864 (3)	0.5608[a]
rSiH / rSiC	0.7937 (2)	0.7909[a]
<HCH / °	108.03(3)	
<HSiH / °	108.42(3)	

[a]Assuming that rSiC remains at 1.8686 Å

The bond ratios of the different structures obtained for methyl silane are compared in Table 6.30.

Table 6.30 Comparison between r_0 ,r_e and r_α structures of Methyl Silane

Method/solvent	rCH / rSiC	rSiH / rSiC
Microwave (r_o)	0.5864 (3)	0.7937 (2)
Infra Red (r_e)	0.5808	0.7909
E5 (r_α)	0.5836 (7)	0.7919 (7)
ZLI 4792 (r_α)	0.5888 (1)	0.7987 (2)
ZLI 3086 (r_α)	0.5825 (10)	0.7920 (12)
ZLI 1083 (r_α)	0.5877 (45)	0.7963 (59)

If the silane coupling is to be used as an indicator for predicting the structure in best agreement with the gas phase structure, then it is expected that the structure obtained in liquid crystal ZLI 4792, which has a silane coupling of -0.24 Hz, will be the most reliable. However, as can be seen in Table 6.30, this gives a structure where rSiC appears a little shorter than is observed in the gas phase. On comparing the HSiH and HCH bond angles as well it is observed that this structure is indeed in closest agreement with that found in the gas phase and infra red predictions.

It is curious that the HSiH angle is slightly smaller in all the liquid crystal structures than is found in the gas phase. This is different to what has been observed previously in this work, where the gas phase structure has tended to lie somewhere between the structures found in ZLI 4792 and ZLI 3086. It can also be noted, however, that less structural variation of the silyl geometry is observed for methyl silane than for any other of the silyl compounds studied in these different solvents. This is presumably a consequence of methyl silane having the least polar side group of the compounds studied.

6.6.3 Barrier to Internal Rotation

Methyl silane has a 3-fold barrier to internal rotation which can be described by the expression

$$V = \frac{1}{2}V_3(1-\cos 3\alpha)+\frac{1}{2}V_6(1-\cos 6\alpha)$$

Where α is the torsion angle between the methyl and silyl ends of the molecule. This is chosen so that the structure is staggered when $\alpha = 0°$.

The barrier has been measured by microwave spectroscopy using several different techniques. It was measured as ~7.1 kJ mol^{-1} by Kilb et al.[24] using doublets in the microwave spectrum caused by coupling of internal and overall rotation. Lide and Coles[25] obtained a value of ~6.8 kJ mol^{-1} from torsional satellites of the J = 0-1 transition. Wong[26] combined anticrossing molecular beam measurements in the ground torsional state (v = 0) with pure rotational spectra taken from v as high as 4. A value for the internal barrier of 7.086 kJ mol^{-1} was found for tortional levels $v \leq 2$. Interestingly, the model used for these calculations broke down for $v \geq 3$ which led to the suggestion that methyl silane may pass from hindered to free rotation as v increases from 2 to 4.

The barrier has also been studied by ab initio calculations. Radom[27] did a calculation at the MP3/6-31G** level which includes p-polarisation functions on the hydrogen atoms and d-functions on heavy atoms. The barrier was found to be 6.3 kJ mol^{-1}. Magnusson[28] used the 6-31G** basis set to obtain a value of 6.1 kJ mol^{-1}. These calculations also predicted that rCSi would be 0.001 Å longer in the eclipsed confirmation than the staggered, as well as changes to the methyl and silyl geometries. It is predicted that despite the energy gain on relaxation during rotation being greater for the methyl group than the silyl group in methyl silane, that the silyl group will undergo the larger changes to bond length and angles.

Whilst microwave results predict a barrier of ~7 kJ mol^{-1} and ab initio a barrier of ~6.2 kJ mol^{-1}, all investigations have agreed that the equilibrium structure is staggered and that the 6-fold potential V_6 is negligible.

The barrier was therefore calculated in the solution phase by assuming that $V_6 = 0$. Internal rotation was modelled by creating a dummy methyl hydrogen, which could be rotated through 360° and its direct dipolar coupling with one of the silyl hydrogen atoms was then calculated at 1° intervals. By using the barrier height as a refining parameter to determine the probability of the torsion at any given angle, and averaging over a full 360° rotation, it was possible to determine the barrier in each of the four solvents.

$$D36 = \frac{\sum_0^{359} D36 e^{-\frac{V_0}{RT}}}{\sum_0^{359} e^{-\frac{V_0}{RT}}}, \text{ where } V_0 = \frac{1}{2} barrier(1 - \cos 3\alpha)$$

The values obtained for the barrier are listed in Table 6.28. As can be seen, the range in barrier height is relatively small, 0.46 (26) kJ mol^{-1}, between the different solvents. The overall size of the barrier is found to be smaller in the solution than the values reported in the gas phase and by ab initio studies. This is surprising as intuitively, it was expected that with restricted motion in the solution phase, the barrier to internal rotation would be greater than found in the gas phase. Unfortunately, conventional NMR studies in isotropic solvents which make use of observations of the coalescence of peaks, can not be used to measure barriers of rotation smaller than 30 - 40 kJ Mol^{-1}.

However, the structures obtained in the solution phase suggest that rSiC is slightly longer in solution than in the gas phase. This would have the effect of reducing the barrier to internal rotation[29] and so supports the measurements of this barrier made in this work. It is also noted that the barrier height is consistent in the four solvents, in that the longer the parameter rSiC, the smaller the barrier appears to be. The barrier

is also found to be particularly sensitive to the value of D_{16}, with a 1% change in D_{16} resulting in a change of ~1.35 kJ mol^{-1} in the barrier.

6.6.4 Conclusion

The structure of methyl silane has been determined in four chemically different liquid crystal environments. It has been shown that there is a solvent dependence on the structure obtained, with the liquid crystal solvent ZLI 4792 resulting in a structure which is in best agreement with that found from microwave studies.

The barrier to internal rotation has also been determined in these liquid crystal environments, and shows the expected decrease in height with increasing SiC bond length. The magnitude of the barrier is smaller than values obtained from microwave and ab initio studies. The most likely explanation to this being that the structure of methyl silane in the solution phase is different to that found in the gas phase and that the technique of LCNMR is very sensitive to small changes in the direct couplings used.

6.7 Conclusion

The structure of a range of compounds of the general formula SiH_3X, where X = Br, Cl, I, F, CN and CH_3 have been studied using a variety of liquid crystal solvents by conventional LCNMR techniques with vibrational corrections being applied to the direct dipolar couplings.

The results obtained are summarised in Table 6.31 and are compared to those found previously be microwave spectroscopy (r_0 structure). HSiH for each solvent was then plotted against the D_{SiH} coupling of silane for each of the different liquid crystal solvents used (Figure 6.9).

Table 6.31 Summary of HSiH angles obtained (°)

Solvent	SiH_3Br	SiH_3Cl	SiH_3I	SiH_3F	SiH_3CN	SiH_3CH_3
ZLI 1167	112.45 (12)	112.38 (10)				
ZLI 3086	110.20 (28)	109.62 (25)	110.37 (20)	113.31 (20)	111.85 (17)	107.95 (4)
ZLI 4792	111.12 (38)	111.05 (12)	111.12 (12)	111.51 (19)	112.36 (12)	108.28 (1)
ZLI 1083	112.56 (12)	112.55 (10)		112.78 (10)	113.64 (11)	108.27 (15)
Mixt. 1	112.98 (12)					
E 7 / E 5	112.98 (12)	112.60 (10)		112.67 (10)	113.68 (11)	108.19 (4)
Gas Phase	110.7	110.6	110.7	110.6	111.6	108.42

Figure 6.9 The variation in HSiH with D_{SiH} (SiH_4) for some silyl compounds

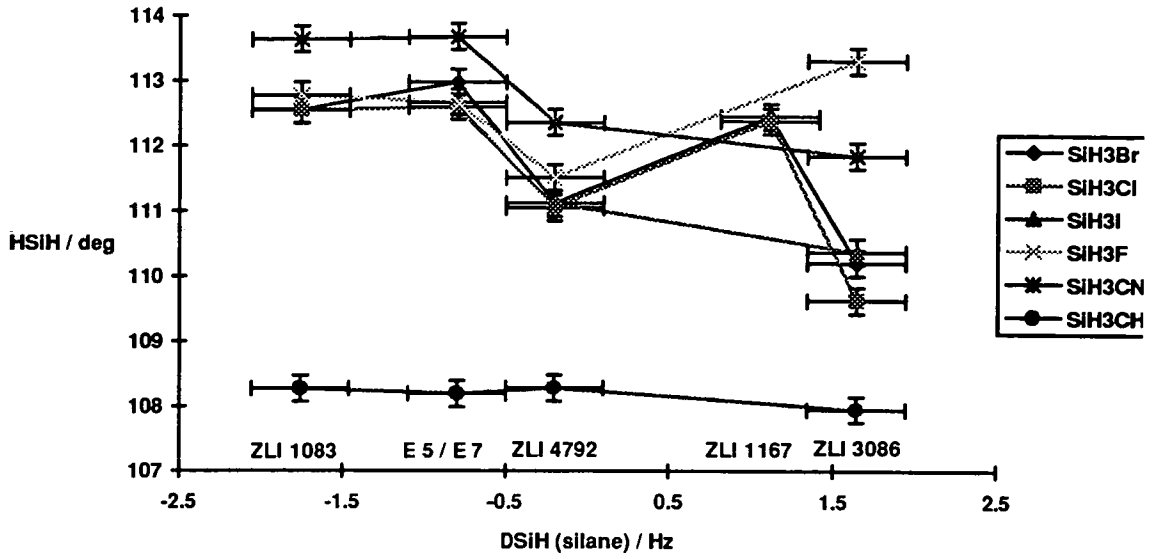

It is observed in Figure 6.9 that with the exception of an anomalous result for silyl fluoride, HSiH is always smallest in liquid crystal ZLI 3086 which is a non-polar solvent. The next smallest HSiH angle is almost always found in ZLI 4792 which is a super fluorinated solvent. It was discovered that both of these solvents give HSiH angles in reasonable agreement with the ground state gas phase values, with ZLI 3086 giving an angle smaller and ZLI 4792 giving an angle larger than is found in the gas phase in almost every case.

All the other liquid crystal solvents used gave rise to HSiH angles that were larger than these. This has been attributed to the presence of cyano groups in these liquid crystals. It is proposed that the cyano group interacts with the silyl unit, forming an five co-ordinate silicon in an S_N2 intermediate. This is observed in the crystalline phase of silyl cyanide and to a lesser extent in the crystalline phase of silyl fluoride and silyl chloride where it is the fluoride and the chloride that interact with the silicon respectively. Some evidence that this is occurring in the solution phase was obtained when it was observed that that the most unstable of the silyl compounds used, silyl iodide, reacted on warming to room temperature with all the cyano containing liquid

crystals it was dissolved in. Also, it is clear from Figure 6.9 and from Table 6.31 that the HSiH angle shows very little variation in HSiH angle in the various cyano containing liquid crystal solvents.

In Chapter 7 the analysis of these compounds is continued by applying a further correction to the direct dipolar couplings. The theory of this has been outlined in Chapter 2 and takes into account the correlation between the vibration and the reorientation of the solute molecules.

References

[1] J.Jokisaari and Y.Hiltunen, Mol. Phys., 50(5), (1983), 1013

[2] C.A.Brookman, 4th year project report., University of Edinburgh, (1989)

[3] W.Schneider and W.Thiel, J. Chem. Phys., 86(2), (1987), 923

[4] S.Cradock, private communication

[5] L.Hedberg and I.M.Mills, J. Mol. Spectr., 160, (1993), 117

[6] R.Kewley, P.M.McKinney and G.Robiette, J. Mol. Spectrosc., 34, (1970), 390

[7] J.L.Duncan, J.L.Harvie, D.C.Mckean and S.Cradock., J. Mol. Struct., 145, (1986), 225

[8] M.D.Harmony, V.W.Laurie, R.L.Kuczkowski, R.H.Schwendemann, D.A.Ramsay, F.J.Lovas, W.J.Lafferty and A.G.Macki., J. Phys. Chem. Ref. Data., 8, (1979), 619

[9] E.A.V.Ebsworth and J.J.Turner, J. Chem. Phys., 36(10), (1962), 2628

[10] R.Ditchfield and L.C.Snyder, J. Chem. Phys., 56, (1972), 5823

[11] G.J.den Otter and C.Maclean, J. Magn. Reson., 5, (1971), 44

[12] J.Lounila and J.Jokisaari, Prog. NMR. Spectrosc., 15, (1982), 249

[13] M.Barfield, Chem. Phys. Letters., 4, (1970), 518

[14] R.Ader and A.Loewenstein, J. Amer. Chem. Soc., 96, (1974), 5336

[15] P.D.Blair, Ph.D. Thesis, University of Edinburgh, (1984)

[16] P.D.Blair, A.J.Blake, R.W.Cockman, S.Cradock, E.A.V.Ebsworth and D.W.H.Rankin, J.Mol. Struct., 193, (1989), 279

[17] P.J.Mathieson, "4th Year Project", University of Edinburgh, (1991)

[18]Derived from the program LEQUOR, P.Diehl, H.P.Kellerhals and W.Niederberger, J. Magn. Reson., 4, (1971), 352

[19] J.L.Duncan, J.L.Harvie, D.C.McKean and S.Cradock, J. Mol. Struct., 145, (1986), 225

[20] R.Ader and A.Loewenstein, J. Amer. Chem. Soc., 96, (1974), 5336

[21] J.Gerritson and C.Maclean, J. Magn. Reson., 5 (1971), 44

[22] A.Komornicki, J. Amer. Chem. Soc., 106, (1984), 317

[23] D.C.McKean, I.Torto, J.E.Boggs and K.Fan, J. Mol. Struct. (Theochem), 260, (1992), 27

[24]R.W.Kilb and L.Pierce, J. Chem. Phys., 27, (1957), 108

[25]D.R.Lide and D.K.Coles, Phys. Rev., 80, (1950), 911

[26]M.Wong, I.Ozier and W.L.Meerts, J. Mol. Struct., 102, (1983), 89

[27]L.Radom, J. Mol. Struct., 126, (1985), 271

[28]E.Magnusson, Aust. J. Chem., 39, (1986), 735

[29] P.R.Schleyer, M.Kaupp, F.Hampel, M.Bremer and K.Mislow, J. Amer. Chem. Soc., 114, (1992), 6791

[30] J.W.Emsley and J.C.Lindon, "NMR Spectroscopy using Liquid Crystal Solvents", Permagon Press, Oxford, (1975)

Chapter 7

A study of Silyl Containing Compounds in the Liquid Crystal Environment - The Correlation between Vibration and Reorientation of the Solute

7 Introduction

In Chapter 2, the correlation between vibration and reorientation of solute molecules in LCNMR experiments was explained. The theory was first introduced by Snijders et al.[1] and then developed by Lounila and Diehl[2,3] for the treatment of more general solute molecules. Several molecules have now been successfully analysed using this approach with great success. These include the structures of hydrogen cyanide[4] cyclopropane[5], iodobenzene[6], benzene and chlorobenzene.[7] A related approach examining the solvent dependence on the structure of solute compounds has also inlcuded iodobenzene[8] as well as acetonitrile[9] and pyrrole.[10]

Two related compounds which have also been studied, and the contribution of this effect taken into account, are methyl iodide and methyl fluoride.[11] It was observed in earlier work[12] that the structure of methyl iodide displayed a strong solvent dependence which was found to be related to the D_{CH} coupling observed from methane also dissolved in the sample tube. A similar effect was found for methyl fluoride.[11] Both of these compounds were found to have HCH angles as much as two degrees larger in the liquid crystal phase than was found in the gas phase. By taking into account this new correction to the LCNMR data it was found that all the experimental data could be refined together to give a satisfactory agreement with the gas phase structure of these compounds.

This same solvent dependence was observed in Chapter 6 and in earlier work[13,14] for silyl containing compounds. It was therefore decided to introduce a correction for this correlation effect in the compounds studied in Chapter 6. The computer program MASTER was obtained from the authors of reference 7. Guidelines for writing input instructions for this program are given in Appendix A and have been adapted from comments and examples from the source code of the program.

MASTER is a least squares refinement program. Because of the need to calculate the correlation between vibration and reorientation of the direct couplings, the harmonic force field for the molecule being studied must also be included in the input. This is

done using subroutines from the program VIBR.[15] Unfortunately, VIBR requires the harmonic force field to be inputted in terms of internal co-ordinate force constants, whereas previous work was carried out using ASYM20 where symmetry co-ordinate force constants were used. This was overcome by using the program UFU[16] to transform the force constants. The advantage of having the force field in the same program as the least squares refinement takes place is that harmonic corrections to the direct couplings can be made *in situ* as the data are refined and the orientation parameter changes.

In Chapter 2 it was explained that to make this additional correction to the direct coupling, it is necessary to calculate the interaction tensor. This can be done as a function of the molecular geometry and two bond interaction parameters, ΔA_{SiH} and ΔA_{SiX}. At the equilibrium geometry the molecular interaction tensor is axially symmetric (around the SiX bond in the case of the silyl halides) and has the anisotropy,

$$\Delta A = \Delta A_{SiX} + 3\Delta A_{SiH}\cos\alpha$$

where α is the HSiH angle. Since the orientation can be defined as

$$S = \frac{3}{4c}\left[e^{c}\left(\int_0^1 e^{cx^2}dx\right)^{-1} - 1\right] - \frac{1}{2}, \text{ where } c = \frac{3\Delta A}{2k_BT}$$

it is possible to use as independent parameters for example ΔA_{SiH} and S which can be determined experimentally from the spectral data. The resulting deformational correction factor in terms of A_{SiH} and c = c(S) is

$$p_{ij}^{d} = -\Delta A_{SiH}\left(\frac{a_1^{ij}}{S} + a_2^{ij} - c\frac{T}{T_0}\left(\frac{a_3^{ij}}{S} + a_4^{ij}\right)\right)$$

This is calculated in the program MASTER using the harmonic force field in the subroutine VIBR.

In Chapter 6, where X = Br, Cl and I, it was only possible to calculate the HSiH angle for SiH_3X. This is because in each experiment only two direct couplings are obtained, one of which is required to determine the orientation parameter. In order to determine the interaction tensor for these molecules and hence make the extra correction to the direct dipolar couplings, it was necessary to find some other piece of information. In the case of methyl iodide and methyl fluoride this extra information was the D_{CH} coupling of methane dissolved in the same sample tube as the solute. In this work silane was used instead and so the D_{SiH} coupling from the silane is the extra information used to allow this correction to be made.

Silane is a tetrahedral molecule and therefore has a zero orientation parameter. This means that there is no harmonic contribution to the dipolar coupling and only the deformational contribution is observed. This is expressed as

$$D_{ij} = p_{ij}^{d}\ ,\ D_{ij}^{e} = -P_2(\cos\beta)a_{ij}\Delta A_{SiH}$$

where $P_2(x) = \frac{1}{2}\left(3x^2 - 1\right)$ is the Legendre polynomial and β is the angle between the magnetic field direction and the director. i.e. the experimental coupling constant of silane is used as a direct measure of the torque acting on the SiH bond. It is assumed that the torques acting on silane will be linearly related to the torques acting on SiH_3X. i.e.

$$\Delta A_{SiH}(SiH_3X) = K_X \Delta A_{SiH}(SiH_4)$$

where K_X is a proportionality constant (dependent on X).

The program MASTER enables this to be done by allowing the observed coupling from the probe molecule (silane in this case) to be entered along with the direct couplings from the solute molecule, and relates this to A_{SiH} by fitting a slope and an intercept to the data. Because it is expected that the least distortion in the solute

structure is when D_{SiH} of silane is zero (i.e. no torques are acting on the bond interaction tensor), the intercept is fixed at zero and only the slope (K_X) is refined.

7.1 Results from Conventional LCNMR study of Silyl Geometries

The silyl geometries of a range of compounds of the general formula SiH_3X (X = Br, Cl, I, F, CN and CH_3) were studied using a variety of liquid crystal solvents by LCNMR spectroscopy, taking account of the vibrational corrections to the direct dipolar couplings only. The results of this work are presented in Chapter 6 where it was observed that the silyl geometry showed a marked solvent dependency. The D_{SiH} direct coupling of silane was also obtained in these experiments and the silyl geometry (HSiH angle) was plotted against this. This plot is shown again as Figure 7.1.

Figure 7.1 The variation in HSiH with D_{SiH} (SiH_4) for some silyl compounds

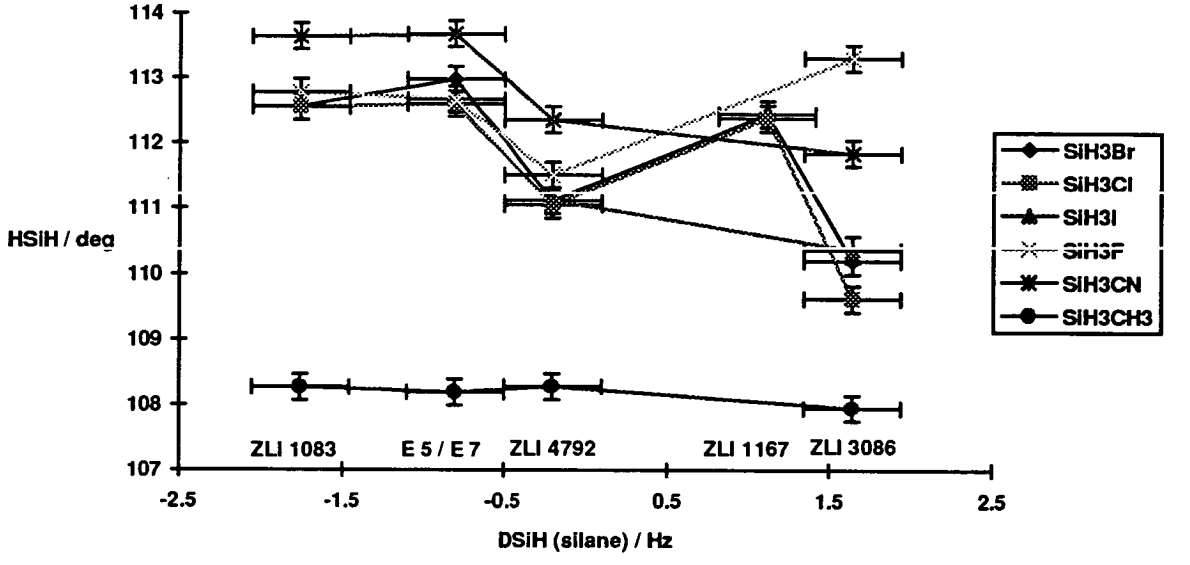

As was discussed in the conclusion to Chapter 6, all the liquid crystals used except for ZLI 4792 and ZLI 3086 (corresponding to D_{SiH} values of silane of -0.2 Hz and 1.65 Hz in the fluorinated and non-polar solvents respectively) contained cyano groups and have led to structures with relatively large HSiH angles as compared to the gas phase structures of these compounds. It was proposed that these cyano containing liquid crystals interact with the silyl solute molecules in solution via the

cyano group resulting in five co-ordinate silicon in an S_N2 type intermediate. This is supported by the very small variation in HSiH angle observed in these liquid crystals despite having comparatively different D_{SiH} couplings from silane. The only significant variations observed in HSiH are between these structures and the two different structures observed in ZLI 4792 and ZLI 3086.

It was also observed that the HSiH angle obtained in the gas phase for each of these compounds lay between the values observed in ZLI 4792 and ZLI 3086, with the angle being smaller than the gas phase value in ZLI 3086 and larger in ZLI 4792. This is significant because the direct dipolar coupling (D_{SiH}) observed in silane changes sign on moving from ZLI 3086 to ZLI 4792, indicating that if the silane is indeed a reliable probe to measure the distortion experienced by the silyl group by the orienting forces of the solvent, then the extrapolated HSiH angle at zero distortion is predicted to be in reasonably good agreement with the value observed in the gas phase.

7.2 Reanalysis of the Silyl Structures Allowing for the Correlation Between Vibration and Reorientation in the Direct Dipolar Couplings

The direct dipolar coupling data obtained in Chapter 6 have been reanalysed using the program MASTER allowing for the correlation between vibration and reorientation of the solute. In all cases, the same harmonic force fields were used as before, but the force constants were converted from symmetry co-ordinate force constants to internal co-ordinate force constants using the program UFU.[16] An example of an input file is given in Appendix A along with instructions for the use of the program.

This theory makes corrections to the direct dipolar couplings for the apparent deformations which result as a neglect of this additional correction. It is unreasonable to expect, however, meaningful results to be obtained when a real deformation is taking place as a consequence of some chemical interaction, like the cyano interaction that is suspected to be taking place in those liquid crystals which contain cyano

groups, and so these results were left out of the refinement. The results obtained after analysis by the program MASTER are presented in Table 7.1. It was not possible to carry out a sensible refinement for silyl fluoride, however, as an anomalous result for the structure in liquid crystal ZLI 3086 was obtained previously. An attempt to refine silyl fluoride using the results obtained in ZLI 1083 instead of ZLI 3086 resulted in an HSiH angle of 110.45 °, but with K_X refining to 43.87 and a p^d correction of 0.75963 Hz for D_{SiH} in ZLI 1083. This resulted in rSiH refining to a larger value than rSiF which was clearly unreasonable.

Table 7.1 Results of the refinement with MASTER

a)

	SiH_3Br		SiH_3Cl		SiH_3I	
Solvent	**ZLI 4792**	**ZLI 3086**	**ZLI 4792**	**ZLI 3086**	**ZLI 4792**	**ZLI 3086**
$p^d D_{HH}$ / Hz	1.00036	1.02839	1.00007	1.02843	1.00045	0.02532
$p^d D_{SiH}$ / Hz	0.99831	1.07972	0.99825	1.09139	0.99890	1.06612
A_{SiH} / 10^{-22} J	-0.62	5.15	-0.47	5.06	-0.54	4.71
A_{SiX} / 10^{-22} J	16.43	11.12	6.61	7.54	20.30	11.89
Szz	0.08749	0.02826	0.03531	0.01101	0.10791	0.03439
K_X	3.12386		2.59656		2.36914	
HSiH / °	111.10		110.83		111.10	
Gas Phase / °	110.7		110.6		110.7	

b)

	SiH_3CN			SiH_3CH_3	
Solvent	**ZLI 4792**	**ZLI 3086**		**ZLI 4792**	**ZLI 3086**
$p^d D_{HH}$ / Hz	0.99376	1.01407	$p^d D_{14}$ / Hz	0.99378	1.00496
$p^d D_{SiH}$ / Hz	0.99315	1.04092	$p^d D_{12}$ / Hz	0.99430	0.99967
$p^d D_{CH}$ / Hz	0.99236	1.00476	$p^d D_{15}$ / Hz	0.99595	0.99908
$p^d D_{CN}$ / Hz	0.99913	1.00517	$p^d D_{56}$ / Hz	1.03800	1.02261
A_{SiH} / 10^{-22} J	-0.70 (9)	5.87 (78)	$p^d D_{67}$ / Hz	1.01523	1.00844
A_{SiC} / 10^{-22} J	23.0 (93)	14.5 (91)	$p^d D_{46}$ / Hz	1.00738	1.00398
A_{CN} / 10^{-22} J	1.9 (97)	3.0 (100)	A_{SiH} / 10^{-22} J	-0.09 (9)	0.88 (89)
Szz	0.13418	0.05643	A_{CH} / 10^{-22} J	4.0 (156)	2.7 (171)
rCSi / rSiH	1.266 (4)		A_{SiC} / 10^{-22} J	12.6 (139)	13.1 (154)
rCN / rSiH	0.753 (2)		Szz	0.04492	0.04917
K_X	3.3566		rCH / rSiC	0.584 (21)	
HSiH / °	112.33		rSiH / rSiC	0.7987 (22)	
Gas Phase / °	111.6		K_X	0.46326	
			HSiH / °	108.26 (6)	
			Gas Phase / °	108.42	
			HCH / °	108.3 (12)	
			Gas Phase / °	108.03	

It is evident that the corrected values for the HSiH angle are larger than the gas phase value for all molecules except methyl silane where HSiH is slightly smaller than the gas phase value and HCH is larger. The differences in angle observed for the other compounds are all remarkably similar. Around 0.4° for the silyl halides and 0.7° for silyl cyanide. This did not come as a surprise since D_{SiH} of silane is just -0.2 Hz in the solvent ZLI 4792 and so the angle always comes out to be just slightly smaller than this. The fact that all compounds give this slightly larger angle than was expected, and because this angle is almost totally dependent on the data from ZLI 4792 (the fluorinated solvent) it was considered that this small enlargement of the angle could be as a consequence of fluorine from the liquid crystal co-ordinating to the silicon from the silyl compounds in the same way as is thought to be the case for cyano containing liquid crystals. This interaction is observed in the crystalline phase of silyl

fluoride[17], where molecules form infinite zigzag chains. Because the interaction does not occur at 180° in the crystal it is only possible to obtain the mean HSiH angle observed which is 111 (5)°. There are obviously large errors associated with this angle but it does imply an opening out of the HSiH angle of silyl fluoride by around 0.4°.

The program MASTER was therefore used to predict the corrections to the direct dipolar couplings for the data obtained in the non polar solvent ZLI 3086. As no functional groups are present in this compound there should be no deformations as a result of specific interactions, and it assumed that any apparent deformations from the microwave structure are a direct consequence of the correlation between vibration and reorientation.

Refinement for each compound was carried out by fixing the structure at that obtained from microwave studies and allowing the anisotropy and slope to refine freely. This refinement is liable to large errors, particularly for silyl bromide, iodide and chloride, as there are three unknowns being determined by just three direct couplings, one of which is D_{SiH} from silane. Also, it is the structures obtained in ZLI 3086 that are most susceptible to errors as a result of small variations in the indirect couplings, J_{ij}. However, the slope obtained from this calculation was then used to determine A_{SiH} in other solvents. This allowed the structure to be refined in these solvents with A_{SiH} fixed by the value of the slope obtained in the ZLI 3086 refinement, Table 7.2.

Table 7.2 Final HSiH angles (°) determined by MASTER

	SiH_3Br	SiH_3Cl	SiH_3I	SiH_3F	SiH_3CN	SiH_3CH_3
K_X	1.67 (36)	1.56 (26)	1.02 (35)	3.98 (6)	1.43 (66)	1.65 (34)
ZLI 3086	110.70 (+50)*	110.60 (+98)	110.70 (+33)	110.60 (-271)	112.00 (+15)	108.42 (+47)
ZLI 4792	111.11 (-01)	111.01 (-04)	111.09 (-03)	110.30 (-121)	112.27 (-09)	108.24 (-04)
ZLI 1083	112.43 (-13)	112.43 (-12)		112.51 (-27)	113.51 (-13)	108.18 (+09)
E 7 / E 5	112.87 (-11)	112.50 (-10)		112.49 (-18)	113.53 (-15)	108.13 (-06)
ZLI 1167	112.39 (-06)	112.30 (-08)				
Mixt. 1	112.87 (-11)					

*Values in brackets are the change in the last two digits of the angle as a result of the correction for vibration and reorientation

The change in HSiH from those calculated previously (using the vibrational corrections to the dipolar couplings only) is always greater for compounds in solvent ZLI 3086. There are two reasons for this, firstly ZLI 3086 gives rise to small orientation parameters and hence small direct dipolar couplings. This results in small corrections to the data having relatively large effects on the structure obtained. The second reason is D_{SiH} of silane in ZLI 3086 is relatively large (~1.9 Hz) compared to values obtained in other solvents, and the solvent with the next smallest dipolar couplings is ZLI 4792 which has D_{SiH} silane smallest of all in magnitude (-0.2 Hz).

In analysing these results, first of all consider the three simplest compounds, silyl bromide, chloride and iodide. For each compound it is only possible to refine the HSiH angle. On examining Table 7.2 it is evident that these compounds have experienced just three different liquid crystalline environments. In each case the data have been refined to match the gas phase value in the non polar solvent, but the HSiH angle refines to values 0.4 (1)° and 1.85 (30)° larger than this for the fluorinated and cyano containing liquid crystals respectively.

A more detailed summary of the refinements are given in Table 7.3 and the relationship between A_{SiH} and A_{SiX} is shown to be approximately linear in Figure 7.2.

Table 7.3 Final Refinement of SiH_3X (X = Br, Cl and I) in MASTER

SiH_3Br	K_{Br} = 1.67 (36)					
Solvent	$p^d D_{HH}$ (Hz)	$p^d D_{SiH}$ (Hz)	A_{SiH} (10^{-22} J)	A_{SiBr} (10^{-22} J)	Szz	HSiH (°)
ZLI 3086	1.01604	1.04497	2.76	8.47	0.02759	110.70
ZLI 4792	1.00086	0.99974	-0.33	16.65	0.08704	111.11 (5)
ZLI 1083	0.99911	0.99591	-2.94	37.45	0.21688	112.43 (2)
E 7	1.00022	0.99833	-1.37	31.77	0.18163	112.87 (3)
Mixt. 1	1.00022	0.99833	-1.34	32.05	0.17730	112.87 (3)
ZLI 1167	0.99880	0.99536	-3.71	42.00	0.24670	112.39 (4)

SiH_3Cl	K_{Cl} = 1.56 (26)					
Solvent	$p^d D_{HH}$ (Hz)	$p^d D_{SiH}$ (Hz)	A_{SiH} (10^{-22} J)	A_{SiCl} (10^{-22} J)	Szz	HSiH (°)
ZLI 3086	1.01860	1.05677	3.03	7.82	0.02297	110.60
ZLI 4792	1.00132	1.00020	-0.28	14.39	0.07471	111.01 (6)
ZLI 1083	0.99969	0.99618	-2.74	32.75	0.18902	112.43 (3)
E 7	1.00095	0.99921	-1.01	28.69	0.15667	112.50 (3)
ZLI 1167	0.99922	0.99508	-3.51	34.25	0.20228	112.30 (4)

SiH_3I	K_I = 1.02 (35)					
Solvent	$p^d D_{HH}$ (Hz)	$p^d D_{SiH}$ (Hz)	A_{SiH} (10^{-22} J)	A_{SiCl} (10^{-22} J)	Szz	HSiH (°)
ZLI 3086	1.01181	1.03045	2.04	8.63	0.03217	110.7
ZLI 4792	1.00092	1.00022	-0.24	19.65	0.10262	111.09 (4)

Figure 7.2 Plot of A_{SiX} (10^{-22} J) versus A_{SiH} (10^{-22} J) for SiH_3X (X = Br, Cl and I)

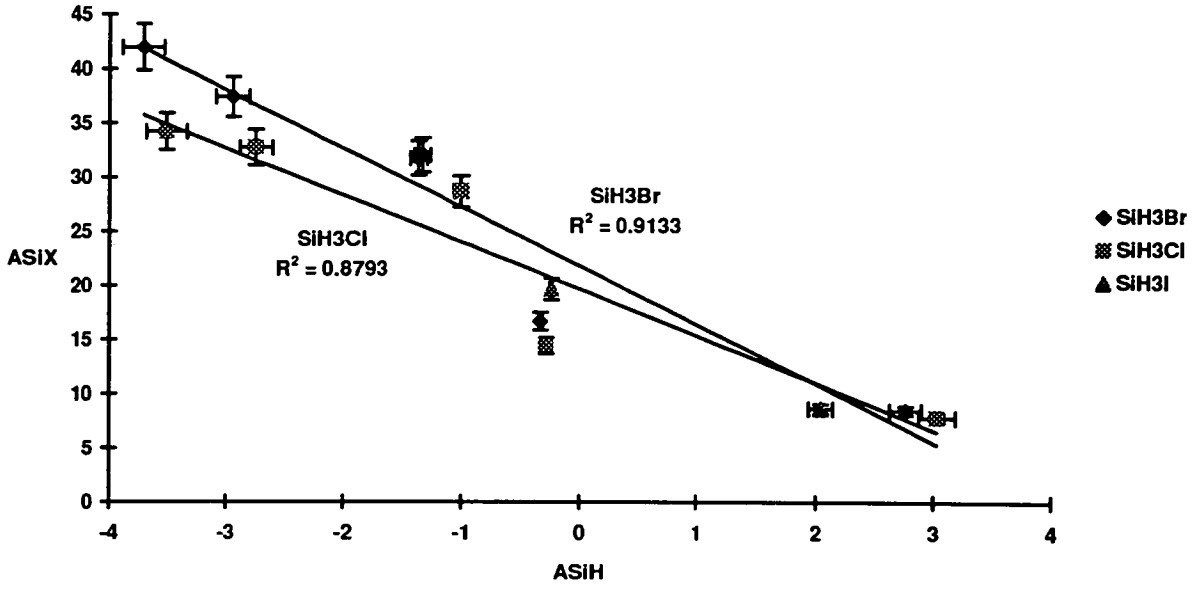

The deviations from a straight line are as a result of the different structures that occur in these different liquid crystals solvents. The larger A_{SiX} for the cyano containing liquid crystals are as a result of slightly shorter rSiH than is found in the fluorinated solvent. Another, potentially large source of error is in the calculation of A_{SiH}. It is likely that the errors associated with calculating D_{SiH} from silane, particularly the uncertainty in the isotropic coupling, J_{SiH}, may contribute to systematic errors for results in different types of liquid crystal solvents.

Next is silyl fluoride. This has an additional coupling to ^{19}F and therefore information can also be obtained about rSiF in the refinement. This is done by keeping rSiH fixed at 1.48 Å. Silyl fluoride gave the most surprising results in this refinement. All four direct couplings (including D_{SiH} in silane) from solvent ZLI 3086 were refined to fit the gas phase structure with an r.m.s. of just 0.07 Hz. Also, when the resultant value for K_F was applied to data in other solvents, equally sensible results were obtained. As in the other silyl halides, the two solvents ZLI 1083 and E 7 which contain cyano groups gave an HSiH angle of 112.5° although the fluorinated solvent, ZLI 4792, gave a slightly smaller angle than was expected on comparison with the other silyl halides, but never the less fits the gas phase structure within experimental errors. The complete results of the analysis of silyl fluoride are given in Table 7.4.

Table 7.4 Final refinement of silyl fluoride

SiH_3F	K_F = 3.98 (6)			
Solvent	**ZLI 3086**	**ZLI 4792**	**ZLI 1083**	**E 7**
$p^d D_{SiH}$ (Hz)	0.91109	0.99809	0.99679	0.99953
$p^d D_{HH}$ (Hz)	0.63753	0.98434	0.98418	0.99205
$p^d D_{HF}$ (Hz)	0.97602	1.00078	1.00002	1.00111
A_{SiH} (10^{-22} J)	7.96	-0.96	-6.73	-3.22
A_{SiF} (10^{-22} J)	6.43	3.10	17.40	17.30
Szz	-0.00839	0.02011	0.12661	0.10646
r_{SiF} / r_{SiH}	1.0743	1.065 (7)	1.108 (1)	1.107 (1)
HSiH (°)	110.60	110.30 (26)	112.51 (2)	112.49 (4)

The bond ratio r_{SiF} / r_{SiH} is consistent with the calculated HSiH angle as rSiF becomes longer with increasing HSiH. The refinement predicts that r_{SiF} is 0.014 (10) Å shorter and 0.050 (3) Å longer than the gas phase value in the fluorinated and cyano containing liquid crystals respectively. This can be compared to a lengthening of 0.010 (1) Å between the observed bond lengths in the gas and crystalline phase. This difference will actually be slightly larger than this as the crystal data was recorded at 96 K and so rSiF in the crystal phase would actually be a little longer at warmer temperatures.

The fact that the structure in the fluorinated solvent has refined to give a shortened rSiF bond length and a smaller HSiH angle to the gas phase is an indication that the errors involved in the direct dipolar couplings obtained in ZLI 3086 and ZLI 4792 have been underestimated. As mentioned before, as a result of the small orientation parameters and direct dipolar couplings, the structure obtained in these solvents is very sensitive to any small variations in the indirect couplings, J_{ij}. The relationship between A_{SiH} and A_{SiF} is shown to be approximately linear in Figure 7.3.

Figure 7.3 Plot of A_{SiF} (10^{-22} J) versus A_{SiH} (10^{-22} J) for SiH_3F

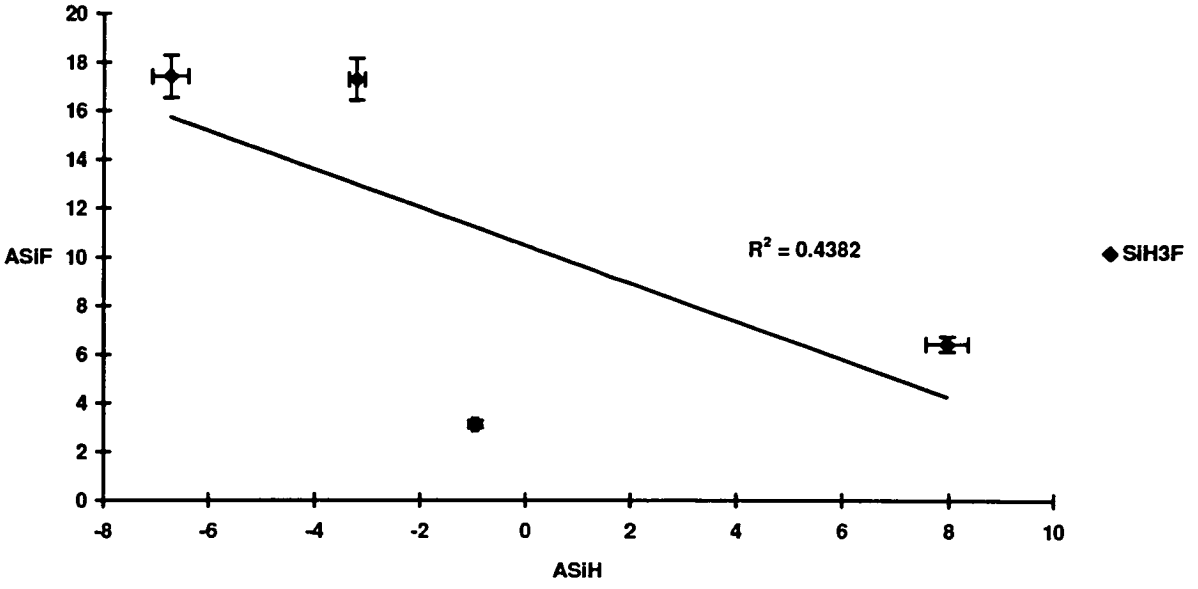

The poor fit to the straight line is largely a result of the ZLI 4792 data. It is clear from this and from the structure and anisotropy (below) that the data in this solvent are less reliable than in the other solvents. It should be remembered in these plots, however, that unlike in the case of the methyl halides where the distortions in methyl structure was shown to be an 'apparent' deformation, in the case of these silyl compounds a significant proportion of the deformations are 'real'.

Another interesting observation from the silyl fluoride refinement was that in changing A_{SiF} to keep rSiF at 1.48 Å, the fit of the D_{HF} coupling began to show some discrepancies. It was reported that J_{HF}^{aniso} is of the order 0.2 - 0.5 % in methyl fluoride.[18] It was therefore decided to estimate the anisotropy in J_{HF} in each of these four solvents for silyl fluoride. This was done as in Chapter 6 for the J_{SiF} coupling by assuming that $\frac{1}{2}J^{aniso}$ is equal to the difference between the experimental and calculated direct dipolar couplings. The results for J_{HF} are given in Table 7.5.

Table 7.5 Anisotropy of the indirect coupling J_{HF}

Solvent	½ J_{HF}^{aniso} (Hz)	Szz	J_{HF}^{aniso} / 2 Szz (Hz)	J_{HF}^{aniso} / 2 D_{HF}^{calc} (%)
ZLI 3086	0.157	-0.00839	18.7 (224)	0.5 (6)
ZLI 4792	-2.182	0.02011	108.5 (300)	2.9 (8)
ZLI 1083	-2.201	0.10646	20.7 (35)	0.6 (1)
E 7	-3.189	0.12661	25.2 (36)	0.7 (1)

Apart from the anomalous result obtained in ZLI 4792, it appears that the anisotropy in J_{HF} is ~0.6 (1) % in silyl fluoride. It is a little surprising that such a good correlation is found when the differences in r_{SiF} are considered. The result in ZLI 4792 may be as a result of inadequate indirect couplings being used. This would also explain both the smaller HSiH angle and rSiF bond length that was observed previously.

The sensitivity of the results obtained in ZLI 3086 and ZLI 4792 are emphasised further in the case of silyl cyanide. When the HSiH angle was fixed at 111.6°, K_{CN} refined to a value of -1.60. This was thought odd since K_X was found to be positive for all the other silyl compounds studied. It was found that by increasing HSiH to 112.0°, K_{CN} became +1.43 which is much more in line with expectations. The results for silyl cyanide in other solvents were not particularly sensitive to this change in sign of K_{CN}, with the maximum change in calculated angle being only 0.03°. It was therefore decided to refine the data for silyl cyanide without the use of D_{SiH} (silane). This is possible for silyl cyanide because of the extra couplings involving ^{13}C and ^{15}N. This resulted in very large errors but results are in good agreement with those obtained using K_X at 1.43.

A plot of A_{SiH} versus A_{SiC} demonstrates the approximate linearity of the relationship between A_{SiH} and A_{SiC} in each of the three refinements (Figure 7.4). and the results obtained are compared in Table 7.6.

Figure 7.4 Plot of A_{SiC} (10^{-22} J) versus A_{SiH} (10^{-22} J) for SiH_3CN

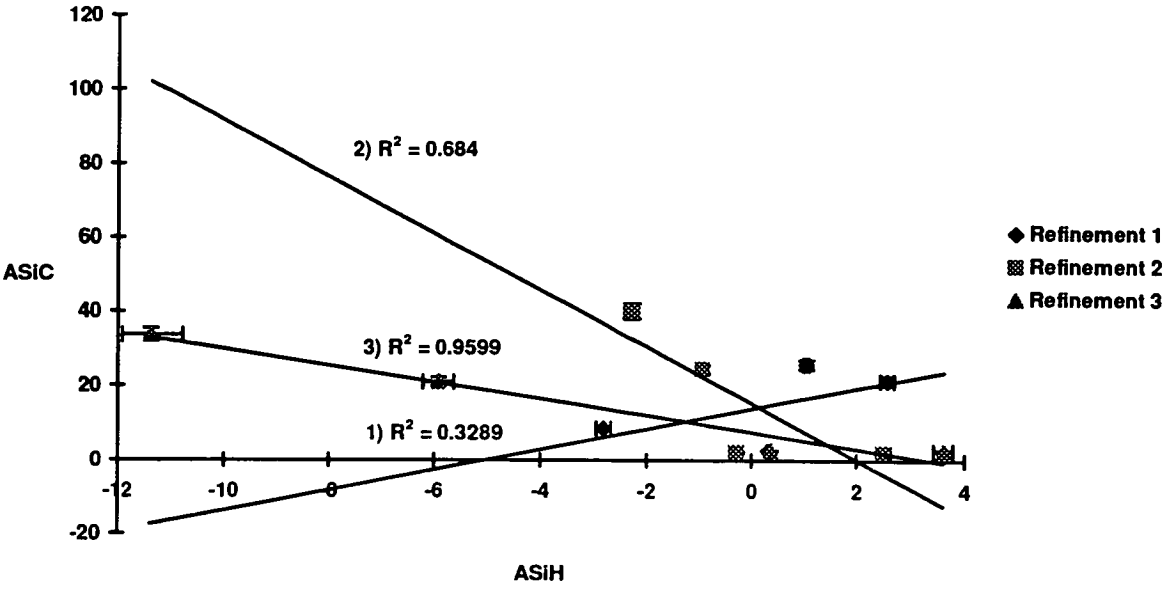

Table 7.6 Results for the three different refinements of silyl cyanide

SiH_3CN	1) K_{CN} = -1.6 (7)			2) K_{CN} = 1.4 (7)			3) Did not use D_{SiH} from silane in refinement					
Solvent	**ZLI 3086**			**ZLI 4792**			**ZLI 1083**			**E 7**		
Refinement	**1**	**2**	**3**	**1**	**2**	**3**	**1**	**2**	**3**	**1**	**2**	**3**
$p^d D_{HH}$ (Hz)	0.98136	1.02708	1.03100	1.01765	1.01652	1.01749	1.01131	0.99377	0.98620	1.00142	0.99929	0.99383
$p^d D_{SiH}$ (Hz)	0.96803	1.03657	1.04526	1.01618	1.01404	1.01613	1.01136	0.99300	0.97908	1.00240	0.99833	0.98784
$p^d D_{CH}$ (Hz)	0.98254	1.02691	1.02954	1.02020	1.01951	1.02011	1.01167	0.99289	0.98802	1.00042	0.99903	0.99552
$p^d D_{NH}$ (Hz)	0.99562	1.00620	1.00719	1.00344	1.00303	1.00347	1.00274	0.99892	0.99635	1.00058	1.00000	0.99825
A_{SiH} (10^{-22} J)	-2.81	2.50	3.61	0.32	-0.29	0.37	2.56	-2.28	-11.35	1.04	-0.93	-5.91
A_{SiC} (10^{-22} J)	8.62	1.95	2.68	2.58	2.17	2.62	21.50	40.17	33.80	28.87	24.53	21.17
A_{CN} (10^{-22} J)	-1.87	11.00	11.61	21.80	21.29	21.54	28.80	4.19	0.85	9.79	9.01	7.04
Szz	0.04891	0.05163	0.05241	0.012515	0.12365	0.12365	0.25588	0.25171	0.25165	0.18532	0.18532	0.18530
r_{CSi} / r_{SiH}	1.243	1.243	1.246	1.253	1.258	1.259	1.284	1.283	1.276	1.280	1.278	1.273
r_{CN} / r_{SiH}	0.777	0.777	0.775	0.776	0.779	0.779	0.780	0.779	0.777	0.777	0.777	0.775
HSiH (°)	111.60	112.00	112.10	112.29	112.27	112.29	113.53	113.51	113.40	113.56	113.53	113.44
	Previous structures											
r_{CSi} / r_{SiH}	1.236			1.264			1.284			1.283		
r_{CN} / r_{SiH}	0.748			0.759			0.786			0.784		
HSiH (°)	111.85			112.36			113.64			113.68		

It was observed that although the anisotropies (A_{SiH}, A_{SiX}) and the deformation corrections vary depending on the refinement carried out, in all cases the HSiH angle and bond lengths are corrected towards their gas phase values. The largest corrections occur when no information from silane is used, but the errors, however, were much larger in these refinements. This is perhaps another indication that it is unreasonable to treat the data in all solvents as being related in the same manner to the coupling observed in silane, especially when it is known that the structure is different in the various solvents. This is particularly obvious in that the goodness of fit (R^2) to a straight line for the anisotropies in refinement three (Figure 7.4), where there is no silane correlation, is much better than in the other two refinements, where A_{SiH} was fixed to be proportional to the silane coupling.

The final molecule studied was methyl silane. It was observed in Table 7.2 and previously in Table 7.1 that methyl silane does not show the same variation in HSiH angle with solvent as has been found for the other silyl compounds studied. The final results of the refinement of methyl silane are given in Table 7.7.

Table 7.7 Final refinement for SiH_3CH_3

Solvent	ZLI 3086	ZLI 4792	ZLI 1083	E 5
$^pD_{SiH1}$ (Hz)	1.02840	0.99014	0.96240	0.99187
$^pD_{H1H2}$ (Hz)	1.01004	0.99231	0.98111	1.00006
$^pD_{CH1}$ (Hz)	1.00526	0.99469	0.98833	1.00059
$^pD_{CH6}$ (Hz)	0.99640	1.04592	1.06961	0.99281
$^pD_{H6H8}$ (Hz)	0.99611	1.01836	1.03077	0.99983
$^pD_{SiH6}$ (Hz)	0.99773	1.00897	1.01501	1.00000
A_{SiC} (10^{-22} J)	12.82	13.00	13.010	5.55
A_{SiH} (10^{-22} J)	3.14	-0.33	-2.81	-1.08
A_{CH} (10^{-22} J)	0.03	4.76	7.21	-1.00
Szz	0.04923	0.04491	0.04599	0.03860
HSiH (°)	108.42	108.28 (7)	108.07 (8)	108.13 (6)
HCH (°)	108.03	108.15 (13)	108.51 (13)	108.16 (15)
r_{CH} / r_{SiC}	0.586	0.586 (2)	0.585 (3)	0.586 (2)
r_{SiH} / r_{SiC}	0.794	0.798 (2)	0.799 (3)	0.795 (2)

As before, methyl silane does not show a large variation in HSiH angle in different solvents but HSiH does have three distinct values depending on whether the solvent is non polar (108.4°), fluorinated (108.3°) and cyano containing (108.1°). However, no such correlation is observed in HCH and it is therefore likely that these variations are largely due to experimental error. For example, these small effects in HSiH could be as a result of relatively small changes in the indirect coupling J_{SiH} between different types of solvents. Another reason why no correlation is observed in HCH is the larger uncertainties associated with these angles. The same magnitude of differences as is observed for HSiH could easily be lost in the case of HCH due to experimental error.

7.3 Correlation between ^1H chemical shift and HSiH angle

In Chapter 6 the chemical shifts of the ^1H spectra of each silyl compound were compared and predictions as to the effect on the indirect couplings, J_{ij}, were made. Here the correlation between ^1H chemical shift and HSiH angle is examined. If the liquid crystal molecules are interacting chemically with the silyl solute in an S_N2 type interaction, then this ought to be reflected in the chemical shift of the ^1H spectra.

If an electron donor such CN^- interacts with the slightly electron deficient silicon atom, then the Si-H bond will change from sp^3 hybridisation towards sp^2 hybridisation. Because the bonding increases in s character, the shielding around the hydrogens decreases resulting in a shift toward low field in the ^1H chemical shift. This was investigated by plotting differences in chemical shift (dω) versus change in HSiH angle (dHSiH) for the compounds studied.

Figure 7.5 Plot of chemical shift (d*w*) versus change in HSiH angle (dHSiH) for the silyl compounds studied

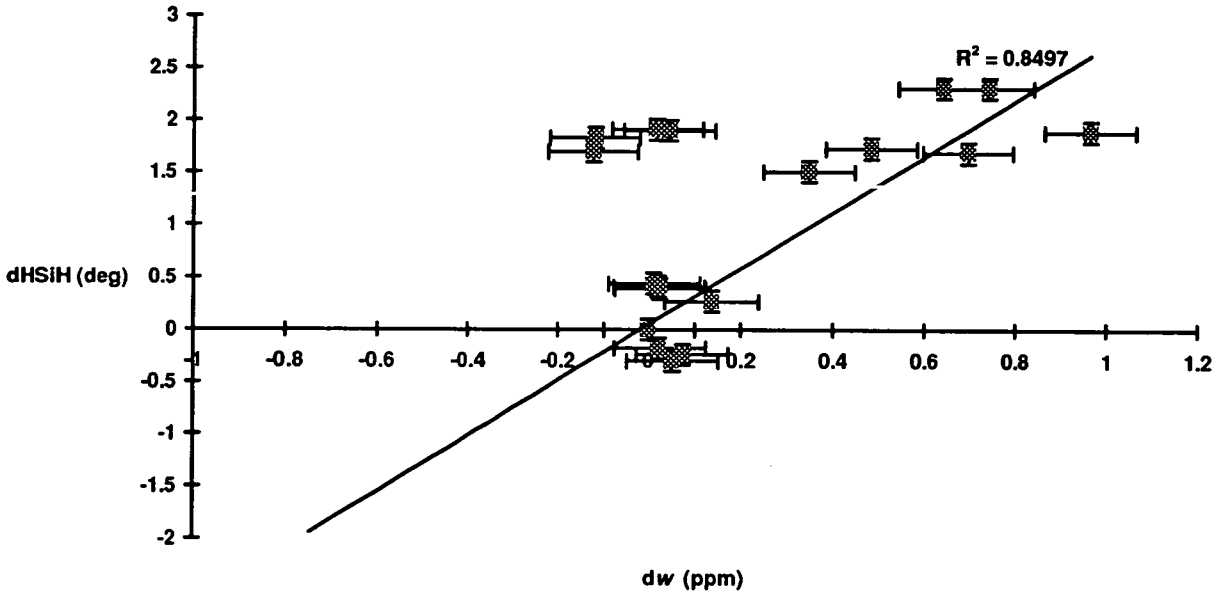

The graph demonstrates an approximate linear relationship between increasing ^1H chemical shift and increasing HSiH angle. The four anomalous data points in the top left corner of the plot have been excluded from this fit. Three of these were obtained

from silyl chloride in ZLI 4792, ZLI 1083 and E7, and the fourth is from silyl fluoride in E7.

7.4 Conclusion

From observing the differences in structure of a range of silyl compounds in various different liquid crystal solvents, it is evident that a significant solvent dependence exists.

This has been investigated by applying a correction which takes into account the correlation between vibration and reorientation of the solute molecules. This ought to remove any variations in results due to differences in the orienting potentials of the different liquid crystals used. This has previously been demonstrated in the case of methyl iodide and methyl fluoride where it was possible to account for apparent distortions of as much as two degrees in the HCH angle of these molecules.[11]

In the case of the methyl halides, the D_{CH} direct dipolar coupling of methane was used as a probe giving extra information on the torques experienced by the CH_3 fragments of the solute molecules. In this work the direct dipolar couplings of silane, D_{SiH}, was used instead as this was believed to be more closely related to the SiH_3 fragments of the silyl compounds being studied.

It has been found that these corrections, although having the correct sign, were not large enough to account for the differences in structure of the silyl compounds studied. In the studies of methyl halides, D_{CH} from methane was found to be as large as 15 Hz in some solvents, whereas in the solvents used here, the largest D_{SiH} coupling observed in silane was 1.9 Hz. Unfortunately no measurements of the coupling of methane have been obtained in the solvents used in this work. It is therefore not possible to determine whether silane is less sensitive to these distortions than methane, or whether this effect is less important in the solvents chosen.

By examining the ^1H chemical shift changes and the observed HSiH angles in these solvents it was observed that some correlation existed. As the chemical shift increases, so does the HSiH angle. This is consistent with the SiH bonds increasing in s character as the silicon changes from sp^3 hybridisation to sp^2 hybridisation as would be observed if the silicon became five co-ordinate.

The differences in HSiH angle in methyl silane were found to be in the opposite direction to that of the other silyl compounds. This is presumably as a consequence of the presence of the methyl group. The ^1H chemical shift does however increase slightly from the non-polar to the fluorinated solvent (0.03 ppm) and again to the cyano containing solvents (0.05 ppm) indicating a weak interaction taking place with the liquid crystal solvent.

It is therefore proposed that the largest effect causing discrepancies between structures obtained in different solvents is specific interactions taking place between the liquid crystal molecules and the silyl solutes. This interaction will be of the form of an S_N2 intermediate as is observed in the crystal structures of these silyl compounds. This would account for the structures in the non-polar solvent being in best agreement with the gas phase structure of each compound (once the correction has been made to account for the torque experienced by the silyl unit), the fluorinated solvent consistently giving an HSiH angle ~0.4° larger than the gas phase value, while the cyano containing solvents consistently give HSiH to be 1.85° larger than the gas phase.

It was also clear from this work that especially with the non-polar and fluorinated solvents which give rise to small orientation parameters and direct couplings that it is important to obtain the indirect couplings, J_{ij}, in the isotropic phase of these solvents. This is because small changes in J_{ij} can result in relatively large changes in the final structure obtained for the compound when the direct couplings are small. With hindsight, many of the difficulties encountered in this work could have been avoided if more accurate indirect couplings had been obtained.

References

[1]J.G.Snijders, C.A.Lange and E.E.Burnell, J. Chem. Phys., 77, (1982), 5386

[2]J.Lounila and P.Diehl, J. Magn. Reson., 56, (1984), 254

[3]J.Lounila and P.Diehl, Mol. Phys., 52, (1984), 827

[4]G.Dombi, P.Diehl, J.Lounila and R.Wasser, Org. Magn. Reson., 22, (1984), 573

[5]M.Kellerhals, P.Diehl, J.Lounila and R.Wasser, J. Mol. Struct., 156, (1987), 255

[6]R.Ugolini and P.Diehl, J. Mol. Struct., 216, (1990), 325

[7]R.Wasser, M.Kellerhals and P.Diehl, Magn. Reson. Chem.., 27, (1989), 335

[8]J.Jokisaari, T.Väänänen and J.Lounila, Mol. Phys., 45, (1982), 141

[9]P.Diehl, J.Jokisaari and F.Moia, J. Mol. Struct., 96, (1982), 107

[10]T.Väänänen, J.Jokisaari, A.Kääriäinen and J.Lounila, J. Mol. Struct., 102, (1983), 175

[11]J.Lounila, P.Diehl, Y.Hiltunen and J.Jokisaari, J. Magn. Reson., 61, (1985), 272

[12]J.Jokisaari and Y.Hiltunen, Mol. Phys., 50, (1983), 1013

[13]P.D.Blair, A.J.Blake, R.W.Cockman, S.Cradock, E.A.V.Ebsworth and D.W.H.Rankin, J. Mol. Struct., 193, (1989), 279

[14]C.A.Brookman, 4th year project report. University of Edinburgh, (1989)

[15]S.Sykora, J.Vogt, H.Bösiger and P.Diehl, J. Magn. Reson., 36, (1979), 53

[16]K.Hedberg, C.R.Pulham, "Personal communication"

[17] A.J.Blake, S.G.D.Henderson, E.A.V.Ebsworth and A.J.Welch, Acta Cryst., Sect. C, 41, (1985), 1141

[18] J.Lounila and J.Jokisaari, Prog. in NMR Spectrosc., 15, (1982), 249

Chapter 8

Final conclusions and further work

8 Final conclusion and further work

In this work the trends in packing of a series of liquid crystal molecules of the formula 4-*n*-alkoxy-4-cyanobiphenyl (*n*-OCB, n = 1-7) were examined and found to be correlated to the mesogenic properties of these compounds.[1] It was observed that when the alkoxy chain was short compared to the length of the cyanobiphenyl 'core' of the molecule (n = 1-4), that only monotropic behaviour occurs. When the 'tail' is of a comparable length to the core (n = 5-7) then nematogenic behaviour is observed and with still longer tails it is smectogenic behaviour that is observed.

In the crystal packing of these compounds, differences in properties are correlated to the degree of imbrication of the molecules. The molecules of the monotropic liquid crystals are arranged in the crystalline phase such that there are many competing inter ring interactions which prevent the persistence on melting of the 'head-to-tail' dimers believed to be present in the mesogenic phases of these compounds.[2,3,4,5,6,7,8,9,10,11] In the nematic liquid crystals, the effect of the lengthening tail is to space out the molecules and reduce the influence of competing inter ring interactions. This results in weaker intermolecular contacts being broken down as the crystal melts with the stronger 'head-to-tail' dimer able to persist. These dimers must then interact with one another, resulting in a mesophase with a small degree of one-dimensional order.

In the crystal structure of these compounds, the molecules arrange themselves into parallel sheets, with the 'head-to-tail' dimers, in the case of nematic liquid crystals, being formed between molecules in adjacent sheets. The crystal structures of *6*- and *7*-OCB demonstrate a distinct layer structure, where it is apparent that the weak van der Waals interactions between hydrogens from the tails of neighbouring molecules is becoming significant, forcing the cores to overlap in the 'head-to-tail' confirmation. It is not difficult to understand that when the 'tail' becomes longer still, the 'head-to-tail' dimers will also be formed within the sheets of molecules enabling a mesophase with a small degree of two-dimensional order to the formed.

The crystal structures of 4-*n*-methoxy-4-cyanobiphenyl (*1*-OCB) and 4-*n*-heptyl-4-cyanobiphenyl (*7*-CB) were determined. That of *1*-OCB was collected at 150 K and found to be in good agreement with that previously determined at ambient temperature.[2] Data for *7*-CB was collected at both ambient and low temperatures with both structures in good agreement with one another. The crystal packing of *7*-CB was found to be similar to that of *7*-OCB, although this is not surprising as both compounds exhibit very similar mesogenic properties.

An additional part of this work was to obtain crystals of adducts formed between liquid crystal and silyl compounds. This proved to be unsuccessful but it is proposed that future attempts at this should concentrate on more polar silyl compounds such as silyl cyanide. Because of the problems experienced in handling these compounds it would also be advisable to concentrate on growing crystals '*in situ*' on the diffractometer using a sealed capillary tube.

The differences in silyl geometry between that obtained in the gas phase and by LCNMR spectroscopy were also investigated using a variety of different liquid crystal solvents. It was found that different silyl compounds all yield structures distorted by a similar amount for any given liquid crystal. Attempts to account for this by introducing an additional correction to the direct dipolar couplings which allows for a correlation between the vibration and re-orientation of the solute molecules[12, 13] were made. Although this proved to be partially successful, it is concluded that the most significant contribution to the distortions of the compounds is as a result of specific interactions between the liquid crystal solvent and the solute. While it was discovered that the structure obtained in a non-polar solvent gave good agreement with the gas phase structures of these compounds, the structures obtained in fluorinated and cyano containing solvents showed consistent deviations from this. The distortion from the cyano containing solvents always being the greatest.

These distortions were found to be consistent with the theory that liquid crystal and solute molecules interact in an S_N2 reaction intermediate as is observed in the crystal phase of these silyl compounds.[14, 15]

For future work in this area it would be interesting if a variety of different non-polar liquid crystals were used. By removing the possibility of specific interactions in the solution phase and taking into account the correlation between the vibration and re-orientation to the direct dipolar couplings it should be possible to obtain accurate, undistorted structures for these compounds in the solution phase.

In doing this it is particularly important that the indirect couplings be measured in the isotropic phase of each solvent used as in this work it was found that because of the small orientation parameter obtained in the non-polar solvent, the final structure was very sensitive to the exact value of these indirect couplings. However, the problems from this can be minimised by refining together data from as many different solvents as possible.

References

[1] Catalogue data, BDH Chemicals Ltd.

[2] L.Walz, H.Paulus and W.Haase, Z. Kristallogr., 180 (1987), 97

[3] P.Mandal and S.Paul, Mol. Cryst. Liq. Cryst., 131, (1985), 223

[4] M.A.Kravers, V.I.Kulishov, A.J.Polschuk and A.S.Tolochko, Sov. Phys. Crystallogr., 37(3), (1992), 375

[5] K.Hori, Y.Koma, A.Uchida and Y.Ohashi, Mol. Cryst. Liq. Cryst., 225, (1993), 15

[6] L.Walz, W.Haase and I.H.Ibrahim, Mol. Cryst. Liq. Cryst., 200, (1991), 43

[7] W.Haase, J.Loub, H.Paulus, M.A.Mokhles and I.H.Ibrahim, Mol. Cryst. Liq. Cryst., 197, (1991), 57

[8] G.V.Vani, Mol. Cryst. Liq. Cryst., 99, (1983), 21

[9] W.Haase, J.Loub and H.Paulus, Z.Kristallogr., 202, (1992), 7

[10] W.Haase, H.Paulus, Z.X.Fan, I.H.Ibrahim and M.Mokhles, Mol. Cryst. Liq. Cryst. (letters), 6(4), (1989), 113

[11] W.Haase, H.Paulus and R.Pendzialek, Mol. Cryst. Liq. Cryst., 100, (1983), 211.

[12] J.Lounila and P.Diehl, J. Magn. Reson., 56, (1984), 254

[13] J.Lounila and P.Diehl, Mol. Phys., 52, (1984), 827

[14]P.D.Blair, A.J.Blake, R.W.Cockman, S.Cradock, E.A.V.Ebsworth and D.W.H.Rankin, J. Mol. Struct., 193, (1989), 279

[15]C.A.Brookman, 4th year project report. University of Edinburgh, (1989)

Appendix A

Instructions and Example File for the Program MASTER

Input instructions for the program MASTER.

The program MASTER has been obtained from R.Wasser, M.Kellerhals and P.Diehl (Magn. Reson. Chem., 27, (1989), 335) and is used principally to calculate corrections to the direct dipolar couplings and refine the structure of your molecule. As many as ten LCNMR data sets can be refined together for a given molecule. The corrections made to the direct couplings are optional and consist of the standard vibrational corrections which can be calculated elsewhere, e.g. BMGV, and a new correction introduced by Lounila and Diehl (Mol. Phys., 52, (1984), 827, J. Magn., Reson., 56, (1984), 254) which accounts for a correlation between the vibration and reorientation of the solute molecules in the liquid crystal environment.

The FORTRAN source code for MASTER is in the directory ~dwhr21/MASTER and the program can be run from any process simply by typing 'master'. NB You must include ~dwhr21/bin in your PATH (edit .bashrc or .profile in your main directory)

The program is dimensioned for 15 atoms, 90 structure parameters and 200 force constants. The main program is used to call the various sub-programs individually in any desired order but in practise the suggested lay out below is probably safest. The input file consists of a series of cards. Each card either calling up a sub-program, passing in the variables controlling the input and output, or supplying the data required for that particular part of the program. Unfortunately, because the various sub-programs were not all originally written for this purpose, there is some information that you have to tell MASTER more than once.

The first part of the input file involves the calculation of the individual atoms of a molecule or a cluster of molecules. This is done using subroutines from the program VIBR.

CARD 1 GEOM calls the subroutine GEOM and passes in the variables INCPS and IOCPS.

As in the majority of subroutines used INCPS describes what is to be read in and IOCPS describes the output that you want.

Here, the digit S (units) refers to the text and structure code
P (tens) refers to the parameters
C (hundreds) refers to the co-ordinates

If any of the three digits are zero then the reading/writing instructions pertaining to the respective data will be ignored. This card is format(A4,10X,I5,I5).e.g.

GEOM 11 000

CARD 2 TITLE GEOM contains a descriptive text, usually indicating where your structure and force-field came from. e.g.

ALLENE FORCE-FIELD HEGELUND ET AL., J. MOL. SPEC. 65, 366 (1977)

CARD 3 STRUCTURE CODE This is where you describe the atom positions, either as straight forward Cartesian co-ordinates or as a series of bonds and angles (degrees).

The cards are arranged as follows:

Each card comprises eight integers N0,N1,N2,N3,NV,IP1,IP2, and IP3 (format 8I5). The cards can be in any order and the list is finished with a blank card. NO is the number of the atom whose position is being specified. The meaning of N1,N2,...,IP3 is a little more complicated and is explained as follows:

The algorithm which is to followed is determined by the integer part of (NV/1000). If this is a zero then the program will use one of the four basic modes or else the algorithm NA will be used. In modes 3 and 4 it is necessary to determine the shape of a triangle (N0,N1,N2). This requires two parameters IP1 and IP2. What these parameters describe is specified by the units of NV. The combinations available are given below where R01 is the distance N0-N1 and A0 is the angle N1-N0-N2 in degrees. If the conditions are met on the right hand side then NV must be negative.

units of NV	IP1	IP2	
0	R01	R02	
1	R01	A1	
2	R01	A2	If R01 < R12 and A0 > 90
3	R01	A0	If R01 > R12 and A2 > 90
4	R02	A2	
5	R02	A1	If R02 < R12 and R02 < 90
6	R02	A0	If R02 > R12 and A1 > 90
7	A1	A2	
8	A0	A1	
9	A0	A2	

The four basic modes are :-

MODE 1 N1,N2, and N3 are all zero or negative and IP1,IP2 and IP3 are the positions of the x, y and z co-ordinates in the parameter list in card 4.

MODE 2 N1 is positive but N2 and N3 are zero or negative. The atom position is the distance IP1 away from atom N1. The bond direction is given by the spherical co-ordinates theta (IP2) and fi (IP3) of the unit vector parallel to N1-N0.

MODE 3 N1 and N2 are positive but N3 is zero or negative. Here you define the orientation of the triangle N0,N1,N2. A plane S is defined by the vector joining the atoms N1 and N2, and a vector on N1 parallel to one of the co-ordinate axes. The co-ordinate axes used is determined by the tens of NV, the values 1,2 and 3 referring to x, y and z. IP3 is then the dihedral angle between S and the plane of the triangle N0,N1,N2, measured in a positive sense from S.

MODE 4 N1,N2 and N3 are all positive. Here the orientation of triangle N0,N1,N2 is determined by a reference to atom N3. There are four ways of doing this chosen by setting the units of NV to 0,1,2 or 3

0 IP3 is the dihedral angle between the planes of the triangles N1,N2,N3 and N0,N1,N2, measured from the former in the sense defined by the cyclic order of the atoms N1,N2 and N3.

1 IP3 is the angle N0-N1-N3. Atom NO must lie above the (oriented) plane of the triangle N1,N2,N3.

2 IP3 is the angle N0-N2-N3. Atom NO must lie above the (oriented) plane of the triangle N1,N2,N3.

3 IP3 is the distance between the atoms N0 and N3. Again, atom NO must lie above the (oriented) plane of the triangle N1,N2,N3.

The special algorithms (NA = 1,2 - see above)

NA = 1 The vector pointing from N1 to N0 is parallel to the vector pointing from N2 to N3. The length is given by IP1.

NA = 2 The projection of the vector pointing from N1 to N0 into the plane of the triangle N1,N2,N3 bisects the compliment of the angle N2-N1-N3. IP1 gives the distance between N0 and N1. IP2 gives the angle between the vector N1-N0 and the plane of the triangle N1,N2,N3. Again, atom NO must lie above the (oriented) plane of the triangle N1,N2,N3.

e.g. Structural code for allene with Cartesian co-ordinates being read in. Remember that the list is terminated with a blank line.

```
1  0  0  0  0  2  7  4
2  0  0  0  0  1  7  4
3  0  0  0  0  7  2  3
4  0  0  0  0  7  1  3
5  0  0  0  0  7  7  6
6  0  0  0  0  7  7  7
7  0  0  0  0  7  7  5
```

CARD 4 NPRM This is just the number of parameters required for the structural code. (format I5) e.g.

```
7
```

CARD 5 : Geometry parameters (8(F10.5)). These are the NPRM parameters required or the structural code. e.g.

```
-0.9329  0.9329  -1.8667 1.8667  -1.3084  1.3084  0.
```

CARD 6 FMAT calls the subroutine FMAT. This subroutine forms the F-Matrix in Cartesian co-ordinates using a list of the contributions to the potential energy expressed in the internal co-ordinates. FMAT passes to this subroutine two numbers IN and OU. The tens of IN refers to the force field code and the units to the force field constants. The hundreds of IO refers to the F-Matrix, the tens and the units being analogous to IN. If any of these are zero the corresponding read (IN) or write (IO) will be ignored. (format(A4,10X,I5,I5)) e.g.

```
FMAT      11 100
```

CARD 7 Definition of Internal Co-ordinates. You need one card for each potential energy function but the order of the cards is not important and the list is terminated with a blank line. Each card starts with two

alphabetic symbols indicating the two interacting internal co-ordinates involved. In the case of the diagonals where only the one internal co-ordinate is involved an asterisk is used as the second symbol. The following types of co-ordinate are available :-

S stretch
B bend (the non-linear case)
L bend (the linear, in-plane case)
O bend (the linear, out-of-plane case)
W wagging
T torsion

Once the type of interaction has been defined, you need to describe what it does. The first number you supply is the position the force constant appears in CARD 9. The remaining numbers are as follows:

S you require two numbers, e.g. the bond N1 and N2
B you require three numbers, e.g. the angle N1-N2-N3
L you require four numbers, e.g. the angle N1-N2-N3 and the plane N1,N3,N4
O you require four numbers, e.g. the angle N1-N2-N3 and the plane N1,N3,N4
W you require four numbers, e.g. the end atom N1, the two anchors N2 and N3, and the apex N4
T you require four numbers, e.g. the atoms N1-N2-N3-N4

** **Warning** ** Remember the symmetry when describing WT modes.

Each card is format (A5,8(I5)) and list is terminated with a blank line.
e.g.

```
S*    1    1    5
S*    1    2    5
S*    1    3    7
S*    1    4    7
S*    2    5    6
S*    2    6    7
B*    3    1    5    2
B*    3    3    7    4
B*    4    1    5    6
B*    4    2    5    6
B*    4    3    7    6
B*    4    4    7    6
SS    5    1    5    2    5
SS    5    3    7    4    7
SS    6    1    5    3    7
SS    6    1    5    4    7
SS    6    2    5    3    7
SS    6    2    5    4    7
SS    7    1    5    5    6
SS    7    2    5    5    6
SS    7    3    7    6    7
SS    7    4    7    6    7
SS    8    1    5    6    7
```

SS	8	2	5	6	7				
SS	8	3	7	5	6				
SS	8	4	7	5	6				
SS	9	5	6	6	7				
SB	10	1	5	1	5	2			
SB	10	2	5	1	5	2			
SB	10	3	7	3	7	4			
SB	10	4	7	3	7	4			
SB	11	1	5	3	7	4			
SB	11	2	5	3	7	4			
SB	11	3	7	1	5	2			
SB	11	4	7	1	5	2			
SB	12	5	6	1	5	2			
SB	12	6	7	3	7	4			
SB	13	5	6	3	7	4			
SB	13	6	7	1	5	2			
SB	14	1	5	1	5	6			
SB	14	2	5	2	5	6			
SB	14	3	7	3	7	6			
SB	14	4	7	4	7	6			
SB	15	1	5	2	5	6			
SB	15	2	5	1	5	6			
SB	15	3	7	4	7	6			
SB	15	4	7	3	7	6			
SB	16	1	5	3	7	6			
SB	16	1	5	4	7	6			
SB	16	2	5	3	7	6			
SB	16	2	5	4	7	6			
SB	16	3	7	1	5	6			
SB	16	3	7	2	5	6			
SB	16	4	7	1	5	6			
SB	16	4	7	2	5	6			
BB	17	1	5	2	3	7	4		
SB	18	5	6	1	5	6			
SB	18	5	6	2	5	6			
SB	18	6	7	3	7	6			
SB	18	6	7	4	7	6			
SB	19	5	6	3	7	6			
SB	19	5	6	4	7	6			
SB	19	6	7	1	5	6			
SB	19	6	7	2	5	6			
BB	20	1	5	6	1	5	2		
BB	20	2	5	6	1	5	2		
BB	20	3	7	6	3	7	4		
BB	20	4	7	6	3	7	4		
BB	21	1	5	2	3	7	6		
BB	21	1	5	2	4	7	6		
BB	21	3	7	4	1	5	6		
BB	21	3	7	4	2	5	6		
BB	22	1	5	6	2	5	6		
BB	22	3	7	6	4	7	6		
BB	23	3	7	6	1	5	6		
BB	23	3	7	6	2	5	6		
BB	23	4	7	6	1	5	6		
BB	23	4	7	6	2	5	6		
T*	24	1	5	7	3				
T*	24	2	5	7	4				
TT	25	1	5	7	3	2	5	7	4

```
SW   26   1   5   6   3   4   7
SW   26   3   7   6   1   2   5
SW   27   2   5   6   3   4   7
SW   27   4   7   6   1   2   5
BW   28   1   5   6   6   3   4   7
BW   28   3   7   6   6   1   2   5
BW   29   2   5   6   6   3   4   7
BW   29   4   7   6   6   1   2   5
W*   30   6   1   2   5
W*   30   6   3   4   7
L*   31   5   6   7   1
O*   32   5   6   7   1
SL   33   1   5   5   6   7   1
SL   34   2   5   5   6   7   1
SO   35   3   7   5   6   7   1
SO   36   4   7   5   6   7   1
BL   37   1   5   6   5   6   7   1
BL   38   2   5   6   5   6   7   1
BO   39   3   7   6   5   6   7   1
BO   40   4   7   6   5   6   7   1
WL   41   6   4   3   7   5   6   7   1
WO   42   6   2   1   5   5   6   7   1
```

CARD 8 NPR This is just the number of force constants that will appear in CARD 9. format (I5). e.g.

```
42
```

CARD 9 FORCE CONSTANTS - these are in the format (8F10.0). The force constants must be in millidyne per angstrom. They are therefore standardised as follows:

S	as the distance between the atoms N1 and N2. i.e. R12
B,L,O	as the angle N1-N2-N3 multiplied by SQRT(R12*R23)
W	as the angle between the vector from N4 to N1 and the (oriented) plane of the atoms N2,N3,N4, multiplied by R14
T	as the angle between the triangles N1,N2,N3 and N2,N3,N4 (looking along N2-N3), measured clockwise form the former to the latter plane, and multiplied by SQRT(R12*R34)

NOTE The line in the source code which standardises the bending force constants has been commented out since GAMP and ASYM20 force constants are already in this form.

Format (8F10.5). e.g.

```
5.6275   9.789    .2515    .2273    -.0235   -.047    .3125    -.07
.547     -.0146   -.0443   -.113    -.0575   .1546    -.1414   .0202
-.004    .0515    .0263    -.1147   .0018    -.1228   -.0008   .08207
.08207   -.0272   .0272    -.0071   .0071    .1222    .2675    .2675
-.3486   .3486    .3486    -.3486   -.0385   .0385    .0385    -.0385
-.0427   .0427
```

CARD 10 NCOR This subroutine computes the vibrational frequencies and the normal co-ordinates of the molecule. It works directly in Cartesian co-ordinates using the F-Matrix formed by the subroutine FMAT. This

subroutine must always be accompanied with the subroutine EIGEN. EIGEN is called by the subroutine NCOR and is responsible for calculating the eigenvalues and eigenvectors of a real symmetric matrix. If the input number INM is non-zero then the atomic masses will be read in. If the hundreds of IO, the output parameter, is positive then masses will be outputted. The tens refer to the vibrational frequencies, and the units to the normal co-ordinates. Format (A4,10X,I5,I5). e.g.

NCOR 1 111

CARD 11 MASSES This card just reads in the atomic masses. format (8F10.5). e.g.

1.008 1.008 1.008 1.008 12. 12. 12.

CARD 12 COVM This subroutine computes the covariance matrices for a predefined set of nuclear pairs using the vibrational frequencies and the normal co-ordinates formed by NCOR. Again, the variable IN and IO are passed in with this card. The tens of IN refer to the reading of the nuclear pairs and the units refers to the temperature. The tens of IO refers to the writing out of the temperature and the units refer to the writing out of computed covariance matrices. Format (A4,10X,I5,I5). e.g.

COVM 11 11

CARD 13 LIST This card contains a list of the nuclear pairs to be considered. They can come in any order with each line being format (2I5). The list is terminated with a blank line. e.g.

1 2
1 3
1 5
1 6
1 7

CARD 14 TEMPERATURE This card allows you enter the temperature in degrees Kelvin using the format F10.0. e.g.

303.

CARD 15 AMPL This subroutine calculates and writes out the mean amplitudes of vibration for specified pairs of nuclei using the covariance matrices from COVM. e.g.

AMPL

CARD 16 DVIB This subroutine has three different entries and it does different things depending on where it is called from.

DVIB Can be used to calculate both the equilibrium and the vibrationally corrected D-Values.

DEQI Can be used to calculate the equilibrium D-Values.

FVIB Can be used to calculate the FI-Tensors.

Again, the variables INCS and IOSR are passed in. INCS refers to what is read in. The tens referring to the list of nuclear pairs (including the code symbols for the nuclei). The units refer to the S-Matrix. IOSR decides what is to be written out. The hundreds refer to the S-Matrix and the units refer to the results (D-Values). Format (A4,10X,I5,I5). e.g.

DVIB 11 11

CARD 17 LISD This is a list of the D couplings required. They MUST be in the same order as they were in COVM and again the list ends with a blank line. This time you must give alphabetic code symbols for each nuclei. The nuclei that the program knows about are H,H1,D,H2,C13,N,N14,N15,O17,F,F19,SI29,P,P31,S33,CL35 and CL37. Along with each symbol the program has the corresponding factors GAMMA*SQRT(H)/(2.*PI). The format is I5,1X,A4,I5,1X,A4. e.g.

1 H 2 H
1 H 3 H
1 H 5 C13
1 H 6 C13
1 H 7 C13

CARD 18 S-MATRIX The S-Matrix is only needed for DVIB and DEQI. It is given on one line with the format 5F10.0 . The parameters come in the order S(XX),S(ZZ),S(XZ),S(XY), and S(YZ). If SXX=SYY then only the order parameter will be calculated. e.g.

.08 -.16

CARD 19 INTER Calculation of the interaction corrections. Only one variable, IOUT, is passed into this subroutine. If IOUT is 1 then the bond scalars XI, XIS and the bond tensors TH, THS will be printed out. This subroutine is used to calculate the value of the interaction elements AL(N),AV(N) and AT(N), where AL is the longitudinal component in the bond direction NI1,NI2. AT is the transversal component, and AV is the component perpendicular to the plane defined by the nuclei NI1,NI2 and NI3.
Format (5X,I5). e.g.

INTER 1

CARD 20 AINT Here you give the number of interactions (bonds) and then the number of different types of interactions (bonds). Format 2I5. e.g.

6 2

CARD 21 DEFINITIONS These are give in the format 5I5. The first two numbers of each card define the bond of interest and fix the direction of the longitudinal component AL. The third number defines an arbitrary third nucleus which is used to fix the plane for the transversal and perpendicular components AT and AV. The fourth number indicates which bond type you are describing. These will range from 1 to the number of different types of bonds that you have indicated exist in CARD 20. The last digit gives the number of equivalent bonds that will be given.

1 5 6 1 1
2 5 6 1 1
3 7 6 1 1
4 7 6 1 1
5 6 1 2 1
6 7 1 2 1

CARD 22 UNIT This subroutine calculates the bond unit vectors using the interaction elements obtained from INTER. If IO is 1 then the unit vectors will be outputted. If output is chosen then the unit vector K'(N) of the N^{th} interaction points along the bond NI1(N) to NI2(N). The unit vector I'(N) is in the plane defined by NI1(N), NI2(N) and NI3(N) and the unit vector J'(N) is perpendicular to this plane. Format A5,I5 e.g.

UNIT 1

CARD 23 SHAPE This subroutine is where you input your experimental D couplings and define the iteration parameters for refinement. The program will then calculate Deq, Dharm and Dint as well as the interaction parameters and the final structure by iteration. When calling SHAPE you can again choose to have output data or not by using the variable IO. i.e. IO = 1 for output. Format A5,I5 e.g.

SHAPE 1

CARD 24 GET PARAMETERS This routine reads in the parameters being used to refine the spectral data. The first two numbers that you give are the number of nuclei (7) and the maximum number of iterations that you wish MASTER to perform (15). The remaining numbers are flags indicating the parameters that you will be giving the program. The first of these is the number of symmetry related nuclei in the molecule (4). The next parameter is the assumed error of the calculation. I am not too sure about this but it is zero in both the example files supplied with the program. Next is the number of angles that you would like the program to tell you about once the refinement has taken place (2). Then comes the nuclei defining the basis bond that the final structure

will be scaled to (5,7) and finally you must tell the program how many sets of spectral data you would like to analyse. If you wish, you can insert some text at the end of this card either to remind you what parameters you are using or just to let you know that the program got this far! Format (I2,I4,6(I5) e.g.

7 15402575 SHAPE

CARD 25 GYROMAGNETIC RATIOS This calls the subroutine IGYRO which reads in the gyromagnetic ratios. Again this card lets you set IO = 1 to get the gyromagnetic ratios printed back out at you. Format A5,I5 e.g.

IGYRO 1

CARD 26 GET GYROMAGNETIC RATIOS This card reads in the values of the gyromagnetic ratios. The values that the program knows about (but still wants you tell it !!!) are : H 346.574, H1 346.574, D 53.201, H2 53.201, C13 87.140, N 25.039, N14 25.039, N15 -35.125, O17 -46.985, F 326.054, F19 326.054, SI29 -68.849, P 140.304, P31 140.304, S33 26.586, CL35 33.961, CL37 28.263, T125 ,-109.492 Format 8F10.5 e.g.

346.574 346.574 346.574 346.574 87.140 87.140 87.140

CARD 27 : IGEOM This subroutine defines which structural parameters that you want to refine. Again this card lets you set IO = 1 to get the selections you have made printed back out at you. Format A5,I5 e.g.

IGEOM 1

CARD 27 GET GEOMETRY ITERATION PARAMETERS This card lets you choose which co-ordinates you want to use in the refinement. The x, y and z co-ordinates are on lines 1,2 and 3 respectively. A one indicates that that co-ordinate is a fixed parameter and a zero indicates that it is free to refine (Z(1) and Z(5)). Format 8I5 e.g.

1 1 1 1 1 1 1
1 1 1 1 1 1 1
0 1 1 1 0 1 1

CARD 28 ISYM This card calls the subroutine ISYM which defines the symmetry related nuclei in the molecule. Again this card lets you set IO = 1 to get the selections you have made printed back out at you. Format A5,I5 e.g.

ISYM 1

CARD 29 GET SYMMETRIES This is where you define the symmetry relations between the nuclei in the molecule. The format is 2(I5),F10.5,3(I5). The first two numbers are the two nuclei that you are placing a constraint on. There are three ways of arranging the remaining numbers depending on the type of constraint you want.

1 Constrain either the x, y or z co-ordinates of the nuclei 1 and 2 to be either the same or opposite one another. This is done by setting the third number to -1 and using the fourth number to select either the x, y or z co-ordinates using the numbers 1,2 or 3 if the nuclei have the same co-ordinate, or -1,-2 or -3 if they are of opposite sign. In this case the final two numbers are left blank.

2 Here the third number is the length of the bond between nuclei 1 and 2. The fourth number again describes the co-ordinate which is to be constrained. What this actually does is conserve the component of the bond length in the direction of the axis specified by the fourth number. The remaining numbers are left blank.

3 This is very similar to 2 but this time the third number is left blank and the bond length is that between the two nuclei specified by the fifth and sixth numbers. e.g.

```
1  2  -1.   3
1  3  -1.  -3
1  4  -1.  -3
5  7  -1.  -3
```

CARD 30 CHOICE OF OUTPUTS This card is format A5,2(I5),F6.3 This is where you get to choose which D values you would like to be calculated. The first thing that you must supply is name for your molecule (A5). The first number you supply determines whether or not you require output of the results. This is normally set at 1 to indicate that that was why you are using the program! The next number is used to indicate which type of calculation you would like. The hundreds indicates that you want D equilibrium calculated, the tens that you want D harmonic to be calculated and finally the units indicates if you would like D interaction calculated. As usual, a 0 in any of these positions will skip that part of the calculation. The final number is an estimate of the error caused by the approximations of the theory. Again, I am not too sure about this but the error is zero in the two example input files supplied with the program. e.g.

```
INDEX  1 0111 0.0
```

CARD 30 GET LIQUID CRYSTAL This card is where you supply the name of the liquid crystal solvent used and let the program know if the solvent aligns parallel or perpendicular to the magnetic field. This is because if the solvent aligns perpendicular to the field then the D-values must be multiplied by -0.5 to convert them to D-values w.r.t the director. The program already knows about the orientation of the following liquid crystals : EBBA, ZLI 1167, ZLI 1132, HAB NEM., HAB SMEC., ZLI 1083, ZLI 1695, PHASE 4, E 48 and HAB SMEC. ANTI.

The format is A15 and if the liquid crystal solvent doesn't appear in the above list then the first three characters must be either PAR (parallel) or PER (perpendicular). e.g.

PHASE 4

CARD 31 GET TEMPERATURE Here the temperature of the experiment is read in using. Format F10.5 e.g.

303.

CARD 32 EXPERIMENTAL Here the experimental direct coupling and standard deviations are read in. These are format 2F10.5 and should be read in the same order as used previously in DVIB. e.g.

715.57 .04
-130.16 .05
193.19 .271
-181.47 .2
-59.06 .26

CARD 34 METHANE COUPLING This card reads in the experimental value of the coupling observed in methane. Format is F10.5 e.g.

7.75

CARD 30-33 are then repeated for the remaining spectra i.e. in this case 2-5 e.g.

ZLI 1167
303.
-387.04 .02
70.79 .02
-92.31 .07
99.16 .06
32.33 .07
-2.18
ZLI 1132
303.
878.77 .04
-160.56 .05
210.71 .18
-225.01 .14
-72.94 .18
-2.
PAR HAB
303.
902.52 .04
-165.51 .05
224.22 .17
-231.72 .13
-75.17 .17
-1.07
E 48
303.
1050.00 .04
-191.65 .05
256.84 .36

-268.45 .28
-87.14 .34
0.03

CARD 34 GEOME The subroutine GEOM is called and a flag is used to indicate if you wish the starting geometry to be outputted. Format A5,I5 e.g.

GEOME 1

CARD 35 GET START GEOMETRY This is where the starting geometry is read in. The format is 8F10.5 The first row contains all the x co-ordinates, the second the y and the third the z co-ordinates. If there are more that eight atoms then continue the x co-ordinates into line two and three as necessary etc. e.g.

.9329	**-.9329**	**0.**	**0.**	**0.**	**0.**	**0.**
0.	**0.**	**.9329**	**-.9329**	**0.**	**0.**	**0.**
1.8667	**1.8667**	**-1.8667**	**-1.8667**	**1.3084**	**0.**	**-1.3084**

CARD 36 IPARA This calls the subroutine IPAR and passes in a flag which determines whether output is given or not. Format is A5,I5 e.g.

IPARA 1

CARD 37 ANISOTROPY This determines whether the anisotropy parameters are to be refined or not. 0 indicates that they are free to refine and 1 means that they are fixed. You need one anisotropy parameter for each type of bond that you have defined in CARDS 20 and 21. The anisotropy is defined from the interaction elements (see CARD 19) such that. Anisotropy = AL(N)-0.5(AT(N)+AV(N))
Format is 8I5 e.g.

0 0

CARD 38 ASYMMETRY For each type of bond you also have some asymmetry. Again, as in CARD 37 these can be left free to refine 0, or be fixed at some value 1. The asymmetry is defined from the interaction elements (see CARD 19) such that. Asymmetry = (AT(N)-AV(N))/AL(N)
Format is 8I7 e.g.

1 1

CARD 39 A' For each type of bond you also have the parameter A'. This is to do with the bond interaction tensor. Again, as in CARD 37 these can be left free to refine 0, or be fixed at some value 1.
Format is 8I7 e.g.

0 1

CARD 37 - 39 are then repeated for each of the remaining spectra.

```
0  0
1  1
0  1
0  0
1  1
0  1
0  0
1  1
0  1
0  0
1  1
0  1
```

CARD 40 DEFINITION OF PARAMETERS The interaction iteration parameters PARA (CARD 41) are linear combinations of the interaction parameters defined by the tensor VARA (CARD 37-39). Here we decide on the linear relationship. Format 8F10.5

EXAMPLE : if we want
PARAMETER1=1.0*INTERACTION(1)+0.0*INTERACTION(2) and
PARAMETER2=0.0*INTERACTION(1)+1.0*INTERACTION(2)
then e.g.

```
1.    0.
0.    1.0
```

CARD 41 PARAS This card calls the subroutine PARA which read in the values for the interaction parameters described in CARD 37-39. Again, setting IN = 1 will output the starting values that you select for these parameters.
Format A5,I5 e.g.

```
PARAS  1
```

CARD 42 ANISOTROPIES These are entered as 8F10.8 e.g.

```
-3.81   11.58
```

CARD 43 ASYMMETRIES These are entered as 8F10.5 e.g.

```
0.
```

CARD 44 A' These are entered as 8F10.5 e.g.

```
0.
```

CARD 42 - 44 are then repeated for each of the remaining spectra

-3.81 11.58
0.
0.
-3.81 11.58
0.
0.
-3.81 11.58
0.
0.
-3.81 11.58
0.
0.

CARD 45 S-CALCULATION This is where the program is given the starting data to solve the orientation parameter for each data set. The format used is A10,I10,3F10.5 The first expression that you supply is an expression letting the program know about the symmetry of the molecule. Unfortunately, the program only appears to know about C3V symmetry, so if this is what you want then you must have C3V as the first three characters in the line. If this is not the case then leave the first three characters blank and a numerical quadrature will be used.

WARNING If the card for C3V symmetry is being used then the symmetry axes must be the Z-axes AND because it is assumed that the molecule is C3V with a linear tail, the co-ordinates must be given such that the three symmetry related atoms come first and the tail comes last. i.e. For a methyl halide, atoms 1,2 and 3 must be the three protons!

The first number that you supply is the number of intervals required for numerical quadrature, the next two are the relative and absolute precision to which S will be calculated and the final value is the minimal change in RMS. where the quadrature can stop. Typical values for these numbers are given in the example. e.g.

C3V 100000 1.0E-3 1.0E-3 .0001

CARD 46 LINME This calls the subroutine LINMET which reads in the parameters required for correlating the methane distortion to the distortion of your molecule. Format is A5,I5 and a 1 indicates that the output is required. e.g.

LINME 1

CARD 47 NPROP This tells the program whether or not methane correlation is to be used. If no methane correlation is required then 0 is used. If n different correlations are required then n is used. Format I5 e.g.

0

CARD 48 PARAMETERS This is only required if CARD 47 is not equal to 0. The format for this line is 3I5,2F10.5 The first two numbers refer to the slope and intercept, either can be 0, free to refine as an iteration parameter, or 1, fixed. The next number indicates the number of the dependent parameter as defined in Card 21 which is a linear function of the methane coupling. The final two numbers are the initial starting values for the slope and intercept.

CARD 49 ANGLES This calls the subroutine IANGL which returns the final value after refinement of any angles that you want to tell it about. This is accompanied with a 1 if you want the value of the angles to be outputted. Format A5,I5 e.g.

IANGL 1

CARD 50 DEFINITION OF ANGLES Here the angles are read in. As an example, the number 1 5 2 would be the angle between atoms 1, 5 and 2. Remember, you can only tell it about the number of angles defined in CARD 24. Format is 8(3I2,4X) e.g.

1 5 2 1 5 6

CARD 51 STOP This brings the input file to a close. e.g.

99

Appendix B

Example LCNMR spectra used in this work

Example LCNMR ^{1}H spectra used in this work

1) Example of a 1st order spectrum of SiH_3Cl
2) Example of a 1st order spectrum of SiH_3F
3) Example of a 2nd order spectrum of SiH_3CH_3
4) Example of a 2nd order spectrum of SiH_3CH_3 (expanded to look for ^{29}Si and ^{13}C satellites)
5) Example of a typical output from the program LCSIM
6) Example of a typical output from the program SLIQUOR

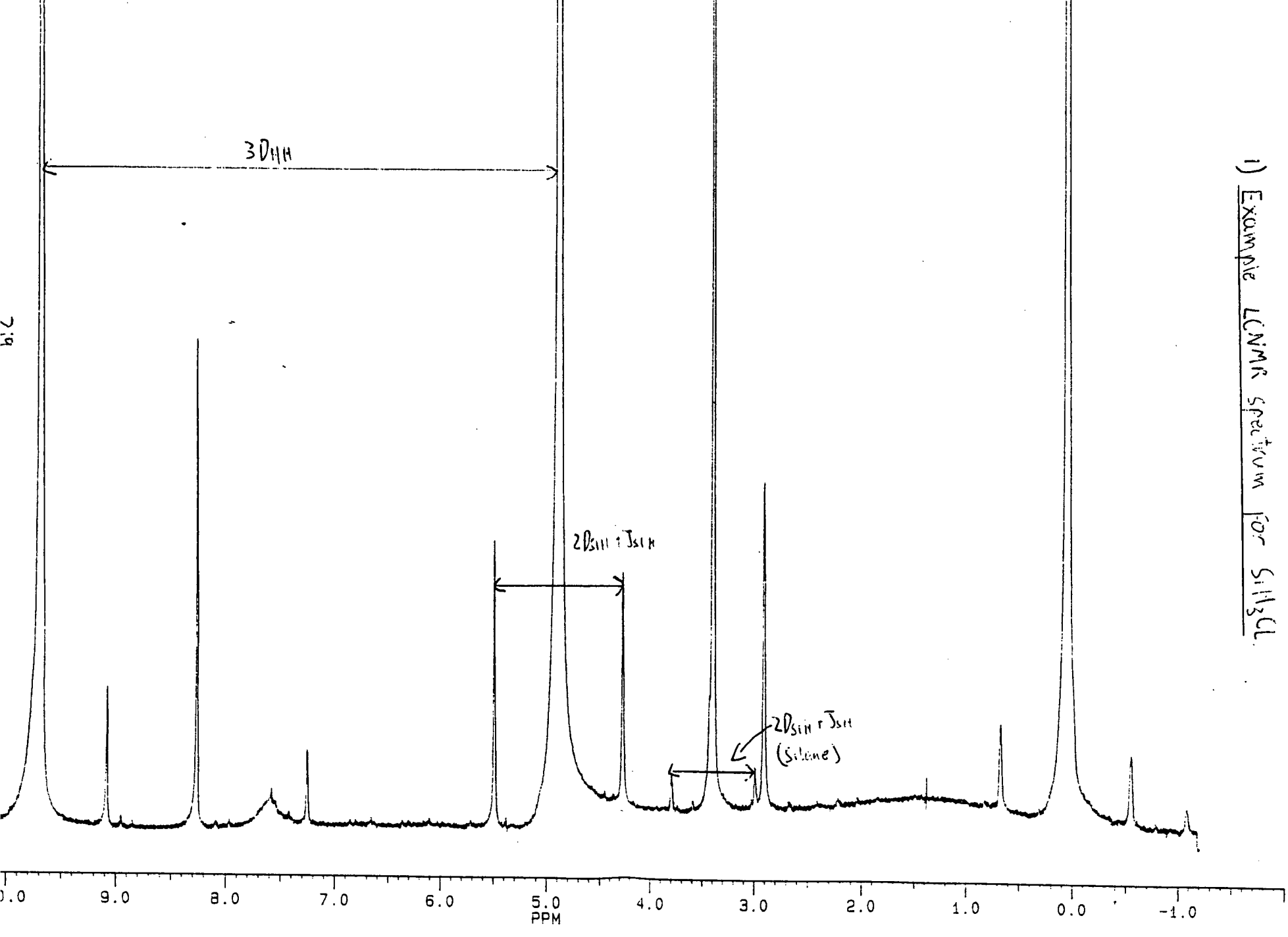

1) Example LCNMR spectrum for SiH_3Cl.

BRUK

KDWR1.100
DATE 1-12
TIME 11:

SF	250
SFO	250
O1	4200
SI	16384
TD	8192
SW	3289
HZ/PT	
PW	
RD	
AQ	
RG	40
NS	915
TE	297
FW	4200
O2	3200
DP	63L
LB	
GB	
CX	
CY	
F1	
F2	
HZ/CM	100
PPM/CM	
SR	2856

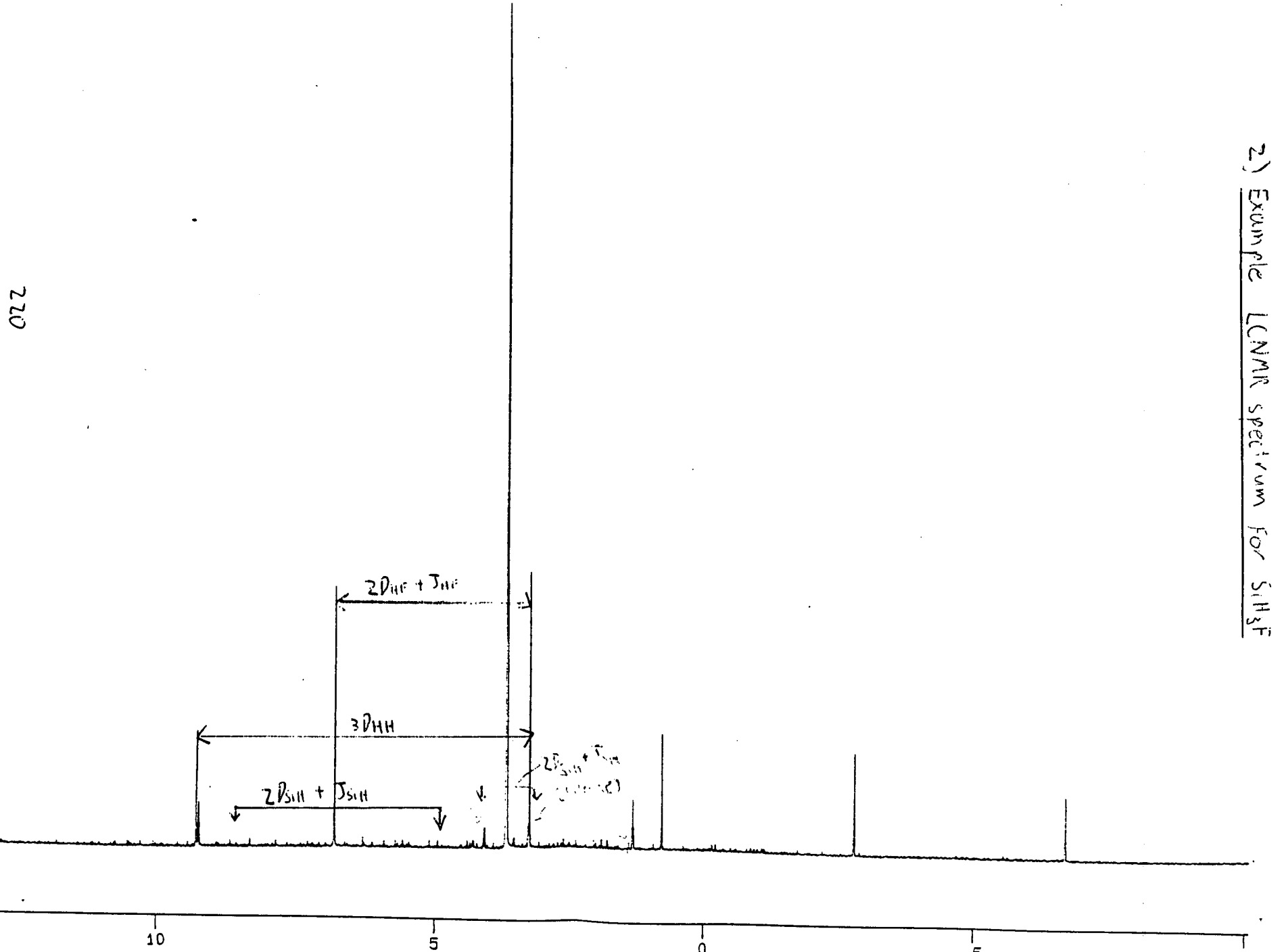

220

BRUKER

IDWR2.100
DATE 4-10-94
TIME 14:26

SF	250.133
SFO	250.130
O1	3536.279
SI	32768
TD	32768
SW	8196.721
HZ/PT	.500
PW	3.0
RD	0.0
AQ	1.999
RG	20
NS	558
TE	297
FW	10300
O2	3200.000
DF	63L PO
LB	0.0
GB	.500
CX	35.00
CY	0.0
F1	4479.47H
F2	-2520.56H
HZ/CM	200.001
PPM/CM	.800
SR	2856.00

2) Example LCNMR spectrum for SiH_3F

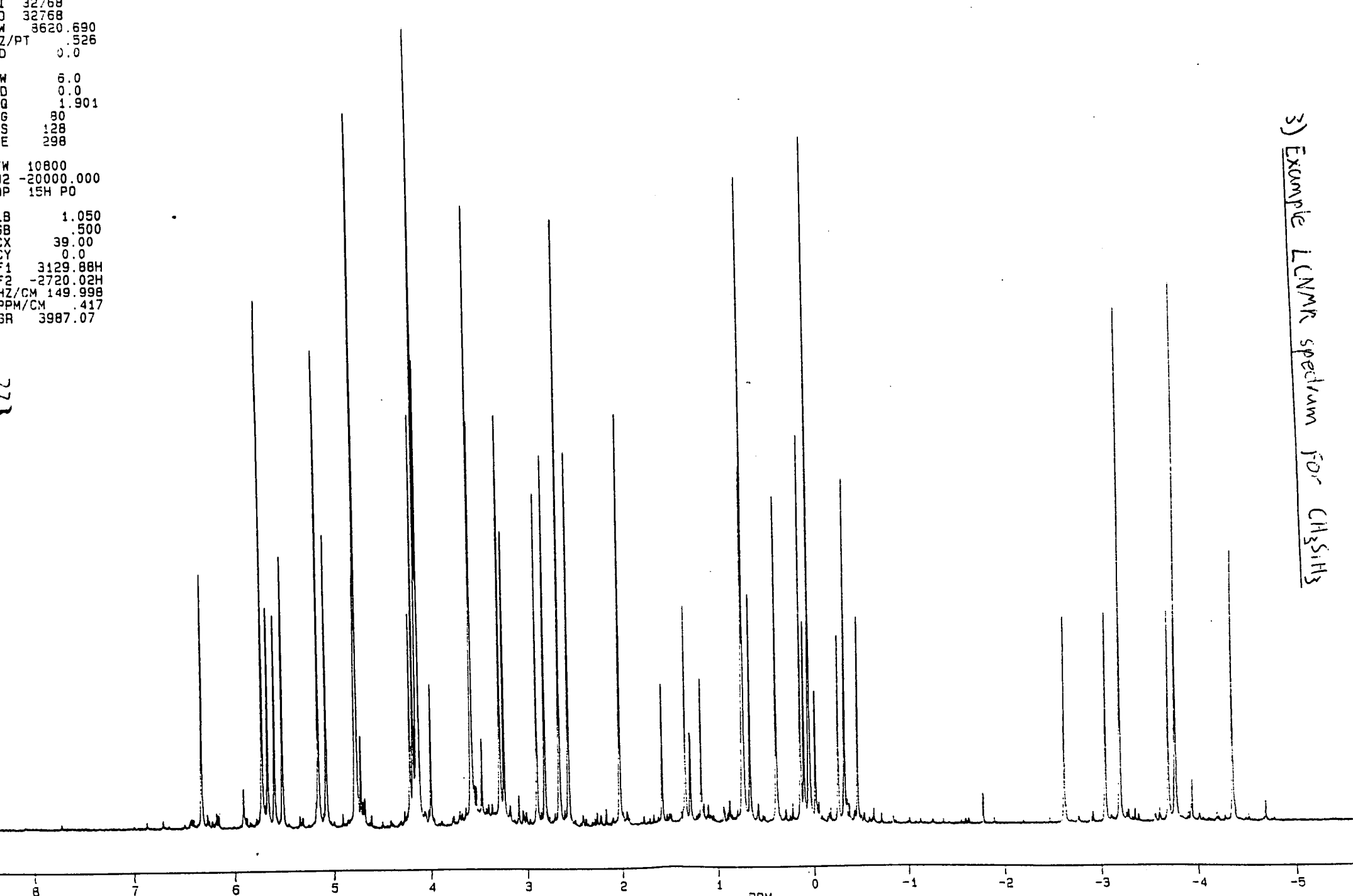

3) Example LCNMR spectrum for CH_3SiH_3

4) Example LCNMR spectrum for CH_3SiH_3 (Expanded)

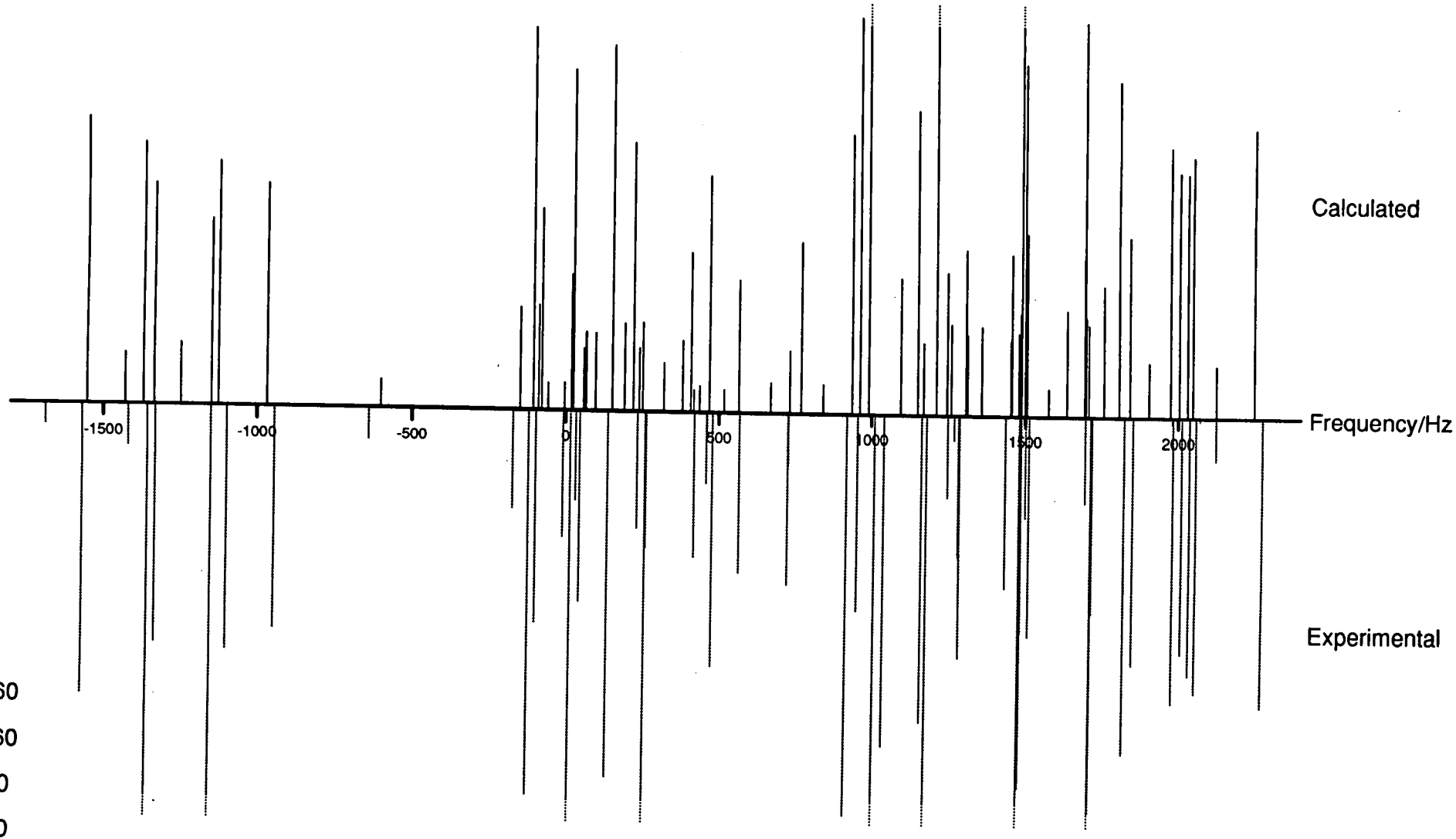

Sxx = -0.02160

Syy = -0.02160

Szz = 0.04320

Sxz = 0.00000

Syz = 0.00000

Sxy = 0.00000

SJ Example LCSIM (Methylsilane)

6) Example SLIQUOR output (cont'd)

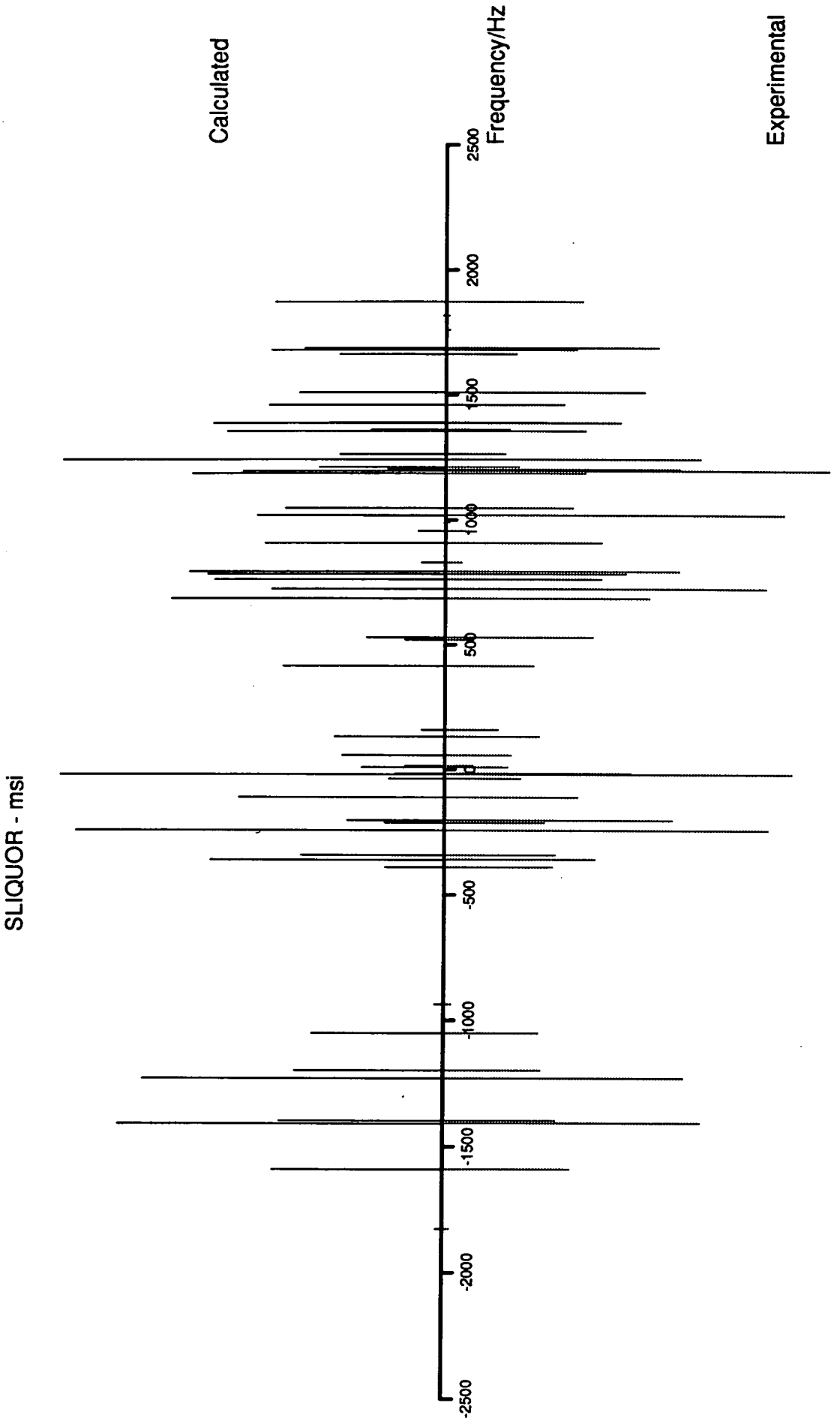

Appendix C

Lecture courses and conferences attended

Lecture Courses

German - Introductory Reading Course, Session 1991/92

NMR Spectroscopy, Dr.I.H.Sadler & Dr.D.Reed

BCA Fourth Intensive Course in X-ray Structural Analysis

Aston University, England, 1993

Industrial Chemistry, Unilever Research & I.C.I.

UNIX I, Edinburgh Regional Computing Centre

UNIX II, Edinburgh Regional Computing Centre

Shell Programming, Edinburgh Regional Computing Centre

Conferences

Fifth European Symposium on Gas Electron Diffraction

Blaubeuren, Germany, 1993

University of Strathclyde Inorganic Club Conference

1991-1994

Departmental Meetings and Seminars, 1991-1994